LEVEL II

12

A039884

Research and Development Technical Report

DELET-TR-74-0109-F

SEALED PRIMARY LITHIUM-INORGANIC ELECTROLYTE CELL

A.N. DEY

P.R. MALLORY & CO., INC.
LABORATORY FOR PHYSICAL SCIENCE
BURLINGTON, MA 01803

JULY 1978

FINAL REPORT FOR PERIOD 1 MARCH 1974 - 31 JULY 1977 and
1 OCTOBER 1977 - 31 MARCH 1978

DISTRIBUTION STATEMENT
APPROVED FOR PUBLIC RELEASE ; DISTRIBUTION UNLIMITED

PREPARED FOR :
US ARMY ELECTRONICS TECHNOLOGY AND DEVICES LABORATORY

ERADCOM
US ARMY ELECTRONICS RESEARCH AND DEVELOPMENT COMMAND
FORT MONMOUTH, NEW JERSEY 07703

Unclassified

SECURITY CLASSIFICATION OF THIS PAGE *(When Data Entered)*

REPORT DOCUMENTATION PAGE

READ INSTRUCTIONS BEFORE COMPLETING FORM

1. REPORT NUMBER: DELET-TR-74-0109-F

2. GOVT ACCESSION NO.

3. RECIPIENT'S CATALOG NUMBER

4. TITLE *(and Subtitle)*: Sealed Primary Lithium-Inorganic Electrolyte Cell

5. TYPE OF REPORT & PERIOD COVERED: Final Report 3/1/74 to 7/31/77 10/1/77 to 3/31/78

6. PERFORMING ORG. REPORT NUMBER

7. AUTHOR(s): A. N. Dey

8. CONTRACT OR GRANT NUMBER(s): DAAB07-74-C-0109

9. PERFORMING ORGANIZATION NAME AND ADDRESS: P. R. Mallory & Co. Inc. Laboratory for Physical Science Burlington, Mass. 01803

10. PROGRAM ELEMENT, PROJECT, TASK AREA & WORK UNIT NUMBERS: 1LI62705AH94-P1-214

11. CONTROLLING OFFICE NAME AND ADDRESS: U.S. Army Electronics Technology & Devices Lab ERADCOM Attn: DELET-PR Ft. Monmouth, New Jersey 07703

12. REPORT DATE: July 1978

13. NUMBER OF PAGES: 241

14. MONITORING AGENCY NAME & ADDRESS *(if different from Controlling Office)*: 249 p.

15. SECURITY CLASS. *(of this report)*: Unclassified

15a. DECLASSIFICATION/DOWNGRADING SCHEDULE

16. DISTRIBUTION STATEMENT *(of this Report)*
Approved for Public Release;
Distribution Unlimited

17. DISTRIBUTION STATEMENT *(of the abstract entered in Block 20, if different from Report)*
Final rept. 1 Mar 74-31 Jul 77 and 1 Oct 77-31 Mar 78,

18. SUPPLEMENTARY NOTES

215 325

19. KEY WORDS *(Continue on reverse side if necessary and identify by block number)*
Inorganic Electrolyte Battery, Thionyl Chloride, Lithium, Lithium Aluminum Chloride, Hermetic Lithium Battery, D Cell, High Energy Density Battery, Explosion Hazards, Differential Thermal Analysis.

land land

20. ABSTRACT *(Continue on reverse side if necessary and identify by block number)*
This report summarizes the R&D activities carried out by P.R. Mallory & Co. on the development of a primary $Li/SOCl_2$ D cell from March 1974 to July 1977 and October 1977 to March 1978.

The original objective of this program was to develop a D cell which is storable and operable in the temperature range of -40 to 160°F and is capable of delivering in excess of 150 WHr/lb at the thirty hour rate and peak power density of

78 07 13 016

215 325

DD FORM 1 JAN 73 1473 EDITION OF 1 NOV 65 IS OBSOLETE

Unclassified

SECURITY CLASSIFICATION OF THIS PAGE *(When Data Entered)*

50 watts/lb and a capacity degradation of less than 10% after one month of storage at 160°F.

We carried out a systematic investigation of the system in an effort to define the intrinsic performance capabilities as well as the limitations of the system. Our basic approach was two fold:

(a) Optimization of the system in order to achieve all the above performance goals in a hermetically sealed D cell structure, and

(b) the identification and definition of problems associated with the system and the development of approaches to solve these problems.

We showed that all the above objectives can be met by the hermetic $Li/SOCl_2$ D cells developed by us. In fact, the low rate D cells developed by us on a separate program delivered capacities of 18 A.Hr at a constant voltage of 3.5 volt corresponding to an energy density of 290 WHr/lb and 20 WHr/in^3 at low drains (0.01-0.03A). High rate cells routinely delivered 12 A.Hr at 1.0A drain corresponding to energy density of 156 WHr/lb and 11 WHr/in^3.

However, we found that the system suffered from two inherent deficiencies:

(a) A voltage delay, particularly at low temperatures after high temperature storage.

(b) A chemical instability that led to an explosion hazard, particularly on shorting and forced as well as on resistive load overdischarge.

We studied the voltage-delay problem in sufficient detail to define its underlying causes and developed several methods for alleviating it. Lowering the electrolyte salt ($LiAlCl_4$) concentration as well as a partial discharge alleviated the voltage delay to an extent that the cells show no voltage delay after a storage of 1 month at 72°C and test at -30°C at currents of 0.25, 1.0 and 3.0A. We consider the problem to be essentially solved for all practical purposes.

We investigated the explosion hazard problem in a phenomenological manner. First we established the conditions under which the hermetic $Li/SOCl_2$ D cells explode. Then we attempted to develop ways and means to prevent the explosion. We found that the lowering of the rate capability may not prevent cell explosions as long as the cell could get hot enough by other extraneous circumstances such as high temperature storage, heavy insulation of the cell wall and so on. We found that low pressure venting is an effective way of preventing cell explosions on external shorts. However, this approach was ineffective in preventing explosions from forced overdischarge. Also, on occasion the cells exploded on resistive load overdischarge. A completely discharged battery, while sitting on the shelf at 25°C, may also explode quite unexpectedly. This is of concern since it is impossible to prevent resistive load overdischarge and/or storage of partially and/or completely discharged batteries in normal use. We believe that this problem needs to be solved before the field use of the system can be recommended particularly in regard to D size cells.

We carried out DTA (Differential Thermal Analysis) studies of the chemical compounds and their mixtures that may be present in a partially discharged $Li/SOCl_2$ cell and identified the exothermic reactants that might either initiate or propagate an explosive reaction in the system. We also found a plausible

(continued)

mechanism for the observed spontaneous explosion of partially discharged cell on storage.

Experimental results of DTA of discharged D cells suggested a method of deactivating the discharged D cells for preventing the spontaneous explosion on casual storage. The efficacy of the approach is yet to be ascertained.

Substantial experimental support has also been obtained for the "hot spot" theory of the cell explosion.

Several empirical approaches to improve the abuse resistance of the hermetic D cells on reversal has been successfully tried, and several safe design features were identified.

All the program tasks have been completed on schedule.

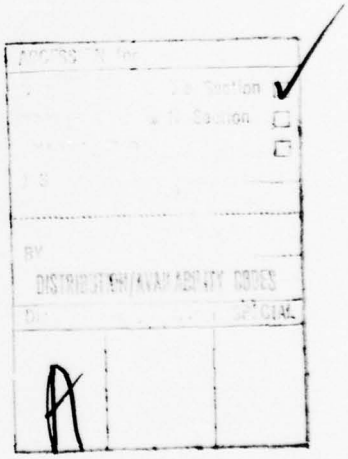

TABLE OF CONTENTS

1. Introduction

The $Li/SOCl_2$ inorganic electrolyte system (1-4) is one of the highest energy density systems known to date. The system consists of a Li anode, a carbon cathode and a $LiAlCl_4$-$SOCl_2$ electrolyte; $SOCl_2$ acts both as solvent and as cathode active material. The Li anode is prevented from reacting with the $SOCl_2$ by virtue of the formation of a LiCl protective film on the Li as soon as it contacts the $LiAlCl_4$-$SOCl_2$ electrolyte according to the reaction.

$$Li + SOCl_2 \longrightarrow 2LiCl + SO \qquad (1)$$

All the experimental facts (5) available to date suggest the reaction (1) as the primary cell reaction. The bi-radical SO is unstable and usually dimerize and then decompose to $S + SO_2$ according to

$$2SO \longrightarrow (SO)_2 \qquad (2)$$

$$(SO)_2 \longrightarrow S + SO_2 \qquad (3)$$

SO may undergo other possible chemical reactions to produce other by-products.

The object of this program is to develop sealed primary lithium-inorganic electrolyte "D" size cells which are operable and storable over the temperature range -40 (-40°C) to 160°F (72°C). Goals of 150 WHr/lb at a 30 hr rate, with peak power density of 50 W/lb and a capacity degradation of less than 10% after one month of storage at 160°F were sought.

We carried out the following tasks under this program.

Task I - Component Capability and Design

The purpose of this phase of the program is to obtain data on: (a) material compatibility, (b) cell optimization with respect to electrode and electrolyte composition and (c) pressure build-up, all of which are necessary for the design of the "D" cells.

We used an accelerated test for the material compatibility studies. Also, we used a non-hermetic 'C' size cell for the optimization and the pressure build-up studies, as the tooling and the parts needed to fabricate this cell were already available in the laboratory.

Task II - Construction of Sealed Portable Battery Cell Prototype

The object of this phase of the program was to develop a D cell and to characterize its performance capabilities at various temperatures, fresh and after storage at temperatures up to 160°F (72°C).

We chose to use a hermetically sealed D cell with a welded top and a G/M seal terminal instead of a crimp sealed cell because of the chemically corrosive and physiologically harmful nature of the $SOCl_2$ vapor. We chose to use a Ni can instead of a stainless steel can because of the possible contamination of Fe, which was known to aggravate the voltage-delay of the system. We demonstrated the high energy density capability and the good capacity retention on storage of these hermetic D cells.

Task III - Study of Voltage-Delay Problem

We showed (4) before the start of the program that the voltage-delay (a phenomenon of instantaneous voltage depression on load and a slow recovery) is a potential problem with this system. We established (4) that the problem was due to the formation of LiCl film on Li, a process which is enhanced by the duration and the temperature of the storage. The object of this task was to develop ways and means to alleviate the problem. We pursued both an empirical and a phenomenological approach consisting of studying the morphology and the growth rate of the LiCl film on Li as a function of the various electrolyte variables. As a result of this study we were able to alleviate the problem to an extent that the cells may be suitable for many applications.

Task IV - Safety Studies. Development of Protection Against Short Circuit and Thermal Runaway

The hermetic D cells were found to explode on short circuiting and forced overdischarge as well as on high rate discharge and on casual storage at ambient temperature in a partially or completed discharged state. The object of this task was to develop ways and means to render the cells safe under normal use and abuse conditions. We pursued a physical approach consisting of the use of a low pressure vent and showed that it was possible to prevent cell explosion from abuses such as shorting by means of a low pressure vent.

Task V - Thermochemical Studies of Pressure Producing Reactions

We carried out DTA (Differential Thermal Analysis) of chemical constituents as well as of the whole D cells and identified the chemicals which could initiate and/or propagate a thermal runaway. The results also suggested possible approaches of deactivating discharged cell so that it may not explode on casual storage.

Task VI - Local Internal Heating of D Cells (To Test the "Hot Spot" Theory of Cell Explosion)

We demonstrated that it was possible to set off a thermal runaway of a discharged D cell by local heating more easily than of a fresh cell, and as such the results supported the "hot spot" theory of cell explosion.

In addition, several empirical approaches were developed, based on our knowledge of the system from the above studies, to alleviate the explosion

hazard on reversal, that may occur in a multicell battery during normal use. The approaches were evaluated using the hermetic D cells. The results were found to be encouraging.

All the above tasks were completed and major portions were reported in thirteen reports and an interim report. We have included all of that and the additional work carried out on Tasks V and VI in this Final Report.

2. Task I - Component Capability and Design

2.1 Material Compatibility Studies

This work was designed primarily to obtain information on the chemical stability of the cell construction materials with the inorganic electrolyte, 1.5(M) $LiAlCl_4$-$SOCl_2$. Two types of materials were examined: (i) Metallic materials, for use on cell can, current collectors, cell terminals and so forth. (ii) Insulating materials, to be used as separators, insulators, sealants, etc. The compatibility of the materials was determined qualitatively by an accelerated test involving refluxing of the specimens of the various materials in 1.5(M) $LiAlCl_4$-$SOCl_2$ electrolyte at a temperature of 85°C (185°F) for approximately one month followed by a microscopic examination of the specimens for degradation. This test condition was considered to be severe enough so that the materials which passed the test were expected to withstand the storage requirements of the "D" cells.

2.1.1 Experimental

2.1.1.1 Materials: Metallic materials were procured as foil, sheet and tube form from Uniform Tube Corporation. Preliminary test tube experiments in our laboratory have shown that metals such as Cu, Fe, cold rolled steel are unstable in this electrolyte even at 25°C. These were excluded from further tests. It was also observed that a metal such as Al was stable by itself in the inorganic electrolyte at 25°C but corroded severely when in contact with carbon; most likely due to the local cell reaction. Ni was found to be stable even in contact with carbon. For this reason, all the metallic materials were spot welded to a carbon electrode on Ni grid (these are identical to the cathodes used for the "C" size cells described later) and then refluxed in the inorganic electrolyte.

The insulating materials were tested in sheet, nonwoven fabric, and molded grommet forms. Several types of rubbers were included in this test.

2.1.1.2 Electrolyte: $LiAlCl_4$ was prepared in the laboratory by melting equimolar mixture of pre-dried LiCl (Foote Mineral) and $AlCl_3$ (Fluka, iron and water free, Columbia Organic Chemical Co.) in argon atmosphere according to a method described elsewhere (1, 6).

$SOCl_2$ was purified by distillation. The distilled product was colorless.

The 1.5(M) solutions of $LiAlCl_4$ in $SOCl_2$ were prepared by dissolving pre-weighed amounts of $LiAlCl_4$ in $SOCl_2$ in a volumetric flask. The electrolyte solutions were colorless to very light amber in appearance.

2.1.1.3 Refluxing Set-up: Refluxing of specimens of the various materials was carried out in pyrex one liter round bottom flasks fitted with a water cooled refluxing condenser. The exit tube of the condenser was connected to a glass tube (by means of a "T" joint) through which a stream of argon was passed continuously. In this manner, entry of air into the flask during refluxing was prevented. Sufficient amount of electrolyte was added to the flask to ensure that all the specimens were submerged in the liquid.

2.1.1.4 Examination of the Specimens: At the completion of refluxing for a definite period of time, the specimens were removed from the flask and were thoroughly washed with water to remove the electrolyte. These were examined under a microscope in order to detect any sign of corrosion or any form of physical changes that could occur as a result of chemical reactions with the electrolyte.

2.1.2 Results and Discussion

The results of the compatibility tests of the metallic materials are shown in Table 1. It appears that all the metals and alloys tested are compatible with the inorganic electrolyte with the exception of Ni-clad steel. It is interesting to note that the steel is dissolved from the exposed edges leaving the Ni foil intact. This suggests that steel may still be used in this system provided it is completely covered with nickel. Nickel plated steel cans are useable for short-term tests. The metals and alloys shown in Table I which were found to be stable in the electrolyte in contact with the carbon cathode, are also expected to be stable in contact with the Li anode as these are not expected to undergo spontaneous electrochemical alloying (7) with Li. Therefore, these metals and alloys should be useable as current collectors for both the Li anode and the carbon cathode for the inorganic electrolyte battery.

The results of the compatibility tests of the insulating materials as shown in Table 2, indicate that glass, Teflon and Kel-F are the only materials that are stable in the inorganic electrolyte.

Viton rubber, although found to be unstable at 85°C, was found to be stable at 25°C for 30 days.

2.2 Optimization Studies

It was shown by several workers (1, 2, 4) that the $LiAlCl_4$-$SOCl_2$ inorganic electrolyte system was superior to other known oxychloride systems in terms of the electrochemical performance of the experimental battery. Behl et al (1) studied a variety of carbon blacks as the substrate for the cathode and found that Shawinigan Black was the best. Teflon was used as a binder for the carbon black cathode and was found to be compatible with the inorganic electrolyte. We showed earlier that the only separator material that was stable in the system was the glass filter paper. Ni was found to be a stable current collector material suitable for both the Li anode and the carbon cathode. Based on this background information, we chose the following specific system for the optimization studies:

TABLE 1

Compatibility Studies of Metallic Material with 1.5 (M) $LiAlCl_4$-$SOCl_2$ Inorganic Electrolyte at 85°C (185°F)

Metallic Materials	Duration of Refluxing at 85°C (days)	Condition of the Samples After Refluxing
Ni Span C	47	Discolored in contact with air
		No sign of corrosion
AM-350	47	" " " " "
Ni-A	47	" " " " "
52 alloy	47	" " " " "
Ni - (99.5%)	47	" " " " "
Inconel 702	47	" " " " "
Inconel 750	47	" " " " "
Inconel 625	47	" " " " "
Invar	47	" " " " "
K-Monel	47	" " " " "
Incoloy 800	47	" " " " "
304 Stainless	45	" " " " "
316 Stainless	45	" " " " "
Monel 400	45	" " " " "
Inconel 600	45	" " " " "
Inconel 601	33	" " " " "
302 Stainless	33	" " " " "
Molybdenum	33	Remained shiny in air
		No corrosion
Tantalum	33	" " " "
Niclad steel sheet (edges not covered by Ni)	32	Steel completely dissolved, Ni part intact

TABLE 2

Compatibility Studies of Insulating Materials with 1.5(M) $LiAlCl_4$-$SOCl_2$ Inorganic Electrolyte at 85°C (185°F)

Insulating Materials	Duration of Refluxing at 85°C (days)	Condition of the Samples After Refluxing
1) 'Webril' nonwoven polypropylene fabric	47	Complete disintegration
2) 'Celguard' polypropylene film	47	" "
3) Glass filter paper	47	Good, no change
4) Epoxy G-10: Epoxy filled fiberglass woven fabric	33	Glass fabric OK; Epoxy disintegrated
5) Polypropylene sheet	46	Dark and brittle
6) PVC sheet	46	Complete disintegration
7) CPVC sheet	46	" "
8) ABS sheet	46	" "
9) Plexiglass sheet	33	" "
10) Rulon rod (a type of teflon)	27	Good, no change
11) Kel-F rod	27	Good
12) Teflon rod	27	Good, no change
13) Butyl rubber(60 d)	15	Disintegrated
14) Neoprene rubber (50 d)	15	"
15) Neoprene rubber (70 d)	15	"
16) Silicone rubber	15	"
17) Viton rubber (70 d)	15	Cracked

Li anode, $SOCl_2$ solvent and depolarizer, $LiAlCl_4$ electrolyte salt, Teflon bonded Shawinigan Black cathode on Ni exmet and glass filter paper separator.

The parameters which need to be defined in the above system are:

1) concentration of $LiAlCl_4$
2) purity or source of $LiAlCl_4$
3) Teflon content of the Shawinigan Black cathode.

Therefore, the optimization studies were carried out with respect to the above three parameters. A factorial matrix was set up using three levels of $LiAlCl_4$ concentration, two sources of $LiAlCl_4$ and three levels of Teflon content. This is shown in Table 3

The test vehicle chosen for the above factorial experiment was a "C" size cell for which most of the hardware and the tooling was already available from our Li/SO_2 battery programs. At least 4 cells were made under each condition and were tested at currents of 0.1, 0.3, 0.5 and 1.0 Amp. All the cells were designed so that the cathode was the capacity limiting electrode. The experimental details are presented below.

2.2.1 Experimental

2.2.1.1 Cell Design: A cut out view of the "C" cell (OD = 0.94", Ht. = 2.00") is shown in Figure 1. A Ni-plated cold rolled steel can was used as a cell container. The Li anode (7.5" x 1.5"), the carbon cathode (8" x 1.5") and the glass filter paper separator were wound into a tight roll and were packaged in the cell can. The electrode terminals in the form of Ni tabs were spot welded to the cell can and the cell top respectively. The cell top comprised a flat Ni washer with a hole at the center which served as electrolyte fill port and as vent. The hole was closed with a viton rubber septum. The Ni top was placed on a viton rubber grommet and an Ni support ring which was placed on the beaded inner wall of the cell can, and the cell top was crimp sealed.

The cells were filled with the electrolyte by means of a hypodermic needle which was pierced through the rubber septum. The cells were evacuated prior to the electrolyte filling. A Ni tab was spot welded on the cell top to keep the rubber septum in position during discharge when the cell pressure increased. If an abnormal pressure build up were to occur, the cell would vent through the hole after breaking the tab under high pressure. In spite of this precaution, of two cells, one cell exploded 0.91 min. after deliberate external shorting, and the other cell vented 1.31 min. after the shorting test.

2.2.1.2 Li-Anode: The Li anodes were made from 0.022" thick Li foil (Foote) and were pressed on a Ni grid.

2.2.1.3 Carbon-Cathode: The carbon cathodes were made by pasting Shawinigan Carbon and an appropriate amount of Colloidal Teflon (du Pont) in water on the Ni exmet (Exmet Corporation) employing the facility used for the

TABLE 3

Extended Factorial Matrix for the Optimization Studies

Teflon Content Wt %	LPS Electrolyte Conc. of $LiAlCl_4$				Foote Electrolyte Conc. of $LiAlCl_4$		
	0.5(M)	1.0(M)	1.5(M)	2.0(M)	0.5(M)	1.0(M)	1.5(M)
10%	0.1A 0.3A 0.5A 1.0A	0.1A 0.3A 0.5A 1.0A	0.1A 0.3A 0.5A 1.0A	0.1A 0.3A 0.5A 1.0A	0.1A 0.3A 0.5A 1.0A	0.1A 0.3A 0.5A 1.0A	0.1A 0.3A 0.5A 1.0A
20%	0.1A 0.3A 0.5A 1.0A	0.1A 0.3A 0.5A 1.0A	0.1A 0.5A 0.5A 1.0A	0.1A 0.3A 0.5A 1.0A	0.1A 0.3A 0.5A 1.0A	0.1A 0.3A 0.5A 1.0A	0.1A 0.3A 0.5A 1.0A
30%	0.1A 0.3A 0.5A 1.0A	0.1A 0.3A 0.5A 1.0A	0.1A 0.3A 0.5A 1.0A	0.1A 0.3A 0.5A 1.0A	0.1A 0.3A 0.5A 1.0A	0.1A 0.3A 0.5A 1.0A	0.1A 0.3A 0.5A 1.0A

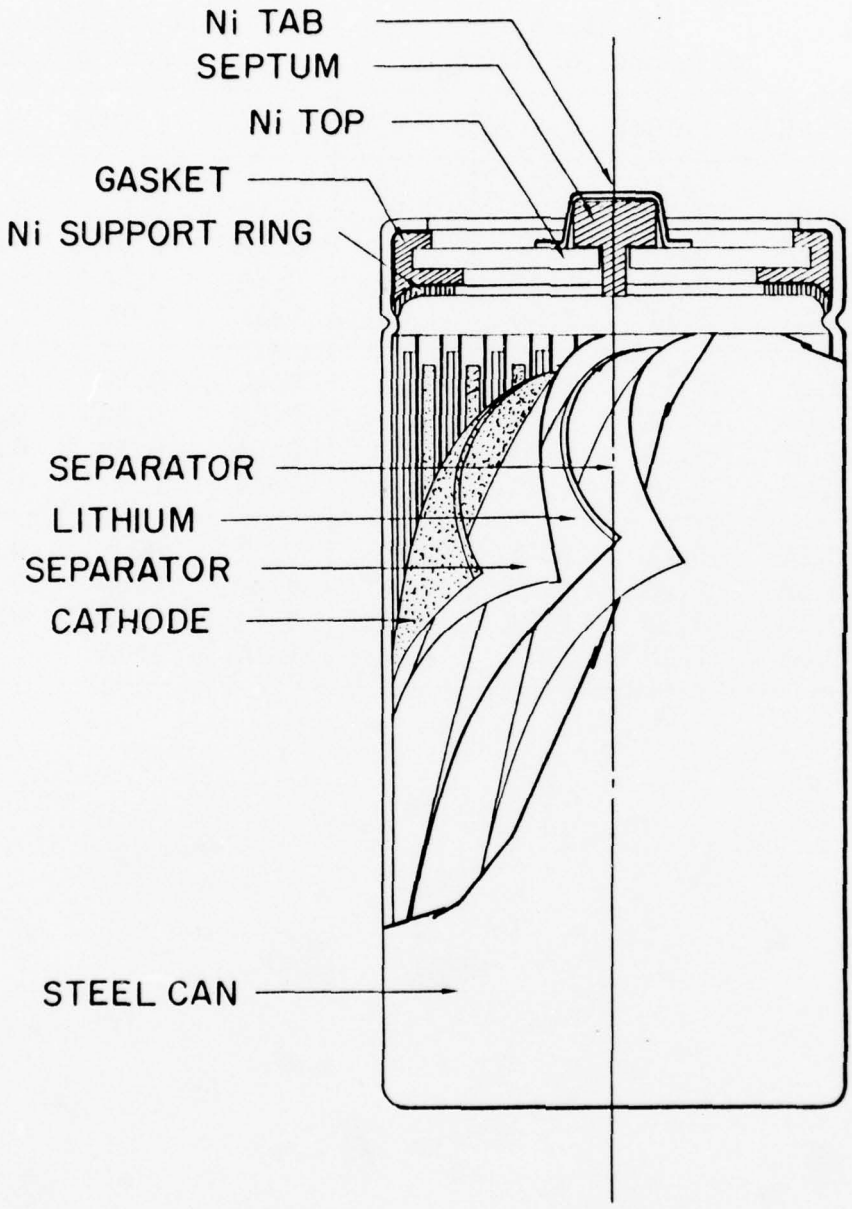

Fig. 1 Cut-out View of the Inorganic Electrolyte "C" Cell

construction of carbon cathodes for Li/SO_2 batteries. The electrodes were vacuum dried according to the method described by Behl et al (1). Each cathode was weighed and the weight of the carbon mix was controlled within 1.65 ±0.2 gm. for each cell. Ni tabs were spot welded to one end of the electrodes prior to its transfer to the dry box (Vacuum Atmosphere).

2.2.1.4 Cell Assembly: The cells were assembled in the argon filled dry box employing pre-dried glass filter paper separators, the carbon cathodes, and the Li anodes. The cells were removed from the dry box after closing them with the rubber grommeted Ni cell top and were immediately crimped.

2.2.1.5 Electrolyte: Two types of electrolytes were used for the optimization studies: (a) as prepared in our laboratory referred to as LPS electrolyte, described earlier; and (b) as prepared from $LiAlCl_4$ received from Foote, referred to as Foote electrolyte. The latter type of electrolyte was prepared by dissolving known quantities of Foote $LiAlCl_4$ in distilled $SOCl_2$. The color of this electrolyte was deep purple and it left an organic residue on the glass vessels after it was washed with water. The chemical composition of this residue has not been determined. However, it is soluble in CCl_4. The LPS electrolyte, on the other hand, was colorless to light amber in appearance and did not leave any residue on the glass after washing with water.

The electrolytes were stored and dispensed from an all-glass (Pyrex) system. The weight of electrolyte added to each cell was recorded and was controlled to within 20 ±2 gms.

2.2.1.6 Cell Testing: The cells were tested at 25°C within 8 hours of cell filling at constant currents of 0.1, 0.3, 0.5 and 1.0 A for each condition of cell construction. In addition, some cells were tested at -30°C at 0.3 Amp. The cell potential was recorded as a function of time and the cell capacities were determined to a 2.0 volt cut off.

2.2.2 Results and Discussion

The results of the factorial experiments are presented in Table 4. The first 4 cells numbering 8, 19, 21 and 22 were all tested at 0.5 A in order to check the variability of the cell. This was found to be quite satisfactory (standard deviation = 0.085 AHr). The capacities of the cells at various currents are shown in the next to the last column. The capacities/gm. of carbon mix in the cathode were also calculated and are shown in the last column.

Typical discharge curves of the "C" cells made under one condition and discharged at 0.1, 0.3, 0.5 and 1.0 A are shown in Fig. 2. The cells showed very flat discharge curves and no voltage delay. This was expected as the cells were tested within eight hours of cell filling. The cell capacity was chosen as the primary response in the factorial experiments. The detailed statistical analysis of the data are available in the first quarterly report (19). According to the analysis, the variables: current (I), source of electrolyte salt (S), electrolyte concentration (C) and Teflon content (T) were all found to be significant.

TABLE 4

The Discharge Data of the Inorganic Electrolyte 'C' Cells Constructed

According to the Factorial Experiments described in Table 3

Cell No	Electrolyte ($LiAlCl_4$) Source S	Electrolyte ($LiAlCl_4$) Concentration(M) C	Cathode, Teflon Content % (wt) T	Cathode Carbon mix weight (gm)	Electrolyte Weight (gm)	Test Current (Amps) I	Cell Capacity to 2.0 Volt (A.hr) Q	Capacity per gm of Carbon Mix
8	LPS electrolyte	1.5	10	--	22.1	0.5	3.70	
19	"	1.5	10	--	21.00	0.5	3.60	
21	"	1.5	10	--	21.50	0.5	3.80	
22	"	1.5	10	--	21.26	0.5	3.65	
23	"	1.5	10	1.44	22.08	0.1	4.84	3.36
24	"	1.5	10	1.42	22.06	0.3	4.11	2.89
25	"	1.5	10	1.50	21.61	0.5	3.55	2.37
26	"	1.5	10	1.59	21.78	1.0	2.40	1.44
27	"	1.5	10	1.66	21.58	0.3 (-30°C)	2.40	1.44
27A	"	1.5	20	1.52	21.97	0.1	4.72	3.10
28	"	1.5	20	1.58	21.83	0.3	3.81	2.41
29	"	1.5	20	1.52	21.99	0.5	3.10	2.04
30	"	1.5	20	1.65	21.68	1.0	2.30	1.39
32	"	1.5	30	1.54	21.09	0.1	4.81	3.12
33	"	1.5	30	1.57	21.66	0.3	4.20	2.67
34	"	1.5	30	1.56	21.97	0.5	3.65	2.34
35	"	1.5	30	1.60	21.02	1.0	2.50	1.56
36	"	1.5	30	1.57	20.08	0.3 (-30°C)	2.19	1.39

TABLE 4 (continued)

The Discharge Data of the Inorganic Electrolyte 'C' Cells Constructed

According to the Factorial Experiments described in Table 3

Cell No	Electrolyte ($LiAlCl_4$) Source S	Electrolyte ($LiAlCl_4$) Concentration(M) C	Cathode, Teflon Content % (wt) T	Cathode Carbon mix weight (gm)	Electrolyte Weight (gm)	Test Current (Amps) I	Cell Capacity to 2.0 Volt (A.hr) Q	Capacity per gm of Carbon Mix
39	LPS electrolyte	1.0	10	1.67	20.75	0.1	5.39	3.23
41	"	1.0	10	1.83	20.23	0.3	4.59	2.51
42	"	1.0	10	1.84	20.53	0.5	4.50	2.44
38	"	1.0	10	---	21.05	0.5	4.40	----
43	"	1.0	10	1.76	20.66	1.0	3.85	2.19
40	"	1.0	10	1.49	18.38	0.3 (-30°C)	2.32	1.56
49	"	1.0	20	1.55	20.16	0.1	5.05	3.26
45	"	1.0	20	1.60	20.43	0.3	4.32	2.70
46	"	1.0	20	1.60	20.50	0.5	3.95	2.47
48	"	1.0	20	1.47	20.89	1.0	2.90	1.97
50	"	1.0	30	1.58	21.04	0.1	4.69	2.97
52	"	1.0	30	1.56	20.94	0.3	4.02	2.58
53	"	1.0	30	1.58	20.14	0.5	3.75	2.37
54	"	1.0	30	1.61	21.19	1.0	2.90	1.80
55	"	0.5	10	1.78	21.42	0.1	4.92	2.76
56	"	0.5	10	1.73	20.62	0.3	3.81	2.20
57	"	0.5	10	1.67	20.47	0.5	2.40	1.44
59	"	0.5	10	1.74	20.62	1.0	1.50	0.86
58	"	0.5	10	1.74	20.34	0.3 (-30°C)	1.86	1.07

TABLE 4 (continued)

The Discharge Data of the Inorganic Electrolyte 'C' Cells Constructed

According to the Factorial Experiments described in Table 3

Cell No	Electrolyte ($LiAlCl_4$) Source S	Electrolyte ($LiAlCl_4$) Concentration(M) C	Cathode, Teflon Content % (wt) T	Cathode Carbon mix weight (gm)	Electrolyte Weight (gm)	Test Current (Amps) I	Cell Capacity to 2.0 Volt (A.hr) Q	Capacity per gm of Carbon Mix
60	LPS electrolyte	0.5	20	1.53	19.58	0.1	4.52	2.95
61	"	0.5	20	1.60	19.75	0.3	3.06	1.91
62	"	0.5	20	1.63	19.59	0.5	2.20	1.35
63	"	0.5	20	1.52	20.99	1.0	1.0	0.66
64	"	0.5	30	1.51	20.90	0.1	4.28	2.83
65	"	0.5	30	1.55	20.09	0.3	3.35	2.16
66	"	0.5	30	1.60	19.39	0.5	2.20	1.37
67	"	0.5	30	1.56	20.24	1.0	1.20	0.77
68	"	0.5	30	1.46	----	0.3 (-30°C)	1.53	1.05
69	Foote electrolyte	0.5	10	1.76	20.29	0.1	4.28	2.43
70	" "	0.5	10	1.88	20.29	0.3	3.20	1.70
71	" "	0.5	10	1.73	20.29	0.5	2.90	1.68
72	" "	0.5	10	1.66	20.62	1.0	2.20	1.32
73	" "	0.5	10	1.65	20.45	0.3 (-30°C)	2.97	1.80
74	" "	0.5	20	1.63	19.79	0.1	3.78	2.32
75	" "	0.5	20	1.40	18.40	0.3	2.82	2.01

TABLE 4 (continued)

The Discharge Data of the Inorganic Electrolyte 'C' Cells Constructed

According to the Factorial Experiments described in Table 3

Cell No	Electrolyte ($LiAlCl_4$) Source S	Electrolyte ($LiAlCl_4$) Concentration(M) C	Cathode, Teflon Content % (wt) T	Cathode Carbon mix weight (gm)	Electrolyte Weight (gm)	Test Current (Amps) I	Cell Capacity to 2.0 Volt (A.hr) Q	Capacity per gm of Carbon Mix
76	Foote electrolyte	0.5	20	1.50	20.24	0.5	2.75	1.83
77	" "	0.5	20	1.60	17.36	1.0	1.85	1.16
79	" "	0.5	30	1.57	19.63	0.1	3.50	2.23
80	" "	0.5	30	1.51	18.16	0.3	2.62	1.73
81	" "	0.5	30	1.60	19.66	0.3	2.54	1.59
82	" "	0.5	30	1.59	19.47	0.5	2.35	1.48
83	" "	0.5	30	1.55	19.87	1.0	1.50	0.97
84	" "	1.0	10	1.67	20.45	0.1	4.10	2.45
85	" "	1.0	10	1.64	20.21	0.3	3.55	2.16
86	" "	1.0	10	1.73	20.00	0.5	2.95	1.70
87	" "	1.0	10	1.60	20.11	1.0	2.15	1.34
88	" "	1.0	10	1.60	20.25	0.3(-30°C)	3.66	2.29
89A	" "	1.0	20	1.57	20.64	0.1	4.28	2.73
90A	" "	1.0	20	1.58	20.84	0.3	3.36	2.13
91A	" "	1.0	20	1.58	20.36	0.5	3.10	1.96
92A	" "	1.0	20	1.63	20.80	1.0	2.40	1.47
93A	" "	1.0	20	1.58	20.27	0.3(-30°C)	3.18	2.01
89	" "	1.0	30	1.57	19.91	0.1	4.25	2.71
90	" "	1.0	30	1.49	19.81	0.3	3.13	2.10
91	" "	1.0	30	1.44	20.14	0.5	2.70	1.87

TABLE 4(continued)

The Discharge Data of the Inorganic Electrolyte 'C' Cells Constructed

According to the Factorial Experiments described in Table 3

Cell No	Electrolyte ($LiAlCl_4$) Source S	Electrolyte ($LiAlCl_4$) Concentration(M) C	Cathode, Teflon Content % (wt) T	Cathode Carbon mix weight (gm)	Electrolyte Weight (gm)	Test Current (Amps) I	Cell Capacity to 2.0 Volt (A.hr) Q	Capacity per gm of Carbon Mix
92	Foote Electrolyte	1.0	30	1.55	19.73	1.0	2.0	1.29
93	"	1.0	30	1.63	20.03	0.3 (-30°C)	3.51	2.15
94	"	1.5	10	1.83	20.43	0.1	4.62	2.52
95	"	1.5	10	1.79	20.68	0.3	3.60	2.01
96	"	1.5	10	1.57	20.46	0.5	2.85	1.81
97	"	1.5	10	1.73	20.69	1.0	2.30	1.33
98	"	1.5	10	1.71	20.26	0.3 (-30°C)	3.42	2.00
104	"	1.5	20	1.79	20.84	0.1	4.78	2.67
105	"	1.5	20	1.77	20.30	0.3	3.42	1.93
106	"	1.5	20	1.65	21.24	0.5	3.10	1.88
107	"	1.5	20	1.62	19.34	1.0	2.00	1.23
99	"	1.5	30	1.75	20.19	0.1	4.13	2.36
100	"	1.5	30	1.77	20.10	0.3	2.94	1.66
101	"	1.5	30	1.85	20.62	0.5	2.80	1.51
102	"	1.5	30	1.73	20.31	1.0	1.90	1.10

TABLE 4 (continued)

The Discharge Data of the Inorganic Electrolyte "C" Cells Constructed

According to the Factorial Experiments described in Table 3

Cell No	Electrolyte ($LiAlCl_4$) Source S	Electrolyte ($LiAlCl_4$) Concentration (M) C	Cathode, Teflon Content % (wt) T	Cathode Carbon mix weight (gm)	Electrolyte Weight (gm)	Test Current (Amps) I	Cell Capacity to 2.0 Volt (A.hr) Q	Capacity per gm of Carbon Mix
117	LPS electrolyte	2.0	10	2.12	22.59	0.1	4.35	2.05
118	"	2.0	10	2.12	22.37	0.3	4.20	1.98
119	"	2.0	10	2.07	22.53	0.5	4.00	1.93
120	"	2.0	10	1.94	22.75	1.0	3.25	1.67
116	"	2.0	10	2.02	22.76	0.3 ($-30^{\circ}C$)	2.82	1.39
113	"	2.0	20	1.62	22.99	0.3	3.68	2.27
114	"	2.0	20	1.51	22.96	0.5	3.52	2.33
115	"	2.0	20	1.58	22.95	1.0	3.05	1.93
122	"	2.0	30	1.88	23.01	0.1	4.20	2.23
123	"	2.0	30	1.82	22.41	0.3	3.90	2.14
124	"	2.0	30	1.89	22.48	0.5	3.77	1.99

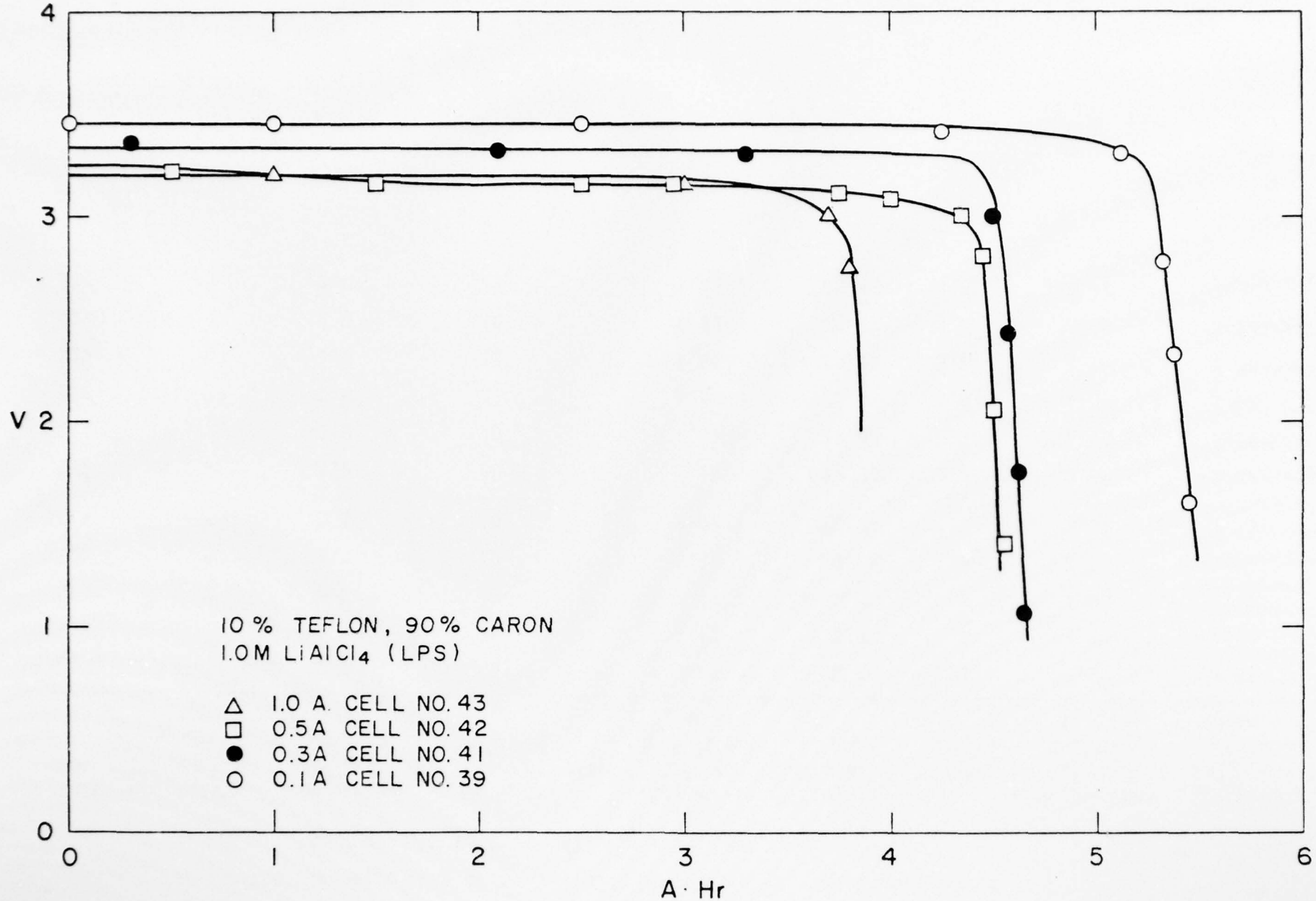

Fig. 2. Typical Discharge Curves of Non-Hermetic 'C' Cells

Among the possible interactions of the above variables, the electrolyte source/electrolyte concentration interaction was found to be the most significant. The analysis of the capacity/gm. of carbon data yielded identical conclusions. The optimum cell performance was realized with 1(M) LPS electrolyte and 10% Teflon in the cathode.

The cell capacity (Q)-current (I) data were also analyzed employing a method developed by Selim and Bro (8) where the capacity-current data were fitted to the equation:

$$Q = \frac{Q_o \tanh\left(\frac{I}{B}\right)^C}{\left(\frac{I}{B}\right)^C} \qquad (4)$$

Where Q_o, B and C are empirical constants which represent: (Q_o) the maximum cell capacity, (B) the current below which the capacity begins to decrease rapidly and (C) the accommodation coefficient which is a measure of how readily the battery can accommodate high discharge rates. The fit of the experimental Q-I data of the "C" cells made under the various conditions to the above expression was found to be satisfactory. The efficacy of this type of analysis has been successfully demonstrated for all types of commercial batteries (8) including the Li/SO_2 organic electrolyte batteries (9). A few typical Q-Log I plots of the inorganic electrolyte "C" cells are shown in Fig. 3 through Fig. 5. Figure 3 compares the Q-Log I plots of cells made with LPS and Foote electrolytes with 10% teflon and 1(M) electrolyte. Figure 4 compares the cell performance at three levels of Teflon content for 1(M) LPS electrolyte and Figure 5 shows the cell performance at three concentrations of LPS electrolyte with 10% Teflon content in the cathode.

The general conclusions are as follows:

(i) The optimal cathode composition is 90% carbon with 10% Teflon binder by weight, and

(ii) The optimal electrolyte concentration is 1.0M $LiAlCl_4$ prepared in the Laboratory by melting anhydrous LiCl and $AlCl_3$ (LPS type).

The above conclusions were based on the performance of the fresh "C" cells tested at 25°C. Whether the conclusion will be valid for tests at temperatures other than 25°C and for storage under various temperatures is yet to be determined.

No attempt has been made to analyze the limited amount of data available for the low temperature (-30°C) performance of the cells.

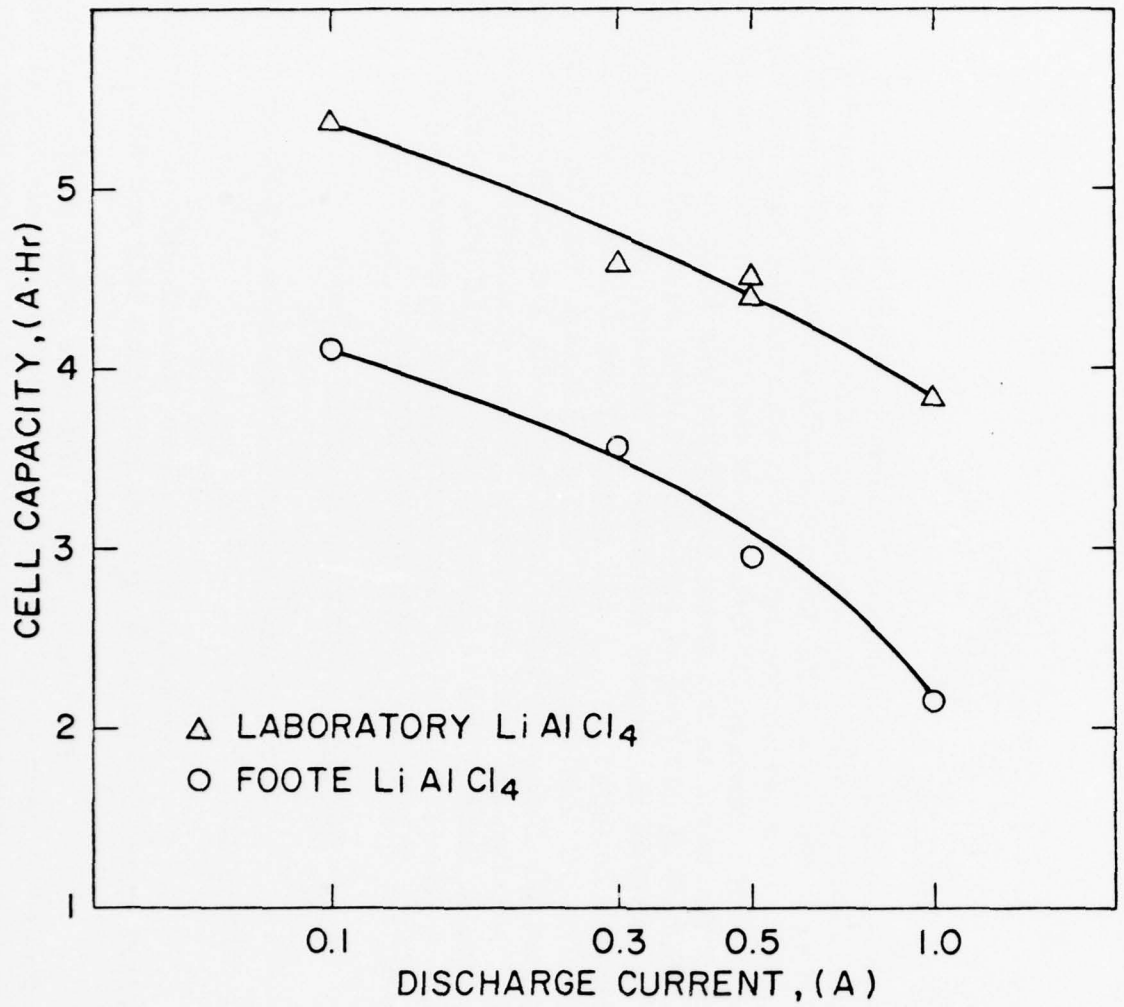

Fig 3. Cell Capacity (Q) vs. Log Current (I) Plots of "C" Cells with 1(M) $LiAlCl_4$ and 10% Teflon for LPS and Foote Electrolyte

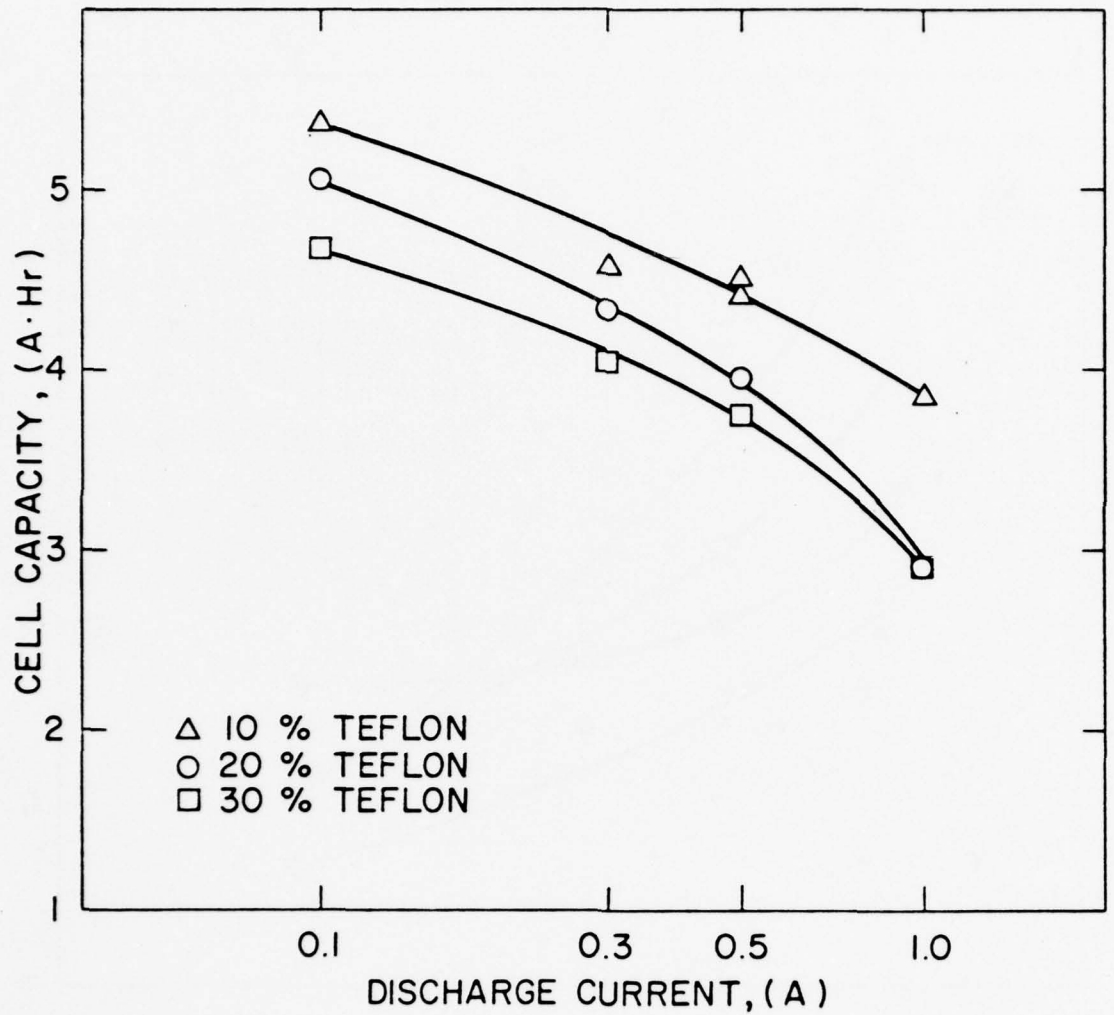

Fig. 4. Cell Capacity (Q) vs. Log Current (I) Plots of "C" Cells with 1(M) $LiAlCl_4$ LPS Electrolyte for 10%, 20% and 30% Teflon in the Cathode

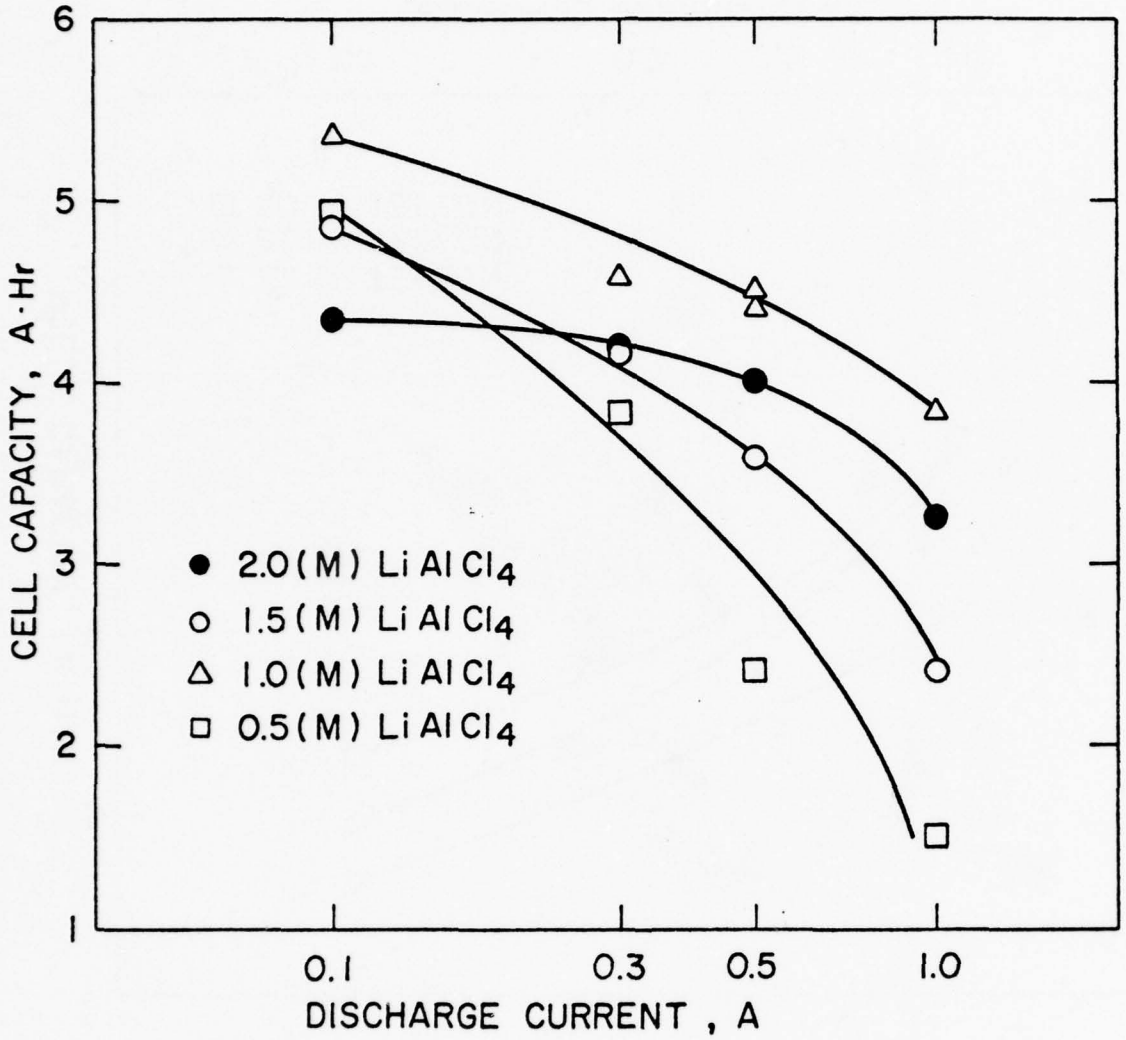

Fig. 5. Cell Capacity Vs Log Current Plots of "C" Cells with 10% Teflon in the Cathode at 0.5, 1.0, 1.5 and 2.0(M) $LiAlCl_4$ LPS Electrolyte

2.3 Pressure Build-Up Studies

The purpose of this study was to determine the internal pressure which was generated during the discharge of the cells in order to design a structurally sound "D" cell which would be able to withstand such pressures without mechanical rupture.

2.3.1 Experimental

The "C" cells made for the optimization studies were modified as shown in Figure 6. The modified "C" cells had an aluminum top (5) which was electrically insulated from both the anode and the cathode and acted as a built-in reference electrode. The rubber septum (3) was tightly held in the aluminum top so that it provided a good seal. The Ni wire (4) passing through the rubber septum acted as a terminal of the battery. The cell bottom was drawn to form a protrusion (10). A male nut (8) was soldered around the protrusion. A "tap a can" valve (12) with a pressure gauge (11) was attached to the cell. All these parts were nickel plated both inside and out. After the discharge of the cells, they were inverted before the needle valve knob (9) was turned to puncture the protrustion of the cell, thereby connecting the pressure gauge with the cell interior. This particular set-up was designed to prevent exposure of the standard commercially available pressure gauges to the corrosive cell electrolyte during the discharge of the cells.

Three cells were made according to the above design and were discharged at 0.5 A to 2.0 volt cutoff at temperatures of 56°, 25°, and -30°C, and internal cell pressures were measured at 25°C.

2.3.2 Results and Discussion

The results are shown in Table 5. The gauge pressure of the cells increased with an increase in the temperature of discharge. The inter al void volume of the "C" cells was approximately 3 cc and the measured internal volume of the pressure gauge, the valves and the connecting tubes, was 5 cc. If the pressure is due to SO_2 generated during the cell discharge according to the cell reaction

$$4Li+2SOCl_2 \longrightarrow 4LiCl+S+SO_2 \qquad (5)$$

the actual cell pressure will be only slightly higher than the gauge pressure and the maximum pressure will be the pressure of liquid SO_2 at 25°C which is approximately 55 PSI. From the point of view of designing "D" cells which can withstand such pressure, we do not anticipate any unusual problems, since the existing organic electrolyte batteries that are being manufactured by P. R. Mallory are capable of withstanding several hundred PSI before any cell venting. We plan to incorporate available Mallory technology in the inorganic electrolyte "D" cell design.

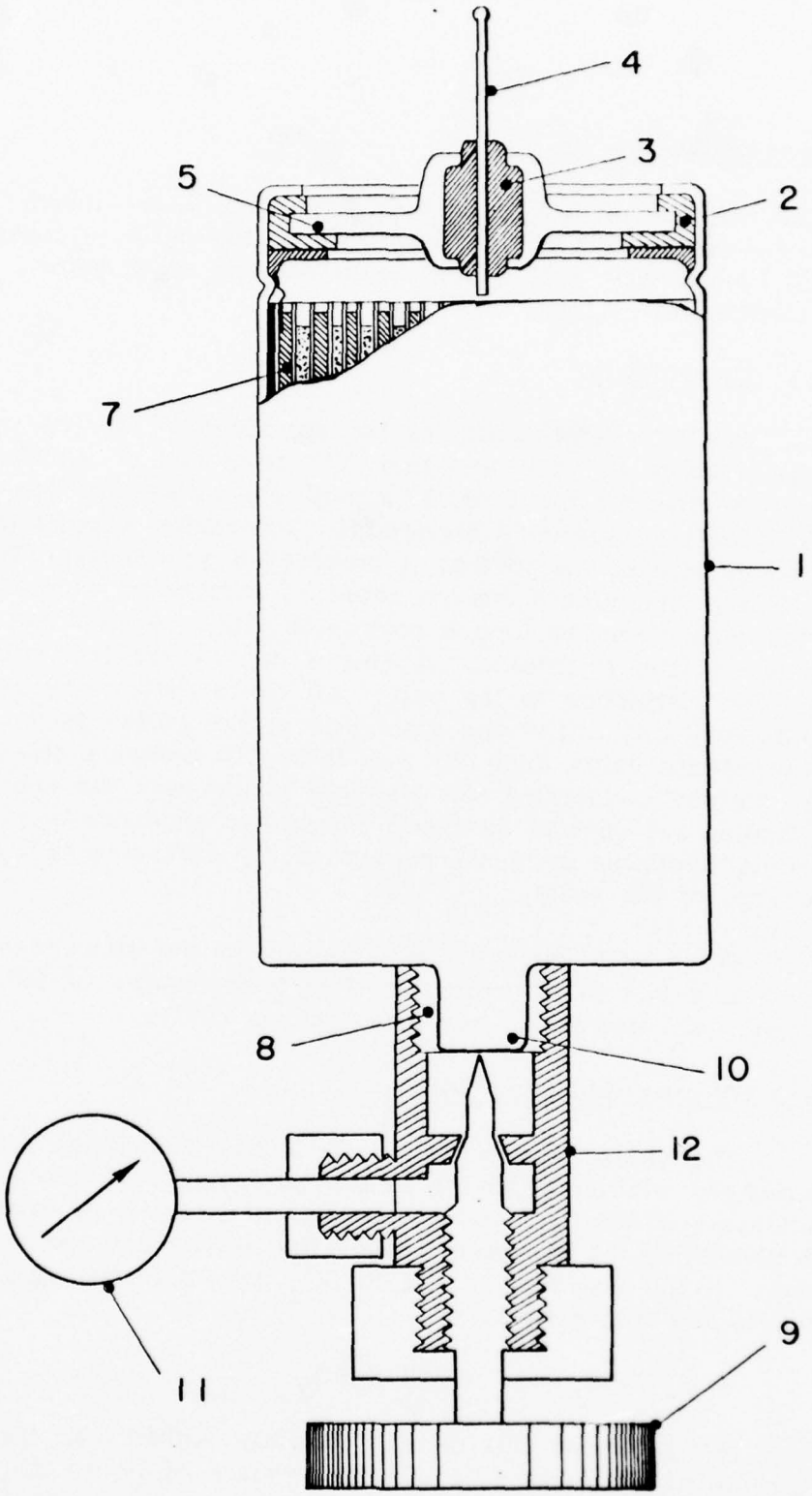

Fig. 6. *Modified "C" Cell for Pressure Build-up Measurements*

TABLE 5

Internal Pressure of the Inorganic Electrolyte 'C' Cell After Discharge*

Cell No	Discharge Temp. °C	Discharge Current (A)	Capacity to 2.0 Volt (A.Hr)	Gage* Pressure (PSI)
15	-30	0.5	2.8	2
16	25	0.5	4.1	10
17	56	0.5	4.4	23

*Pressures measured at 25°C, including gauge volume.

2.4 General Conclusions from Task I.

The activities under Task I were completed on schedule. Based on the results, we made the following choice of materials of cell construction and the cathode and electrolyte compositions for the "D" cells to be designed and constructed under Task II.

Material for "D" cell Can and Top:	Nickel
Material for Cathode Collector:	Nickel
Material for Anode Collector:	Nickel
Material for Separator:	Glass filter paper
Terminal Insulation:	Glass to Metal Hermetic Seal Terminal
Cell Closure Means:	Welding
Electrolyte:	1M$LiAlCl_4$ LPS Electrolyte
Cathode Composition:	90% carbon with 10% Teflon binder by weight

We chose a hermetic structure for the "D" cell, instead of a crimped seal structure because of the non-hermeticity of the crimped type elastomeric seals and the possible danger of slow leakage of physiologically harmful and chemically corrosive $SOCl_2$ vapor. The only plastic material that is stable with the system is Teflon (also Kel-F) which is not elastomeric in nature. Hence, the crimped seal with the teflon gaskets are liable to leak due to the deformation of the Teflon gasket under stress and subsequent flow.

Therefore, the only reasonable choice for the inorganic electrolyte "D" cell design is a hermetic glass-to-metal seal terminal with welded top.

3. Task II - Construction of Sealed Portable Battery Cell Prototypes

The essential purpose of this task is to design, construct and evaluate sealed practical cells under a variety of drains, temperatures of operation and storage conditions in order to define the capabilities as well as the limitations of the $Li/SOCl_2$ inorganic electrolyte system. The "D" size cell was selected by ECOM as a vehicle to accomplish the above. We took the following precautions in the design of the D cells.

(i) Compatible materials were used for the construction of the cell. The compatibility (19) was determined by refluxing the cell construction materials in the inorganic electrolyte (1.5 M $LiAlCl_4$-$SOCl_2$) at 85°C for one month followed by examination of the materials as well as the electrolyte for any sign of degradation. Based on these studies, Ni was chosen as the material for cell can, cell top and the current collectors for the Li anode and the carbon cathode. Glass filter paper was chosen as the separator material.

(ii) The cell was designed to be truly hermetic as determined by the Veeco helium leak detector. We considered the hermeticity of the cells to be essential because of (a) the toxic and the corrosive nature of $SOCl_2$ and (b) the possible ambiguity of the cell evaluations if leakage of $SOCl_2$ from the cell or of air into the cell were to occur. Glass-to-metal seals and welding were used to close the cells.

(iii) The electrodes were designed with as large an area as possible to keep the current density as low as possible under any drain of the cell. According to our earlier studies (4) we found that the voltage delay of the inorganic electrolyte C cells after high temperature storage was more severe at the higher current density than at the lower current density. Therefore, the highest electrode area was expected to result in the least voltage delays under comparable conditions of storage and discharge.

3.1 The Design and Construction of the Hermetic "D" Cell

The cross sectional view of the Hermetic "D" cell design is shown in Figure 7. The cell uses a wound type of electrode configuration as in the "C" cell. The physical dimensions of the electrodes which were chosen based on our experience with the Li/SO_2 "D" cells are as follows:

Carbon Cathode: 20" x 1.75"; 0.019" thick

Li anode: 20" x 1.50"; 0.017" thick

The wound electrode assembly is packaged in the Ni can (OD: 1.297", L: 2.375", wall: 0.019") and the electrode tabs are spot welded to the cell

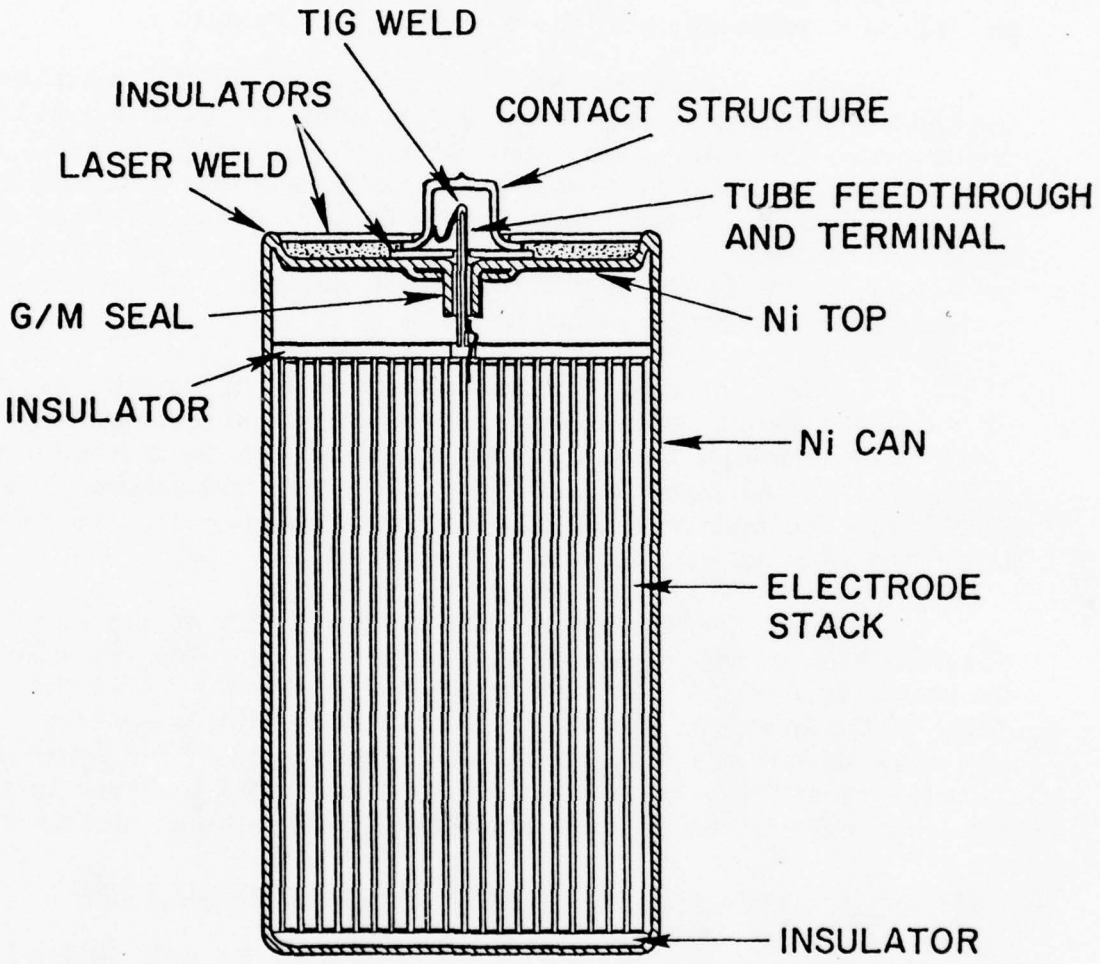

Fig. 7. Cross Sectional View of the Hermetic "D" Cell

can and the tube feedthrough of the G/M Seal, which is pre-welded at the center of the Ni can top. The Ni cell top is welded to the Ni can in the dry box. The cells are evaculated through the tube feedthrough and are filled with electrolyte from an all glass (Pyrex) container. After the electrolyte filling, the tube feedthrough is closed by welding. The cell is hermetically closed at this stage and is ready for the discharge and storage tests. Normally, the contact structure shown in Fig. 7 is not attached to the cells made for our evaluation. Electrical connections are made directly to the cell can and the tube feedthrough.

A photograph of a finished "D" cell and the electrode assembly are shown in Fig. 8. The hermeticity of all the cells were checked using a Veeco helium leak detector prior to the electrolyte filling. The effectiveness of the final cell closure by welding of the tube feedthrough was checked under a microscope and these were found to be excellent. In addition, all the cells were weighed before and after the electrolyte filling as well as before testing, in order to ensure the total hermeticity of the cells. All the cells tested were found to be hermetic and exhibited no electrolyte loss under any of the storage conditions.

In order to maintain a minumum variability of the "D" cell performance, we kept the following parameters constant within the specified limits for all the "D" cells made for fresh and storage tests.

Cathode Composition: 90% Shawinigan Carbon; 10% Teflon

Electrolyte Composition: 1.0(M) $LiAlCl_4$ in distilled $SOCl_2$

The electrolyte solution had the same appearance as distilled $SOCl_2$ which was very light amber to colorless

$LiAlCl_4$: Made from pre-dried LiCl, and iron and water free (Fluka) $AlCl_3$ by melting to a nearly colorless liquid. The possible moisture contamination of the Salt was virtually eliminated by this melting process.

Electrolyte Weight/D Cell: 45 ± 5 gm
Weight of Carbon/D Cell: 5.1 ±0.75 gm
Weight of Finished D Cell: 100 ± 5 gm

3.2 Test Program for the Shelf Life Evaluation of the "D" Cells

We tested "D" cells at constant current of 0.1, 0.25, 0.5, 1.0 and 3.0A at temperatures of 25°C, -30°C and -54°C in order to determine the performance profile of the fresh cells.

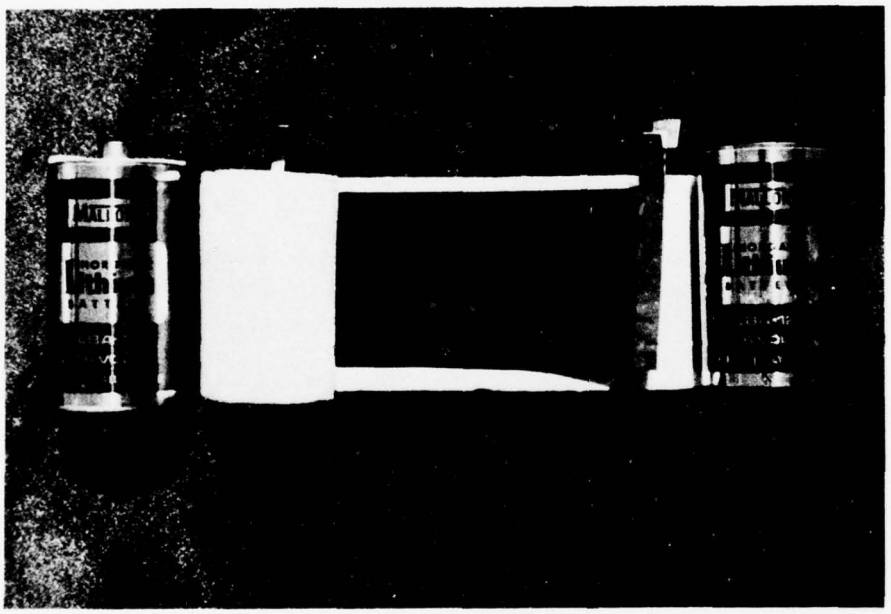

Fig. 8. Photograph of the Hermetic D Cell and the Electrode Assembly

Thereafter, we stored the cells at temperatures ranging from 25°C to 72°C for various periods of time ranging from 1 week to 2 years and tested the cells at 25°C and at -30°C at currents of 0.25, 1.0 and 3.0A. The storage and test schedules are shown below.

Storage Temperature (°C)	Storage Durations	Test Temperature (°C)	Test Current (A)	Total No. of Cells
	1 week	25, -30	0.25, 1.0, 3.0	6
72°C	2 weeks	25, -30	0.25, 1.0, 3.0	6
	1 month	25, -30	0.25, 1.0, 3.0	6
	3 months	25, -30	0.25, 1.0, 3.0	6
	2 weeks	25, -30	0.25, 1.0, 3.0	6
55°C	1 month	25, -30	0.25, 1.0, 3.0	6
	3 months	25, -30	0.25, 1.0, 3.0	6
	6 months	25, -30	0.25, 1.0, 3.0	6
	1 month	25, -30	0.25, 1.0, 3.0	6
45°C	3 months	25, -30	0.25, 1.0, 3.0	6
	6 months	25, -30	0.25, 1.0, 3.0	6
	1 year	25, -30	0.25, 1.0, 3.0	6
	3 months	25, -30	0.25, 1.0, 3.0	6
25°C	6 months	25, -30	0.25, 1.0, 3.0	6
	1 year	25, -30	0.25, 1.0, 3.0	6
	2 years	25, -30	0.25, 1.0, 3.0	6

We monitored the initial cell voltage-time characteristics of each cell on load using a high-speed brush recorder in order to determine the time taken for the cell voltage to recover to 2.0 volt from a lower initial voltage. This time is defined as <u>voltage delay.</u> Fresh cells normally do not show any voltage delay since the initial cell voltage remains above 2.0 volt on load. The voltage delay occurs as a result of storage and according to our experience, (4) this is symptomatic of the soluble depolarizer systems, such as $Li/SOCl_2$. We anticipate this voltage delay to be one of the limitations of this system and therefore, we planned to ascertain the degree of severity of the problem for the hermetic $Li/SOCl_2$ "D" cells as reliably as possible.

3.3 Results

3.3.1 Fresh Tests

Five cells were tested fresh at 25°C, -30°C and -54°C at currents of 0.1, 0.25, 0.5, 1.0 and 3.0A.

The 25°C discharge curves of the D cells are shown in Fig. 9. The cells did not show any voltage delay and the cell capacities decreased with increasing drain as expected. The cell capacity versus current plots are shown in Fig. 10. It is noted that the cell capacity remained relatively unchanged up to 0.25A and it began to decrease significantly above 1.0A. The limiting capacity of the cell or the maximum capacity of the cell as obtained by extrapolation to very low currents, was approximately 12AHr. The capacity realized at 1.0A drain was still 10.5AHr, thus indicating a significantly high rate capability of the cell. The apparent current densities based on the geometric surface area of both sides of the carbon cathode corresponding to the various drains are as follows:

Drain (Amps)	Cathode Current Density (mA/cm^2)
0.1	0.22
0.25	0.55
0.50	1.10
1.0	2.20
3.0	6.60

These are moderate current densities for a soluble depolarizer system even at a drain as high as 1A for the D cell.

Five cells were tested fresh at -30°C after a two-hour stand at -30°C., at currents of 0.1, 0.25, 0.5, 1.0 and 3.0A. The discharge curves are shown in Fig. 11. All the cells showed a sharp drop of voltage on load and a relatively fast recovery followed by a slow recovery of the cell voltage. The voltage delay was more severe at higher current. It is evident, that even the fresh cells tend to exhibit the voltage delay phenomenon at -30°C particularly at high drains; whereas, they do not at 25°C. Furthermore, the voltage regulation as well as the cell capacities were considerably inferior at -30°C, particularly at drains of 0.25A or higher, as shown in Fig. 11. The end points were very poorly defined and the discharge curves showed more than one plateau.

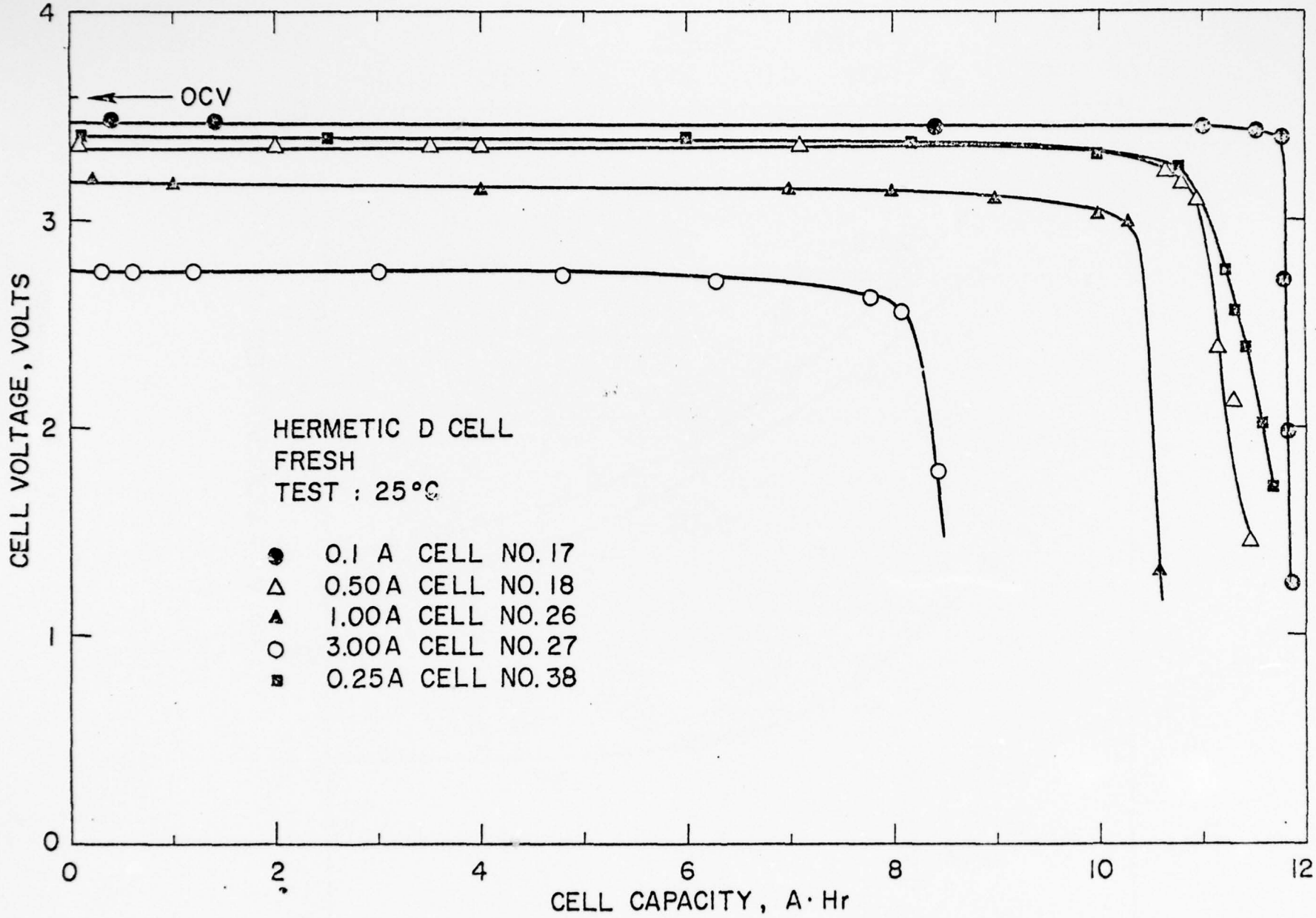

Fig. 9. Discharge Curves of the Fresh Li/$SOCl_2$ D Cells at 25°C on Constant Currents of 0.1, 0.25, 0.5, 1.0 and 3.0A

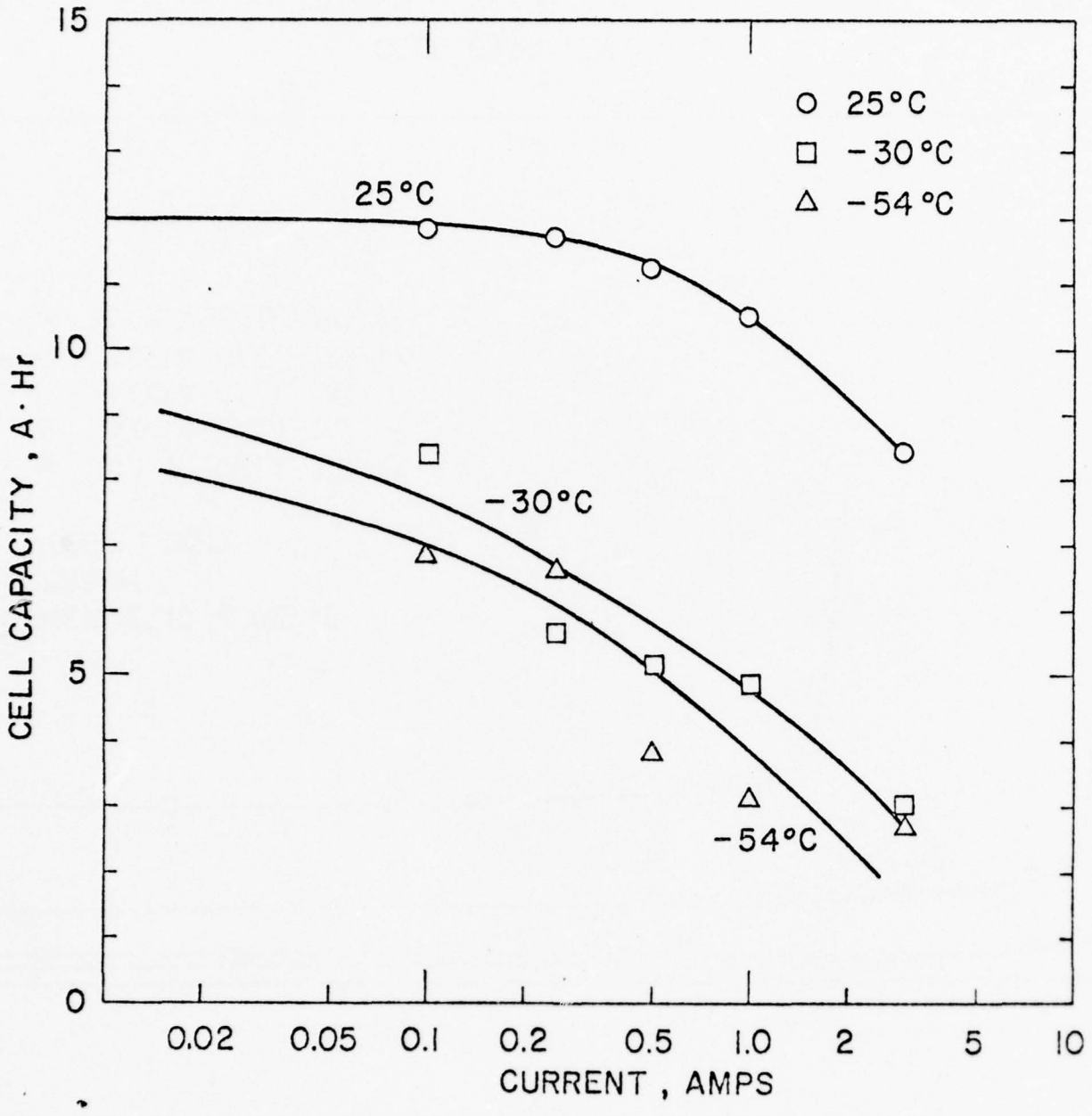

Fig. 10. Cell Capacity vs Log current Plots of Li/$SOCl_2$ D Cells at 25°, -30° and -54°C Tests

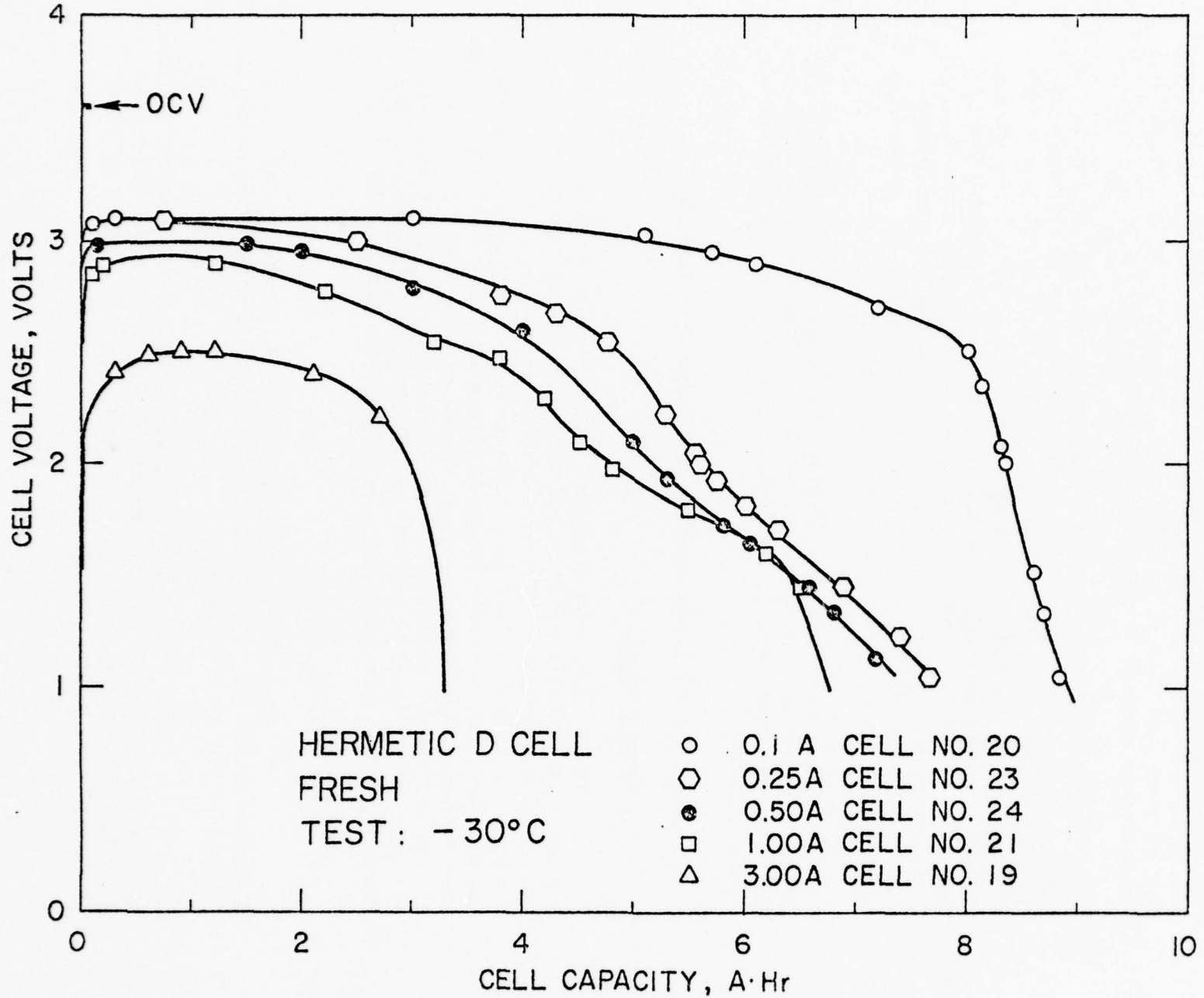

Fig. 11. Discharge Curves of Fresh Li/$SOCl_2$ D Cells at -30°C on Constant Currents of 0.1, 0.25, 0.50, 1.0 and 3.0A

A batch of D cells was tested at -54°C at currents of 0.1, 0.25, 0.5, 1.0 and 3.0A and the discharge curves are shown in Fig. 12. The cell performance at -54°C appeared to be similar to that at -30°C. This may be seen from Fig. 10, where the cell capacities are plotted against the discharge currents for the various temperatures.

The fresh cells showed a voltage delay at -54°C just as they did at -30°C. The voltage delays were quite severe at high currents. For example, at 0.5A, the cell voltage dropped to 1.0 volt and it took 115 seconds for the cell voltage to recover to 2.0 volt. At 3A the cell voltage became negative and remained negative for 50 seconds and it took more than 1000 seconds for the cell voltage to rise above 2.0 volt. Thus, the voltage delay phenomenon exists even for the freshly made cells if the cells are discharged at low temperatures (-30° or lower) and at drain rates of 0.5A (1.1 mA/cm^2) or higher.

The energy densities (WHr/lb and WHr/in^3) of the D cells are plotted as a function of the power density (W/lb) and are shown in Fig. 13. The superiority of the system in terms of energy density is clearly shown.

All the fresh test results are tabulated in Table 6.

3.3.2 Storage Tests

The D cells were routinely tested at constant currents of 0.25, 1.0 and 3.0A at 25°C and at -30°C after each storage interval at the respective temperatures. The tests included monitoring of the initial voltage-time profile on load on a high-speed Brush recorder to determine the time taken for the cell voltage to recover to 2.0 volt from the initial lower voltage. Thereafter, the cell voltage was monitored as a function of time in order to determine the cell capacity to 2.0 volt. The test circuitry was designed to cut off the current to the cell as the cell voltage reached 1.0 volt thus preventing any overdischarge of the cell.

3.3.2.1 72°C Storage

The test results after the various storage periods up to 3 months at 25° and -30°C tests after 4 weeks of storage are shown in Figures 14 and 15 respectively.

The voltage delay has been arbitrarily defined as the time (seconds) taken for the cell voltage to reach 2.0 volt after the initial instantaneous voltage drop. It is shown in the sixth column of Table 7. The initial drop in cell voltage on load is shown in the fifth column.

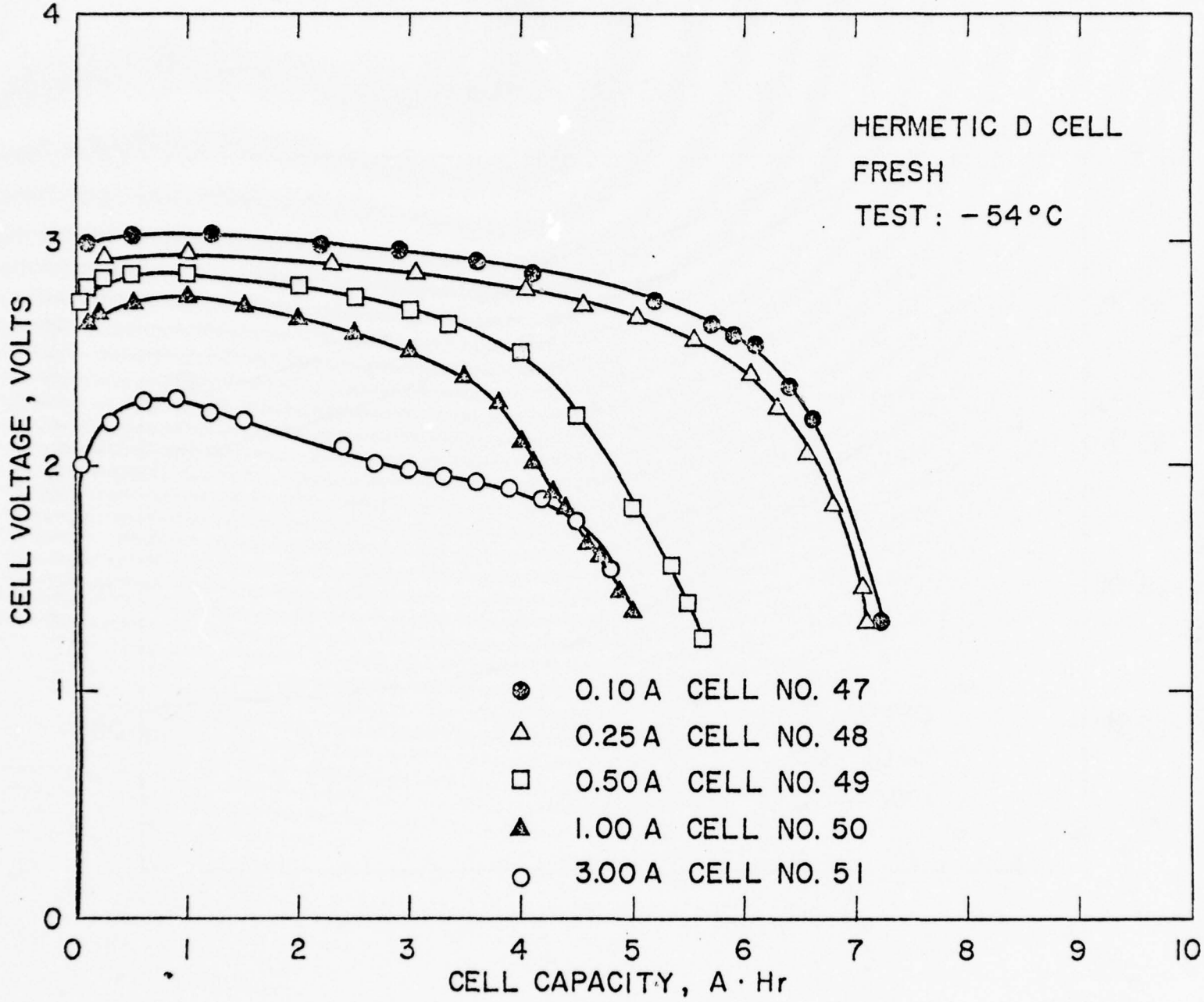

Fig. 12. Discharge Curves of Fresh Li/$SOCl_2$ D Cells at -54°C on Constant Currents of 0.1, 0.25, 0.5, 1.0 and 3.0A

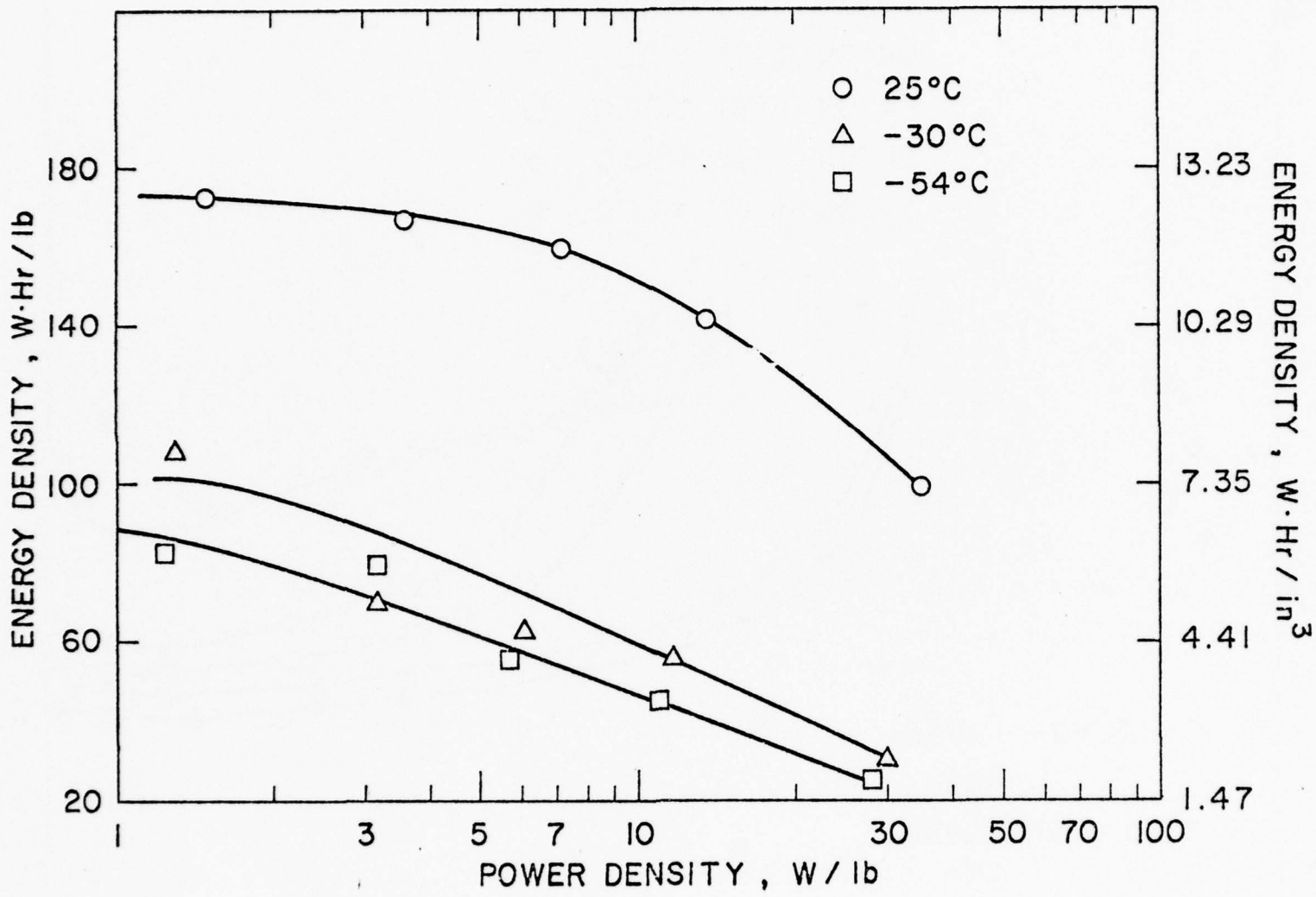

Fig. 13. Plots of Gravimetric and Volumetric Energy Densities of the Li/$SOCl_2$ D Cells as a Function of Power Density at 25°, -30° and -54°C Tests

TABLE 6

Discharge Data of $Li/SOCl_2$ Inorganic Electrolyte "D" Cells (Fresh) at Various Temperatures

Cell No.	Test Temperature (°C)	Test Current (Amps)	Average Cell Operating Voltage	Cell Capacity to 2.0 Volt (A.Hr)	Total Energy (W.Hr)	Energy Density	
						WHr/lb	WHr/in^3
17	25	0.10	3.45	11.83	40.8	176	12.9
38	25	0.25	3.30	11.72	38.7	167	12.3
18	25	0.50	3.30	11.25	37.1	160	11.8
26	25	1.00	3.10	10.50	32.6	141	10.3
27	25	3.00	2.7	8.40	22.7	98	7.2
20	-30	0.10	3.0	8.35	25.0	108	7.9
23	-30	0.25	2.9	5.60	16.2	70	5.1
24	-30	0.50	2.8	5.20	14.6	63	4.6
21	-30	1.00	2.7	4.85	13.0	56	4.1
19	-30	3.00	2.3	3.00	7.0	30	2.2
47	-54	0.10	2.8	6.80	19.0	82	6.0
48	-54	0.25	2.75	6.65	18.3	79	5.8
49	-54	0.50	2.65	4.80	12.7	55	4.0
50	-54	1.00	2.56	4.10	10.5	45	3.3
51	-54	3.00	2.15	2.70	5.8	25	1.8

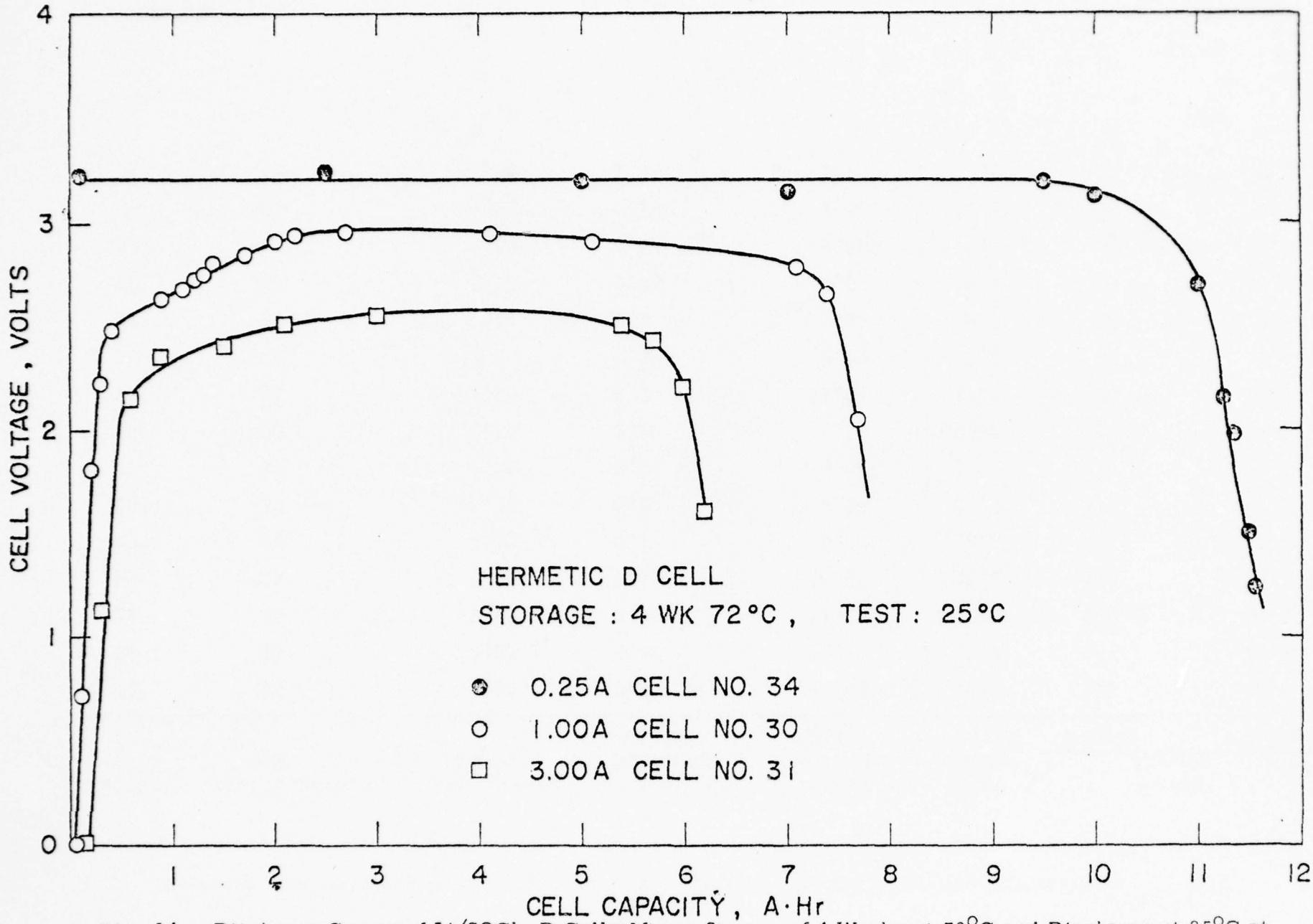

Fig. 14. Discharge Curves of $Li/SOCl_2$ D Cells After a Storage of 4 Weeks at 72°C and Discharge at 25°C at Currents of 0.25, 1.0 and 3.0A

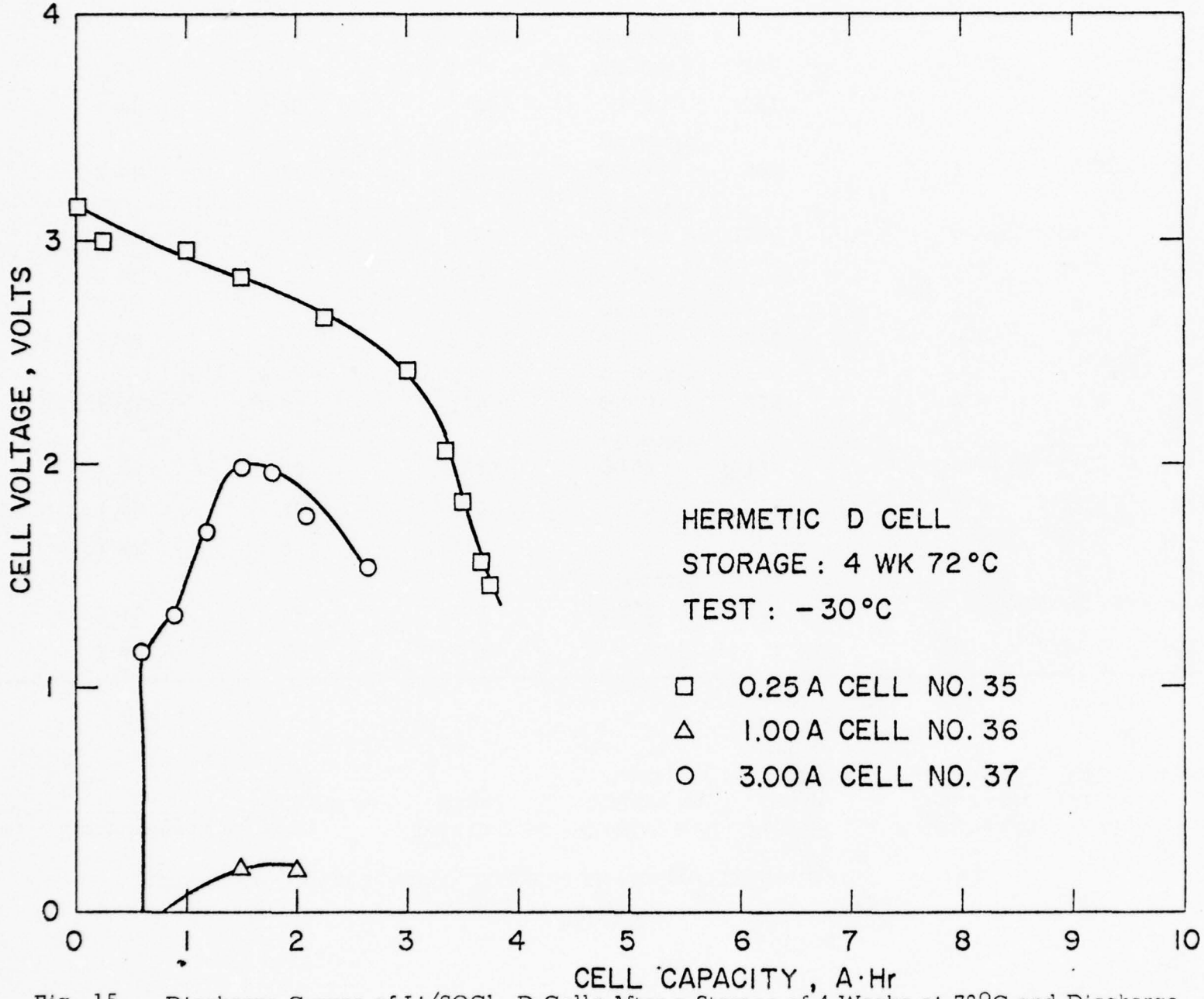

Fig. 15. Discharge Curves of Li/$SOCl_2$ D Cells After a Storage of 4 Weeks at 72°C and Discharge at -30°C at Currents of 0.25, 1.0 and 3.0A

TABLE 7

Discharge Data of $Li/SOCl_2$ Inorganic Electrolyte "D" Cells After Storage at 72°C

Cell No.	Storage Duration	Test Temperature (°C)	Test Current (Amps)	Starting Cell Voltage on Load	Voltage Delay Time Taken to reach 2.0 Volts (sec)	Cell Capacity to 2.0 volt (A.Hr)	Total Energy (WHr)	Energy Density WHr/lb	Energy Density WHr/in^3
4	1 wk	25	0.25	1.9	1	10.7	35.3	152	11.2
5	1 wk	25	1.0	<1.2 off scale	625	Recorder paper jammed			
7	1 wk	25	1.0	---	---	9.4	28.6	124	9.1
6	1 wk	25	3.0	1.9	912	6.3	13.8	60	4.4
8	1 wk	-30	0.25	<1.2 off scale	135	4.5	11.7	51	3.7
10	1 wk	-30	1.0	<1.2 off scale	215	3.4	8.3	36	2.6
9	1 wk	-30	3.0	<1.2 off scale	320	0.95	2.2	10	0.7
28	2 wk	25	0.25	0.7	2	11.3	36.2	156	11.5
13	2 wk	25	1.0	<1.2 off scale	1000	8.45	24.5	106	7.8
14	2 wk	25	3.0	<1.2 off scale	396	7.3	18.2	79	5.8
29	2 wk	-30	0.25	2.6	<1	3.2	8.5	37	2.7
15	2 wk	-30	1.0	<1.2 off scale	292	3.25	8.1	35	2.6

TABLE 7 (continued)

Discharge Data of $Li/SOCl_2$ Inorganic Electrolyte "D" Cells After Storage at 72°C

Cell No.	Storage Duration	Test Temperature (°C)	Test Current (Amps)	Starting Cell Voltage on Load	Voltage Delay Time Taken to reach 2.0 Volts (sec)	Cell Capacity to 2.0 Volt (A.Hr)	Total Energy (WHr)	Energy Density WHr/lb	Energy Density WHr/in
16	2 wk	-30	3.0	-7.04	970 sec to 1.0V, never reached 2.0 Volt				
34	4 wk	25	0.25	2.6	<1	11.3	35.0	151	11.1
30	4 wk	25	1.0	<-1.2 off scale	800	7.6	21.3	92	6.8
31	4 wk	25	3.0	-8.0	634	6.0	13.8	60	4.4
35	4 wk	-30	0.25	2.4	<1	3.37	9.3	40	3.0
36	4 wk	-30	1.0	-9.0	3450 to 0 volt never reached 1.0 volt				
37	4 wk	-30	3.0	<-13.0 volt off scale	1635 barely reached 2.0 volt				
64	3 mo	25	0.25	-5.0	5000	9.5	31.4	136	10.0
63	3 mo	25	1.00	-8.0	1440	7.1	19.9	86	6.3
62	3 mo	25	3.00	-11.0	1670	4.8	10.6	46	3.4
68	3 mo	-30	0.25	-10.0	1800	1.5	4.1	18	1.3
69	3 mo	-30	1.0	-15.0	4200 to -1.0 volt never reached 0 volt				
70	3 mo	-30	3.0	-15.0	875 to 1.0 volt never reached 2.0 volt				

It is noted that the voltage delay varies from less than a second to thousands of seconds depending upon the length of the storage, the test temperature and the test current. It appears that for storage durations of 4 weeks or less, the voltage delay is quite moderate at the 0.25A test current both at 25° and -30°C. However, this is no longer true after 3 months of storage at 72°C; the voltage delay is severe at all currents. The general worsening of the delay with increasing current and decreasing test temperature is evident.

A plot of the realized cell capacity at the various currents at 25° and -30°C, after various periods of storage at 72°C is shown in Fig. 16. The capacity retention at the low rate (0.25A) of discharge at 25°C is good even after 3 months of storage at 72°C. However, the capacity losses are quite significant at high rates (1A and 3A) of discharge. This indicates a lessening of the rate capability of the system with the duration of storage rather than an intrinsic loss of the cell capacity. The capacity retention appears to be particularly poor at -30°C, the cells lose capacity progressively with an increasing storage period at all currents. This may be attributed to a loss of the rate capability of the system which is further reduced by the lowering of the test temperature (-30°C).

3.3.2.2 55° Storage

The cell discharge data after the various periods of storage up to six months at 55°C are tabulated in Table 8. The cell capacity versus storage duration plots are shown in Fig. 17.

The voltage delays became increasingly severe with an increasing storage duration, but significantly less than that after 72°C storage. It is interesting to note that although the voltage delay was quite severe, there was no significant capacity loss at 25°C on a 0.25A discharge after storage for six months at 55°C. The intrinsic capacity of the cell remains unchanged on storage; only the rate capability of the cells is reduced.

3.3.2.3 45°C Storage

The test results after the various periods of storage up to one year at 45°C are shown in Table 9. The capacity versus storage duration plots are shown in Fig. 18. In general, the cells maintained their intrinsic capacity well even after 1 year of storage at 45°C. The voltage delay, though severe at high rates, was absent at 0.25A at -30°C even after 1 year at 45°C.

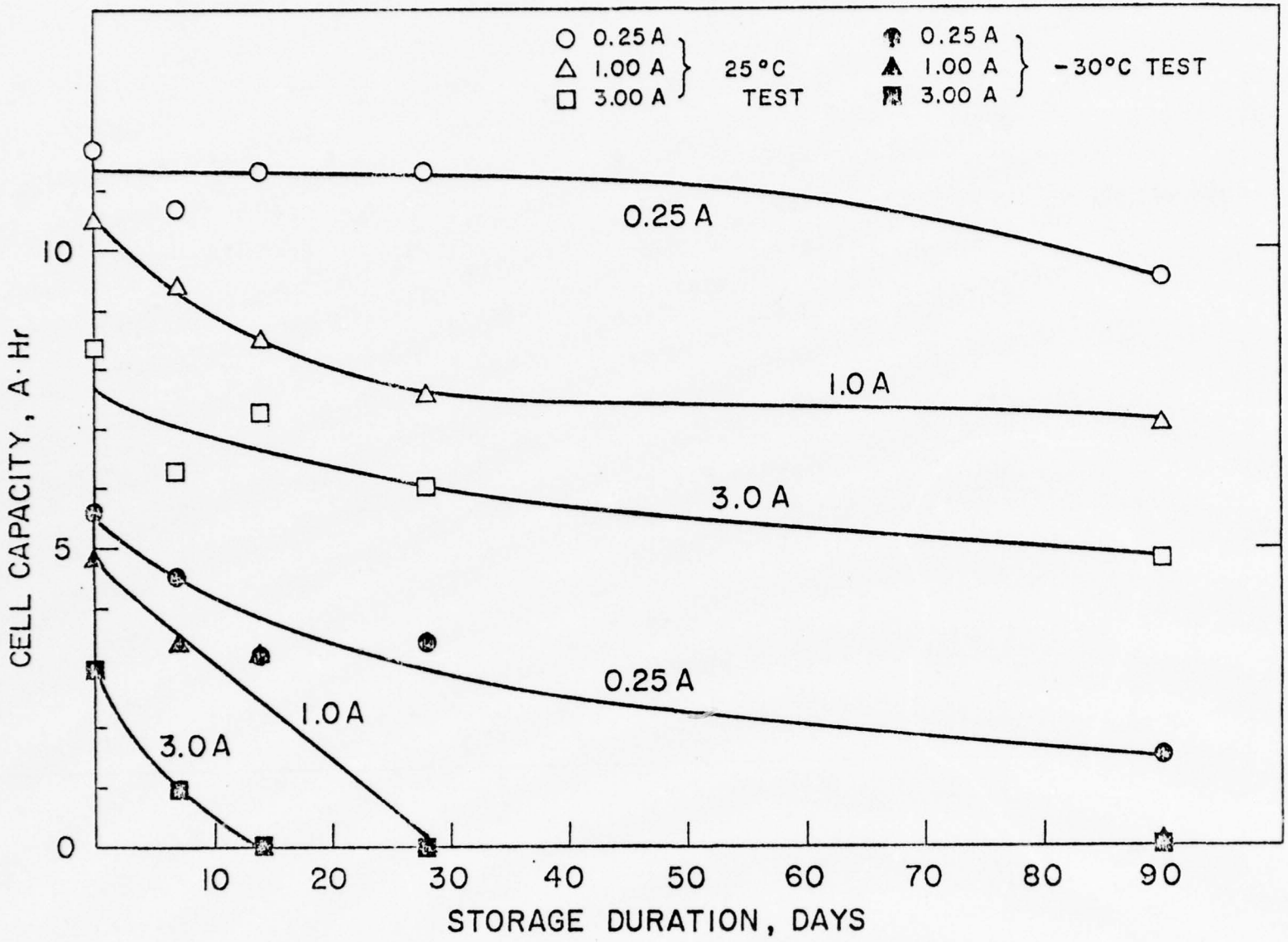

Fig. 16. Plots of Li/$SOCl_2$ D Cell Capacities to 2.0 Volt as a Function of Storage Duration at 72°C, Test at 25° and -30°C at Currents of 0.25, 1.0 and 3.0A.

TABLE 8

Discharge Data of $Li/SOCl_2$ Inorganic Electrolyte "D" Cells After Storage at 55° C

Cell No.	Storage Duration	Test Temperature (°C)	Test Current (Amps)	Starting Cell Voltage on Load	Voltage Delay Time Taken to reach 2.0 Volts (sec)	Cell Capacity to 2.0 Volt (A.Hr)	Total Energy (Whr)	Energy Density WHr/lb	WHr/in
32	2 wk	25	0.25	3.2	0	10.5	35.2	152	11.2
11	2 wk	25	1.0	<-1.2 off scale	137	9.5	28.5	123	9.0
33	2 wk	25	3.0	0.70	271	8.5	22.1	95	7.0
39	2 wk	-30	0.25	3.3	0	4.3	11.4	49	3.6
12	2 wk	-30	1.0	<-1.2 off scale	122	3.6	8.8	38	2.8
40	2 wk	-30	3.0	-4.5	249	2.0	4.2	18	1.3
41	4 wk	25	0.25	3.4	0	10.0	34.0	147	10.8
42	4 wk	25	1.0	-5.7	17	9.8	30.9	133	9.8
43	4 wk	25	3.0	-7.2	77	7.8	20.3	88	6.4
44	4 wk	-30	0.25	<-1.2 off scale	102	4.9	13.2	57	4.2
45	4 wk	-30	1.0	-7.0	110	4.1	10.3	44	3.3
46	4 wk	-30	3.0	-7.5	345	Barely reached 2.0 volt			
72	3 mo	25	0.25	<-1.2	15	11.6	38.3	165	12.1
73	3 mo	25	1.0	<-1.2	25	8.8	26.4	114	8.4
74	3 mo	25	3.0	<-1.2	300	6.2	15.8	68	5.0

TABLE 8 (continued)

Discharge Date of $Li/SOCl_2$ inorganic Electrolyte "D" Cells After Storage at 55°C

Cell No.	Storage Duration	Test Temperature (°C)	Test Current (Amps)	Starting Cell Voltage on Load	Voltage Delay Time Taken to reach 2.0 Volts (sec)	Cell Capacity to 2.0 Volt (A.Hr)	Total Energy (WHr)	Energy Density WHr/lb	Energy Density WHr/in^3
75	3 mo	-30	0.25	-5	< 1	5.6	15.1	65	4.8
76	3 mo	-30	1.0	-5	135	4.6	11.5	50	3.6
77	3 mo	-30	3.0	-5	185	1.7	3.7	16	1.2
90	6 mo	25	0.25	< -1.2	1460	11.0	34.7	150	11
91	6 mo	25	1.00	< -1.2	720	5.7	14.8	64	4.7
102	6 mo	25	3.00	< -1.2	660	6.4	14.4	62	4.6
100	6 mo	-30	1.00	2.5	540	6.5	18.2	79	5.8
99	6 mo	-30	3.00	< -1.2	1000	2.0	4.8	21	1.5

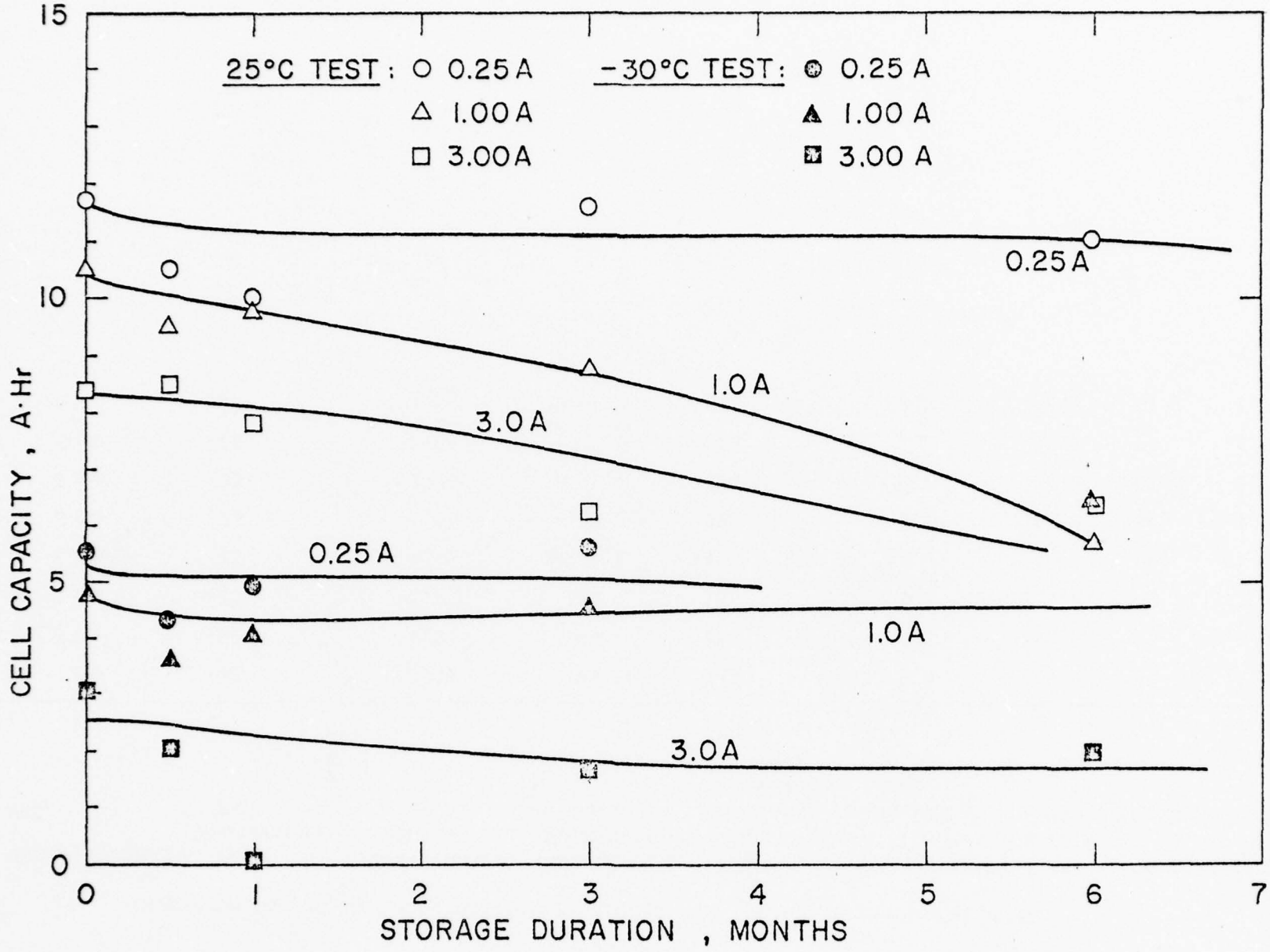

Fig. 17. Plots of $Li/SOCl_2$ D Cell Capacities to 2.0 Volt as a Function of Storage Duration at 55°C, Test at 25° and -30°C at Currents of 0.25, 1.0 and 3.0A

TABLE 9

Discharge Data of $Li/SOCl_2$ Inorganic Electrolyte 'D' Cells After Storage at 45°C

Cell No.	Storage Duration	Discharge Temperature (°C)	Discharge Current (amps)	Starting Cell Voltage on Load	Voltage Delay Time Taken to Reach 2.0 Volts (sec)	Cell Capacity to 2.0 Volt (A.Hr)	Total Energy (WHr)	Energy Density	
								WHr/lb	WHr/in^3
80	1 mo	25	0.25	<-1.2	< 1.0	12.2	40.3	174	12.8
79	1 mo	25	1.0	2.8	0	10.1	30.3	131	9.6
78	1 mo	25	3.0	-5.0	< 1.0 to zero volt, never reached 2.0 volt				
83	1 mo	-30	0.25	<-1.2	90	6.1	16.5	71	5.2
82	1 mo	-30	1.0	<-1.2	115	4.5	11.3	49	3.6
81	1 mo	-30	3.0	<-1.2	150	2.3	5.2	22	1.7
87	3 mo	25	0.25	0.7	26	11.5	37.4	161	11.9
88	3 mo	25	1.00	2.3	0	10.1	30.8	133	9.8
89	3 mo	25	3.00	<-1.2	110	7.7	20.0	66	6.3
92	3 mo	-30	0.25	<-1.2	110	3.9	10.0	43	3.2
93	3 mo	-30	1.00	<-1.2	360	2.7	6.3	27	2.0
94	3 mo	-30	3.00	<-1.2	520	1.3	2.5	11	0.8
96	3 mo	-30	0.25	0.6	350	3.1	8.2	35	2.6
97	3 mo	-30	1.00	<-1.2	370	3.2	7.8	34	2.5
98	3 mo	-30	3.00	<-1.2	520	1.9	4.5	19	1.4
91	6 mo	25	0.25	2.0	0	10.8	34.0	147	10.8
94C	6 mo	25	1.0	1.7	72	8.3	24.1	104	7.6
98C	6 mo	25	3.0	<-1.2	480	5.0	11.5	50	3.6
287	6 mo	-30	0.25	<-1.2	The cell was inoperable (bad cell)				
281	6 mo	-30	1.0	<-1.2	72	6.2	15.5	67	4.9
284	6 mo	-30	3.0	<-1.2	720	Negligible Capacity above 2.0 volt 3.6 AHr to 1.5 volt.			

TABLE 9 (continued)

Cell No.	Storage Duration	Discharge Temperature (°C)	Discharge Current (amps)	Starting Cell Voltage on Load	Voltage Delay Time Taken to Reach 2.0 Volts (sec)	Cell Capacity to 2.0 Volts (A.Hr)	Total Energy (WHr)	Energy Density	
								WHr/lb	WHr/in^3
110	1 yr	25	0.25	2.3	0	10.3	33.0	142	10.5
103	1 yr	25	1.0	<-1.2	510	5.8	16.2	70	5.1
105	1 yr	25	3.0	<-1.2	187	6.2	17.0	73	5.4
112	1 yr	-30	0.25	2.8	0	4.2 (7.0)	11.5	50	3.6
113	1 yr	-30	1.0	<-1.2	300	2.1 (4.5)	5.7	24	1.8
132	1 yr	-30	3.0	<-1.2	Never recovered above 2 volts; 1.4AHr to 1.5 volts				

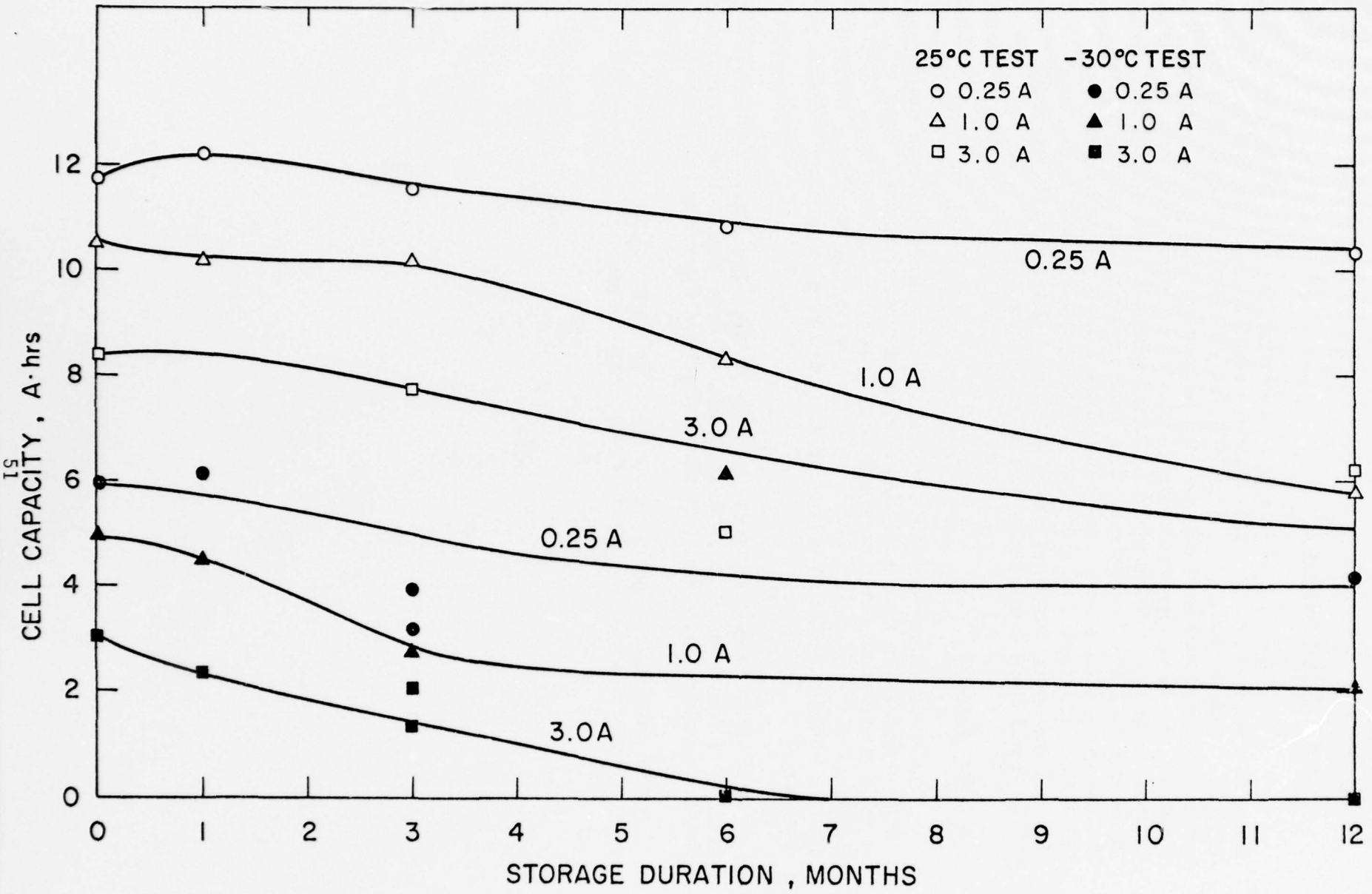

Fig. 18. Capacity Retention of $Li/SOCl_2$ D Cells on Storage at 45°C

3.3.2.4 25° Storage

The test results are summarized in Table 10 for the storage up to two years at 25°C. The capacity retention plots are shown in Fig. 19. Unfortunately, the data at 0.25A on 25°C discharge after 2 years of storage were lost because of a malfunction of the test equipment. However, the capacity-storage time plots for 1.0A test indicate that the intrinsic capacity of the cells most likely remained virtually intact. There was certainly no capacity loss after 1 year. The voltage delays did become severe after 2 years of storage, but there was no delay at 25°C for 0.25A test. After 2 year's storage, and at -30°C test, the cell voltage never recovered above 2.0 volt. This is most liekly due to the insufficient conductivity of the anode film.

3.4 Conclusions

The unoptimized hermetic Li/$SOCl_2$ D cells are capable of delivering energy densities in excess of 100 WHr/lb at power densities of 30 W/lb, at room temperature, with excellent voltage regulations. At lower temperatures (-30° and -54°C) both the energy density (at any power density) and the voltage regulation deteriorates, giving rise to multiple voltage plateaus.

The cells experience severe voltage delays after storage, the severity of which increases with increased storage temperature, increased storage duration, decreased test temperature and increased test current.

The cells exhibit no significant loss of stoichiometric capacity on storage, only the rate capability of the cells are reduced.

TABLE 10

Discharge Data of $Li/SOCl_2$ Inorganic Electrolyte 'D' Cells After Storage at 25°C

Storage Duration	Test Temperature (°C)	Test Current (Amps)	Starting Cell Voltage On Load	Voltage Delay Time Taken to Reach 2.0 Volts (sec)	Cell Capacity to 2.0 Volt (A.Hr)	Total Energy (WHr)	Energy Density WHr/lb	Energy Density WHr/in^3
3 mo	25	0.25	1.5	0.5	11.1	36.6	158	11.6
3 mo	25	1.00	1.2	0.5	9.8	29.9	129	9.5
3 mo	25	3.00	0.1	160	7.6	19.8	86	6.3
3 mo	-30	0.25	2.5	0	3.5	9.1	39	2.9
3 mo	-30	1.00	<-1.2	74	4.0	10.0	43	3.2
3 mo	-30	3.00	<-1.2	160	2.5	5.6	24	1.8
6 mo	25	0.25	2.0	0	10.9	36.0	155	11.4
6 mo	25	1.00	2.6	0	10.9	33.8	146	10.7
6 mo	25	3.00	-0.2	120	7.5	19.5	84	6.2
6 mo	-30	0.25	-0.3	170	3.7	9.8	42	3.1
6 mo	-30	1.00	<-1.2	210	5.1	12.2	53	3.9
6 mo	-30	3.00	<-1.2	240	2.1	4.7	20	1.5
1 yr	25	0.25	1.7	<0.1	13.2	43.6	189	13.8
1 yr	25	1.00	-0.9	123	12.8	38.4	166	12.2
1 yr	25	3.00	<-1.2	117	8.4	22.7	98	7.2
1 yr	-30	0.25	<-1.2	411	2.0	5.6	24	1.8
1 yr	-30	1.00	<-1.2	369	3.5	9.3	40	3.0
1 yr	-30	3.00	<-1.2	210	2.8	7.0	30.0	2.2
2 yr	25	0.25	3.15	0	Data lost; test equip. malfunction			
2 yr	25	1.00	1.60	480	8.0	24.0	104	7.6

TABLE 10 (continued)

Discharge Data of $Li/SOCl_2$ Inorganic Electrolyte 'D' Cells After Storage at 25°C

Storage Duration	Test Temperature (°C)	Test Current (Amps)	Starting Cell Voltage on Load	Voltage Delay Time Taken to Reach 2.0 Volts (Sec)	Cell Capacity to 2.0 Volt (A.Hr)	Total Energy (WHr)	Energy Density WHr/lb	Energy Density WHr/in^3
2 yr	25	3.00	<-1.2	180	5.5	15.4	67	4.9
2 yr	-30	0.25	<-1.2	∞	0	--	--	--
2 yr	-30	1.00	<-1.2	∞	0	--	--	--
2 yr	-30	3.00	<-1.2	∞	0	--	--	--

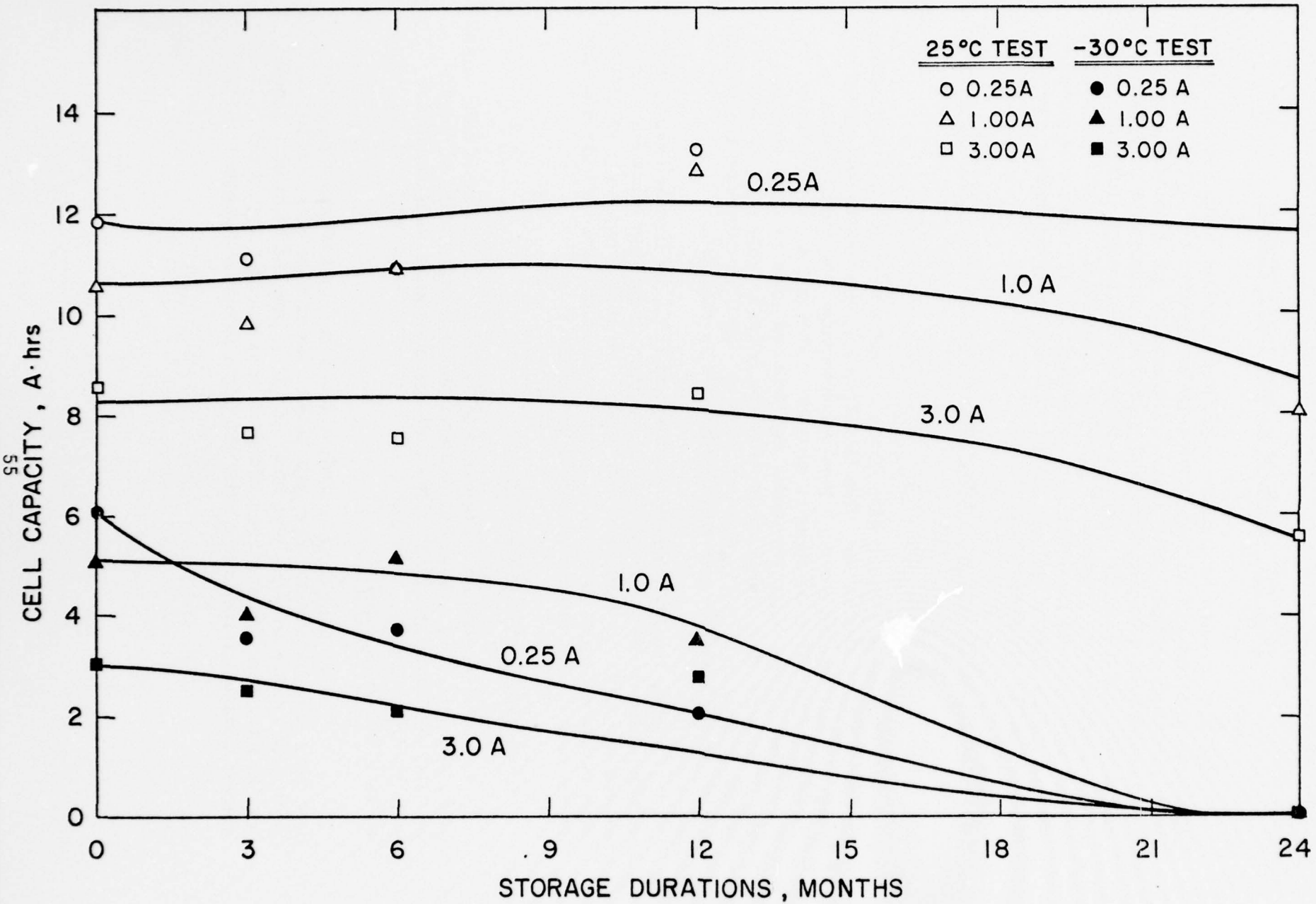

Fig. 19. Capacity Retention of Li/$SOCl_2$ D Cells on Storage at 25°C.

Task III. Study of Voltage Delay Problem

We first pursued an intuitive empirical approach consisting of partial discharge and constant current pulsing for alleviating the voltage delay after 72°C storage and -30°C tests. The results are discussed here. We then pursued a phenomenological approach consisting of studying the morphology and the growth characteristics of the Li anode film, the cause of the voltage delay problem, in an effort to establish a cause and effect relationship between the electrolyte variables, the Li anode film growth characteristics and the voltage delay. The experimental details and the results are presented here.

4.1 The Empirical Approach: Effect of Partial Discharge, 72°C Storage

4.1.1 Experimental

We made a group of Li/$SOCl_2$ D cells with 20" x 1.75" carbon cathodes and Li anodes and 1(M) $LiAlCl_4$-$SOCl_2$ electrolyte and stored them at 72°C for one month. Then we determined the voltage delay of these cells at -30°C at currents of 0.25, 1.0 and 3.0A and partially discharged (0.3-0.5A.Hr) the cells and returned them to 72°C storage. The cells were then tested again after the second, third and the sixth month of storage at 0.25, 1.0 and 3.0A at -30°C to determine the voltage delay, *if any, without any significant drain in capacity*.

After the sixth month of storage at 72°C, we first determined the voltage delay of the cells at -30°C and then completely discharged all except two cells at 0.25, 1.0 and 3.0A. We tested two cells at 25°C at a constant current of 0.25A in order to determine the intrinsic capacity of the cells. The results are described below.

4.1.2 Results and Discussion

The results are summarized in Table 11. Of the three cells tested at 0.25A, none showed any voltage delay even after six months of storage at 72°C and tests at -30°C. The cells also retained their capacities well as determined by discharging one cell at -30°C (5AHr) and two cells at 25°C (11.2, 8.2AHr).

Of the three cells tested at 1.0A, one cell was accidentally lost after the first month, one cell showed no voltage delay below 3 months of storage at 72°C and test at -30°C and the third cell showed significant voltage delays even after the first month. Both cells became completely inoperable after the sixth month of storage.

TABLE 11

Cell No.	Test Current	Capacity Disch. After 1st Test (A.Hr)	Voltage Delay at -30° Test After Storage at 72°C for Periods of (Months) 1	2	3	6	Capacity Recovered After 6 Mo. at 72°C (A.Hr.)	(Test Temp
179	0.25	0.5	0	0	0	0	5	(-30°C)
183	0.25	0.5	0	0	0	0	11	(25°C)
187	0.25	0.5	0	0	0	0	8.2	(25°C)
200	1.0	0.5	0	-	-	-	-	
209	1.0	0.5	50	40	200(3.0A)	∝	0	(-30°C)
211	1.0	0.5	0	0	0	∝	0	(-30°C)
218	3.0	0.3	20	52	130	∝	0	(-30°C)
219	3.0	0.3	120	55	150	∝	0	(-30°C)
222	3.0	0.3	200	92	370	∝	0	(-30°C)

All the three cells tested at 3.0A, showed voltage delays from the first to the third month of storage and became virtually inoperable at -30°C after the sixth month of storage.

4.1.3 Conclusion

We conclude that partial discharge coupled with intermittent anodic pulsing decreases the severity of the voltage delay. It is interesting to note that such conditioning did not lead to any drastic loss of the intrinsic capacity. However, the low temperature voltage delay is still quite substantial at high rates. It is not clear which of the two factors, partial discharge and intermittent anodic pulsing, is responsible for the improved voltage delay characteristics.

4.2 The Phenomenological Approach: SEM Studies on the Li Anode Film in the Inorganic Electrolytes

We showed earlier (4) that the voltage delay of the Li/$SOCl_2$ inorganic electrolyte cells was due to the Li anode which was covered by a protective film. We found this film to consist primarily of LiCl crystals. The thickness of the film increased with an increasing storage duration and an increasing storage temperature giving rise to more and more severe voltage delays. We believe that the instantaneous drop of the cell voltage on load is caused by the protective film. Initially, anodic dissolution of Li is highly localized and occurs at pinholes and other imperfections of the protective film. Probably, the film is dislodged mechanically or fractured when sufficient Li has dissolved underneath the film. This gives rise to the voltage recovery. SEM examinations of the Li anode surface before and after the anodic pulse showed this clearly (4). Based on this model of the voltage delay process, it appears that both the morphology and the thickness of the protective film may have an important effect on the voltage delay characteristics of the system.

We demonstrated earlier (4) the usefulness of the SEM technique for studying the Li anode film, and we have continued to use this technique. Our primary objective is to examine the effect of the electrolyte variables on the Li anode film that is visible at moderate SEM magnifications (100-1000).

We found earlier (10) that the film growth on Li in $SOCl_2$ alone is substantially less than in 1.8(M) $LiAlCl_4$-$SOCl_2$, as may be seen from Fig. 20 and 21 which shows Li surfaces exposed to 1.8(M) $LiAlCl_4$-$SOCl_2$ at 55°C for 590 hrs and to distilled $SOCl_2$ at 78°C for 624 hours, respectively. $LiAlCl_4$ appears to participate actively in promoting the film growth. The concentration of $LiAlCl_4$ would be expected to affect the

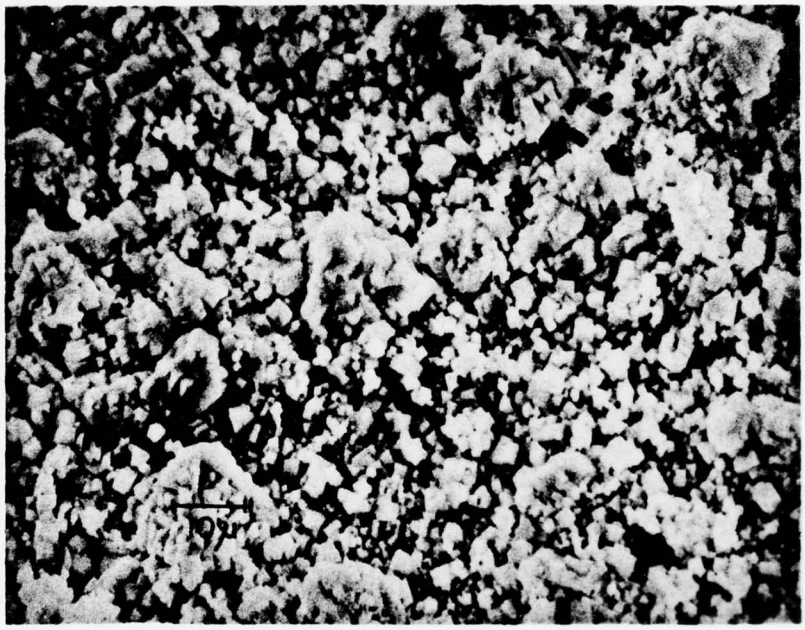

Fig. 20. SEM photograph of Li surface exposed to 1.8 (M) $LiAlCl_4$-$SOCl_2$ for 590 hours at 55°C, magnification 1000.

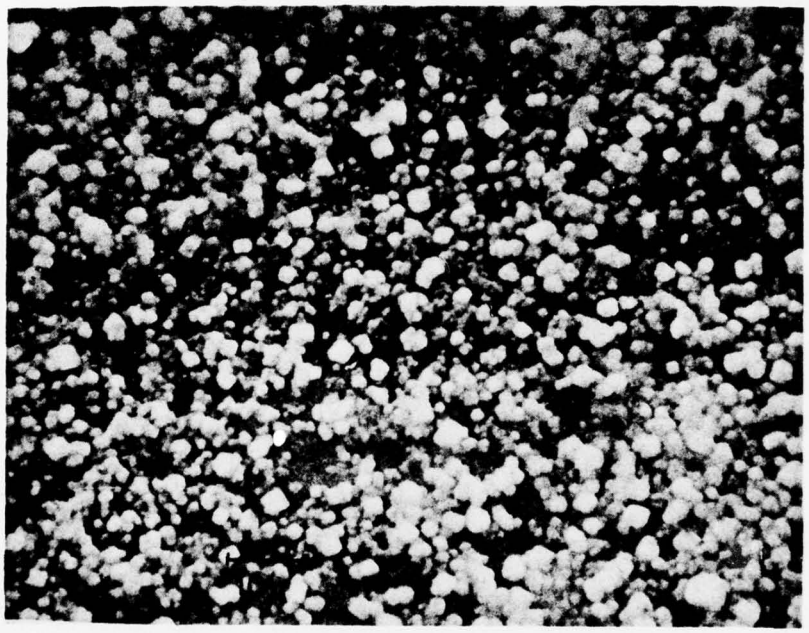

Fig. 21. SEM photograph of Li surface exposed to distilled $SOCl_2$ for 624 hours at 78°C, magnification 1000.

rate of film growth in the sense that a lower salt concentration will lessen the voltage delay. We planned to study the growth of the Li film in 0.5(M) and 0.25(M) $LiAlCl_4$-$SOCl_2$ solutions at 72°, 55° and 25°C.

The other variables we were interested in examining included the common electrolyte impurities such as H_2O and $AlCl_3$. The latter is used in preparing $LiAlCl_4$ and is highly soluble in $SOCl_2$. A finite amount of the above impurities are thought to be present in even the purest electrolytes. The electrolytes prepared in our laboratory normally contain less than 10 ppm H_2O according to our analysis. It is of interest to determine the effect of higher (0.01 and 0.1%) water content on the Li film. The amount of free $AlCl_3$ in $LiAlCl_4$ is not known. We planned to add 1% and 10% by weight of $AlCl_3$ to the regular 1(M) $LiAlCl_4$-$SOCl_2$ electrolyte to determine their affect on the Li film formation.

The substances formed during discharge or from the spontaneous decomposition of $SOCl_2$ were other electrolyte variables that we were interested in examining. SO_2 and S_2Cl_2 are two examples. We chose to use approximately 10% by weight of these chemicals in the regular 1(M) $LiAlCl_4$-$SOCl_2$ electrolyte. SO_2 is known to react with Li to form a protective film. The chemical composition of the film is most likely $Li_2S_2O_4$. In $SOCl_2$, the Li anode film is composed of LiCl. It is of interest to determine whether there is a mixed film when Li is kept in a mixture of SO_2 and $SOCl_2$. The presence of other film forming materials such as $Li_2S_2O_4$ may also affect the morphology of the LiCl film. It is of interest first of all to determine whether there is any effect on the film as seen by SEM, and next, to determine whether or not this leads to a shorter voltage delay in the actual cells.

At the very early stages of our investigation (11) we found electrolyte impurities such as iron to be harmful to the storability of the system. This might be due to the shuttling effect of iron which may deposit on Li and set up a local cell action and subsequently redissolve in the electrolyte. We found that it was not possible to protect iron cathodically by Li metal in the $LiAlCl_4$-$SOCl_2$ electrolytes. For this reason, we chose an all nickel can for the D cell (12). Our earlier observations (11) were confirmed by workers at GTE (13) who used nickel plated steel cans as cell containers. The voltage delay observed by them was considerably more severe than that observed by us. These types of impurities were not included in the present study.

The experimental details and the results are described below.

4.2.1 Experimental

The Li anode films were formed by immersing Li specimens in inorganic electrolytes having various compositions, and the surface of the specimens was examined in the Scanning Electron Microscope (SEM). The Li specimens were made by pressing Li discs (OD: 0.5") on a stainless steel stud on which a layer of expanded Ni was prewelded as shown in Fig. 22. The Li specimens were stored in the various inorganic electrolytes in a glass jar with a screw-cap cover with a teflon washer. These containers were stored at 25°C, 55° and 72°C. The Li specimens were removed from the glass jars at various intervals and were examined in the SEM after they had been washed quickly in distilled propylene carbonate to remove $LiAlCl_4$. The effectiveness of the seal and the transfer operations were checked by measuring (14) the moisture content of the electrolyte stored in a similar jar at 72°C for 8 weeks. There was no increase in the moisture content due to the storage and the transfer. The effectiveness of the washing step in terms of complete removal of $LiAlCl_4$ was checked by examining the Li surface with EDAX-707 (x-ray energy dispersive analyzer) which was attached to SEM. The absence of Al in the film ensured the effective removal of $LiAlCl_4$. Control experiments were carried out to ensure that the treatment with distilled propylene carbonate did not alter the Li anode surface.

The surface features of the Li film were examined at various magnifications ranging from 100 to 10,000X and were photographed for detailed analysis. Attempts were made to section the Li anodes to determine the thickness of the film. The measurements were extremely difficult, and the results were not always satisfactory.

The various electrolytes selected for the study include:

1. 0.5(M) $LiAlCl_4$-$SOCl_2$
2. 0.25(M) $LiAlCl_4$-$SOCl_2$
3. 1.0(M) $LiAlCl_4$-$SOCl_2$ + 1gm $AlCl_3$/100ml of electrolyte
4. 1.0(M) $LiAlCl_4$-$SOCl_2$ + 10gm $AlCl_3$/100ml of electrolyte
5. 1.0(M) $LiAlCl_4$-$SOCl_2$ + 0.01gm H_2O/100ml of electrolyte
6. 1.0(M) $LiAlCl_4$-$SOCl_2$ + 0.1gm H_2O/100ml of electrolyte
7. 1.0(M) $LiAlCl_4$-$SOCl_2$ + 10gm S_2Cl_2/100ml of electrolyte
8. 1.0(M) $LiAlCl_4$-$SOCl_2$ + 17.3gm SO_2/100ml of electrolyte

All the above electrolytes were stored with lithium specimens at 72°, 55° and 25°C. At least 10 samples were stored at each temperature, making a total of more than 240 samples.

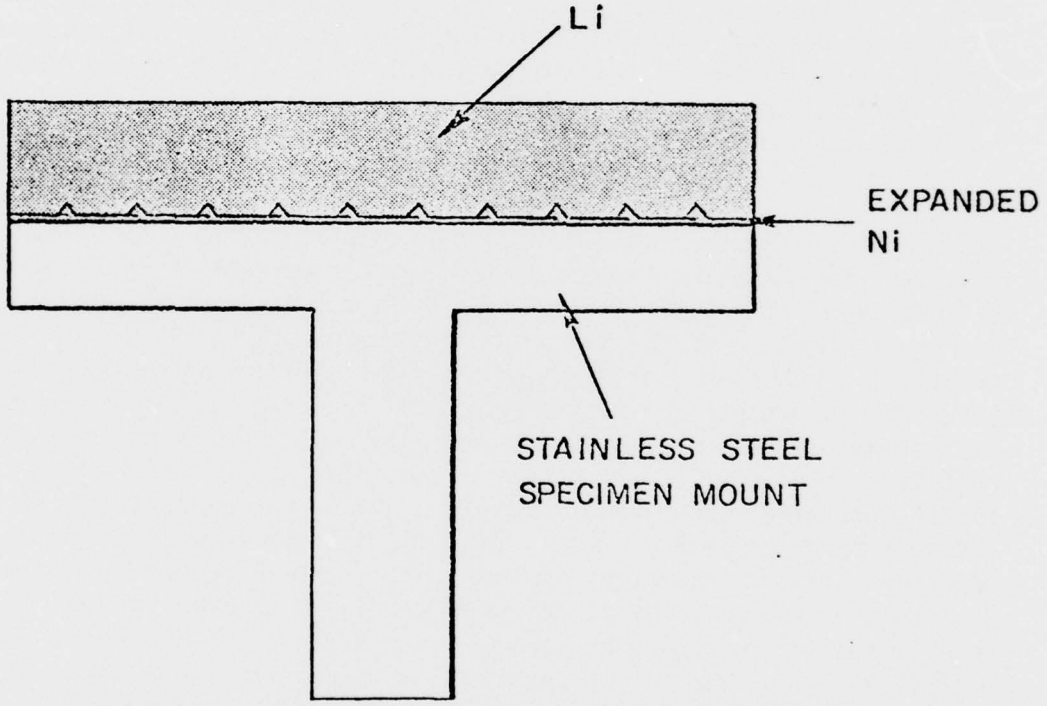

Fig. 22. Cross Sectional View of the Li Specimen Mounted on Stainless Steel Specimen Mount

4.2.2 Results and Discussion

4.2.2.1 Effect of Electrolyte Variables on the Li Film Morphology

The SEM photographs of the Li film formed in the 1(M) $LiAlCl_4$-$SOCl_2$ electrolytes containing 1% $AlCl_3$, 0.01% H_2O, 10% S_2Cl_2 and 17.3% SO_2 are shown in Figures 23, 24, 25 and 26 respectively. The film morphologies are shown at two magnifications viz 200X and 1000X. The film morphologies were also studied in 0.5M and 0.25M $LiAlCl_4$-$SOCl_2$ electrolytes, and were found to be very similar to those observed in the 1.8M $LiAlCl_4$-$SOCl_2$ electrolytes (Fig. 20). Some typical morphologies in the 0.5M electrolytes are shown in Fig. 27. The film morphologies were studied as a function of storage temperatures and the storage durations as well. It is clear from Figures 23, 24 and 25 that the addition of $AlCl_3$, H_2O and S_2Cl_2 did not cause any significant change in the morphology. However, the addition of SO_2 caused a marked change in the film morphology. The growth of the LiCl crystals was found to be quite orderly, as shown in Fig. 26. The behavior persisted as a function of storage temperatures and durations.

Thus, two general types of film morphologies were observed. One consists of a cluster type of growth over a bed of small crystals; the clusters became taller and thicker with storage and finally a third layer of smaller crystals grow on top of all this. This is shown schematically in Fig. 28 (a) which represents the type of growth experienced in all the inorganic electrolytes studied, particularly at lower temperatures except the electrolyte with 17.3% SO_2. In the case of the SO_2 containing electrolyte large well defined cubic crystals grow in a regular manner over a bed of small crystals; the large crystals become larger and larger on storage and cover the whole surface shown schematically in Fig. 28 (b). Although the latter type of growth was reported (15) to cause less voltage delay, the experimental data available are insufficient to confirm that. However, it is important to note that it is possible to change the morphology of the Li film by the electrolyte variables and as such, the approach of improving the voltage delay characteristics of the cells by changing the electrolyte variables may be successful.

4.2.2.2 Effect of Electrolyte Variables on the Li Film Growth Rate

The Li film growth rates were measured by measuring the Li film thickness as a function of storage duration and storage temperatures. The Li film growth rate curves in 0.5M and 0.25M $LiAlCl_4$-$SOCl_2$ electrolytes at 25°, 55° and 75°C are shown in Figures 29 and 30 respectively. The film thickness increases with the storage duration,

(a)

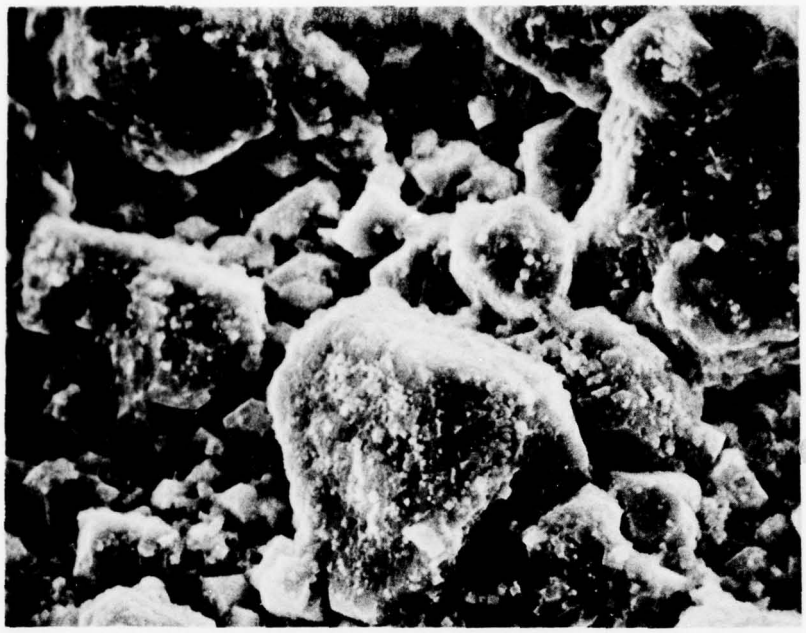

(b)

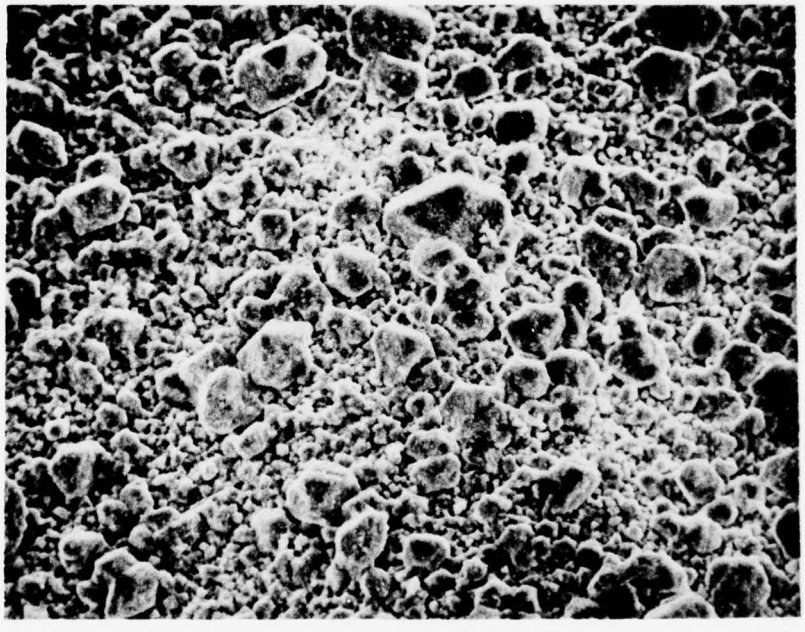

Fig. 23. SEM Photographs of Li Surface Exposed to 1.0 (M) $LiAlCl_4$-$SOCl_2$ + 1% $AlCl_3$ for 26 Days at 72°C. (a) 1000X (b) 200X; Film Thickness: 100 microns.

(a)

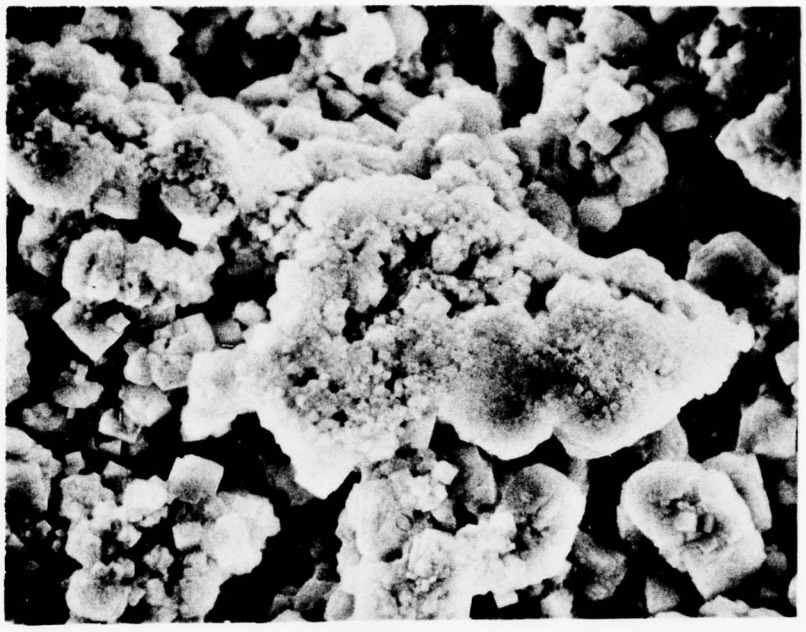

(b)

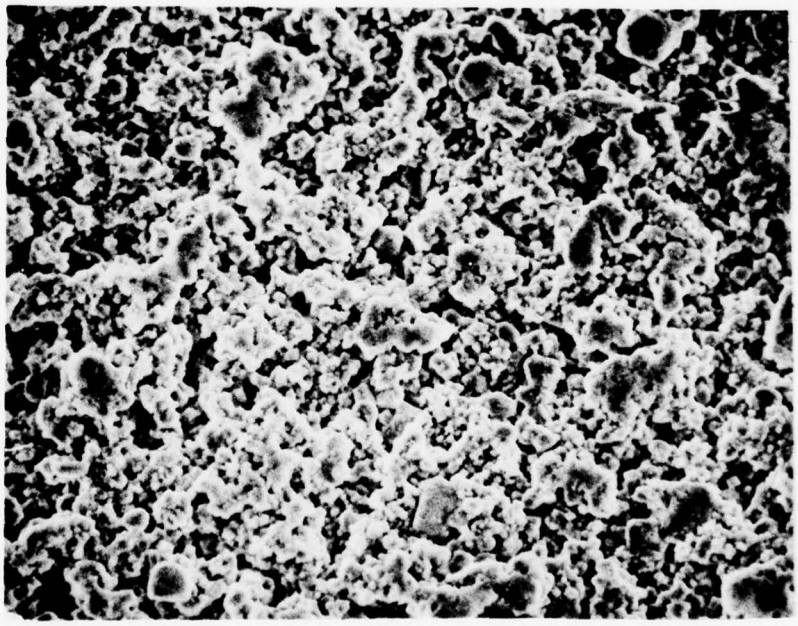

Fig. 24. SEM Photograph of Li Surface Exposed to 1.0 (M) $LiAlCl_4$-$SOCl_2$ + 0.01% H_2O for 71 Days at 55°C. (a) 1000X (b) 200X; Film Thickness: 100 microns.

(a)

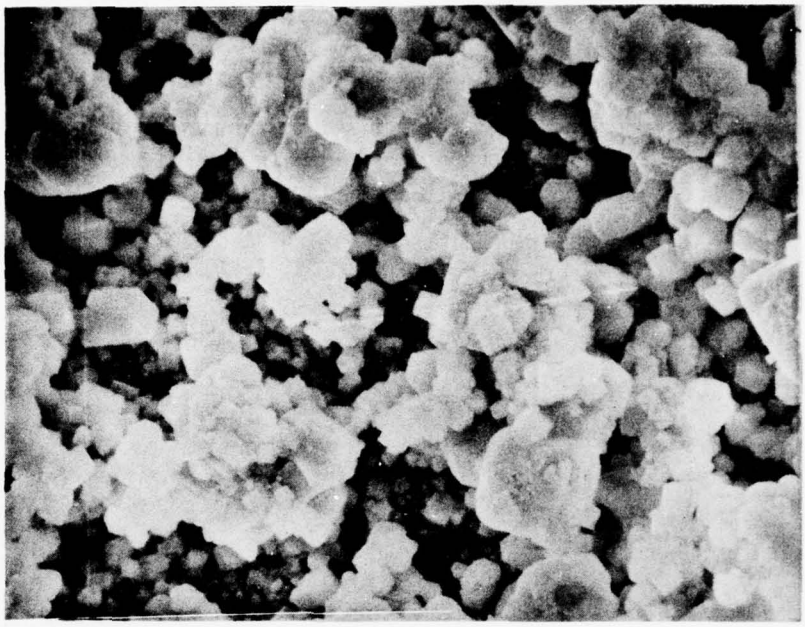

(b)

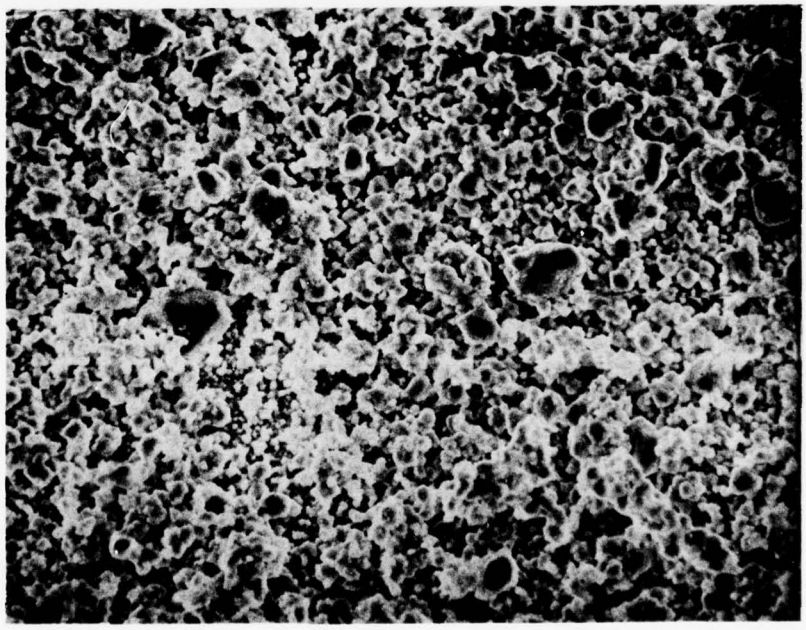

Fig. 25. SEM Photograph of Li Surface Exposed to 1.0 (M) $LiAlCl_4$-$SOCl_2$ + 10% S_2Cl_2 for 16 Days at 72°C. (a) 1000X (b) 200X; Film Thickness: 50 microns.

(a)

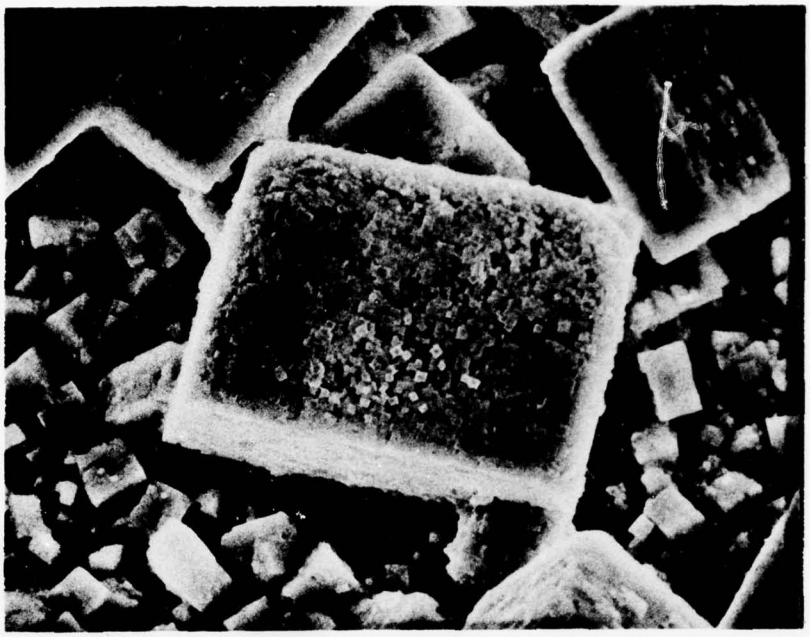

(b)

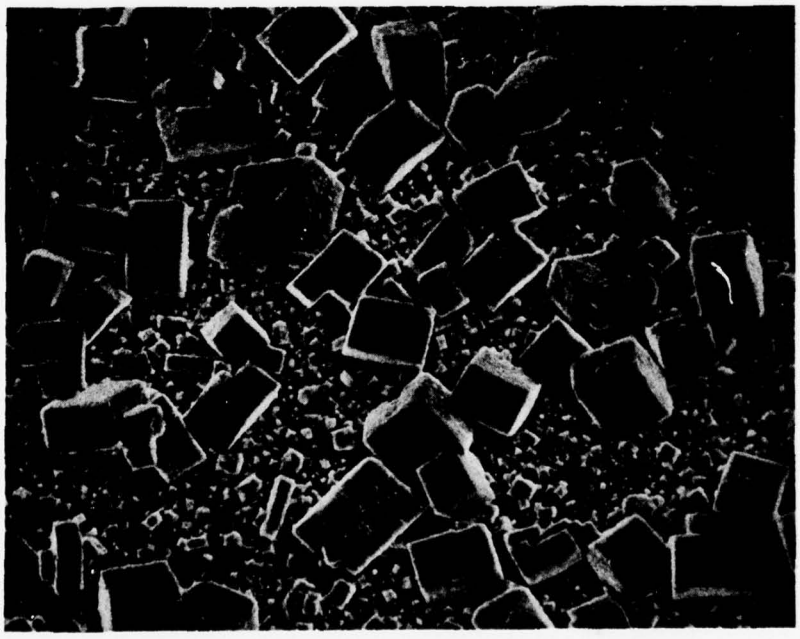

Fig. 26. SEM Photograph of Li Surface Exposed to 1.0 (M) $LiAlCl_4$-$SOCl_2$ + 17.3% SO_2 for 8 Days at 72°C. (a) 1000X (b) 200X; Film Thickness: 50 microns.

(a)

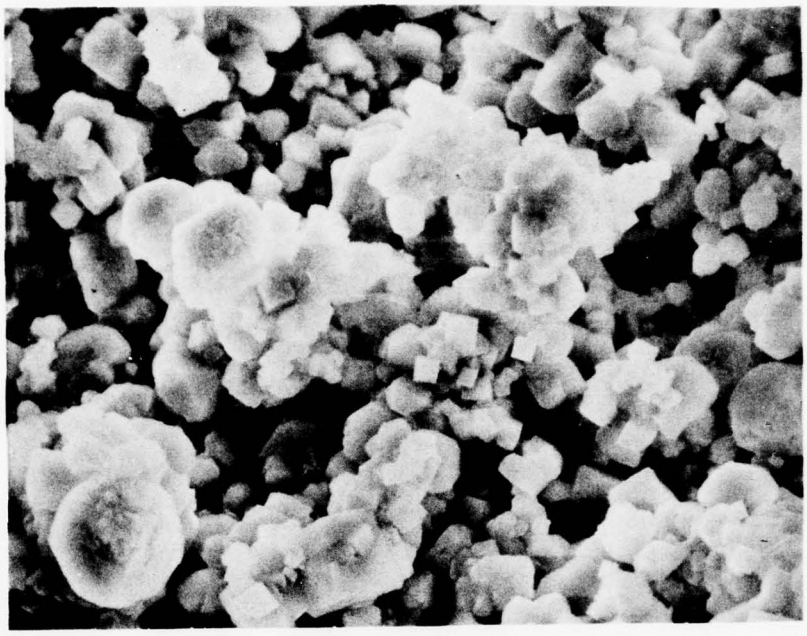

(b)

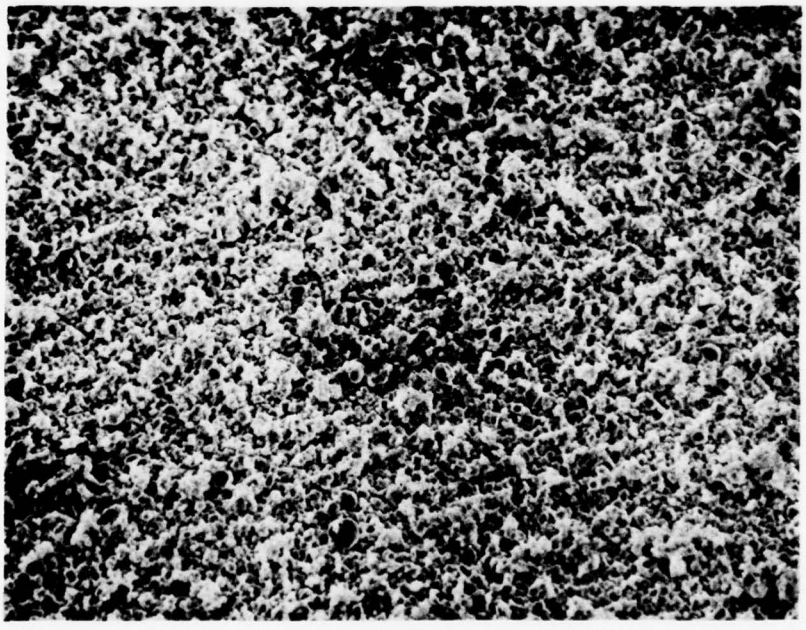

Fig. 27. SEM photographs of Li surface exposed to 0.5 (M) $LiAlCl_4$-$SOCl_2$ for 8 days at 72°C,
(a) 1000x (b) 100x; film thickness: 100 microns.

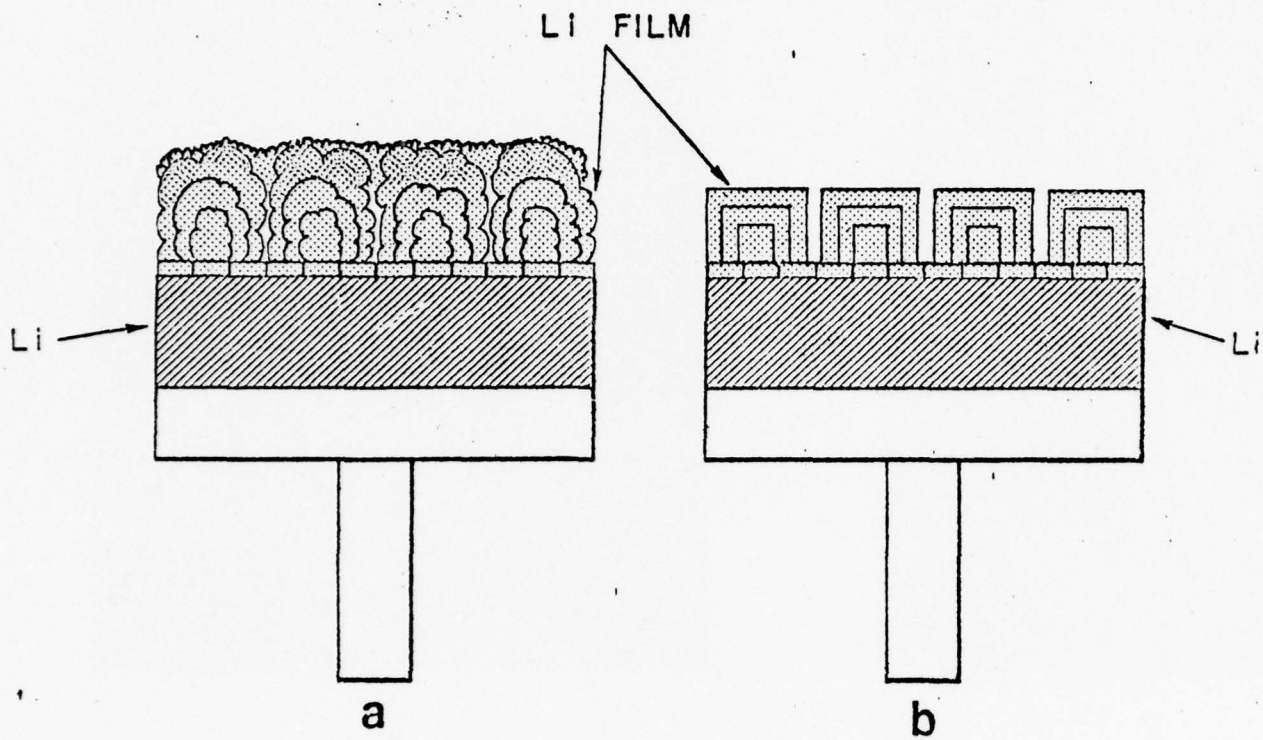

Fig. 28. Schematic Representation of Two Types of Film Crowth:
(a) Formation of Tall Clusters Over a Bed of Small Crystals.
(b) Formation of Large Crystals Over the Bed of Small Crystals.

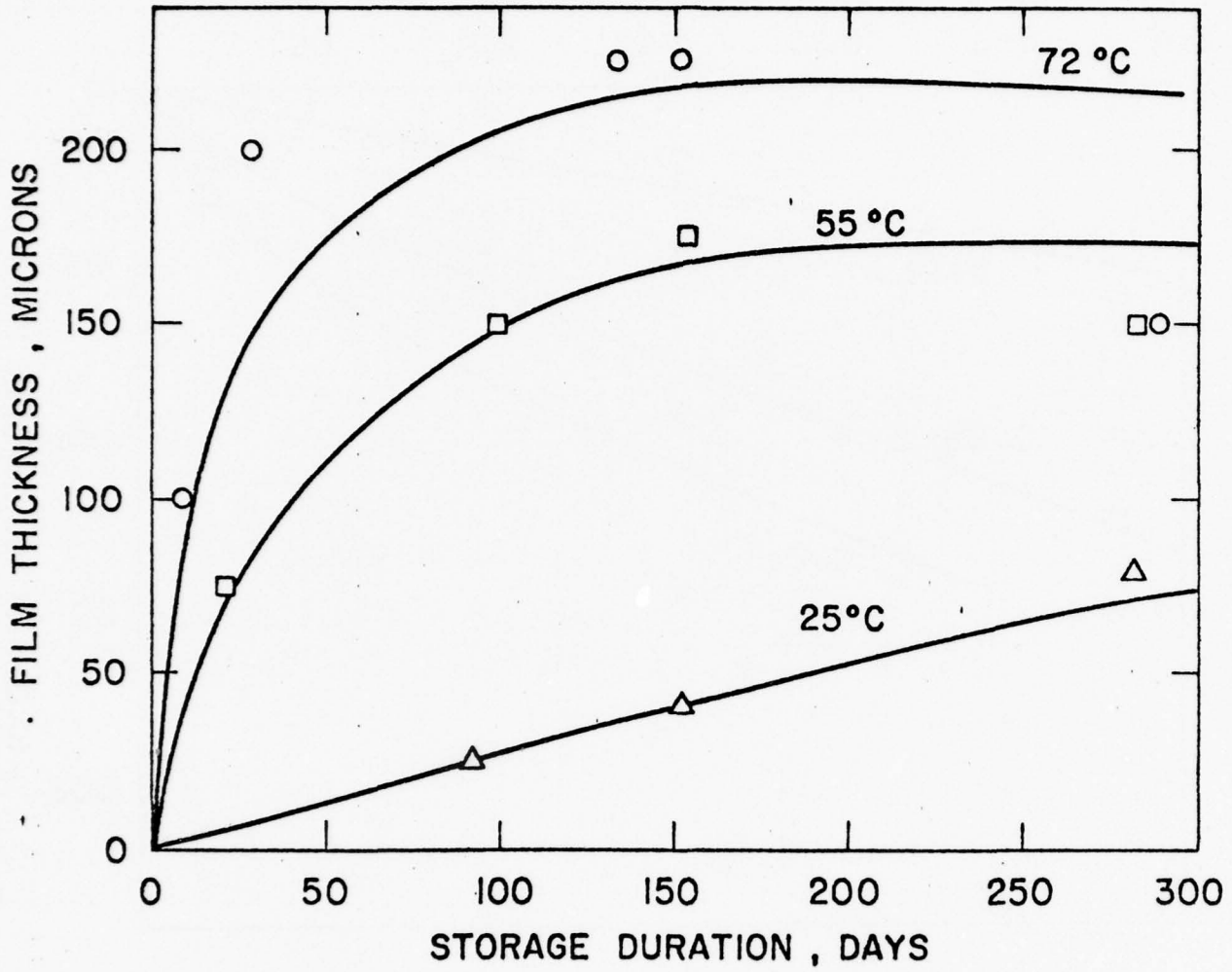

Fig. 29. Li Film Growth on Storage in 0.5 (M) $LiAlCl_4$-$SOCl_2$ at 72°, 55° and 25°C

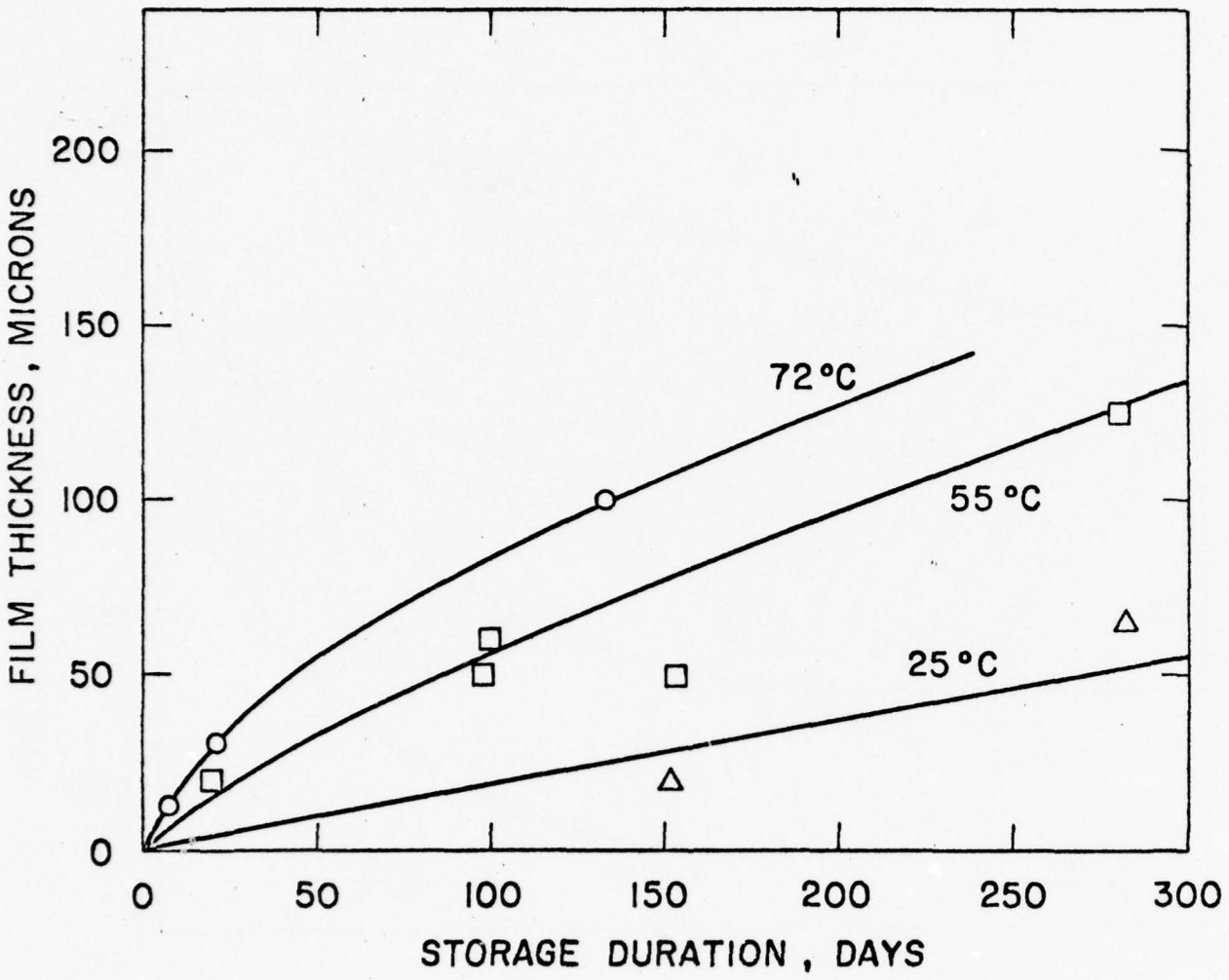

Fig. 30. Li Film Growth on Storage in 0.25 (M) $LiAlCl_4$-$SOCl_2$ at 72°, 55° and 25°C

and the growth rate increases with an increase in the storage temperature. Also, the film growth rates are significantly higher in the 0.5M electrolyte compared to that in the 0.25M $LiAlCl_4$-$SOCl_2$ electrolyte at all three temperatures. This is in accord with the observation (10) that in pure $SOCl_2$ the Li film forms very sparsely as shown in Fig. 21 compared to that in $LiAlCl_4$-$SOCl_2$ solutions. The possibility of reducing the film growth by reducing the salt ($LiAlCl_4$) concentration in the inorganic electrolyte is thus demonstrated.

The film growth rates in 1M $LiAlCl_4$-$SOCl_2$ with 0.1% and 0.01% H_2O were found to be identical, as shown in Figures 31 and 32 respectively.

The Li samples (thickness: 381 microns) were found to be completely reacted with the electrolyte in 75 days at 55°C in the 1M $LiAlCl_4$-$SOCl_2$ electrolyte containing 10% $AlCl_3$. Thus, high concentration of $AlCl_3$, a common impurity in $LiAlCl_4$ was found to be deleterious. However, the growth rate in 1% $AlCl_3$ (Fig. 33) was found to be very similar to that in 0.5M $LiAlCl_4$-$SOCl_2$.

The growth rate curves in 1M $LiAlCl_4$-$SOCl_2$ with 10% (6 wt %) S_2Cl_2 at 72°, 55° and 25°C are shown in Fig. 34. The film appears to grow continuously without any sign of leveling off at the lower temperature.

The Li film growth rates in 1M $LiAlCl_4$-$SOCl_2$ with 17.3% SO_2 (11 wt %) at 72, 55°, and 25°C are shown in Fig. 35. At 72°C, the Li film grows rapidly at first and then asymptomatically reaches a value significantly lower than the film thickness observed in all the previous electrolytes.

The results indicate that the Li film growth rates can be altered significantly by electrolyte variables such as the $LiAlCl_4$ concentration.

4.2.2.3 A Tentative Model for the Li Film Growth

The Li metal used in all the studies mentioned was processed by the manufacturer in dry air (RH $\simeq$ 2%) instead of in dry argon. This is possible because of the low reactivity (16) of Li metal with dry O_2, CO_2 and N_2. Moisture enhances the rate of the above reactions leading to the tarnishing of the Li foil. It is reasonable to assume that the apparent stability of Li in dry air is due to the kinetic inhibition of the following thermodynamically favorable reactions which lead to the presence of Li_2O, LiOH, Li_2CO_3 and Li_3N films on the Li surface.

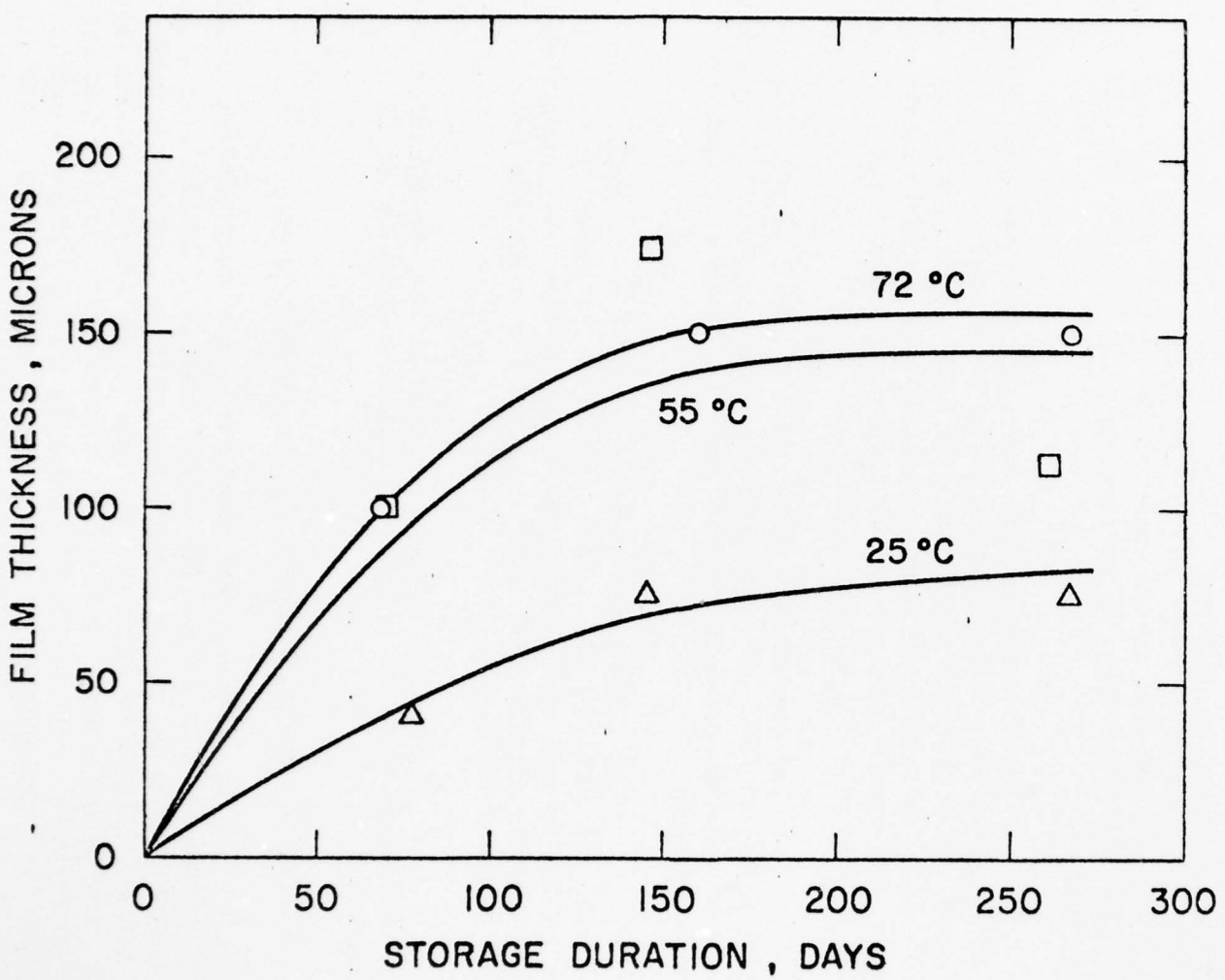

Fig. 31. Li Film Growth on Storage in 1.0 (M) $LiAlCl_4$-$SOCl_2$ + 0.1% H_2O at 72°, 55° and 25°C

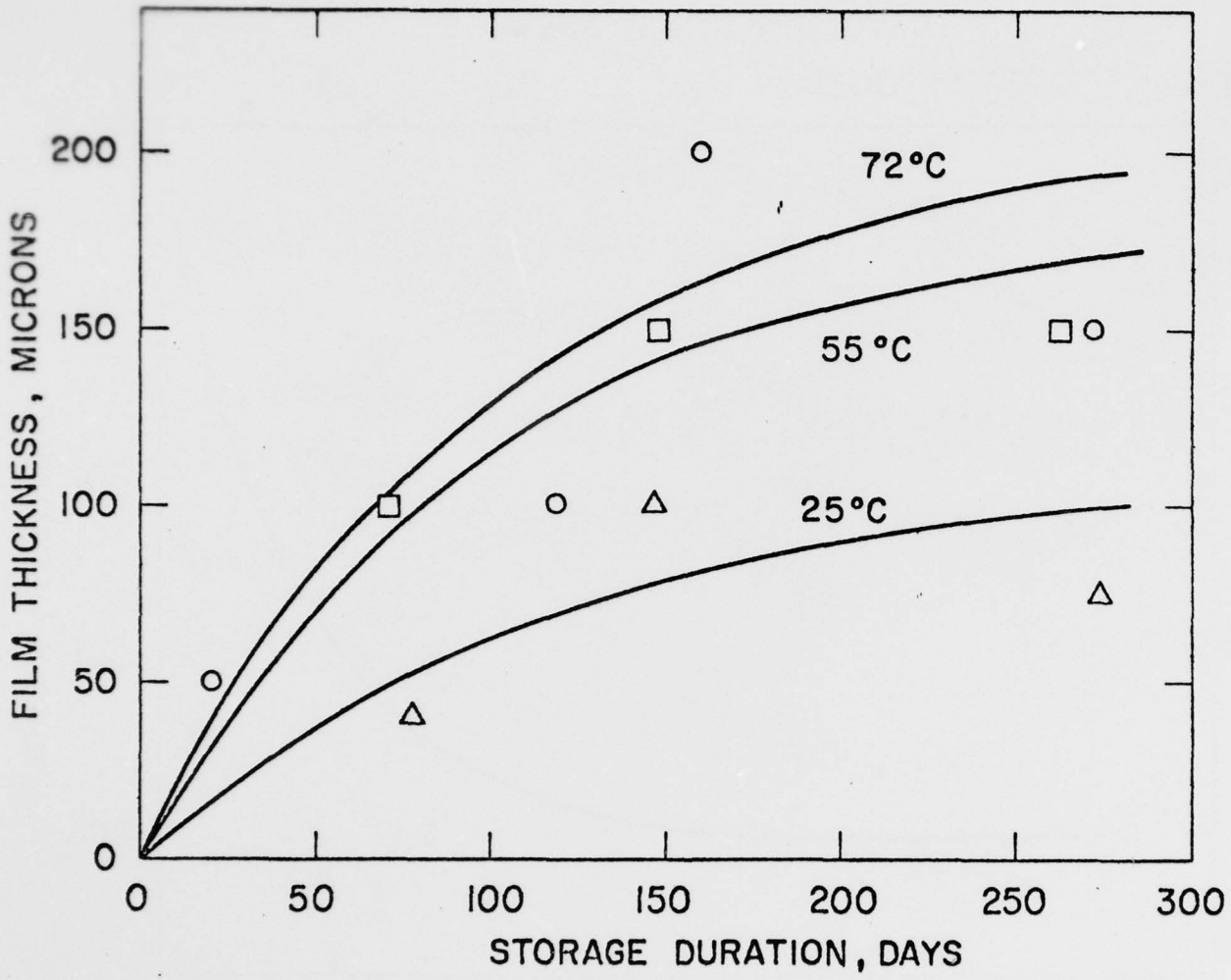

Fig. 32. Li Film Growth on Storage in 1.0 (M) $LiAlCl_4$-$SOCl_2$ + 0.01% H_2O at 72°, 55° and 25°C

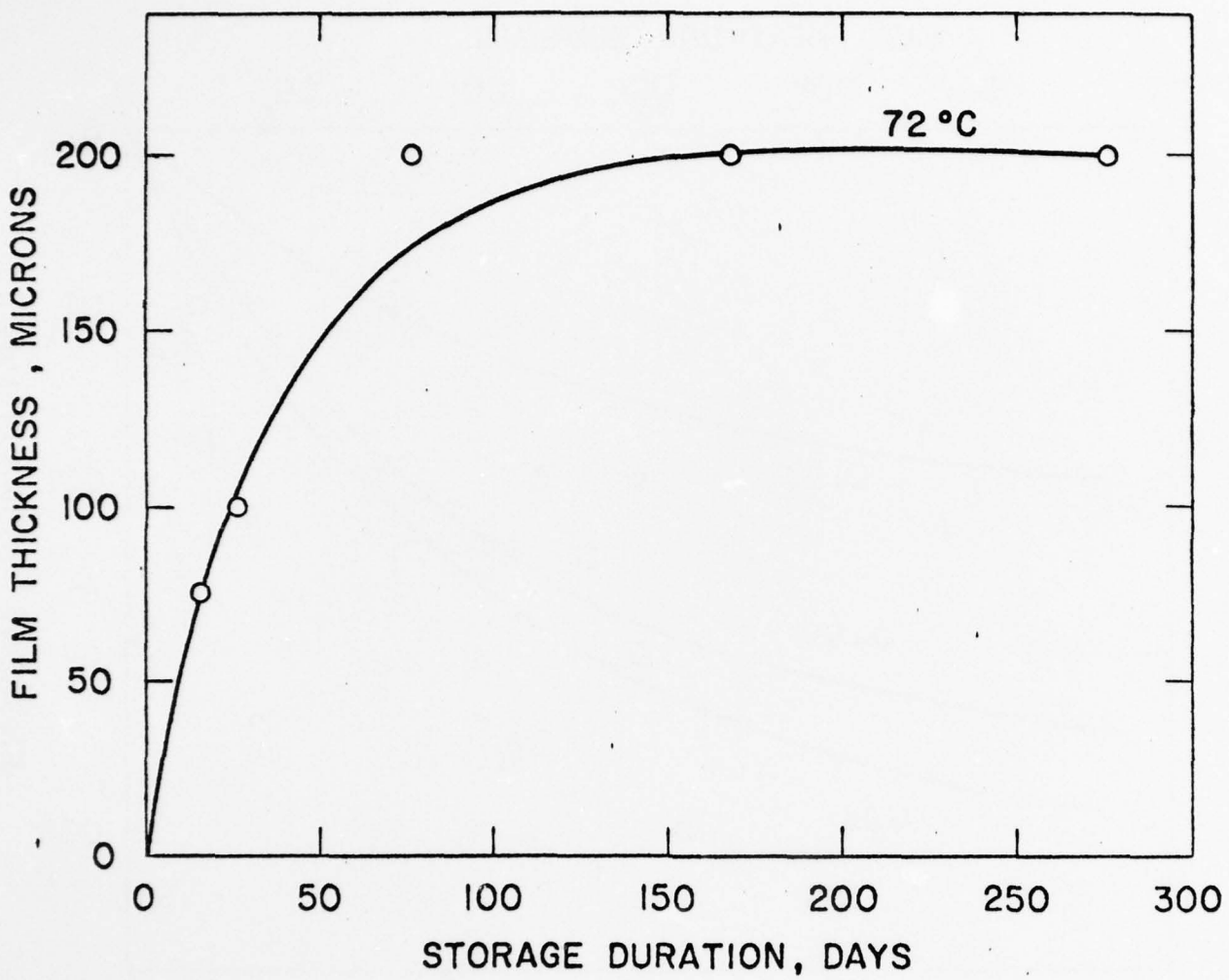

Fig. 33. Li Film Growth on Storage in 1.0 (M) $LiAlCl_4$-$SOCl_2$ + 1% $AlCl_3$ at 72°C

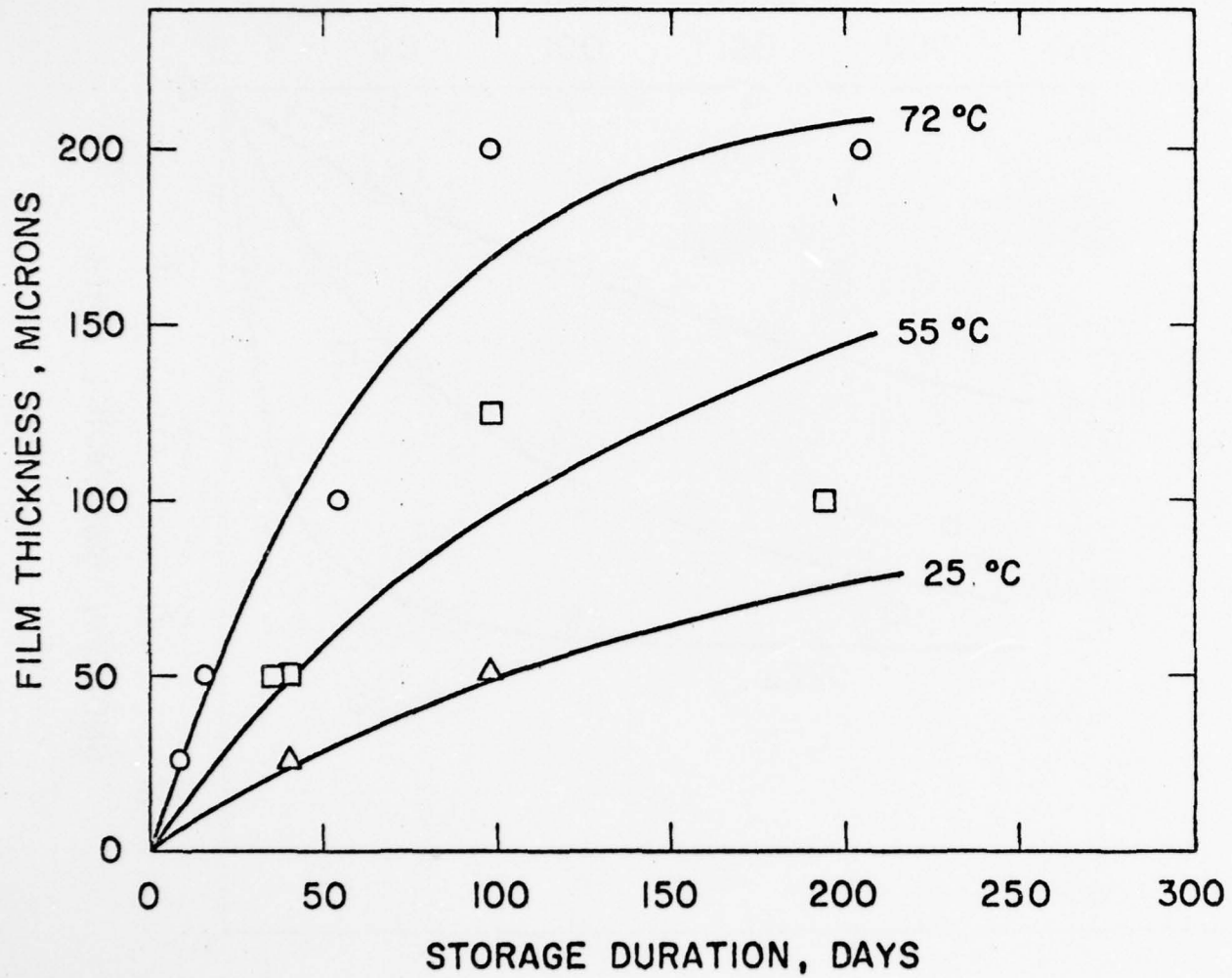

Fig. 34. Li Film Growth on Storage in 1.0 (M) $LiAlCl_4$-$SOCl_2$ + 10% S_2Cl_2 (6wt%) at 72°, 55° and 25°C

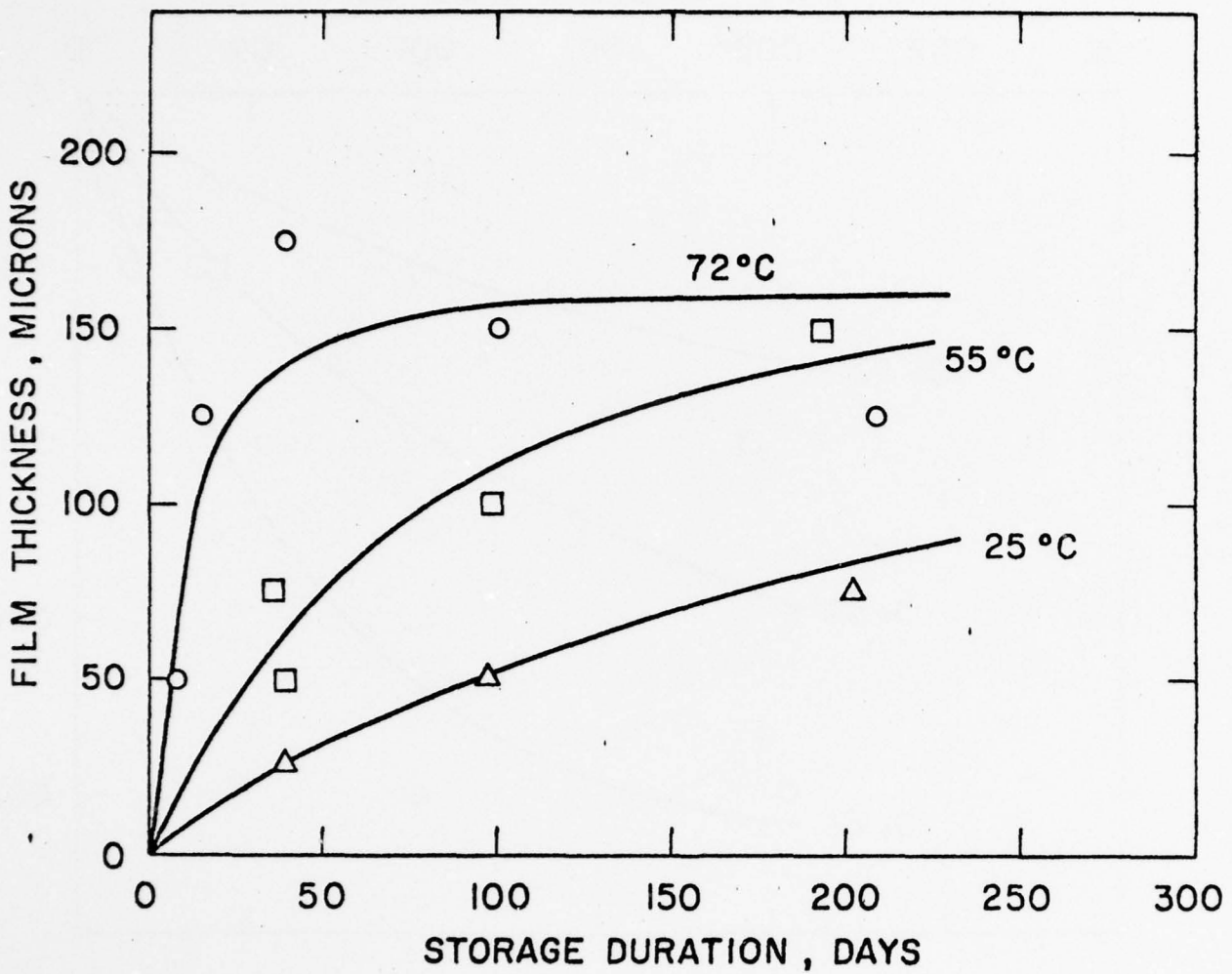

Fig. 35. Li Film Growth on Storage in 1.0 (M) $LiAlCl_4$-$SOCl_2$ + 17.3% SO_2 at 72°, 55° and 25°C

$$6\ Li + N_2 \longrightarrow 2\ Li_3N \qquad (6)$$

$$\Delta H = -94.4\ K.Cal$$

$$4\ Li + O_2 \longrightarrow 2\ Li_2O \qquad (7)$$

$$\Delta H = -284.8\ K.Cal$$

$$2\ Li + H_2O + CO_2 \longrightarrow Li_2CO_3 + H_2 \qquad (8)$$

$$\Delta H = -138.7\ K.Cal$$

$$2\ Li + 2H_2O \longrightarrow 2\ LiOH + H_2 \qquad (9)$$

$$\Delta H = -117.4\ K.Cal$$

The effectiveness of the above protective coatings may be judged, according to Pilling-Badworth ratio (R) (17).

$$R = \frac{V_s}{nV_{Li}} \qquad (10)$$

V_s = molar volume of the Li compound

n = no. of gram atoms of Li in one mole of the compound

V_{Li} = gram atomic volume of Li

which has to be close to or greater than unity to provide corrosion protection. The R values of some of the Li compounds are shown in Table 12. It appears that both LiOH and Li_2CO_3 films are expected to be protective in nature. However, LiOH forms monohydrate and could continue (16) to react further with Li metal and other Li film forming materials such as Li_3N to continue the film buildup without giving any protection. Li_2O and Li_3N form porous films since the R values are less than one. Only Li_2CO_3 can provide good protection by virtue of high R value. Therefore, it is reasonable to assume that before the Li metal is brought in contact with the inorganic electrolyte, the metal surface is already coated with (i) a very thin protective less porous film of Li_2CO_3 and (ii) a porous film of Li_2O and Li_3N. On contact with the $SOCl_2$, the Li_2CO_3 film may chemically react to form the protective film LiCl as

$$Li_2CO_3 + SOCl_2 \longrightarrow 2\ LiCl + CO_2 + SO_2 \qquad (11)$$

Table 12.

Pilling-Bedworth Ratio of Some Li Compounds

Li Compounds	$R = \frac{\text{molar vol. of compound}}{\text{no. of gm. atom of Li} \times \text{gm. atomic vol. of Li}}$
Li_2O	0.57
Li_3N	0.64
LiOH	1.26
Li_2CO_3	1.34
LiCl	1.58

The rate of the LiCl film forming reactions in the regions covered with Li_2CO_3 is expected to be low because of the slow diffusion of the reacting species through the Li_2CO_3 and LiCl ($R > 1$) protective films. The bed of small LiCl crystals as depicted in Fig. 44 (a) and (b) may have formed in these regions.

In view of the fact that Li was found to be non-reactive (16) towards dry O_2 and CO_2 even at temperature as high as 250°C, it is reasonable to assume that the major portion of the Li surface remains covered by the less porous protective film of Li_2CO_3 and very minor portions of the Li surface are covered by the porous Li_2O and Li_3N films. The growth of tall stacks of LiCl crystals as shown in Fig. 28 may have occurred in the latter regions covered by the porous Li_2O and Li_3N films, since the rate of reaction with $SOCl_2$ is expected to be greater. The general observation in regard to the growth of clusters of large crystals (Fig. 27) or single large crystals (Fig. 26) over a bed of uniformly grown smaller crystals, is explained in this manner. According to this model, the thin films which are present on the Li surface prior to its contact with the electrolyte controls the initial phase of the LiCl growth in the inorganic electrolytes.

The subsequent growth of the LiCl film is controlled by the electrolyte variables. In view of the fact that the SEM pictures of LiCl films (which are as thick as 384 microns) were taken without applying any conductive coating such as vapor deposited Al or Au, as is customary for photographing the non-conducting oxides such as Al_2O_3 on Al or Ta_2O_5 on Ta, it is reasonable to assume that the LiCl crystals grown in the inorganic electrolyte containing $LiAlCl_4$-$SOCl_2$ must have sufficient defects (caused by the impurities in the crystal) to make them electronically conducting. One may then view the growth of LiCl film as a result of a local cell reaction which is shorted through the LiCl film as schematically shown in Fig. 36. The anodic reaction involving the dissolution of Li occurs near the pores of the film and the cathodic reaction involving the formation of LiCl occurs on the LiCl film itself thus causing the LiCl crystals and the film to grow. The steps that could control this film growth are as follows:

1. Li^+ transport through the pores.
2. Electronic conduction of the LiCl film.
3. Li^+ ion conduction of the LiCl film.

Both the steps 2 and 3 can be eliminated since the film growth is dependent on the $LiAlCl_4$ concentration, indicating the step 1 as the controlling step for the film growth.

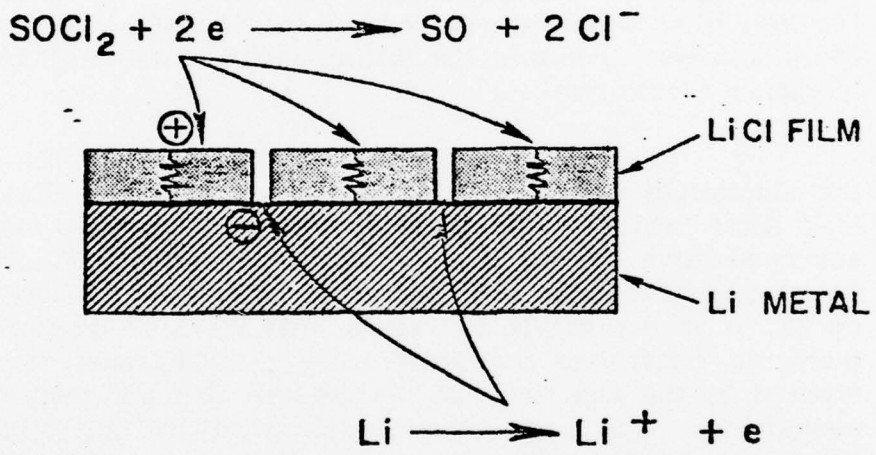

Fig. 36. Schematic Representation of Film Growth by Local Action Through the Pores of the Electronically Conducting Film

Thus, the rate of film growth $\frac{d\Theta}{dt}$ can be related to either

(i) The surface concentration of the pores, or

(ii) the length of the pores or (iii) both.

(i) Film Growth Controlled by The Surface Concentration of Pores

The surface concentration of the pores can be expressed as the portion of the surface not covered by the film $(A - \Theta)$ where Θ is the LiCl film area.

The rate of film growth can be expressed as:

$$\frac{d\Theta}{dt} = k\ (A - \Theta) \tag{12}$$

Where K is the rate constant. Integration yields:

$$\Theta = A(1 - e^{-kt}) \tag{13}$$

when $t = O$, $\Theta = O$; and when $t \simeq \infty$, $\Theta = A$

This represents an asymptotic type of growth. According to this type of growth, Θ increases rapidly at first and then slowly levels off. The LiCl film growth in the electrolyte with SO_2 gives rise to this type of growth (Fig. 35). The large crystals which grow eventually cover the pores (Fig. 26) and stop further film growth.

(ii) Film Growth Controlled by The Length of the Pores

As the film grows thicker, the length of the pores increases, thus, impeding the transport of Li^+. Therefore, the rate of growth is inversely proportional to the film thickness.

$$\frac{d\Theta}{dt} = \frac{k}{\Theta} \tag{14}$$

Integration yields:

$$\Theta = (2kt)^{1/2} \tag{15}$$

This is the well-known parabolic law of film growth. According to this the growth of the film continues without approaching an asymptotic value.

The Li film growth in all the electrolytes studied except the SO_2 containing electrolyte, particularly at lower temperatures, conforms to this type of behavior (Figures 29-32, 34 & 35). Thus, the tentative model of film growth proposed above qualitatively conforms to all the experimental observations. The data available to date are insufficient to do any quantitative analysis, and it is in fact likely that pore concentration and pore length both affect the growth kinetics.

4.3 The Effect of Electrolyte Variables on the Energy Density and the Voltage Delay of the Hermetic D Cells

We found from the SEM studies that the concentration of $LiAlCl_4$ in $SOCl_2$ had a significant effect on the Li anode film growth. We planned to evaluate the effect of the $LiAlCl_4$ concentration on the voltage delay characteristics of the $Li/SOCl_2$ D cell. But before that, we decided to determine the effect of the $LiAlCl_4$ concentration on the rate capability and the energy density of the fresh $Li/SOCl_2$ cells.

4.3.1 Effect of Salt ($LiAlCl_4$) Concentration on the Energy Density of the Hermetic D Cells

4.3.1.1 Experimental

Hermetic D cells were made in Ni cans with G/M seals and welded tops using the methods described earlier. The electrode dimentions of both the Li anode and the carbon cathode were 20" x 1.75". The electrolytes were made according to the procedure described earlier. The cells were discharged at constant currents at ambient (25°C) temperature within one week of electrolyte filling.

4.3.1.2 Results and Discussion

The capacity-rate curves of the $Li/SOCl_2$ D cells with 1.8, 1.0, 0.5, 0.25 and 0.1 (M) $LiAlCl_4$-$SOCl_2$ electrolytes are shown in Fig. 37. The lowering of the $LiAlCl_4$ concentration beyond 1 (M) leads to a lowering of the rate capability of the cells but an increase in the intrinsic capacity (capacity at low rate) of the cells. The latter has been found to be true in C size cells, and was presumed to be due to the increased precipitation of $LiAlCl_4$ in the cathode with the higher initial $LiAlCl_4$ concentration in $SOCl_2$ which is depleted on discharge.

Thus, the lowering of the $LiAlCl_4$ concentration appears to be beneficial with respect to the cell capacity at low rates, but detrimental with respect to the rate capability insofar as the fresh performance at room temperature is concerned.

The performance characteristics of all the above cells are summarized in Table 13.

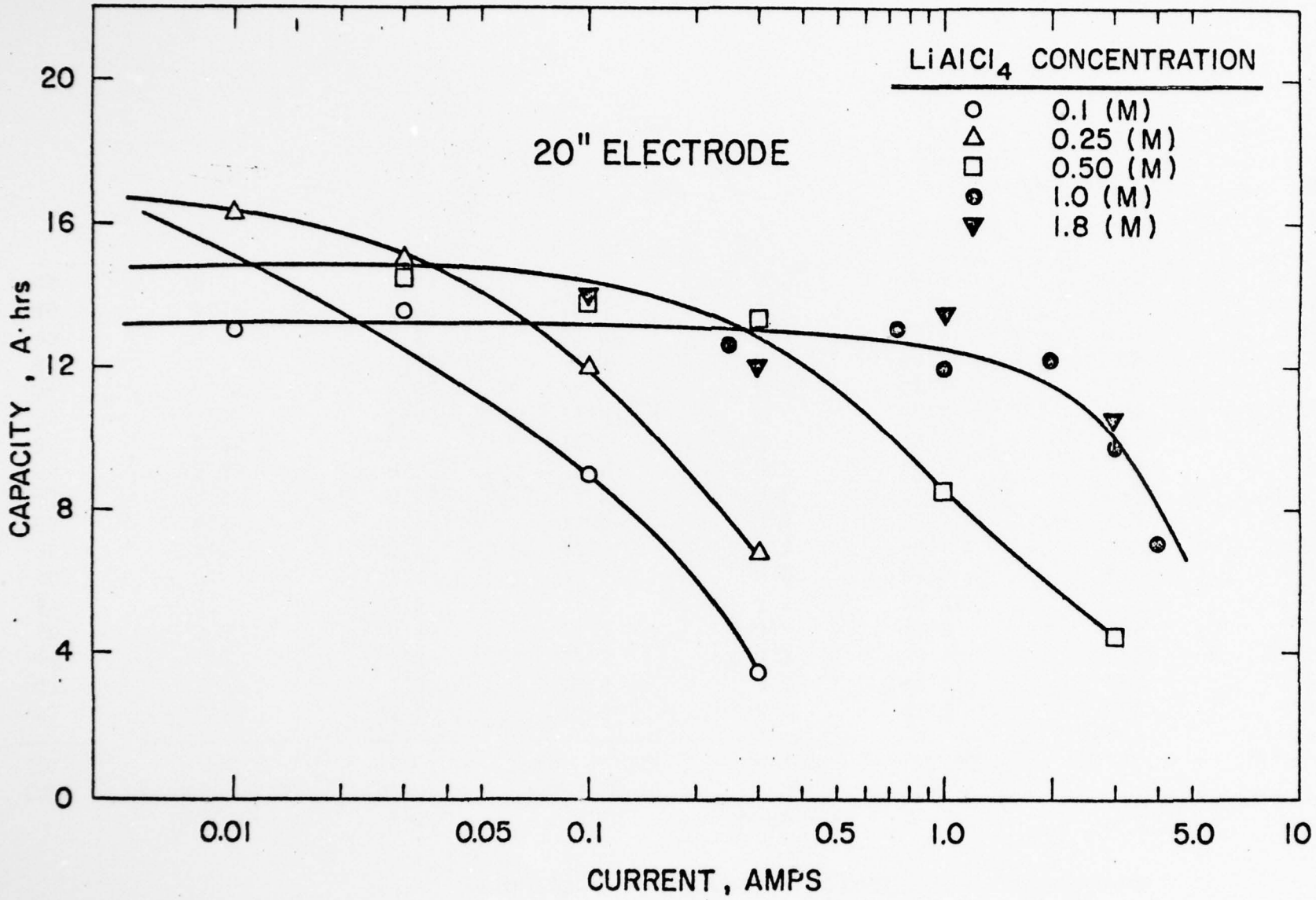

Fig. 37. Capacity Rate Curves of Li/$SOCl_2$ D Cells with 1.8, 1.0, 0.5, 0.25 and 0.1 (M) $LiAlCl_4$-$SOCl_2$ Electrolyte

Table 13. Performance Characteristics of the $Li/SOCl_2$ D Cells with 1.8, 0.5, 0.25 and 0.1 M $LiAlCl_4$-$SOCl_2$ Electrolytes

Cell No.	$LiAlCl_4$ Concentration (M)	Test Current (A)	Cell Capacity to Volt (A.Hr)	Average Cell Voltage	Total Energy (W.Hr)	Energy Density	
						W.Hr/lb	W.Hr/in^3
51	1.8	3.0	10.5	2.8	29.4	127	9.3
47	1.8	1.0	13.5	3.2	43.2	187	13.7
49	1.8	0.3	12.0	3.3	39.6	171	12.6
50	1.8	0.1	13.8	3.4	46.9	202	14.9
37	0.5	3.0	4.5	2.7	12.2	52	3.9
40	0.5	1.0	8.5	3.0	25.5	110	8.1
38	0.5	0.3	13.4	3.2	42.9	185	13.6
39	0.5	0.1	13.8	3.4	46.9	202	14.9
41	0.5	0.03	14.5	3.5	50.8	219	16.1
34	0.25	0.3	6.8	3.0	20.4	88	6.5
35	0.25	0.1	12.1	3.3	39.9	172	12.7
36	0.25	0.03	14.9	3.4	50.7	219	16.1
33	0.25	0.01	16.3	3.5	57.1	246	18.1
42	0.1	0.3	3.5	3.0	10.5	45	3.3
43	0.1	0.1	8.9	3.2	28.5	123	9.0
46	0.1	0.03	13.7	3.4	46.6	201	14.8
45	0.1	0.01	13.1	3.5	45.9	198	14.6

4.3.2 Effect of Electrolyte Variables on the VoltageDelay of $Li/SOCl_2$ Hermetic D Cell

From the SEM studies we found that electrolyte variables affected the morphology and the growth rates of the Li anode film. The purpose of this investigation was to determine the effect the above changes might have on the voltage delay of the $Li/SOCl_2$ D cells. We found that a lowering of the $LiAlCl_4$ concentration in the electrolyte resulted in a lowering of the rate of film growth. Although we carried out the SEM studies using only two $LiAlCl_4$ concentrations, viz. 0.5 and 0.25(M) we felt that it is necessary to examine the voltage delay characteristics of the cells with a wider range of salt concentrations since the quantitative cause and effect relationship between the Li film and the voltage delay may be quite complicated. According to our model, the initial voltage depression on load occurs as a result of the concentration polarization across the pores of the LiCl film on the Li anode. A lowering of the $LiAlCl_4$ concentration leads to a thinner LiCl film and a smaller pore length, thus decreasing the concentration polarization. But, at the same time, the lowering of the $LiAlCl_4$ concentration also leads to a decrease of the electrolytic conductivity, thus leading to an increase in the anode polarization. Therefore, it is necessary to determine the optimum $LiAlCl_4$ concentration where the above opposing effects are minimized for a minimum initial anode polarization. This can be accomplished by experiments with actual cells.

We found that S_2Cl_2 (electrolyte additive) did not change either the morphology or the film growth rates in any significant way. We included it in this investigation also in order to determine whether S_2Cl_2 might affect the voltage delay of the D cells. We included the SO_2 additive in this study, in view of its dramatic effects on the LiCl film morphology. The experimental details and the results are presented below.

4.3.2.1 Experimental

$Li/SOCl_2$ D cells were made with the following electrolyte variables, using the methods and the procedure described in the previous section.

1. 1.8 (M) $LiAlCl_4$-$SOCl_2$
2. 1.0 (M) $LiAlCl_4$-$SOCl_2$
3. 0.5 (M) $LiAlCl_4$-$SOCl_2$
4. 0.25 (M) $LiAlCl_4$-$SOCl_2$
5. 1.0 (M) $LiAlCl_4$-$SOCl_2$ + (6 Wt.%) S_2Cl_2
6. 1.0 (M) $LiAlCl_4$-$SOCl_2$ + (11 Wt.%) SO_2

All the cells were fitted with low pressure vents.

The cells were stored at 72°C and were taken out every month and were cooled to -30°C for at least two hours and the voltage delays were measured at constant currents of 3.0, 1.0 and 0.25A. As soon as the cell voltage reached 2.0 volt, the tests were discontinued and the cells were re-stored at 72°C. The cell voltages were recorded on a strip chart recorder to determine the initial voltage depression and the subsequent recovery. The cells which exhibited no voltage depression below 2.0 volt on load were considered to have no voltage delay. The cells which exhibited an initial voltage depression on load to a voltage below 2.0 volt, were considered to have a voltage delay measured as the time required for the voltage to reach 2.0 volt. The cells which did not recover to a 2.0 volt level within an hour of test, were considered to have infinite voltage delay and to be inoperative.

4.3.2.2 Results and Discussion

The results of the voltage delay tests are shown in Table 14.

The voltage delay measurements of $Li/SOCl_2$ hermetic D cells having 1.8 and 1.0 (M) $LiAlCl_4$-$SOCl_2$ electrolytes were made after a storage of 1, 2 and 3 months at 72°C. The cells with 0.5 (M) and 0.25 (M) electrolytes were tested after 1, 2, 3 and 4 months at 72°C. The cells with 6 wt% S_2Cl_2 were tested after 1, 2, and 3 months at 72°C; these results are also shown in Table 14. The results indicate a gradual alleviation of the voltage delays with a decrease in the $LiAlCl_4$ concentration from 1.8 (M) to 0.5 (M). At 0.25 (M), the voltage delays are somewhat longer. According to our model of the voltage recovery after the initial depression, the anode dissolution of Li occurs through the pores of the LiCl film. A simple explanation for the observed behavior based on this model is as follows: The thicker film at high salt concentrations (1.8M) results in longer pores and, hence, longer voltage delays. The thinner film at lower salt concentrations has shorter pores, and, therefore, shorter voltage delays. However, at even lower salt concentrations, viz, 0.25 (M), the conductivity of the electrolyte is reduced substantially, thus impeding the mass transport necessary for a rapid voltage recovery. Thus, a minimum in the hypothetical voltage delay vs salt concentration curve should occur between the 0.25 (M) and the 1.8 (M) points on the curve, and this minimum is probably near the 0.5 (M) point.

The voltage delays of the cells with S_2Cl_2 in the 1(M) $LiAlCl_4$-$SOCl_2$ electrolyte after 3 months at 72°C, appear to be similar to that of the cells without S_2Cl_2.

Table 14. Voltage-Delay Characteristics of Li/$SOCl_2$ D Cells with the Various Electrolytes; Storage at 72°C, Test at -30°C

Electrolyte	Test Current (A)	Voltage-Delay(Seconds) on Storage of 1 Month	2 Months	3 Months
1.8 (M) $LiAlCl_4$-$SOCl_2$	3.0	23	∝	∝
	3.0	33	∝	∝
	3.0	31	∝	∝
	1.0	No-delay	∝	∝
	1.0	No-delay	∝	∝
	1.0	No-delay	300	∝
	0.25	No-delay	No-Delay	∝
	0.25	No-delay	No-delay	No-delay
	0.25	No-delay	No-delay	∝
	0.25	No-delay	No-delay	No-delay
1.0 (M) $LiAlCl_4$-$SOCl_2$	3.0	162	∝	606
	3.0	204	-	-
	3.0	∝	-	-
	1.0	No-delay	No-delay	220
	1.0	No-delay	-	-
	1.0	No-delay	No-delay	No-delay
	1.0	27	No-delay	1380
	0.25	No-delay	No-delay	No-delay
	0.25	No-delay	No-delay	No-delay
	0.25	No-delay	No-delay	No-delay

Table 14. Voltage-Delay Characteristics of Li/$SOCl_2$ D Cells with the Various Electrolytes; Storage at 72°C, Test at -30°C (cont.)

Electrolyte	Test Current (A)	Voltage-Delay (Seconds) on Storage of: 1 Month		2 Months	3 Months	4 Months
0.5 (M) $LiAlCl_4$-$SOCl_2$	3.0	290		172	-	900
	3.0	177		665	-	∝
	1.0	No-delay		No-delay	-	No-delay
	1.0	No-delay		No-delay	-	No-delay
	0.25	No-delay		No-delay	-	No-delay
	0.25	No-delay		No-delay	-	No-delay
0.25 (M) $LiAlCl_4$-$SOCl_2$	3.0	124	(1Ω)	No-delay	-	-
	3.0	352		464	300	300
	3.0	No test		300	570	∝
	1.0	110		290	186	∝
	1.0	525		261	No-delay	390
	1.0	120	(3Ω)	1150	720	1500
	0.25	No-delay		55	No-delay	420
	0.25	No-delay		350	No-delay	300
	0.25	No-delay	(300Ω)	No-delay	No-delay	No-delay

Table 14. Voltage-Delay Characteristics of $Li/SOCl_2$ D Cells with the Various Electrolytes; Storage at 72°C, Test at -30°C (cont.)

Electrolyte	Test Current (A)	Voltage-Delay (Seconds) on Storage of 1 Month	2 Months	3 Months
1 (M) $LiAlCl_4$-$SOCl_2$ + 6% S_2Cl_2	3.0	138	900	∝
	3.0	156	∝	-
	3.0	138	660	∝
	1.0	No-delay	∝	∝
	1.0	No-delay	330	∝
	1.0	No-delay	No-delay	300
	0.25	No-delay	No-delay	∝
	0.25	No-delay	No-delay	No-delay
	0.25	No-delay	No-delay	No-delay
1 (M) $LiAlCl_4$-$SOCl_2$ + 11% SO_2	3.0	No-delay	--	--
	1.0	No-delay	--	--
	0.25	No-delay	--	--

Only three of the ten cells with 1.0 (M) $LiAlCl_4$-$SOCl_2$ + 11 Wt % SO_2 electrolyte survived the first month of storage at 72°C, the rest vented during the 72°C storage due to the excessive pressure caused by the SO_2. Three cells were tested at the three currents and showed no voltage delay. However, these cells vented during the second month of storage at 72°C. We repeated this experiment with cells having high pressure vents.

Unfortunately, these cells leaked at the end of one month. The weight loss of these cells as well as the voltage delays at -30°C test, are shown in Table 15. Note that the cells showed reasonably good voltage delay characteristics in spite of the electrolyte loss. Two cells were discharged at 25°C at 1.0 and 0.25A. The capacity recovered was 10.8 and 13.4A.Hr respectively, indicating no significant capacity loss as a result of the storage.

It is important to note that all the cells in Table 14 showed no delay when tested at 25°C after the various storage periods.

4.3.3 Conclusion

The $LiAlCl_4$ concentration in $SOCl_2$ was found to have a significant effect on both the intrinsic energy density and the voltage delay characteristics of the Li/$SOCl_2$ D cells. We found 1.0 and 0.5 (M) $LiAlCl_4$-$SOCl_2$ to be the best from both the energy density and the voltage delay point of view.

Addition of 6 % S_2Cl_2 did not have any significant effect on the voltage delay characteristics of Li/$SOCl_2$ D cells.

Evidence regarding the effect of SO_2 on the voltage delays remained inconclusive because of the premature cell leakage.

In general, the voltage delay characteristics of the hermetic D cells were found to be superior to those reported by others (13).

Table 15. Voltage-Delay Characteristics of $Li/SOCl_2$ D Cells with (11 wt %) SO_2 in 1 (M) $LiAlCl_4$-$SOCl_2$ Electrolyte; 1 Month Storage at 72°C, Test at -30°C

Wt. Loss (gm)	Voltage-Delay at -30°C		Capacity at 25°C	
	Current (A)	Delay (Sec)	Current (A)	Capacity (A. Hr)
4.8	3.0	240	1	10.8
0	3.0	180		
10.3	3.0	∝		
11.4	3.0	∝		
2.2	1.0	No-delay		
13.6	1.0	∝		
12.1	1.0	∝		
2.8	0.25	No-delay	0.25	13.4
17.8	0.25	No-delay		
9.8	0.25	No-delay		

5. Task IV - Safety Studies: Development of Protection Against Short Circuit And Thermal Runaway

It was discovered that the $Li/SOCl_2$ D cells exploded on 10A discharge. The cells also exploded on external shorting in spite of an operational vent designed to open at 500-550 PSIG. The wall temperature-time plot of a D cell after external shorting is shown on Fig. 38. The opening of the vent did not result in any significant cooling of the cell.

Two approaches were pursued in an effort to alleviate the explosion hazard.

(i) Low pressure venting to cool the cell before it reached the critical temperature, and

(ii) A chemical approach based on the identification of the chemical combinations (present in the cell) capable of sustaining a thermal runaway and the development of possible methods of deactivating these.

5.1 Low Pressure Venting

5.1.1 Venting at 0 PSIG

We showed that venting at 500 PSIG did not prevent explosion on shorting. Next, we attempted to vent D cells at 0 PSIG on shorting. We accomplished this by fabricating cells according to the methods described earlier, but by keeping the electrolyte fill port open after the cell filling. The cells were fitted with a thermocouple on the outer wall which was insulated thermally by wrapping several layers of the glass filter paper and asbestos sheet around the cell. The short circuit current and the wall temperature of the cell were monitored as a function of time after shorting. The test results for three D cells are shown in Fig. 39. The behavior of all three cells was qualitatively similar. The short circuit current rose to approximately 24 A within a short time after the shorting and then decreased rather rapidly. The cell temperature increased for the first 3 or 4 minutes, reached a maximum, and then declined slowly. The cell venting began visibly within a minute or two of the cell shorting. There was no explosion, bulging or any other damage, internal or external to the cell.

The results indicate that it is possible in principle to prevent explosion of $Li/SOCl_2$ on shorting by means of venting. Since venting at 500 PSIG did not work, and venting at 0 PSIG did, there must be a safe venting pressure between 0 PSIG and 500 PSIG. It is,therefore,necessary to investigate the internal cell pressure as a function of the various abuse conditions in order to determine this maximum safe venting pressure.

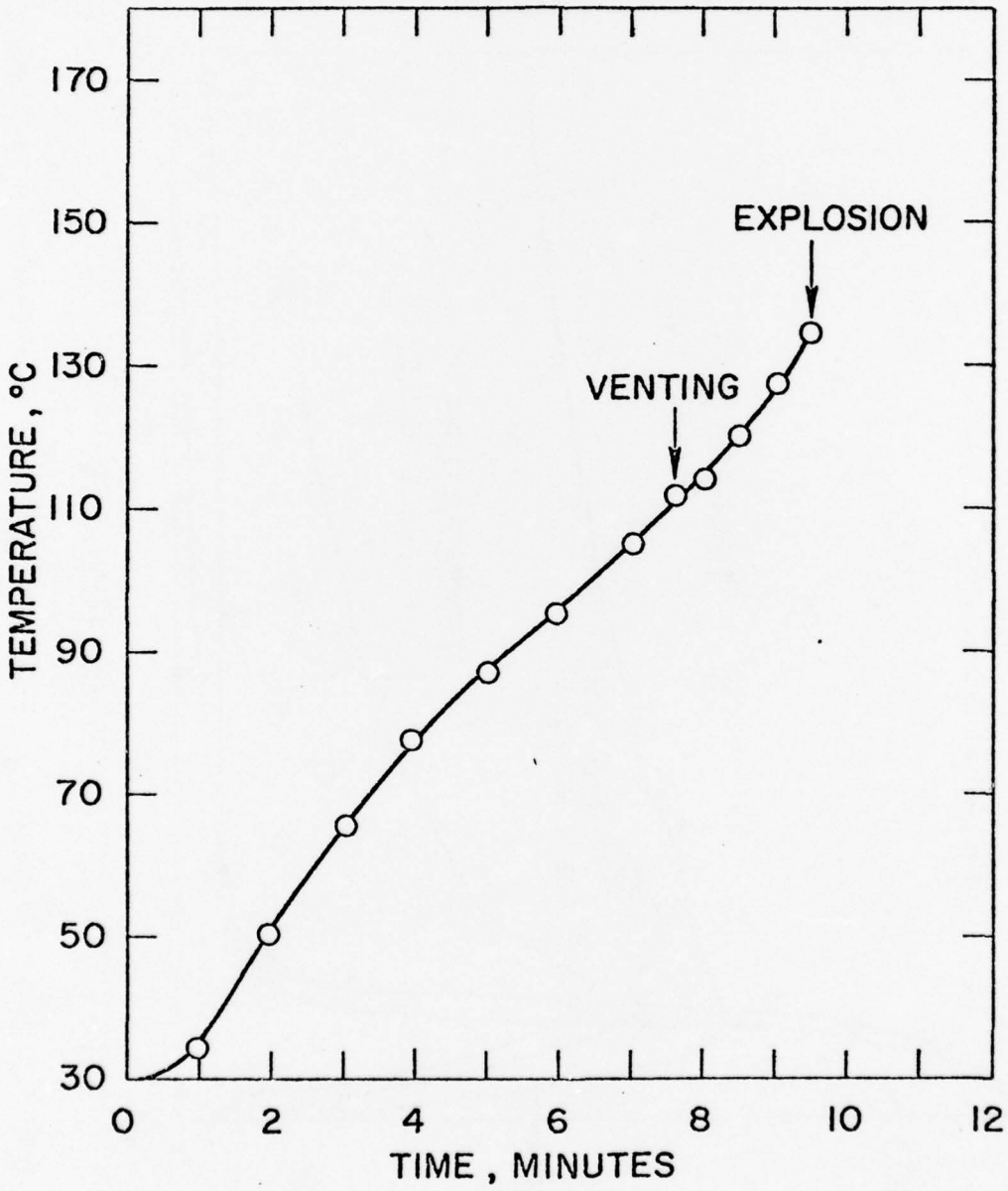

Fig. 38. Plot of the Skin Temperature of a Li/$SOCl_2$ D Cell as a Function of Time After Shorting the Cell Externally

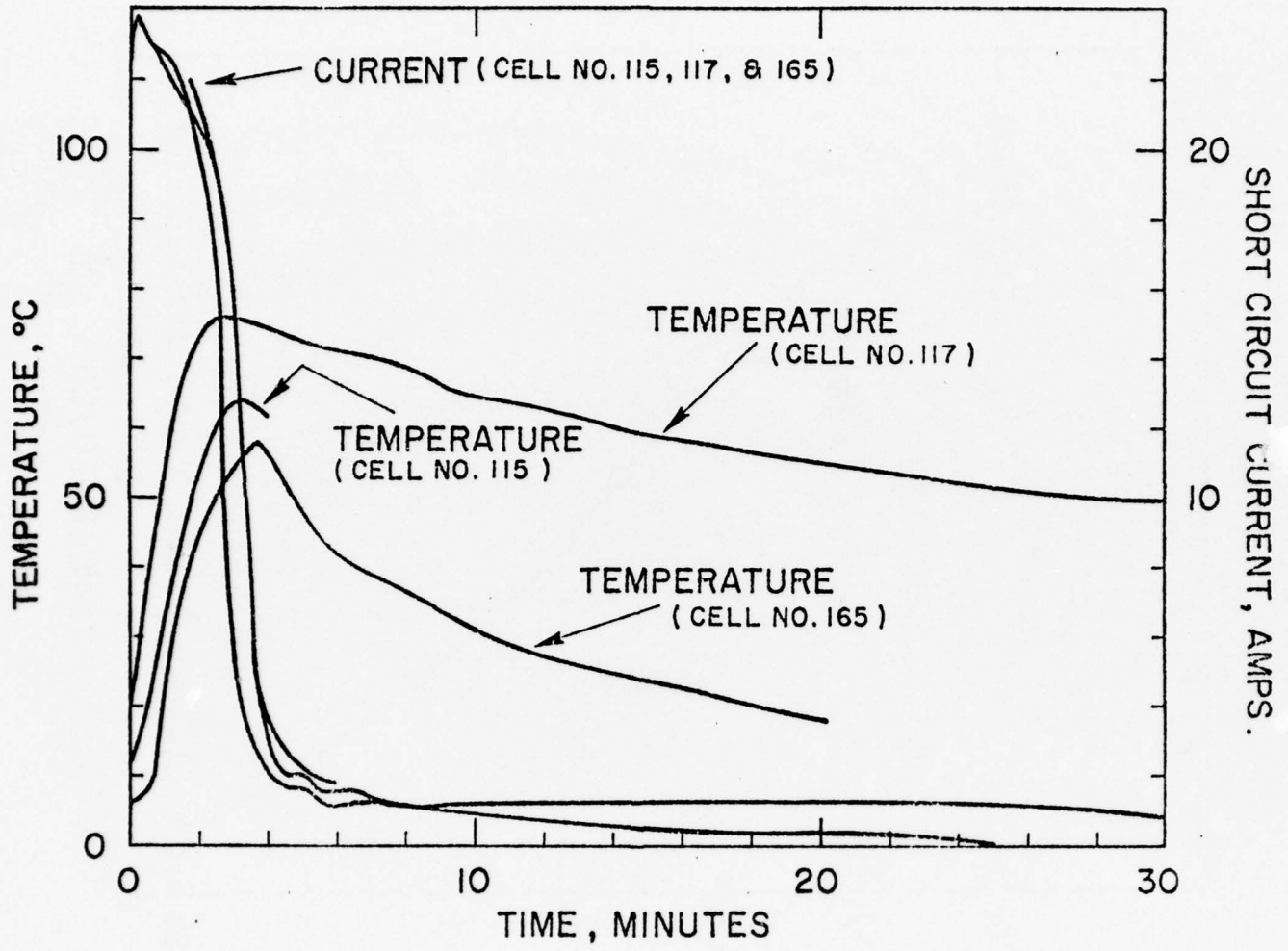

Fig. 39 Plots of the Skin Temperature and the Short Circuit Current of Li/$SOCl_2$ D Cells With the Open Electrolyte Fill Port as a Function of Time after Shorting the Cell Externally.

5.1.2 Quantitative Measurements of Cell Pressures and Temperatures On Short Circuiting

We attempted to determine the safe venting pressure by quantitatively measuring the pressure-temperature characteristics of the D cells under external heating and shorting conditions. We also designed and built a device which allowed us to vent the cell from a remote position as the cell internal pressure rose to a certain value. The experimental details and the results are presented here.

5.1.2.1 Experimental

D cells were made with 20" x 1.75" electrodes in Ni cans with G/M seals employing the methods described earlier. The cells were filled with 1(M) $LiAlCl_4$-$SOCl_2$ electrolyte through the electrolyte fill port and the electrolyte fill ports were temporarily closed with a rubber plug instead of a permanent seal by welding as is the normal practice. The electrolyte fill port was used for monitoring the internal cell pressure as well as for venting when desired. A schematic view of the device built for this purpose is shown in Figure 40. The device has a teflon nest mounted on a hinged steel plate that supports the D cell which is wound with heating tape and insulation. A thermocouple is attached to the outer wall of the cell for monitoring the temperature of the cell. The hinged steel plate is kept in a horizontal position by means of a latch which can be opened by an electromechanical actuator. A top steel plate which can be clamped down by means of a threaded rod is positioned on the cell top by means of several 'O' rings which provides a seal as well as electrical insulation. The electrolyte fill port is electrically connected to the top steel plate and is positioned in a hole drilled in the top plate. A pressure transducer is screwed into the other end of the hole, thus connecting with the interior of the cell through the electrolyte fill port. A tab welded to the cell can is one terminal of the cell, the electrolyte fill port electrically connected to the steel device is the other terminal. Note that the cell can is electrically insulated from the device by means of the teflon nest and the rubber 'O' ring seal at the top. The electrical insulation at the top is further improved by a thin disc of teflon on the cell top.

The transducer was calibrated before each experiment using a pressure gauge connected to a gas cylinder which was in turn connected to an empty D cell can (with tube feed through) placed in the teflon nest of the device. The calibration of the transducer did not change during the experiments which included several explosions. The transducer and the electromechanical actuators were protected by the heavy steel plates within which the cell was located.

The device was kept behind protective shields in the safety room which had electrical connections through the wall. All the measuring instruments including the switch for actuating the vent were placed outside the safety room away from the device. It had provisions for allowing the cell to vent at will by means of the electromechanical actuator that pulls the latch that clamps the middle steel plate (supporting the cell) against the cell. When actuated, the middle plate drops down to expose the electrolyte fill port to the atmosphere. It was planned to vent the cell when the cell pressure reached 200 and 400 PSI in order to determine the highest safe venting pressure. We already knew that it was unsafe to vent the cells at 500 PSI.

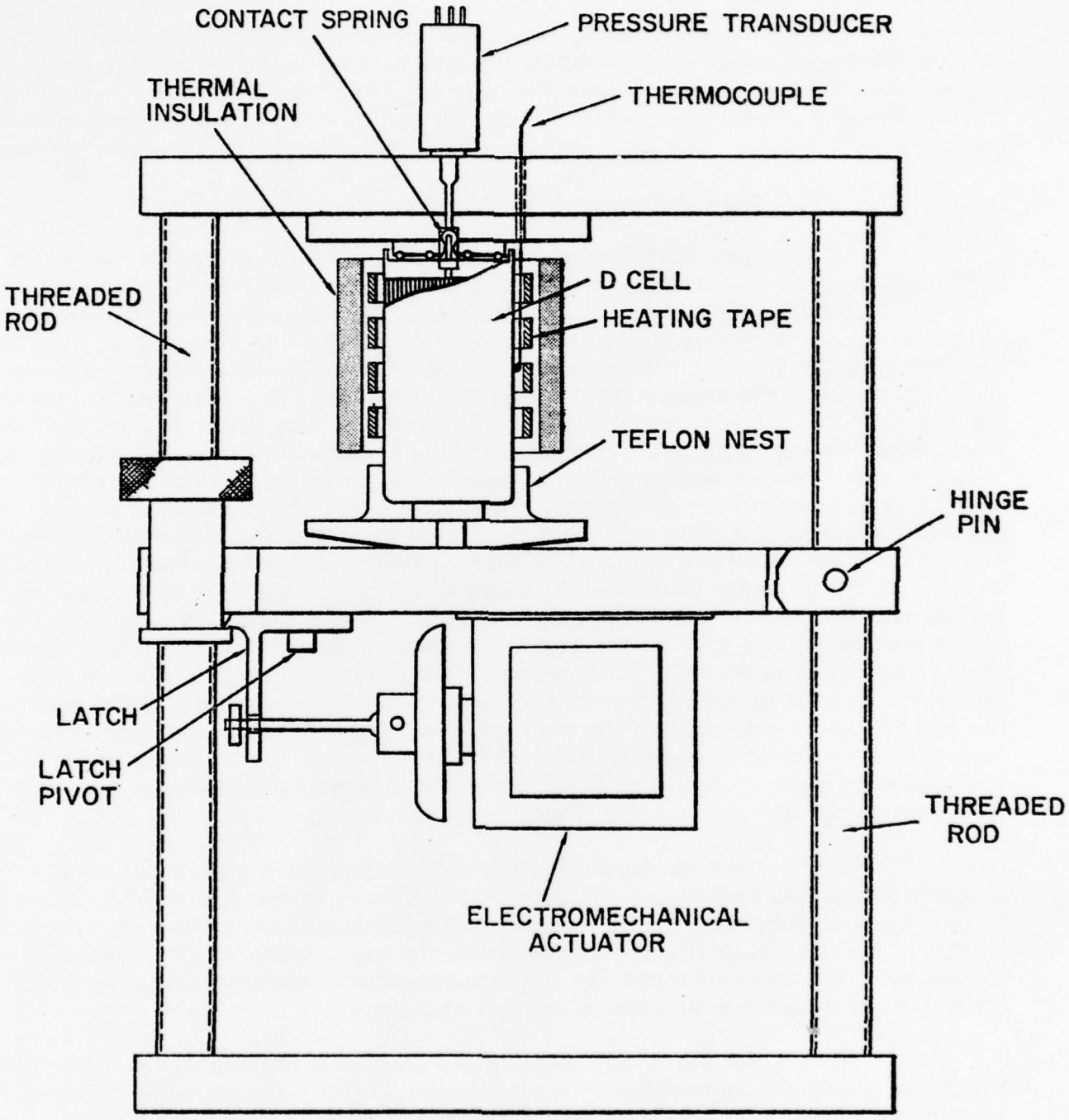

Fig. 40. Schematic View of the Device for Measuring Internal Cell Pressure and for Cell Venting by Remote Control.

5.1.2.2 Results and Discussion

We ran several experiments consisting of heating the cell externally and monitoring the internal pressures in order to check out the dependability of the device. We also ran several shorting experiments to establish the general pressure-time characteristics on shorting. The results of two specific experiments are described below.

In the first experiment one freshly made D cell with open electrolyte fill port and a thermocouple fitted to the cell wall with insulation was mounted in the device (Fig. 40) and was externally shorted through a 1 milliohm shunt. The pressure, the wall temperature, the voltage and the short circuit current of the cell were all monitored as a function of time on strip chart recorders. The results of the first experiment are shown in Fig. 41. On shorting, the cell voltage initially plummeted to 0.15 volt and then rose gradually to 0.65 volt and began to decline slowly. The short circuit current also rose gradually after the initial fluctuation to 19.5 A and then began a slow decline. The cell temperature and the cell pressure increased rather slowly during the first minute. Thereafter the temperature rose steadily to 115°C. The pressure rose steadily to approximately 160 PSI, and began to rise rather sharply thereafter. The cell was vented through the electrolyte fill port by means of the electromechanical actuator as soon as the pressure reached 195 PSI. The cell temperature began to decline steadily right after the venting. There was no cell explosion. The results indicate that cell venting below 200 PSI may prevent explosions.

We carried out another shorting experiment with another fresh D cell after readjusting the latch mechanism of the device. The plots of pressure, temperature, short circuit current and the voltage as a function of time after the shorting are shown in Fig. 42. Again the plots were the same as in the previous experiment. The cell pressure rose rather gradually to 150-200 PSI and then began to rise very sharply. All these experiments indicate that the pressure-time plots after shorting tend to have two slopes, with a transition region around 150-200 PSI. The cell pressure rose to 400 PSI when the switch for the vent was pressed. The cell exploded right at that instant. It was not clear whether the vent mechanism really opened prior to the explosion. However, it is clear that the cell may explode at 400 PSI. The temperature at which the explosion occurred was 140°C.

5.1.2.3 Conclusions

The following conclusions were drawn from the quantitative measurements of the pressure and temperature on cell heating and cell shorting.

1. The rate of increase of cell pressure on shorting has a transition region around 150-200 PSI above which the rate is significantly higher.

2. Cell venting below 200 PSI may prevent cell explosions on shorting.

Fig. 41. Plots of Pressure, Temperature, Voltage and Current as a Function of Time on Shorting the D Cells and Venting at 200 PSI.

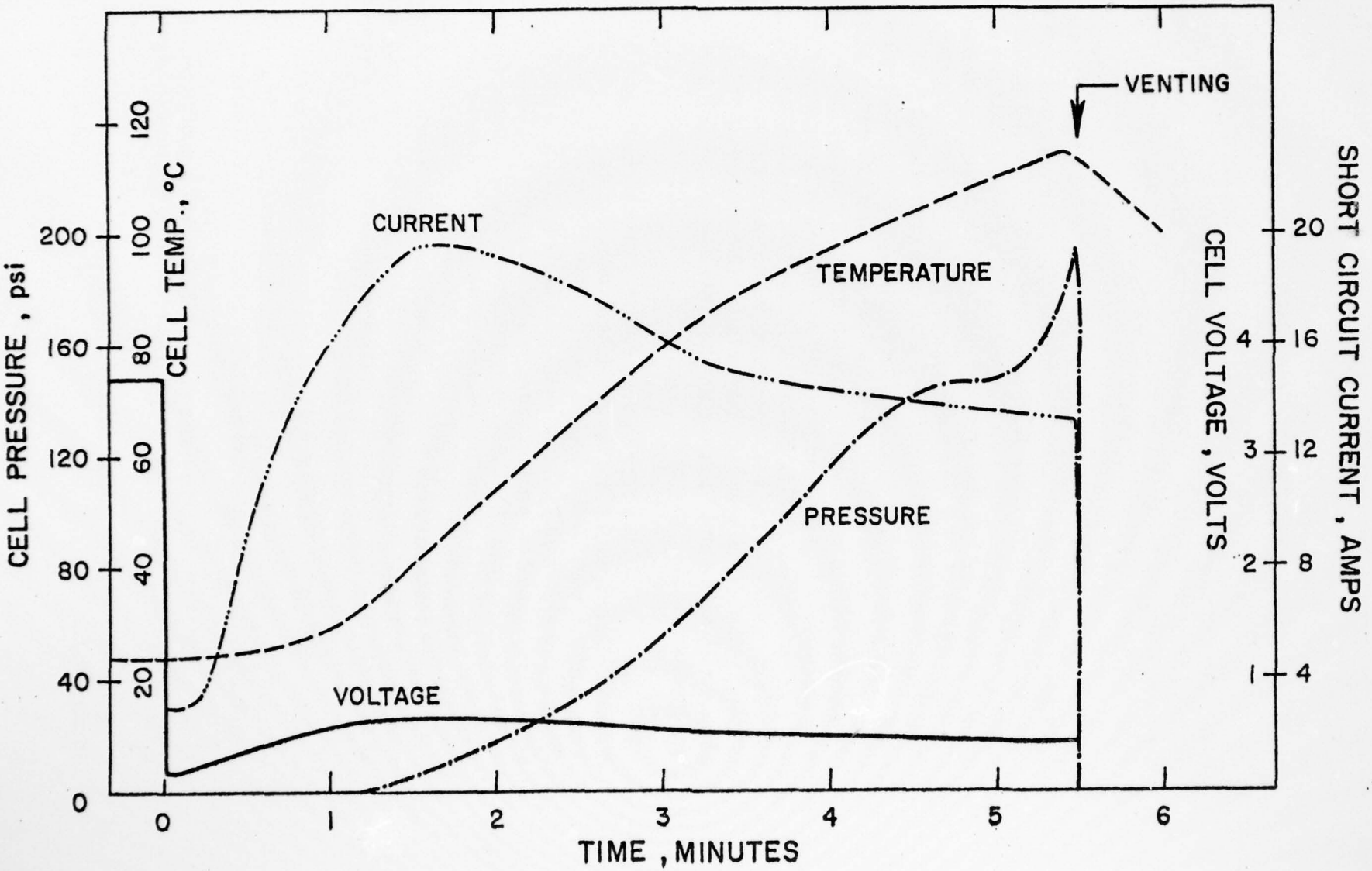

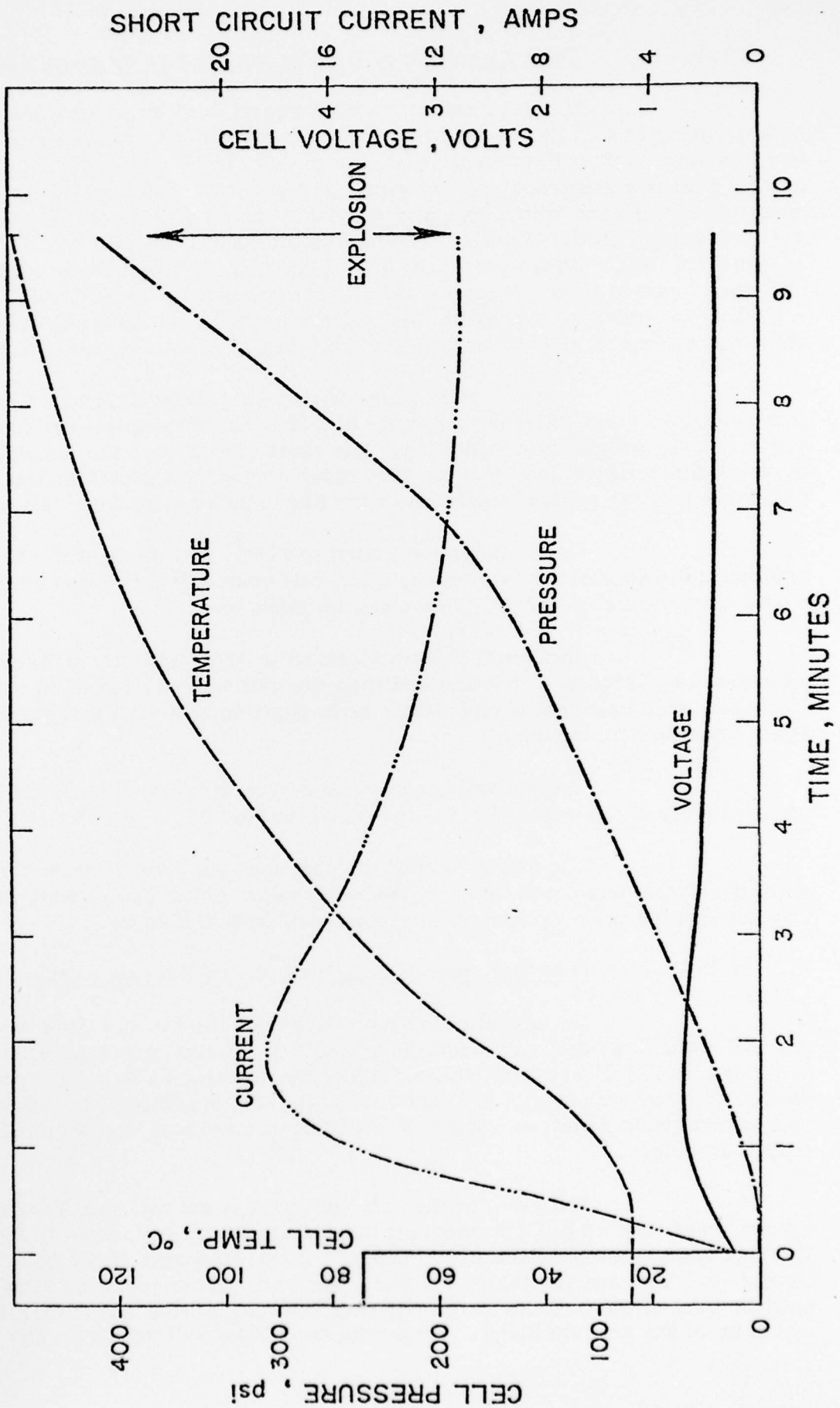

Fig. 42. Plots of Pressure, Temperature, Voltage and Current as a Function of Time on Shorting the D Cell and Venting at 400 PSI.

5.1.3 Short Circuiting of D Cells With A Low Pressure Vent

We used existing experimental vent structures developed on a company funded project in order to determine the effectiveness of low pressure venting in preventing explosions of the D cells. We carried out the first few experiments with empty D size cans fitted with these vents and pressurized the cans with a gas from a cylinder to determine the pressures at which the vent opened on the D cells. The venting pressures were 114, 126, 108, 114, 106 and 132 PSIG. These pressures were significantly lower than the 200 PSI which had been found to be the probably safe limit for venting. $Li/SOCl_2$ D cells made with this low pressure vent were then tested for explosion hazards under external shorting conditions at 25°C and 72°C. The results are discussed below.

Seven D cells were shorted externally at 25°C. The wall temperature of these cells were monitored with a thermocouple. All seven cells vented safely without any explosion. The short circuit current, the wall temperatures at which the cells vented, and the time taken to vent are shown in Table 16. Note that there is quite a bit of variation of the above parameters from cell to cell.

One D cell was heated to 72°C, and the heater was turned off and the cell was shorted externally. This cell vented in 3 minutes after shorting at a wall temperature of 117°C. There was no explosion.

Another D cell was heated to 72°C and the wall temperature was maintained at 72°C for 1.5 hours and then the cell was shorted without shutting off the heat. This cell vented one minute after shorting at a wall temperature of 105°C. Again there was no explosion.

Typical wall temperature-time plots on shorting of the cells, one at 25°C and the other at 72°C are shown in Fig. 43.

The above results indicate that explosions caused by external shorting may be prevented by using a low pressure vent. The venting time and the venting temperature appeared to vary somewhat from cell to cell.

5.1.4 Overdischarge of D Cells with Low Pressure Vents

We investigated the efficacy of the low pressure vent in preventing cell explosions that may occur as a result of a forced overdischarge that might occur in a multicell battery. This was done by discharging D cells with a low pressure vent at constant currents of 0.5 and 0.25 A and the discharge was continued after the cell voltage went negative. The cell wall temperature was monitored using a thermocouple as before.

The plots of the cell voltage and the cell wall temperature as a function of time on a 0.5 A constant current discharge are shown in Fig. 44. The cell voltage dropped sharply at the end of the discharge and dropped to approximately -0.3 volt and fluctuated a little. The cell wall temperature remained steady until the end of the cell discharge and then it began to rise and it rose to 34°C at which point the cell exploded. There was no evidence of venting. The cell was

TABLE 16.

Venting Time, Venting Temperature and Short Circuit Current of $Li/SOCl_2$ D Cells With Low Pressure Vent

Cell No.	Short Circuit Current (A)	Venting Time After the External Short (mt)	Venting Temperature °C	Remarks
251	37	5	93	No explosion
256	22	1.2	110	"
258	22	5.3	120	"
259	22	1.2	95	"
262	24	6.0	120	"
263	22	2.2	100	"
264	--	3.4	130	"

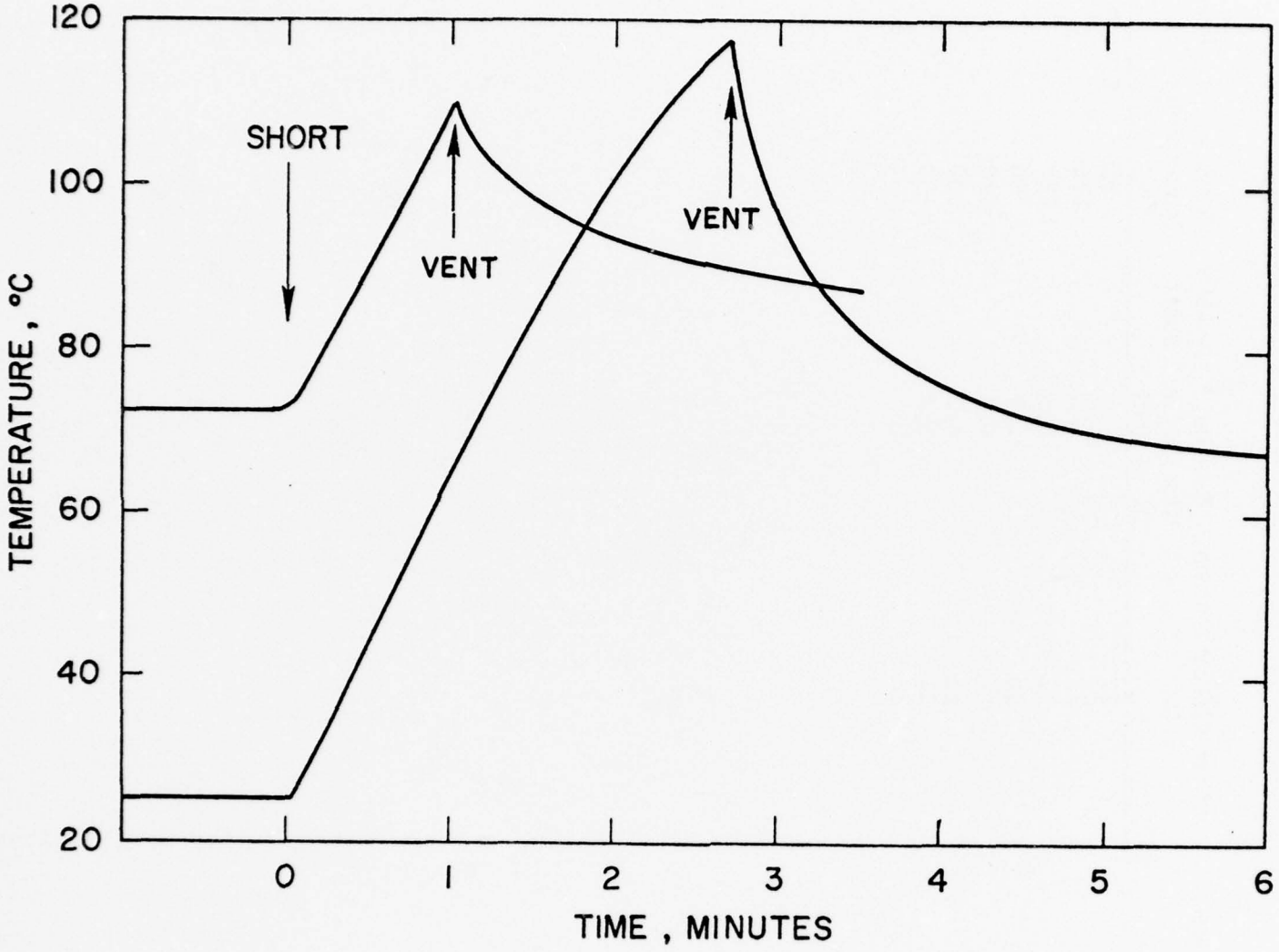

Fig. 43. Wall Temperature-Time Profile of Li/$SOCl_2$ Hermetic D Cells With Low Pressure Vent on Shorting at 25° and 72°C

Fig. 44. Cell Voltage and Cell Temperature-Time Profile of D Cells with Low Pressure Vent on Forced Discharge at 0.5A.

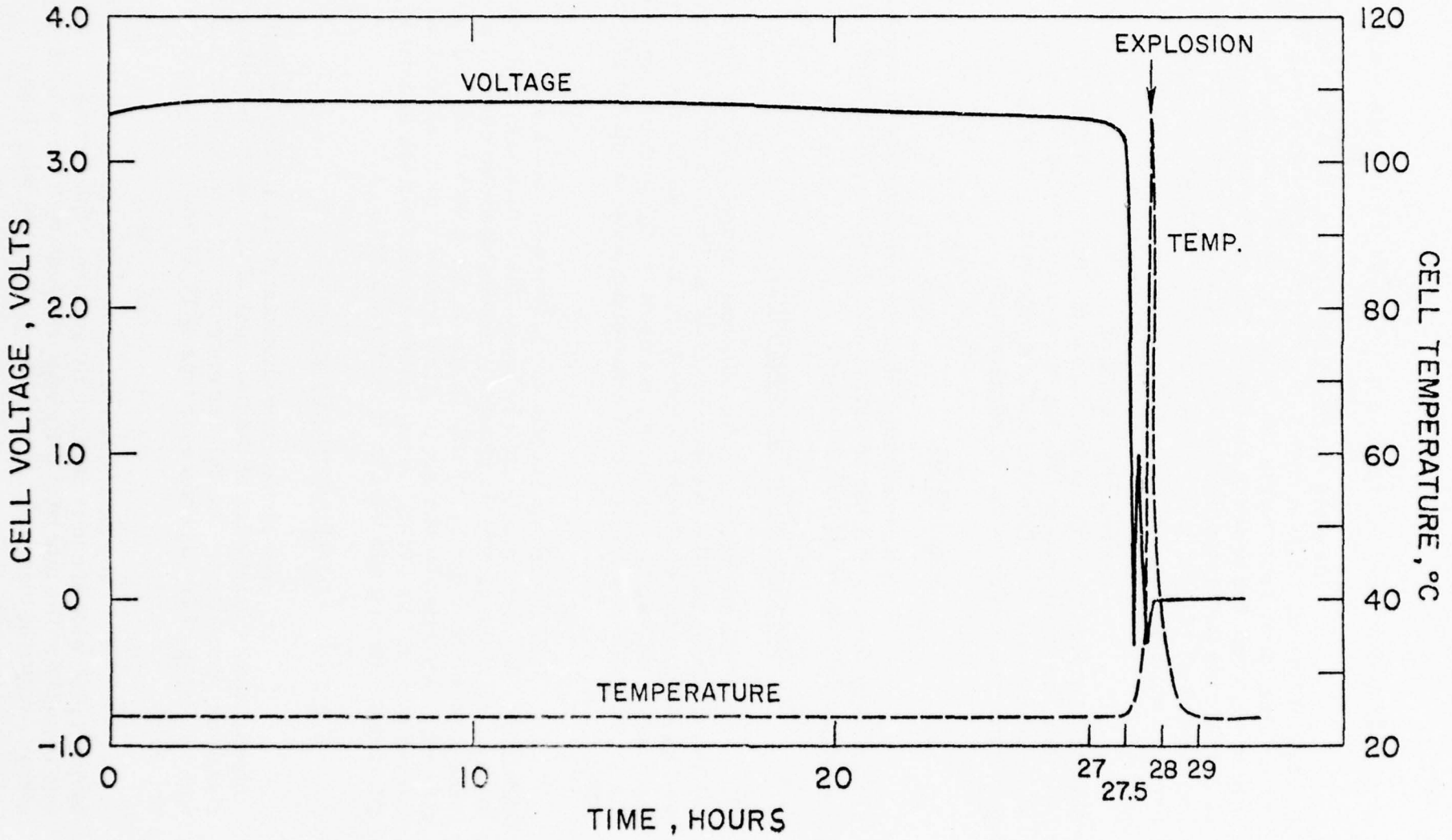

overdischarged for only 0.3 hours at 0.5 A before the cell exploded.

The plots of cell voltage and the cell wall temperature as a function of time on a 0.25 A constant current discharge are shown in Fig. 45. The cell ran for 51 hours before the voltage dropped erratically to -0.3 volt and then to -0.5 volt and began to oscillate. The cell temperature remained constant at 24°C during the discharge then began to rise at the end of the cell discharge and leveled off at 39°C in 6.5 hours of overdischarge at which point the cell exploded violently.

It should be noted that in both the above experiments, the cell wall temperature at which the cells exploded were 34 and 39°C, respectively. The cells had low pressure vents but that did not prevent the explosions. Therefore, it is reasonable to conclude that low pressure venting is not an effective means of preventing cell explosion due to overdischarge.

5.1.5 Conclusions

It was concluded that the explosion due to shorting could be prevented by the use of a low pressure vent. However, it is ineffective in preventing explosions caused by cell reversals.

5.2 Reduction of the Rate Capability

We attempted to reduce the rate capability of the D cells by decreasing the electrode lengths, keeping the width and the weight of the electrodes as well as the quantity of electrolyte constant. We evaluated the electrochemical performance as well as the explosion hazards of D cells with two sizes of electrodes viz 11.5" and 7". The length of the electrodes used for all the previous tests was 20".

All the earlier D cells had 1.5" wide Li anodes and 1.75" wide carbon cathodes. This was used in order to reduce the incidence of cell shorting during the winding of the electrode assembly. A modification of the cell winding apparatus made it possible to use 1.75" wide Li anode along with 1.75" wide carbon cathode for cell construction without any shorting problem during cell winding. The electrode lengths were 20" as before. A few cells were tested fresh in order to determine the effect this change might have on the cell capacity.

5.2.1 Electrochemical Performance

The performance characteristics are summarized in Table 17. Performance characteristics of the two types of 20" electrode cells are also included for comparison. The cell capacity-current semilog plots of the D cells with two types of 20" and one each type of 11.5" and 7" electrodes are shown in Fig. 46.

The substantial increase in the rate capability of the cells having 1.75" wide anode is particularly striking. The increase in the Li anode area was only 17%. The rate capability was increased by a factor of almost three. The energy density of the D cells on 0.25 A test was 184 Whr/lb and 13.5 WHr/in^3. In

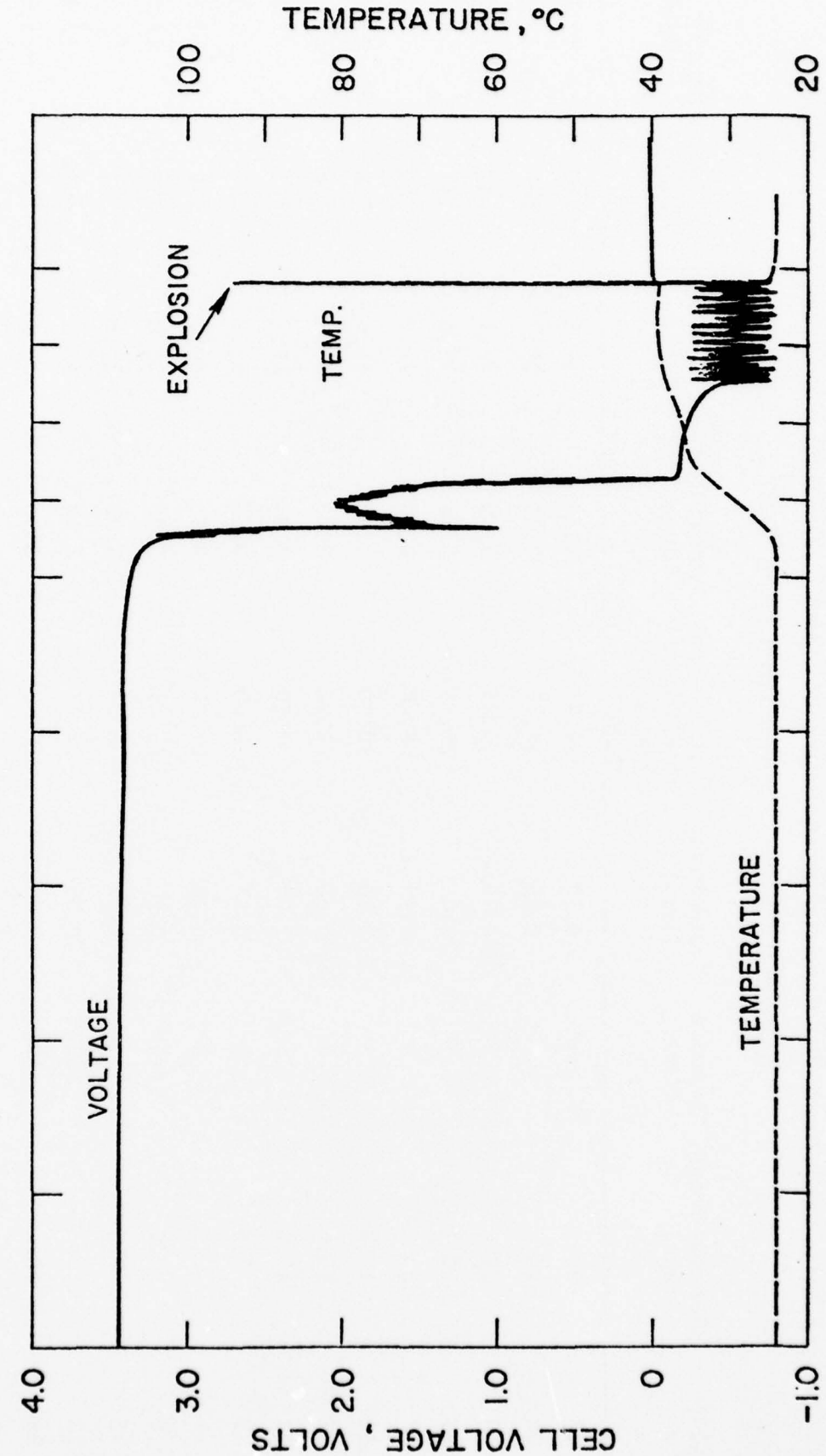

Fig. 45. Voltage and Temperature-Time Profiles of D Cells with Low Pressure Vent on 0.25A Forced Discharge.

TABLE 17.

Discharge Date of $Li/SOCl_2$ Inorganic Electrolyte D Cells with Various Electrode Lengths and Anode Widths

Cathode Width = 1.75"; Test Temperature: 25°C

Cell No.	Electrode Length (inch)	Li Anode Width	Test Current (Amps)	Cell Capacity to 2.0 volt Cutoff (A.Hr)	Average Cell Voltage	Total Energy (W.Hr)	Energy Density WHr/lb	Energy Density WHr/in^3
17	20	1.5"	0.10	11.83	3.45	40.8	176	12.9
38	20	1.5"	0.25	11.72	3.30	38.7	167	12.3
18	20	1.5"	0.50	11.25	3.30	37.1	160	11.8
26	20	1.5"	1.0	10.50	3.10	32.6	141	10.3
27	20	1.5"	3.0	8.40	2.70	22.7	98	7.2
55	11.5	1.5"	0.10	10.75	3.40	36.6	158	11.6
57	11.5	1.5"	0.50	9.25	3.20	29.6	128	9.4
58	11.5	1.5"	1.00	7.60	3.05	23.2	100	7.3
1	7.0	1.5"	0.25	8.80	3.35	29.5	127	9.3
7	7.0	1.5"	0.05	11.67	3.50	40.8	176	12.9
6	7.0	1.5"	0.1	10.81	3.40	36.8	159	11.7
5	7.0	1.5"	1.0	5.20	3.05	15.9	67	5.0
103	20	1.75"	0.25	12.7	3.35	42.5	184	13.5
95	20	1.75"	1.00	12.0	3.00	36.0	156	11.4
108	20	1.75"	0.75	13.2	3.10	40.9	177	13.0
109	20	1.75"	2.00	12.2	2.70	32.9	142	10.4
101	20	1.75"	3.00	9.7	2.55	24.7	107	7.8
104	20	1.75"	4.00	7.2	2.20	15.8	68	5.0

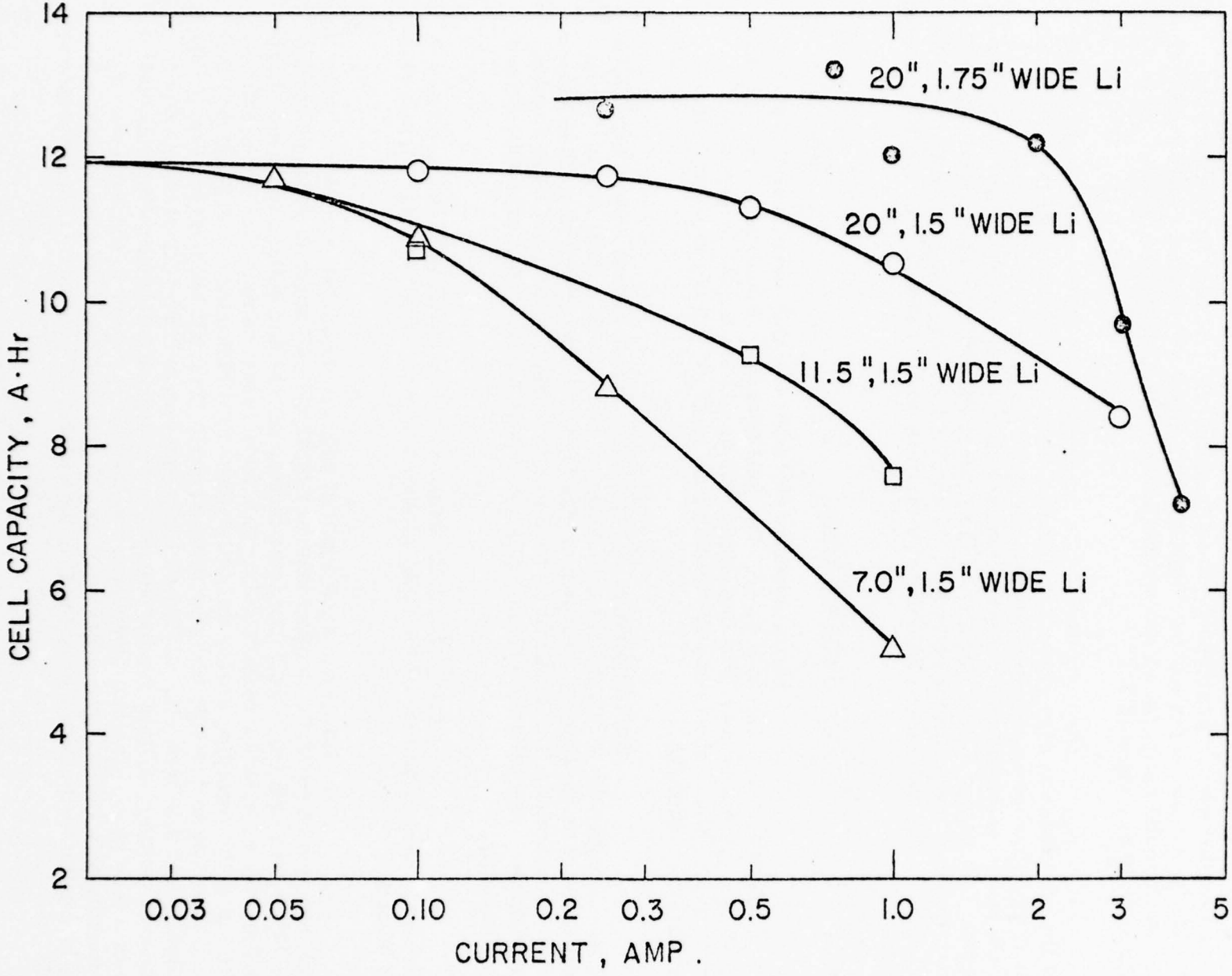

Fig. 46. Plots of Capacity Versus Logarithm of Discharge Current of the Li/$SOCl_2$ D Cells With Varying Electrode Lengths

view of the fact that the above energy densities were realized without any optimization with respect to the electrode geometries, the potentially realizable energy densities that may be achieved by suitable optimization appear to be attractive. We did in fact develop a low rate high energy density D cell on a separate program by experimental optimization and we realized energy densities of 20 WHr/in^3 and 290 WHr/lb at a drain of 0.03 A.

The reduction in rate capability with the decrease in the length of the electrodes is also shown. It is noted that at 0.05 A drain the D cell with all the three sizes of electrodes delivered the same capacity (11.7 AHr), and at 1.0 A drain the 7" electrode cell delivered almost half the capacity of the 20" electrode cells. The energy density penalty of the D cells with shorter electrodes becomes significant at some current between 0.05 and 0.10 A. The rate capability of the 7" electrode cells was almost an order of magnitude smaller than that of the 20" electrode cells.

5.2.2 Short Circuiting Tests

The temperature-time plot after the shorting of a D cell with 11.5" electrode is shown in Fig. 47. The cell temperature increased steadily after shorting, the cell vented, and then exploded, as did the D cells with the 20" electrodes. Thus, shortening of the electrode to 11.5" did not prevent the cell explosion on shorting.

The temperature and the short circuit current versus time plots of two D cells with 7" electrodes are shown in Fig. 48. The short circuit current rose sharply to 18-20 Amps and then dropped gradually to almost negligible values in twenty minutes. The temperature rose to approximately 90°C and then dropped very slowly. The behavior of both cells were quite similar both quantitatively and qualitatively.

Shorting of D cells with 7" electrodes did not lead to an explosion. The appearance of the cells remained unchanged without any visible sign of bulging.

However, when a D cell with 7" electrodes was shorted after the cell was heated to 72°C, (a simulation of accidental cell shorting while on storage at 72°C), the cell exploded. The temperature, current and voltage plots are shown in Fig. 49, a, b, and c respectively. The short circuit current shot up beyond 25 A, the top of the recording scale, the cell voltage first plummeted to 0.5 volt and then rose instantly to 1.3 volt and then dropped again. The cell temperature first dropped slightly and then took off. A slight hump in the temperature-time plot was due to the cell venting. Within approximately five minutes of cell venting the cell blew up with a loud bang. The skin temperature of the cell just prior to the explosion was approximately 130°C. The behavior of this D cell with the 7" electrode was found to be similar to the behavior of the D cells with the 20" electrodes when shorted at 25°C.

Although, the above results indicated the apparent ineffectiveness of this approach, we examined the possibility of making the D cells safe by reducing the rate capability in much more detail on another program. We found that

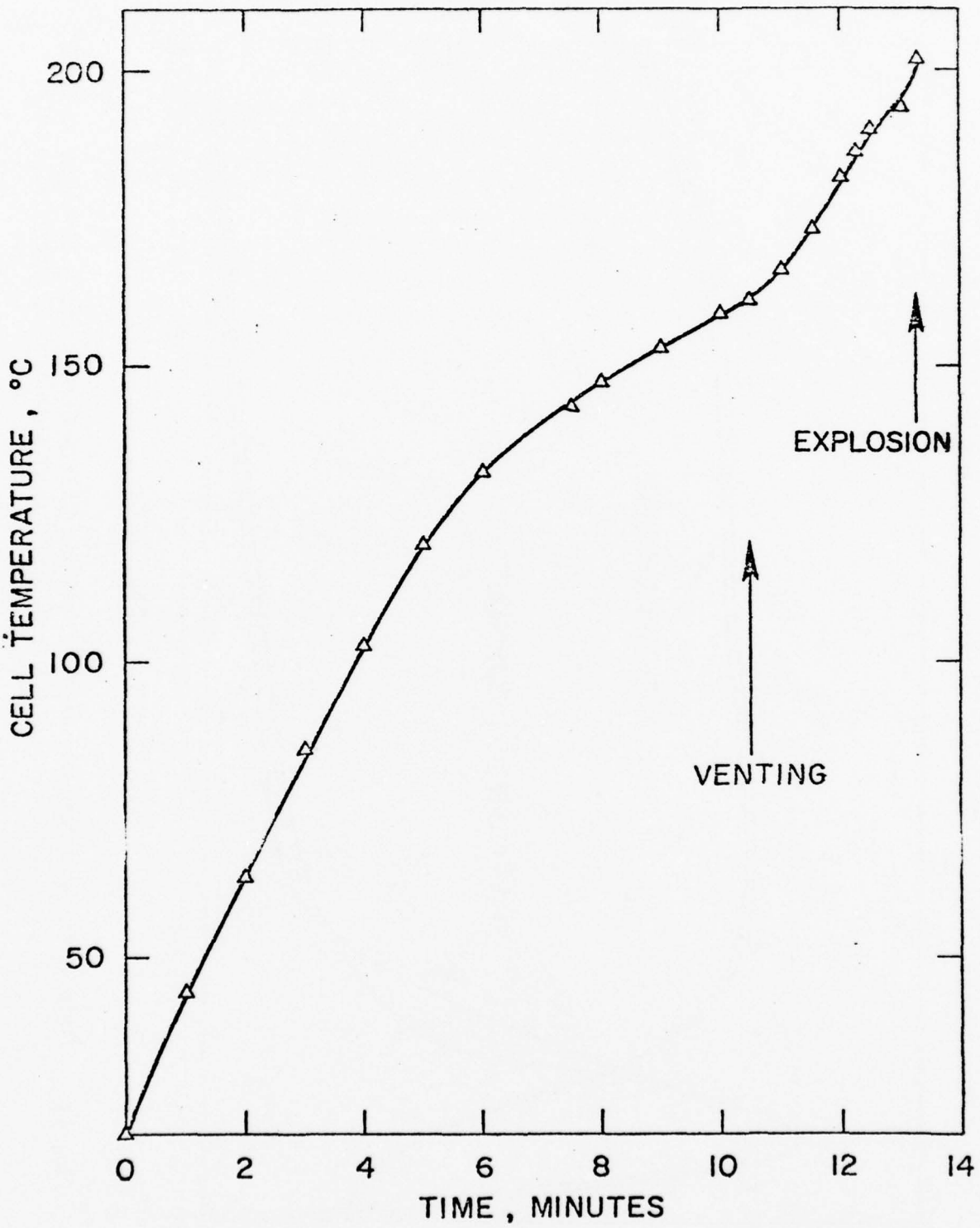

Fig. 47. Plot of the Skin Temperature of a Hermetic Li/$SOCl_2$ D Cell With 11.5" Electrode as a Function of Time After Shorting Externally.

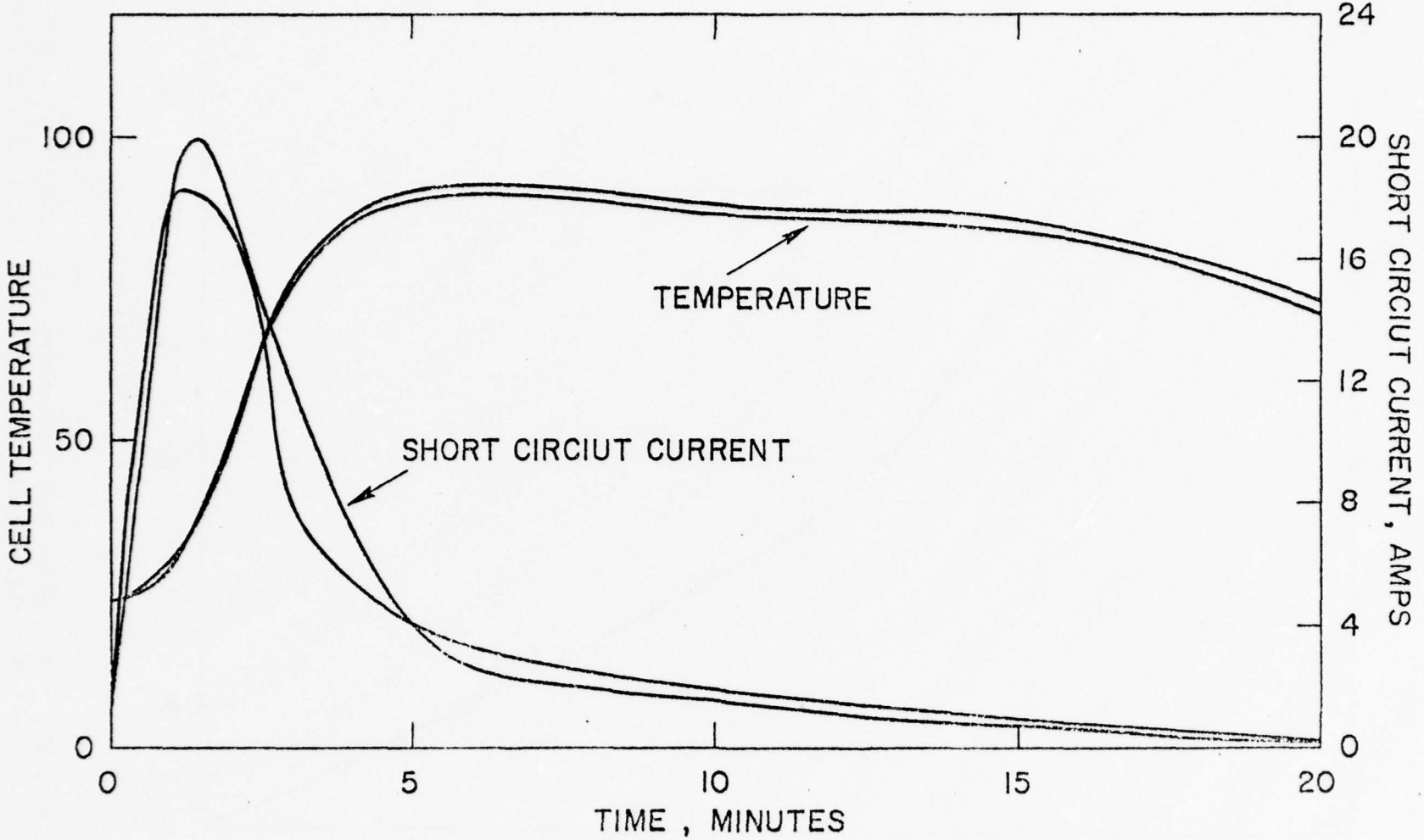

Fig. 48 Plots of the Skin Temperature and the Short Circuit Current of the Hermetic Li/$SOCl_2$ D Cells with 7" Electrode as a Function of Time After Shorting Externally.

a) Skin Temperature-Time Plot of D Cells With 7" Electrode on Pre-Heating to 72°C and Shorting

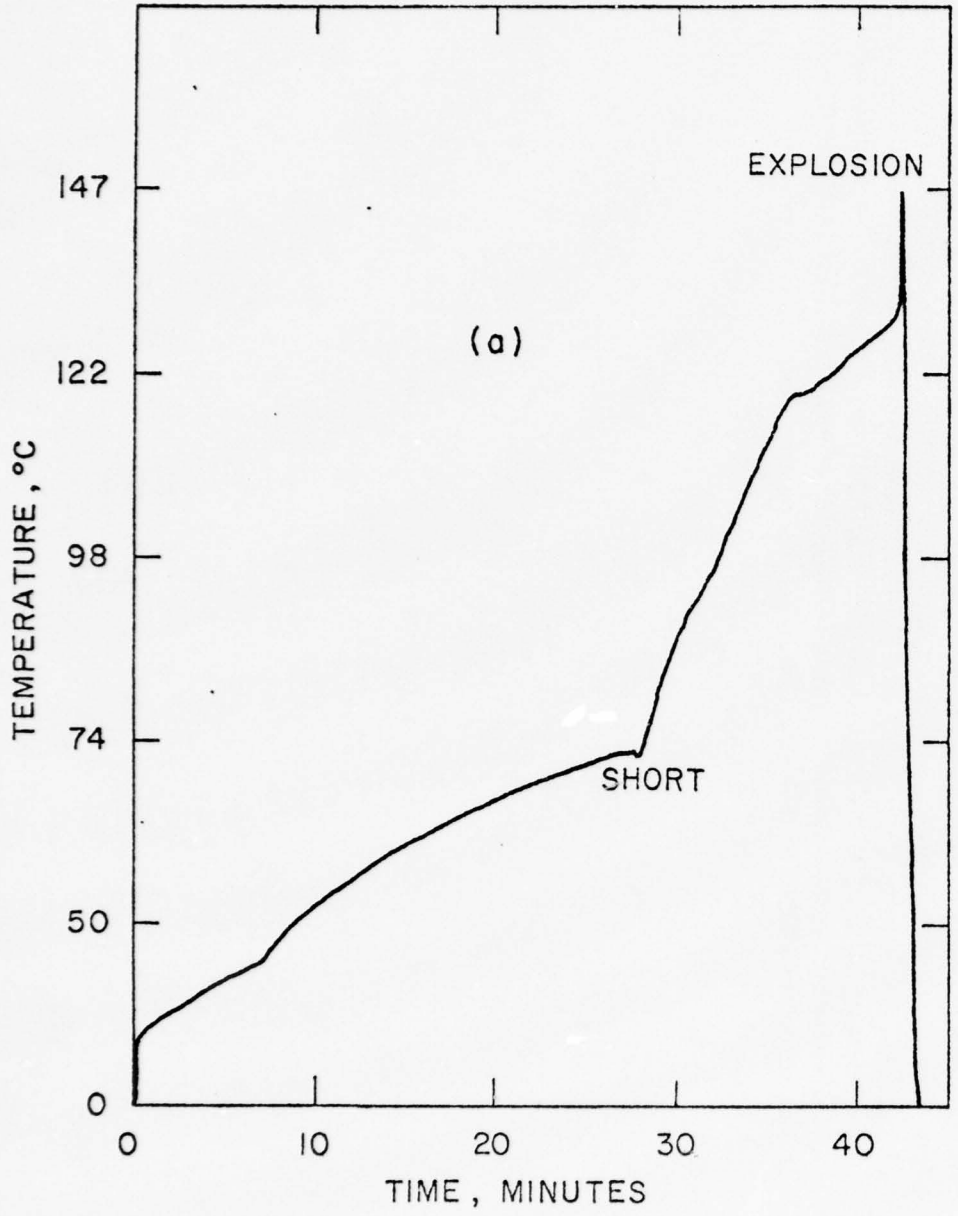

b) Current-Time Plot of the Above After Shorting

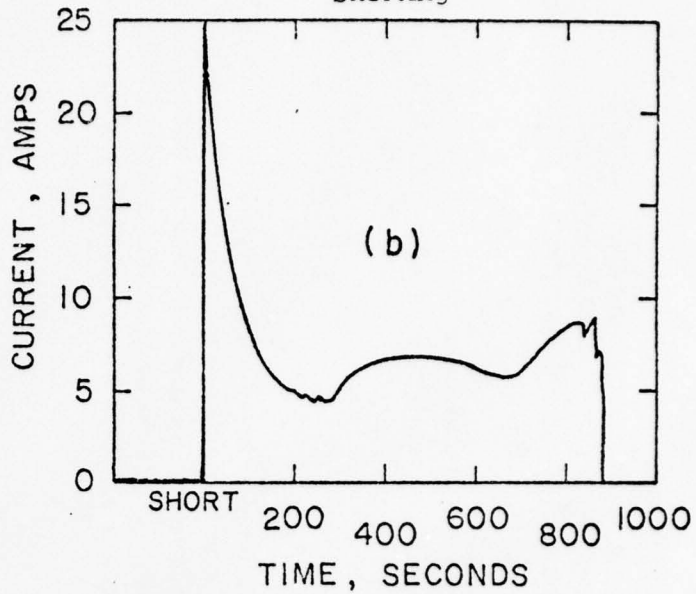

c) Voltage-Time Plot of the Above After Shorting

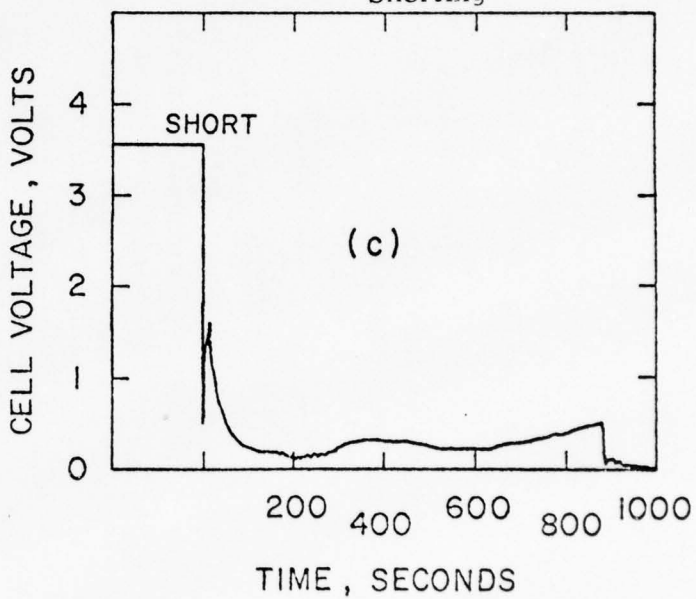

Fig. 49.

it is indeed possible to prevent any cell explosion or venting on short circuit by reducing the rate capability of the cells without sacrificing the energy density of these cells at low rate. Indeed, these cells delivered 280 WHr/lb and 18 WHr/in^3 corresponding to a cell capacity of 17-18 AHr at 0.03 A. At high rate, the safe cells performed poorly, e.g. 4 A·Hr at 1.0 A.

Unfortunately, the "safe" cells exploded on cell reversal at currents of 0.01 A and 0.03 A. The cell voltages were around -0.01 to -0.03 volts at the point of explosion.

5.2.3 Conclusion

It is possible to prevent cell explosions on external shorting by reducing the rate capability of the cells sufficiently. However, this does not prevent cell explosions on voltage reversal even at as low a current as 0.01 A from the D size cell. Voltage reversal is not an uncommon occurrence in series connected multicell batteries where one cell may have a slightly lower capacity than the others.

5.3 General Conclusions

It was shown that both the low pressure venting and the reduction of the rate capability of the cells prevented cell explosion on accidental short circuiting, but could not prevent explosion on forced overdischarge (voltage reversal) even at currents as low as 0.01 A for the D cell. This restricts the use of the present generation of $Li/SOCl_2$ cells to a single cell application, since series connected multicell batteries are liable to cause voltage-reversals in cells having a slightly lower capacity than the others.

6. Task V - Thermochemical Studies of Pressure Producing Reactions

The deficiencies of the physical approaches in rendering the $Li/SOCl_2$ D cell safe on voltage reversal and the reported infrequent incidence of spontaneous explosion of partially discharged cells on storage (with or without a resistive load) led us to consider the thermo-chemical approach for the solution of the safety problem. The premise is that an understanding of the chemistry and thermochemistry of the chemicals present in the $Li/SOCl_2$ cell at the various states of storage and discharge will ultimately be useful in formulating an acceptable solution to the general problem. As a first step we carried out Differential Thermal Analyses (DTA) of the chemical compounds and their mixtures that may be present in a partially discharged $Li/SOCl_2$ cell. The objects were (a) to identify the exothermic combinations that could initiate and propagate an explosive reaction, (b) to determine the temperature at which these could occur, and (c) to distinguish between exothermic thermal runaways and endothermic pressure bursts.

We also carried out exothermicity measurements on the various chemicals (present in partially discharged cells) when combined at room temperature. This is different from DTA in that the temperature rise of the various chemical combinations will be measured at room temperature. The purpose was to identify the chemical species which could spontaneously start an exothermic reaction inside the cell to provide the high temperature needed locally for the thermal runaway. Once the specific chemicals which may trigger the spontaneous explosions are identified, it may then be possible to control them by chemical and/or physical means.

In addition we carried out differential thermal analyses of discharged hermetic $Li/SOCl_2$ D cells to characterize the nature of the instability that is generated on discharge with the hope of finding ways and means to stabilize the cells.

6.1 Differential Thermal Analysis of $Li/SOCl_2$ Cell Constituents

Our initial results on the DTA analysis of the cell reaction products indicated that the technique was useful in distinguishing between a pressure burst and a thermal runaway. The former was endothermic, whereas the latter was exothermic. The technique was also found to be useful in determining the temperatures at which the above processes are likely to occur. However, the interpretation of some of the results was complicated because of the reactivity of the thermocouple wire (chromel-alumel) with the chemical to be analyzed. The sample container

used, as shown in Fig. 50, was a sealed glass ampoule with Pt wire feed-through, the thermocouple wires were welded to the Pt wires inside the ampoule. We chose a sealed sample container as opposed to an open glass tube, as is customary for DTA analysis, because of the reactivity of relatively volatile $SOCl_2$. The physical contact of the thermocouple wires with the chemicals increased the sensitivity of the measurements, but it also allowed the thermocouple wires to be attacked by reactive substances, particularly, S. We found that the DTA thermograms of S resulted in exothermic peaks corresponding to its reaction with the thermocouple wires which were found to be disintegrated at the end of the run. In order to avoid this problem, we re-designed the sample container so that the thermocouple wires are physically isolated from the chemicals. The details of the design of the sample container and the results of the DTA analysis of the various cell reaction products using the container are discussed below.

We also found that the furnace, provided for the DTA analysis of corrosive chemicals, was too fragile to withstand the minor explosions resulting from the experiments. We designed and fabricated a new furnace using an aluminum body instead of pyrex.

6.1.1 Experimental

A cross sectional view of the new sample container is shown in Fig. 51. It has a thermocouple well at one end of the container. The thickness of the glass of the thermocouple well was kept at a minimum in order to maintain a reasonable sensitivity. The sample container was filled with the desired chemicals from the end opposite the thermocouple well and was frozen using liquid nitrogen and then evacuated and sealed with a flame. The absence of any feed-through ensured the hermeticity of the containers. Leaky containers result in spurious endotherms.

The earlier furnace was modified by replacing the pyrex body with a thick-walled aluminum cylinder (Fig. 52). Also, the furnace was used in an inverted position in order to ensure that the chemicals in the sample container remain in contact with the thermocouple well.

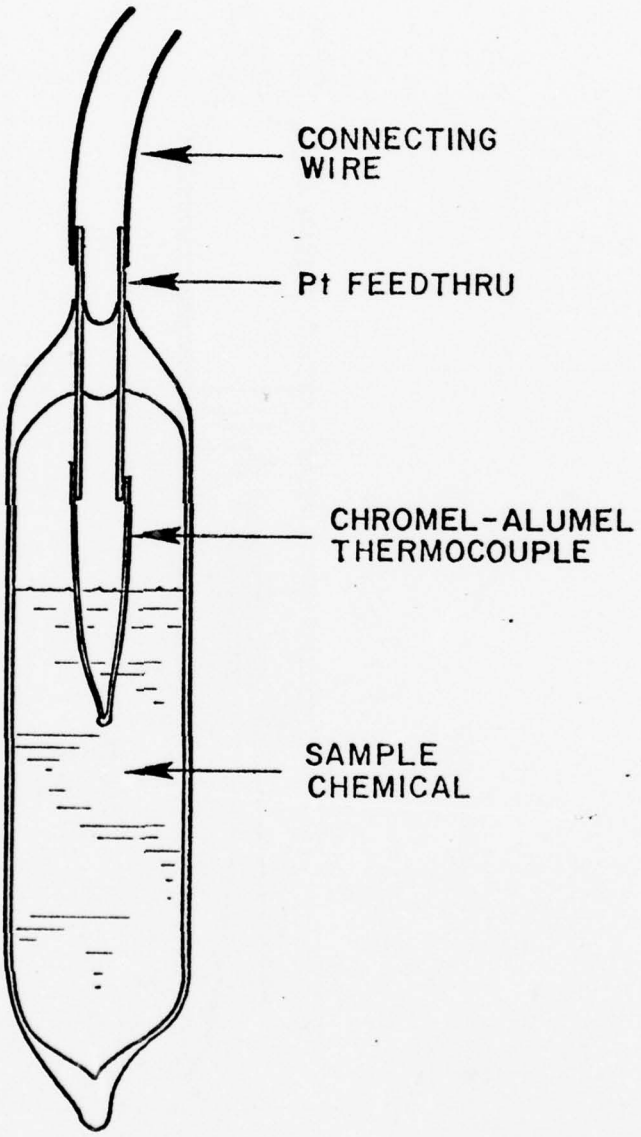

Fig. 50. Cross sectional view of the hermetic sample container

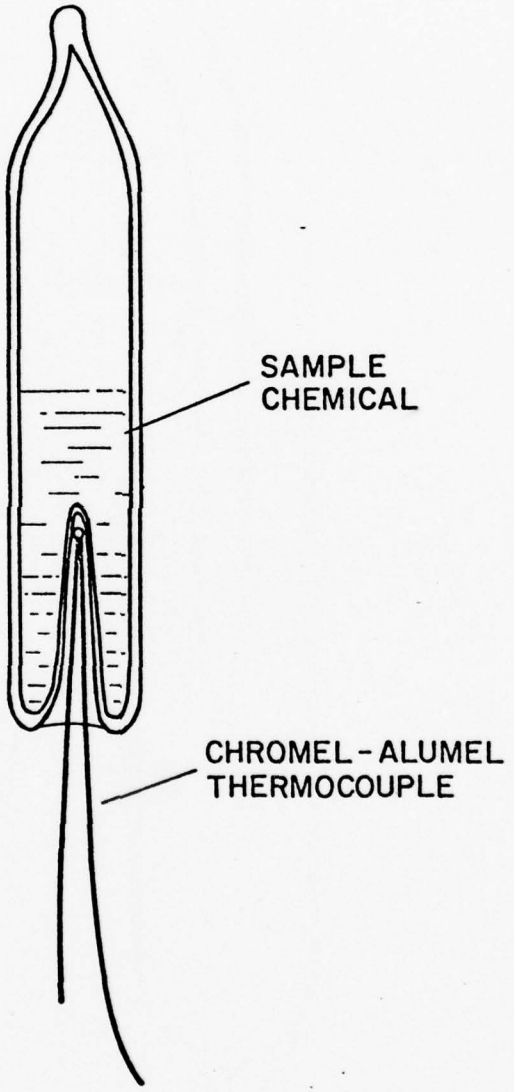

Fig. 51. The Sample Container with a Thermocouple Well

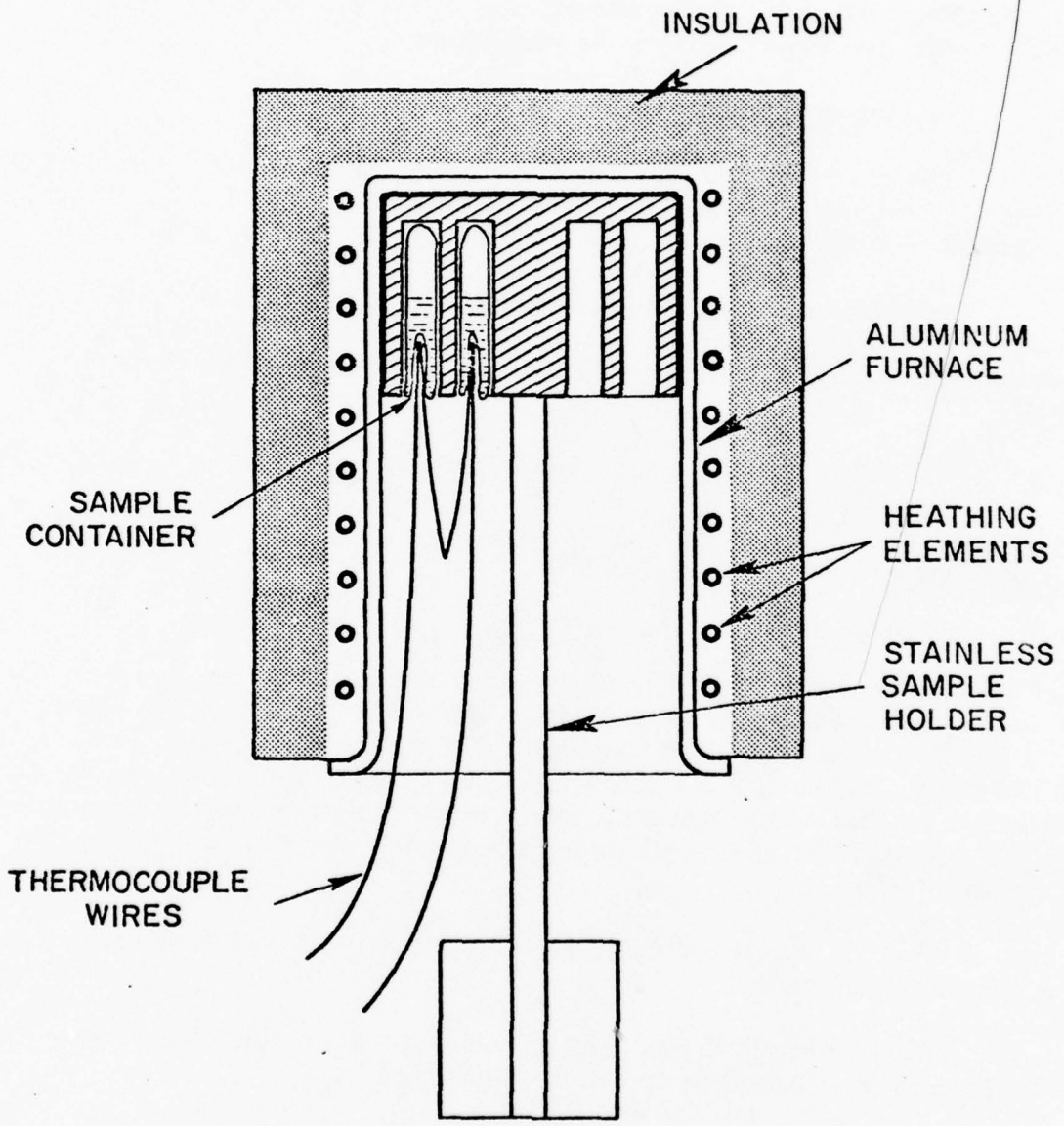

Fig. 52. Cross-Sectional View of the DTA Furnace with the Sample Holder

The sample temperature was increased from room temperature (25°C) to a maximum of 300°C, at an average rate of 10°C/minute. The linearity of the temperature-time profile was found to be adequate for our purpose. Both the sample temperature and the differential temperature were recorded in a dual channel strip chart recorder. The reproducibility of the measurements was checked by replication, and it was found to be satisfactory.

6.1.2 Results and Discussion

The chemical species known or presumed to be present in the partially discharged Li/$SOCl_2$ cells are: Li, $SOCl_2$, $LiAlCl_4$, sulfur, SO_2, LiCl, Li_2SO_3, Li_2S, Glass, Carbon, Teflon, Nickel, Kovar, and Trace Impurities (H_2O, etc.).

In addition, transient species may be present that are formed from the primary cell reaction product, SO, (18). In addition to SO they include $(SO)_2$, S_2O and polymeric $(S_mO)_n$ which may be formed as a result of the chemical reactions 16-19.

$$2Li + SOCl_2 \longrightarrow 2\ LiCl + SO \quad (16)$$

$$2SO \longrightarrow (SO)_2 \quad (17)$$

$$(SO_2) + SO \longrightarrow S_2O + SO_2 \quad (18)$$

$$(S_2O)_x \longrightarrow (S_mO)_n + SO_2 \quad (19)$$

Any and all of the above species, along with the other chemical species that may have been formed by chemical interactions between the above listed species, may be responsible for the initiation and the propagation of the thermal runaway encountered in the thionyl cells. For our initial studies we restricted ourselves to the stable chemical species. Our first objective was to identify the potential species or combination of species that may cause either a pressure burst and/or a thermal runaway on external heating.

The DTA results of the above stable materials and their various combinations are discussed here.

The blank DTA thermogram of two Al_2O_3 specimens are shown in Fig. 53 which represent a base line for all the thermograms.

1. Lithium

The DTA thermogram of pure Li (0.015 gm) at 5°C/min heating rate is shown in Fig. 54. The endotherm at 180°C represent the melting of Li and the two sharp exotherms at 195° and 202° represent the exothermic reaction between Li and the glass sample container. The glass sample container broke and stuck to the sample holder. The results indicate that the Li-glass reaction is a potential contributor to the thermal runaway.

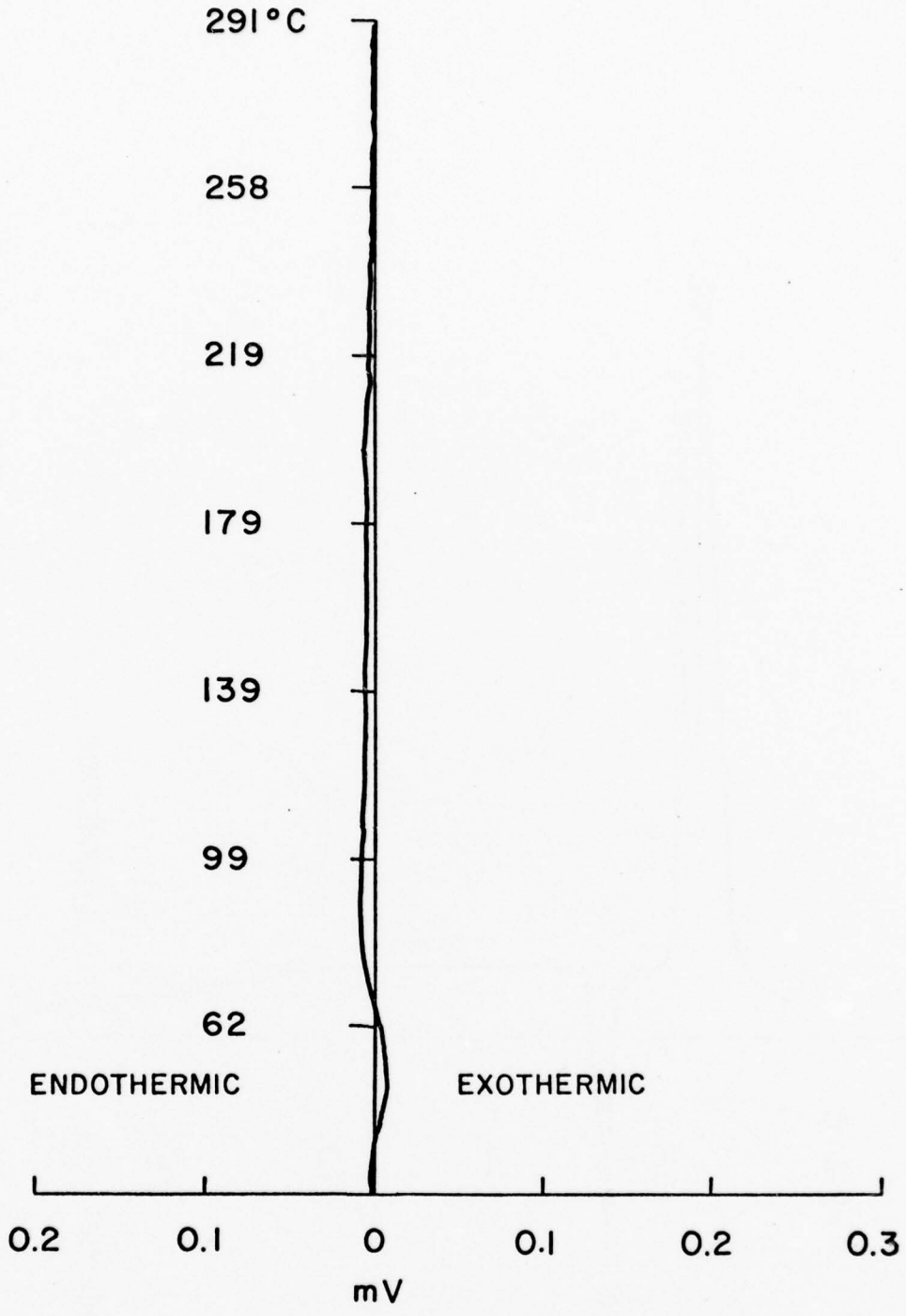

Fig. 53. Thermogram of Al_2O_3 Sample (Blank)

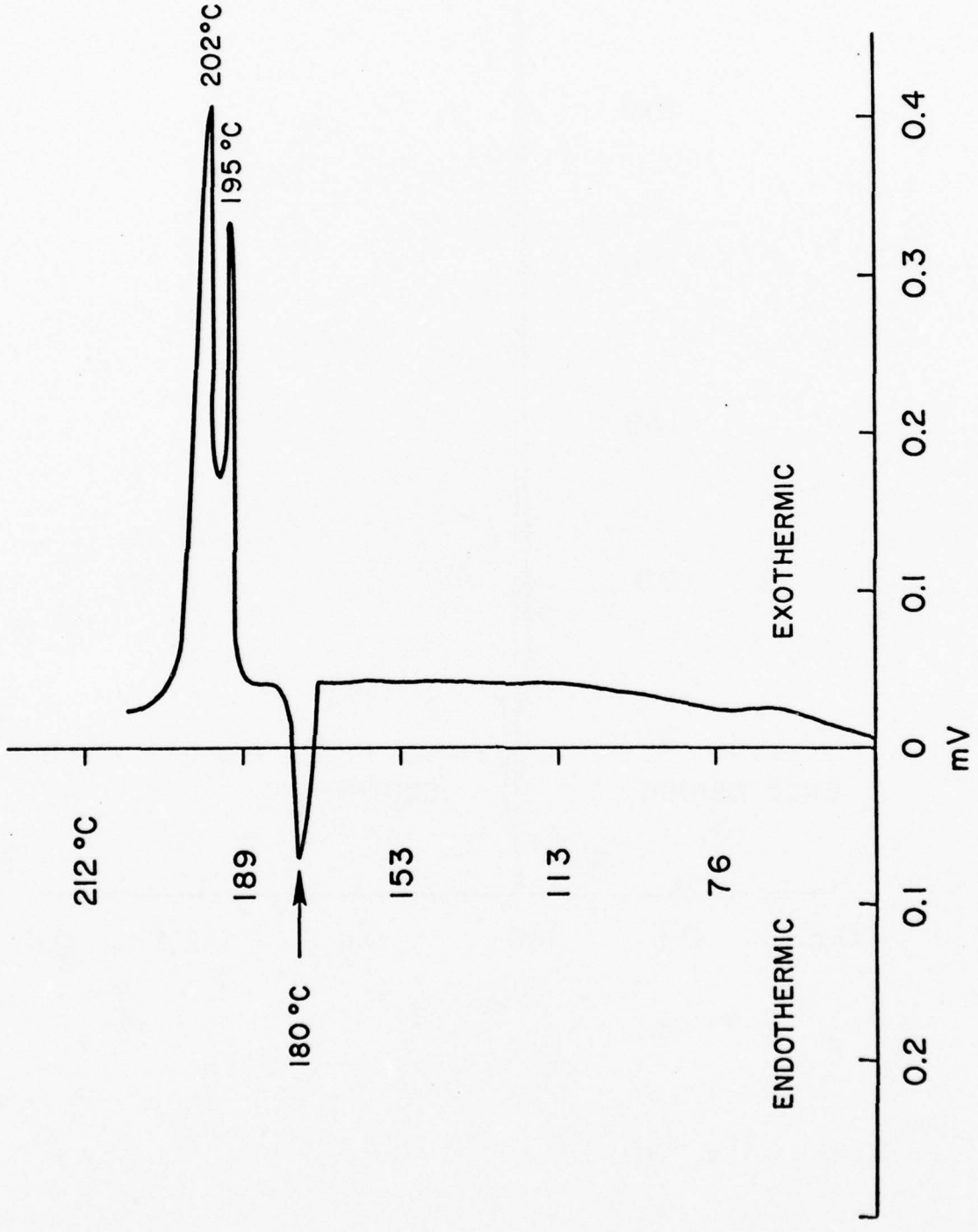

Fig. 54. Thermogram of Li, Sample #101

2. Sulfur

The thermogram of S (0.12 gm) at 5°C/min. is shown in Fig. 55. The broad endothermic transition at 45° represent the base line drift due to thermal lag of the sample and not a real transition. The two real endothermic transitions at 106° and 121°C represent the melting of two types of sulfur e.g. rhombic (α) and monoclinic (β).

3. Thionyl Chloride ($SOCl_2$)

The thermogram of $SOCl_2$ (0.161 gm) at 5°C/min heating rate is shown in Fig. 56. There is no transition prior to the endothermic bursting of the sample at 231°C, most likely due to the pressure generated by the decomposition of $SOCl_2$ to SO_2 and Cl_2, known to occur at elevated temperatures.

4. Carbon Cathode

The thermogram of carbon cathode (0.023 gm) at 5°C/min did not show any transition indicating that the material is stable in glass sample container within the temperature range examined.

5. Electrolyte Salt ($LiAlCl_4$)

The thermogram of $LiAlCl_4$ (0.142 gm) at 5°C/min heating rate is shown in Fig. 57. The endotherm at 118°C represents the melting of $LiAlCl_4$. The materials appear to be stable.

6. Lithium Chloride (LiCl)

The thermogram of LiCl (0.118 gm) at 5°C/min is shown in Fig. 58. The small endotherm at 143°C probably represents dehydration.

7. Lithium Sulfide (Li_2S)

The thermogram of Li_2S (0.043 gm) at 10°C/min heating rate is shown in Fig. 59. There is no transition within the temperature range examined.

8. Lithium Sulfite (Li_2SO_3)

The thermogram of Li_2SO_3 (0.079 gm) as received from supplier (Fisher Scientific) is shown in Fig. 60 at 10°C/min heating rate. The endotherms at 183° and at 214°C represent dehydration as the material was in the hydrated form. The thermogram after vacuum drying at 75°C for 8 hours still showed those two endotherms indicating inadequate drying. The thermogram after vacuum drying at 135°C for 20 hours showed no endothermic transitions indicating completion of the drying of Li_2SO_3.

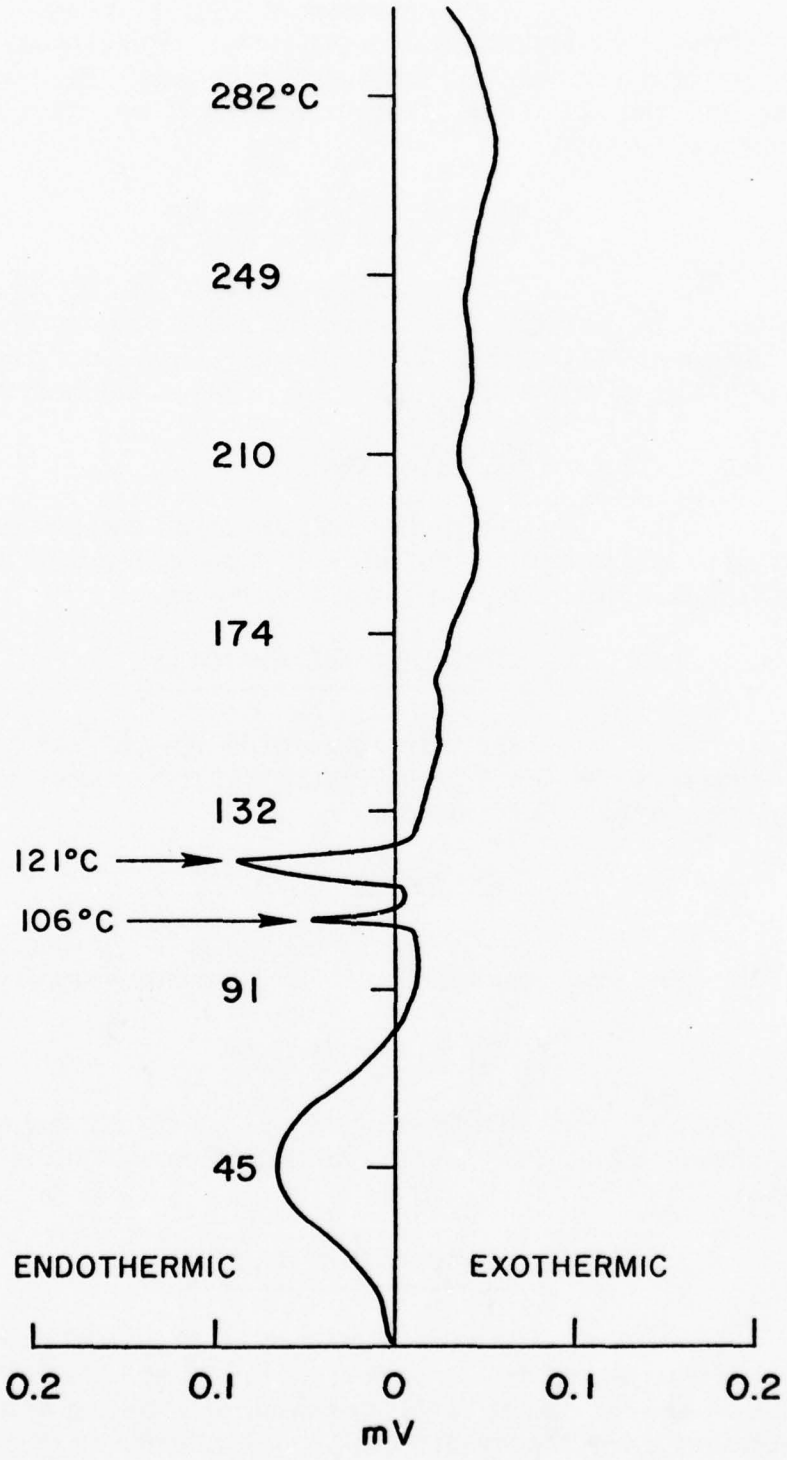

Fig. 55. Thermogram of S, Sample #102

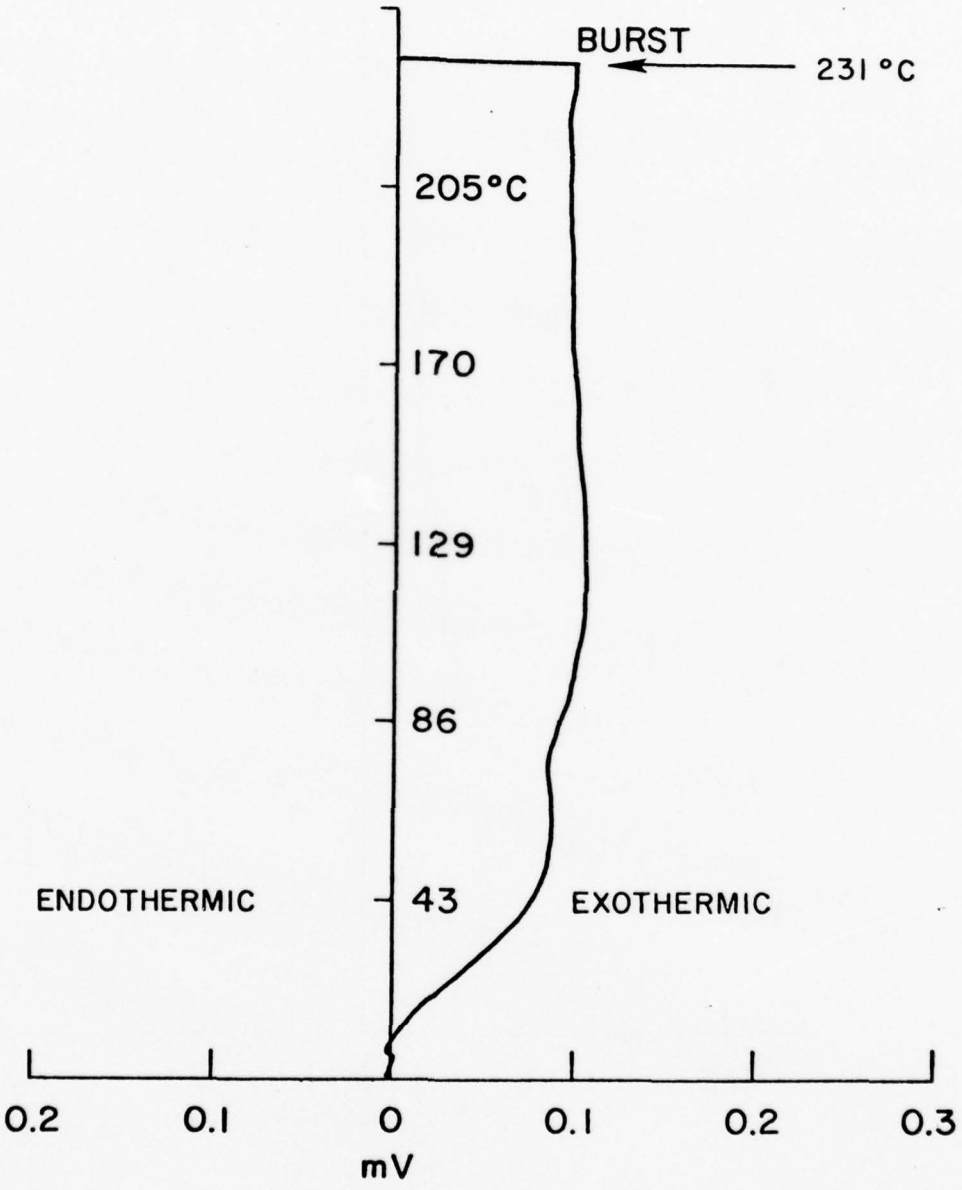

Fig. 56. Thermogram of $SOCl_2$, Sample #105

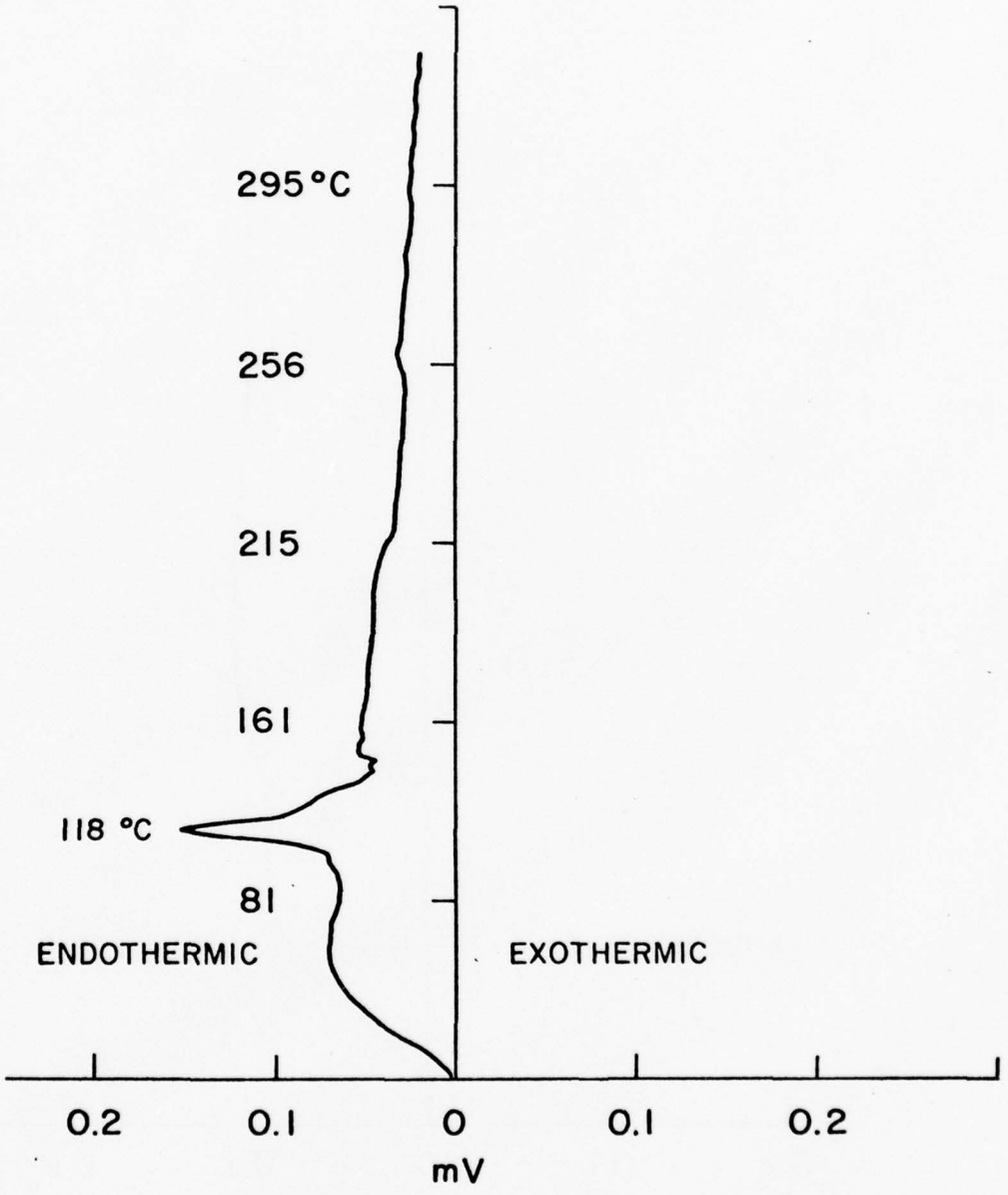

Fig. 57. Thermogram of $LiAlCl_4$, Sample #112

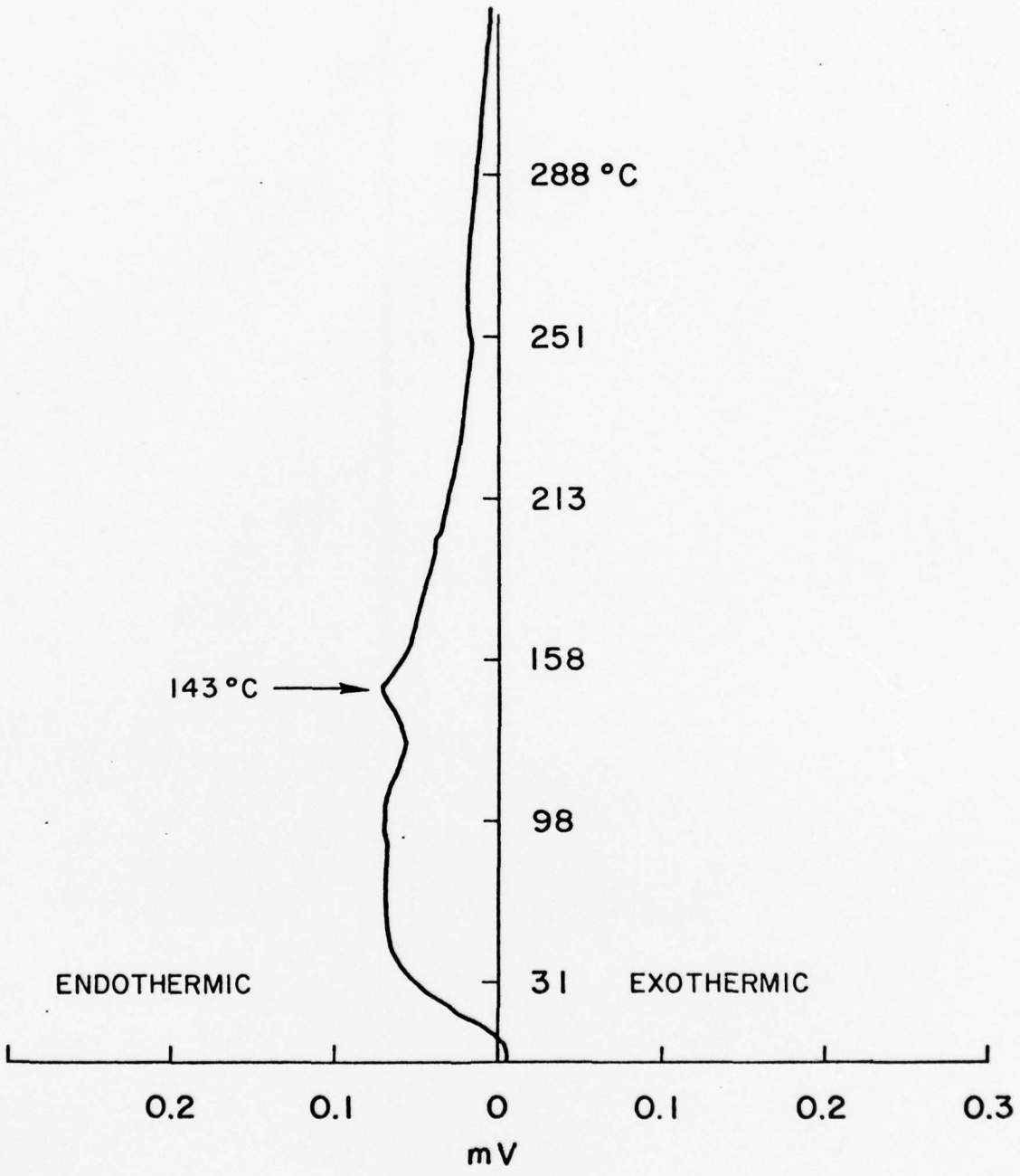

Fig. 58. Thermogram of LiCl, Sample #113

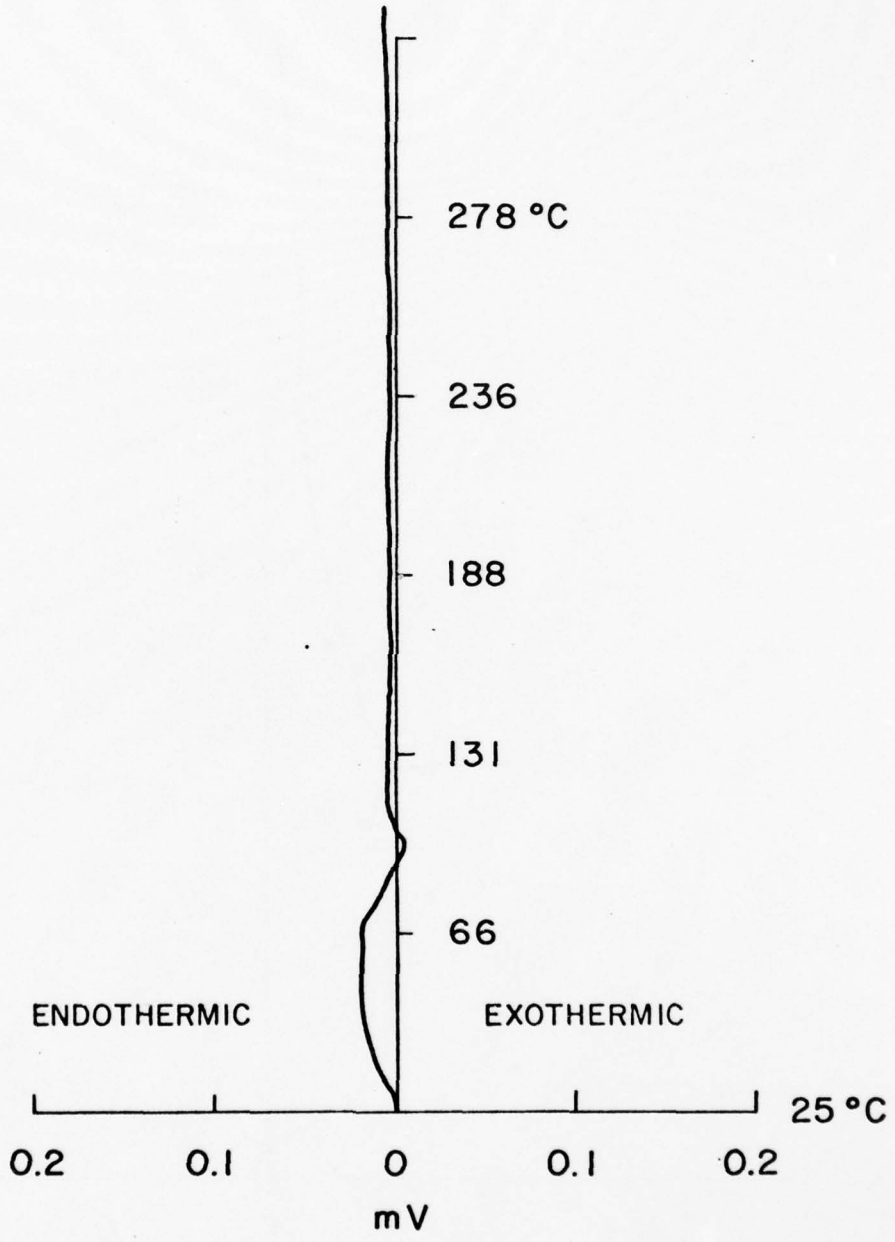

Fig. 59. Thermogram of Li_2S, Sample #37

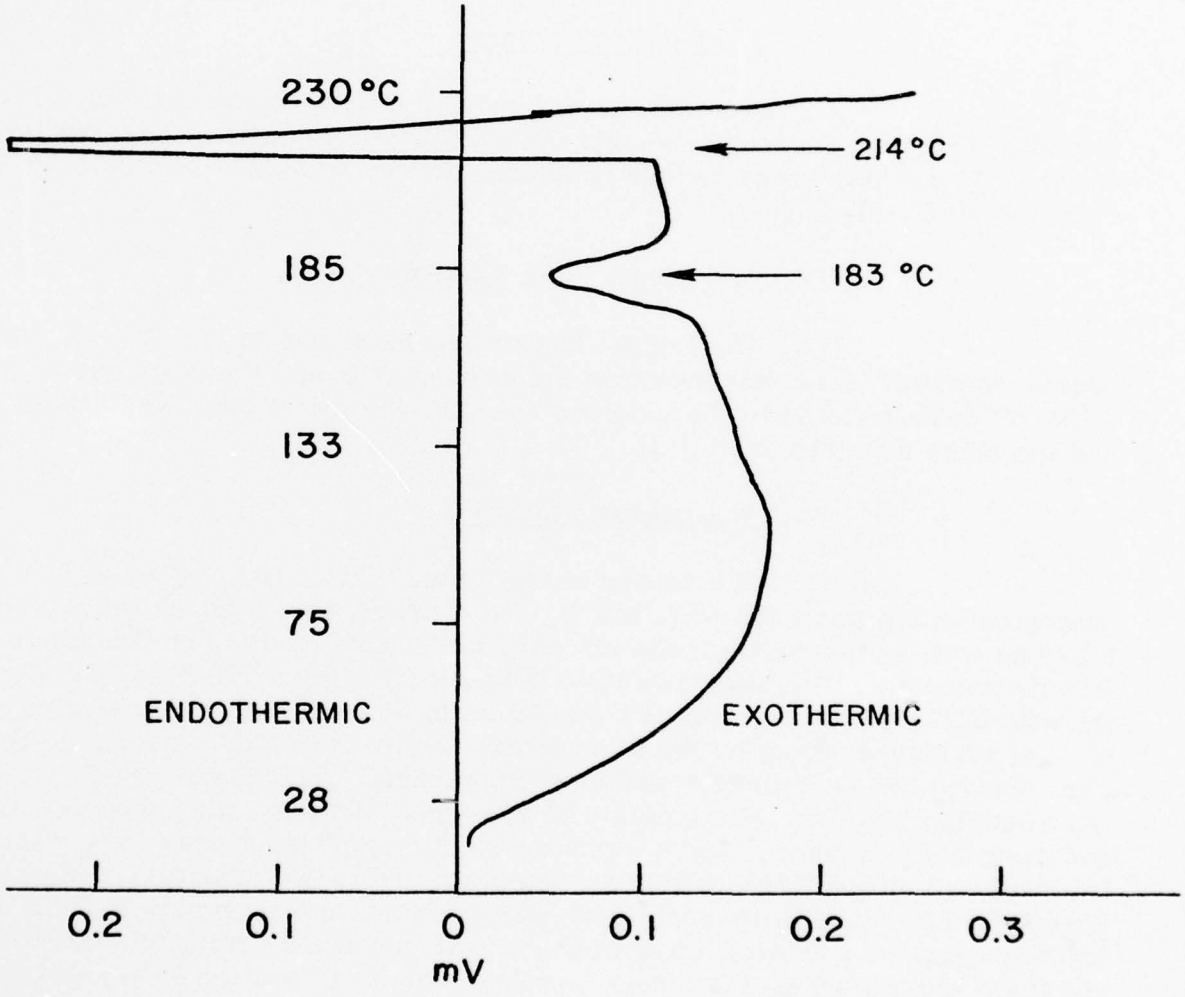

Fig. 60. Thermogram of Li_2SO_3, Sample #60

9. Lithium Oxide (Li_2O)

The thermogram of Li_2O (0.043 gm), as shown in Fig. 61, showed no transitions indicating its thermal stability.

10. $Li + SOCl_2$

A typical thermogram at 10°C/min is shown in Fig. 62. The endothermic transition at 189°C represents melting of Li and the exothermic blast at 227°C represents a thermal runaway.

11. Li + Carbon Cathode

A typical thermogram (10°C/min) is shown in Fig. 63. The endotherms at 184°C represent Li melting; the exothermic transitions represent the reaction of Li with the glass sample container which was found to be cracked and stuck to the sample holder.

12. Li + Glass Paper (Separator)

The typical thermogram as shown in Fig. 64 indicates an endotherm at 187°C corresponding to the melting of Li and the large exotherms at 208°C corresponding to the vigorous combustive type of reaction between Li and the glass separator material.

13. Thermograms of Li + S

We carried out DTA analyses of 10 samples of Li + S having various proportions of Li and S. The purpose was to check the reproducibility as well as to ascertain any effect of the sample weights on the nature of DTA thermograms. One representative thermogram is shown in Fig. 65. The reproducibility of the thermograms was found to be excellent. The relative weights of Li and S had no effect on the thermograms within the limits examined. The thermogram showed two endothermic peaks at approximately 112°C and 122°C, corresponding most likely to the melting points of two types of sulfur, viz, rhombic (113°C) and monoclinic (120°C). There was a very large exothermic peak, occurring in the temperature range of 150° to 184°C, corresponding to a combustion. The heat generated during this exothermal peak was such that the temperature of the sample holder increased by 10°C. Most of the Li was consumed during this combustion, and there was no endothermic peak corresponding to Li melting at higher temperatures.

The data indicated that the exothermic Li + S reaction occurs at a temperature higher than the melting point of S and lower than the melting point of Li when they are present in a dry state. The Li was used as a foil and the S was in powder form.

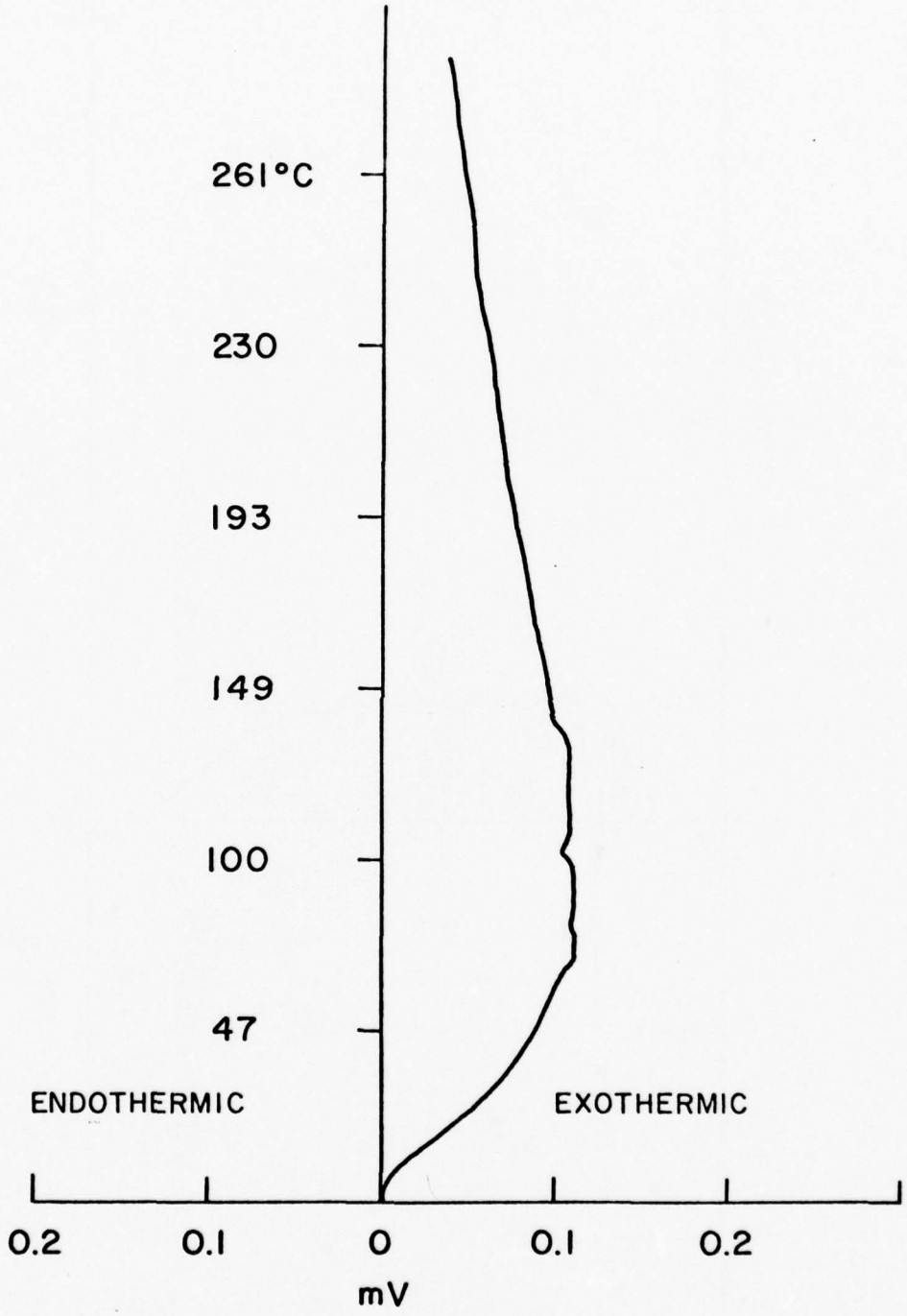

Fig. 61. Thermogram of Li_2O, Sample #73

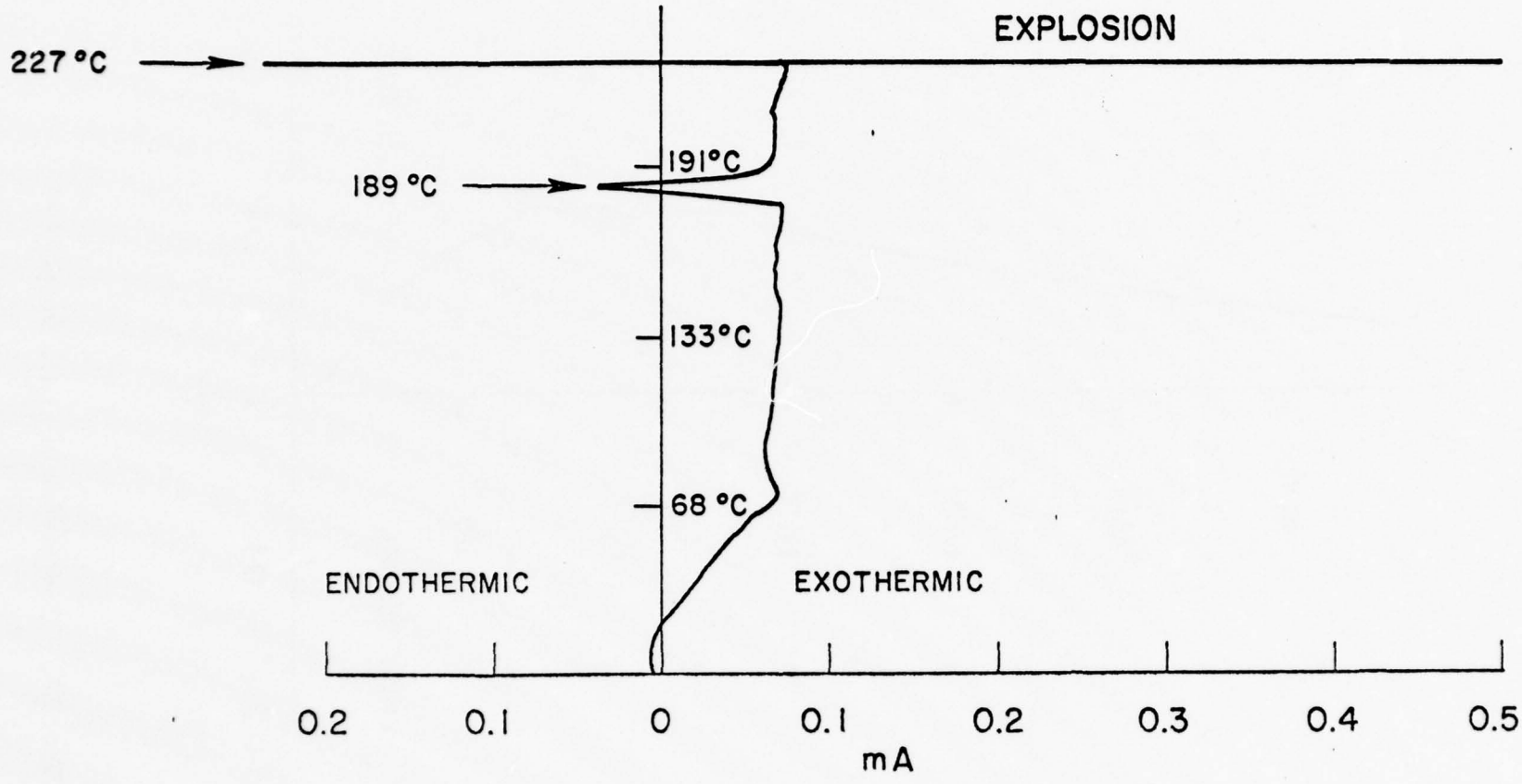

Fig. 62. Thermogram of Li (0.013) + $SOCl_2$ (0.167), Sample #26

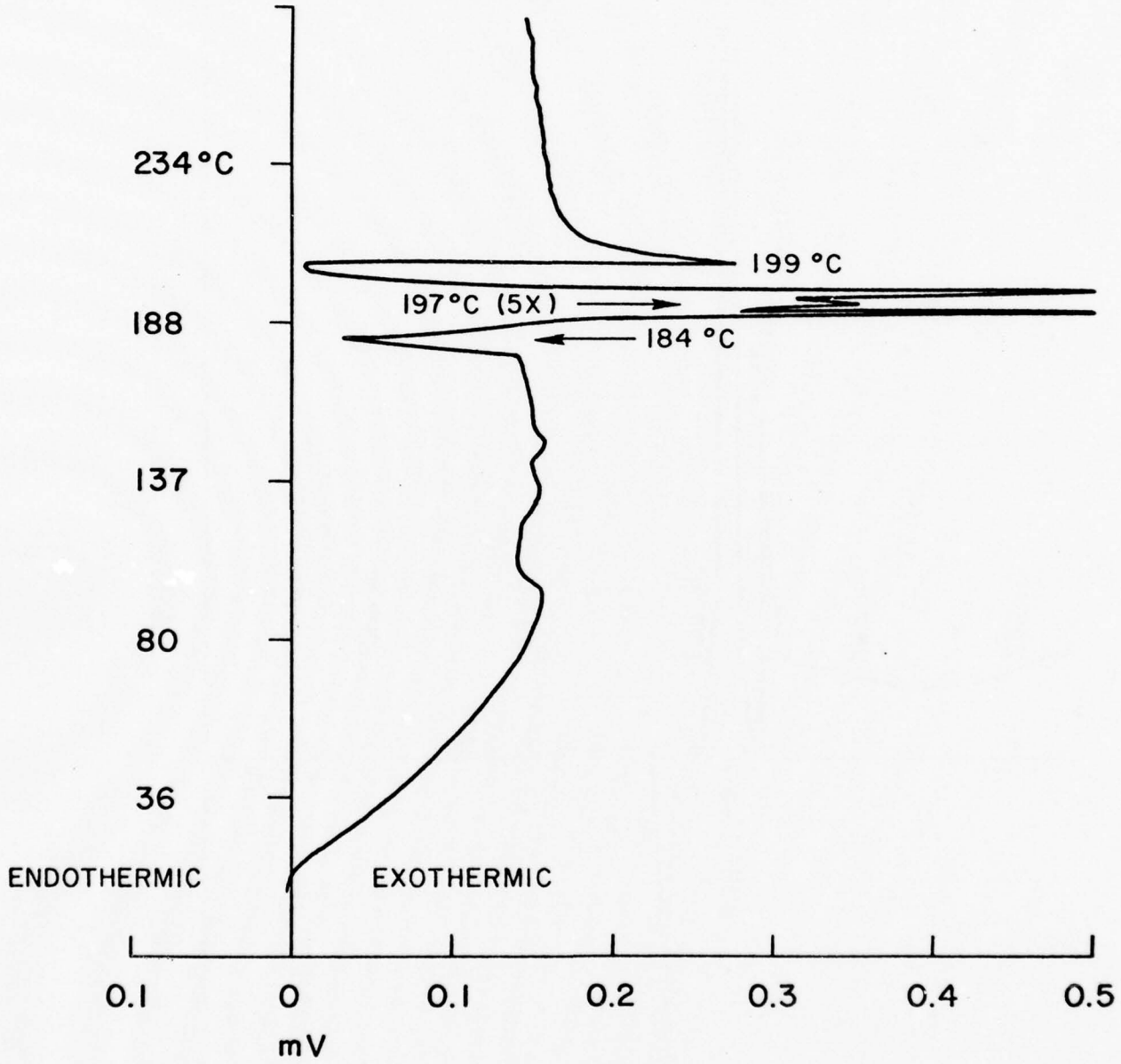

Fig. 63. Thermogram of Li + Carbon Cathode, Sample #85

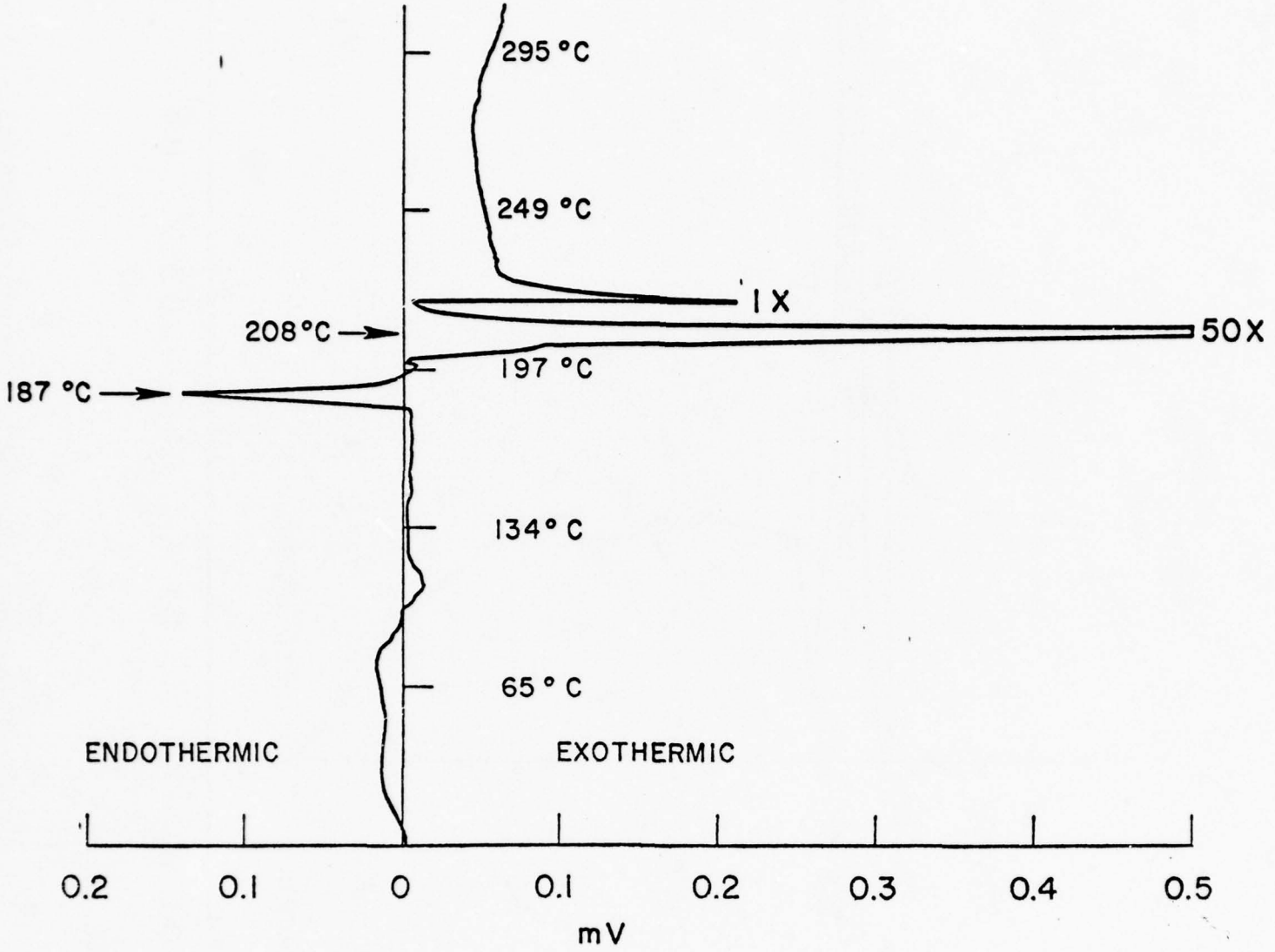

Fig.64. Thermogram of Li (0.011) + glass separator (0.008), Sample #39

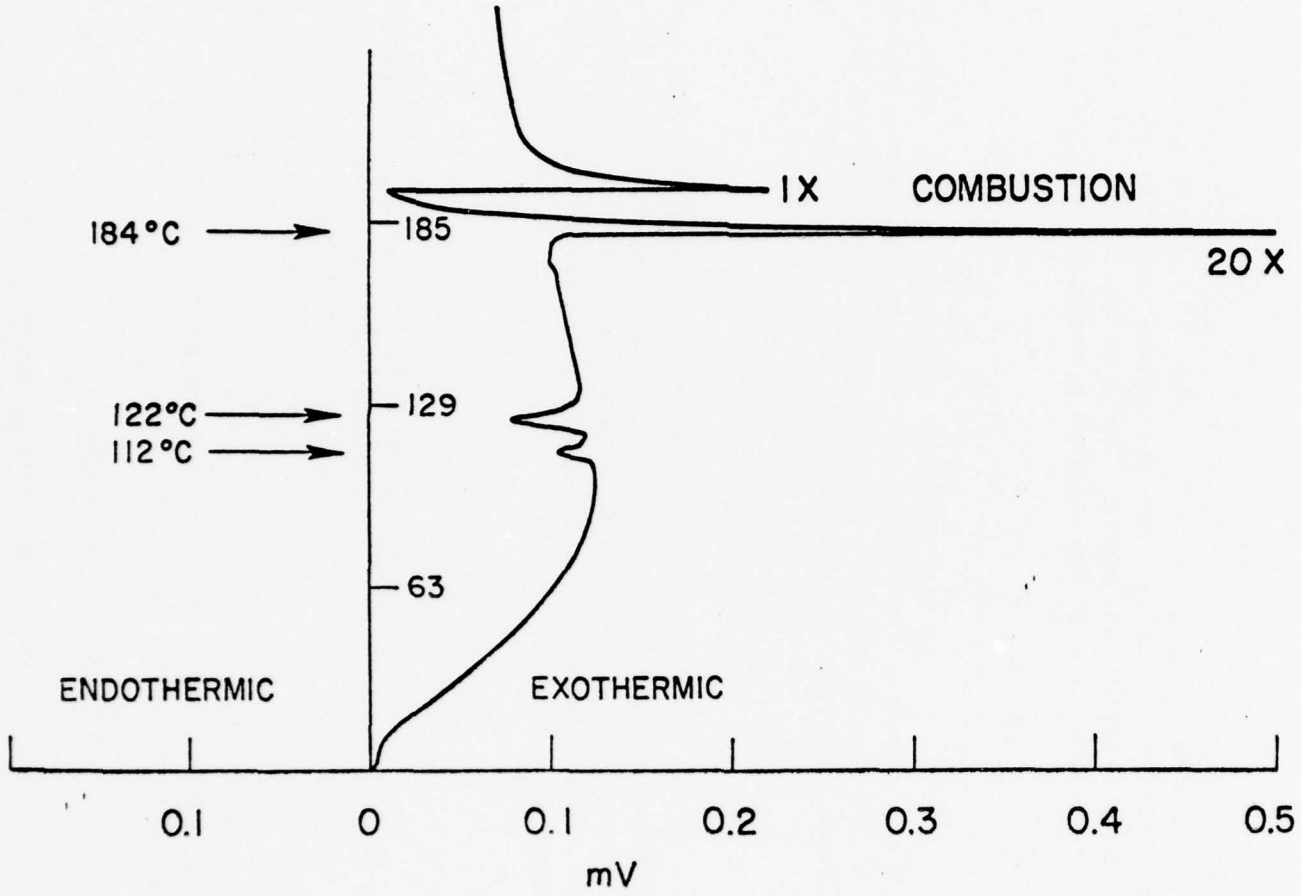

Fig. 65. Thermogram of Li (0.014) + S (0.021), Sample #43

14. $Li + Li_2S$

The thermogram showed only one endothermic peak at 194°C indicating the melting of Li. The materials appear to be stable.

15. $Li + Li_2SO_3$

The thermogram of $Li + Li_2SO_3$, H_2O (monohydrate) is shown in Fig. 66, and the thermogram of $Li + Li_2SO_3$ (anhydrous) is shown in Fig. 67. The exothermic peak at 139°C in Fig. 66 appears to be associated with the reaction between Li and H_2O from the monohydrate. The endothermic peak at 109° and the large exothermic peak at 174°C which are present in both Fig. 66 and 67, are most likely due to the reaction between Li and Li_2SO_3.

16. $SOCl_2 + S$

The thermogram is shown in Fig. 68. There was one very small endothermic peak at 72° followed by a sharp endothermic peak at 107°C, most likely due to the dissolution of S. The sample container burst at 236°C with a large endotherm indicating a pressure burst.

17. $SOCl_2 + Li_2S$

A typical thermogram at 10°C/min heating rate is shown in Fig. 69. There were two small exothermic transitions at 74° and 167°C and a very large exothermic transition at 145°C prior to the usual endothermic burst at 207°C. All of these could be potential contributors to a thermal-runaway, either as initiators or as propagators or both.

18. $SOCl_2 + Li_2SO_3$

The thermogram of $SOCl_2 + Li_2SO_3$, H_2O (monohydrate) showed no transitions prior to the endothermic burst at 76°C. This was most likely due to the hydrolysis of $SOCl_2$ from the H_2O of the monohydrate to form SO_2 and HCl, the pressure of which ruptured the glass sample container. The thermogram of $SOCl_2$ and Li_2SO_3 (anhydrous) as shown in Fig. 70 had three small exothermic transitions at 83°, 112° and 167° prior to the endothermic burst at 171°C. The reactions corresponding to the exothermic transitions are not known. These may also contribute to a thermal runaway.

19. S + Carbon Cathode

The thermogram as shown in Fig. 71, consists of three endothermic transitions, two of which at 118° and 134°C represent the melting of two types of sulfur and the small third one at 184°C probably represents dehydration of the cathode.

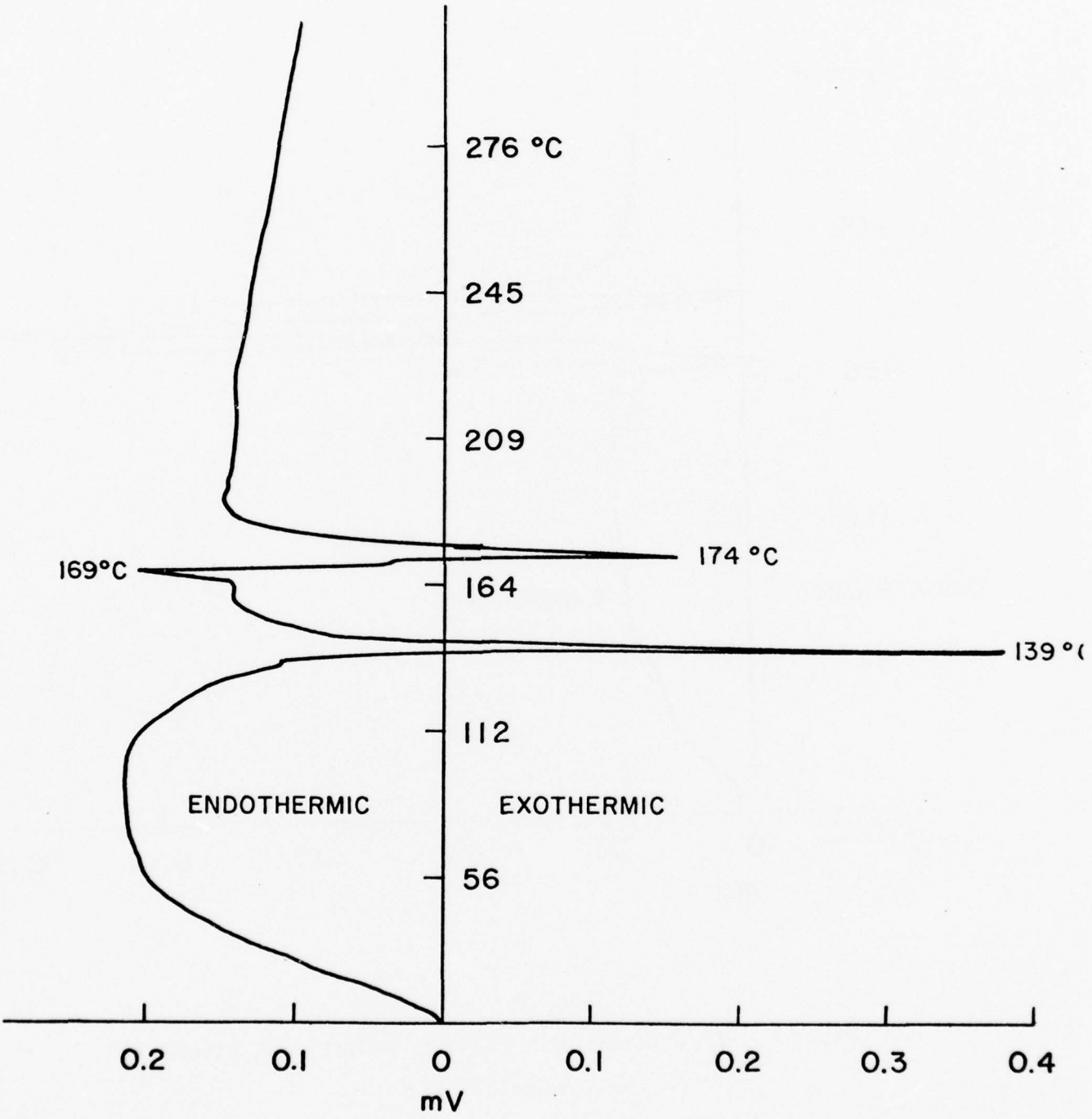

Fig. 66.. Thermogram of Li + $Li_2SO_3 \cdot H_2O$, Sample #61

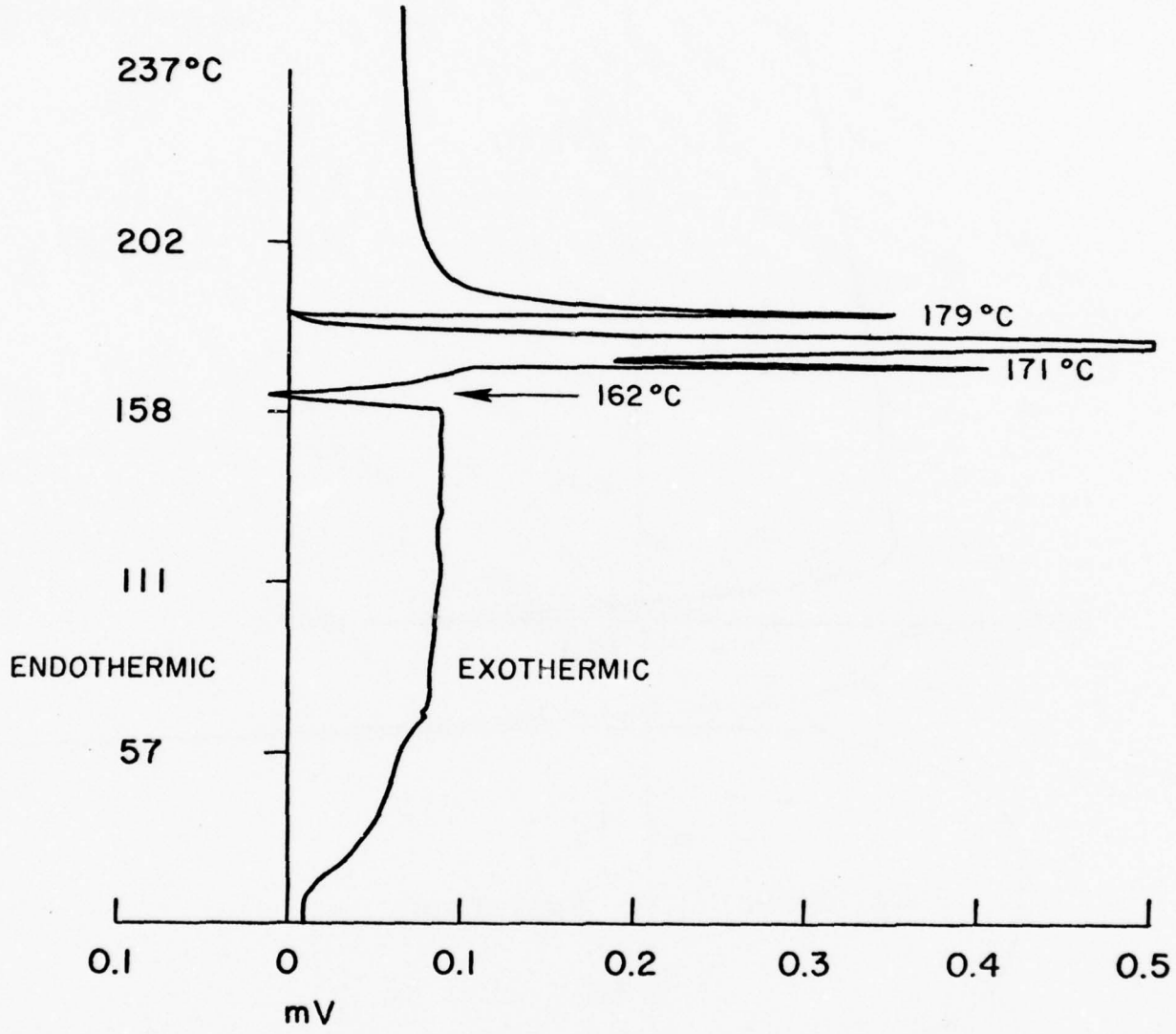

Fig. 67. Thermogram of Li + Li_2SO_3 (Anhydrous), Sample #75

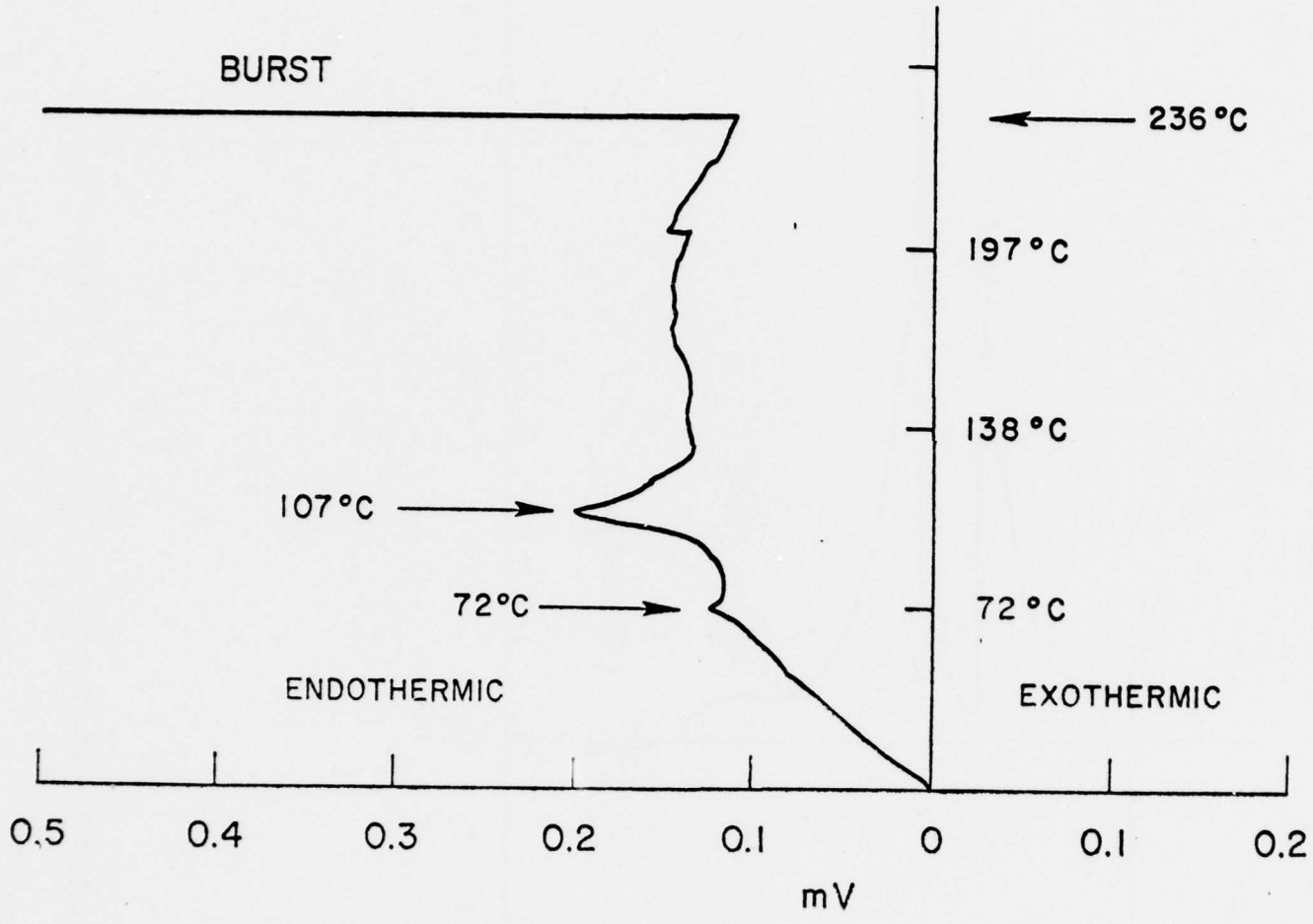

Fig. 68. Thermogram of S (0.087) + $SOCl_2$ (0.128), Sample #27

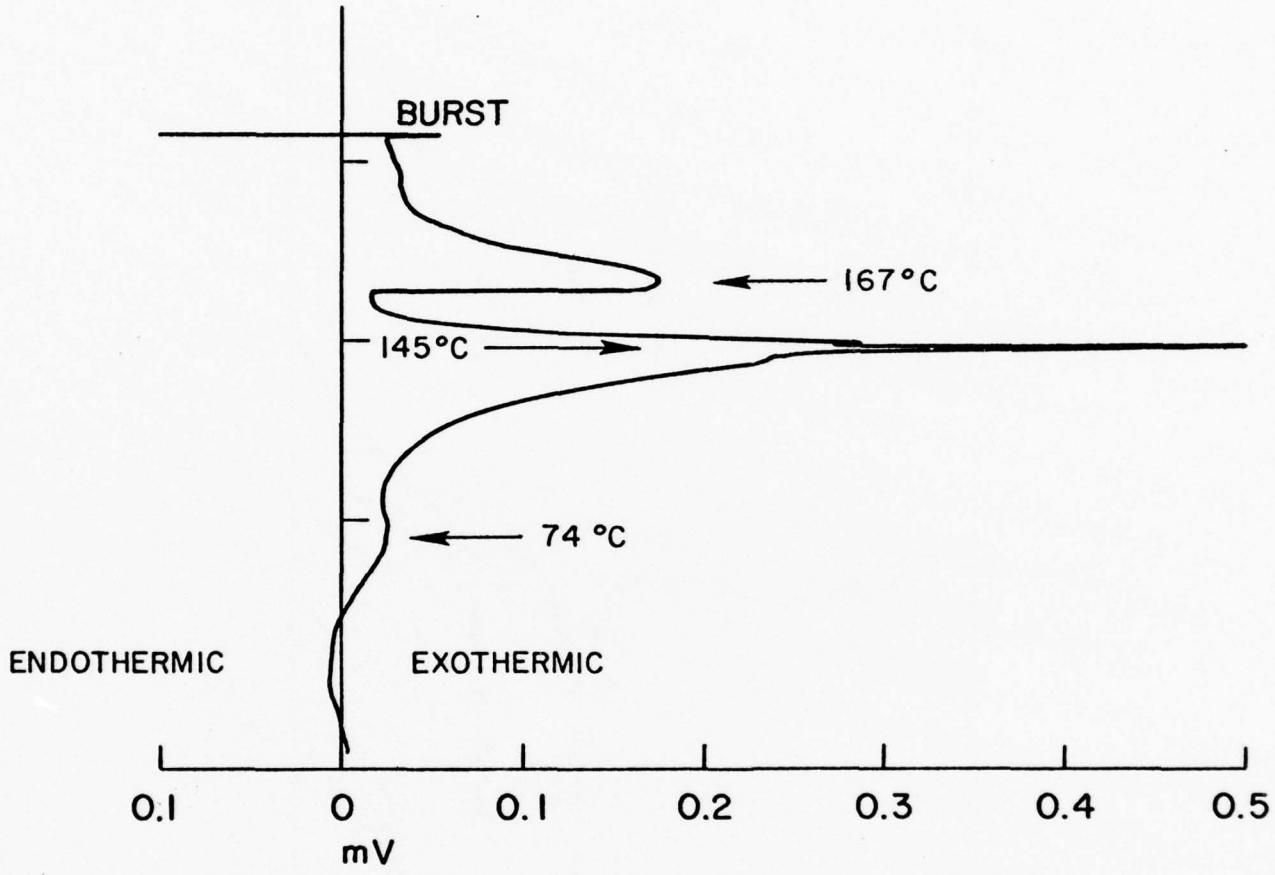

Fig. 69. Thermogram of $Li_2S + SOCl_2$, Sample #57

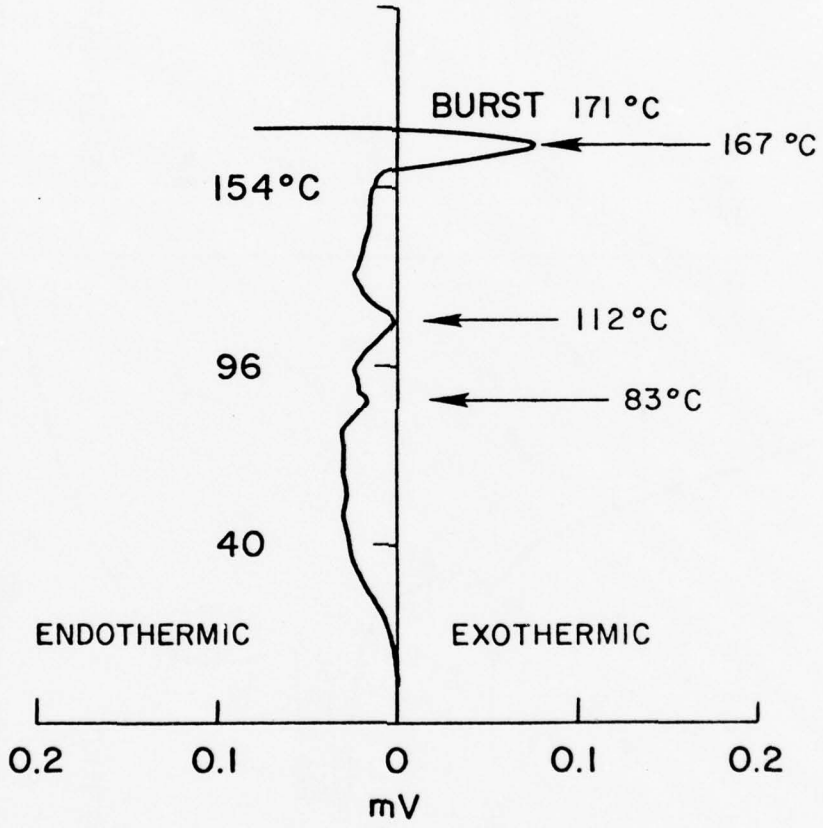

Fig. 70. Thermogram of Li_2SO_3 + $SOCl_2$, Sample #82

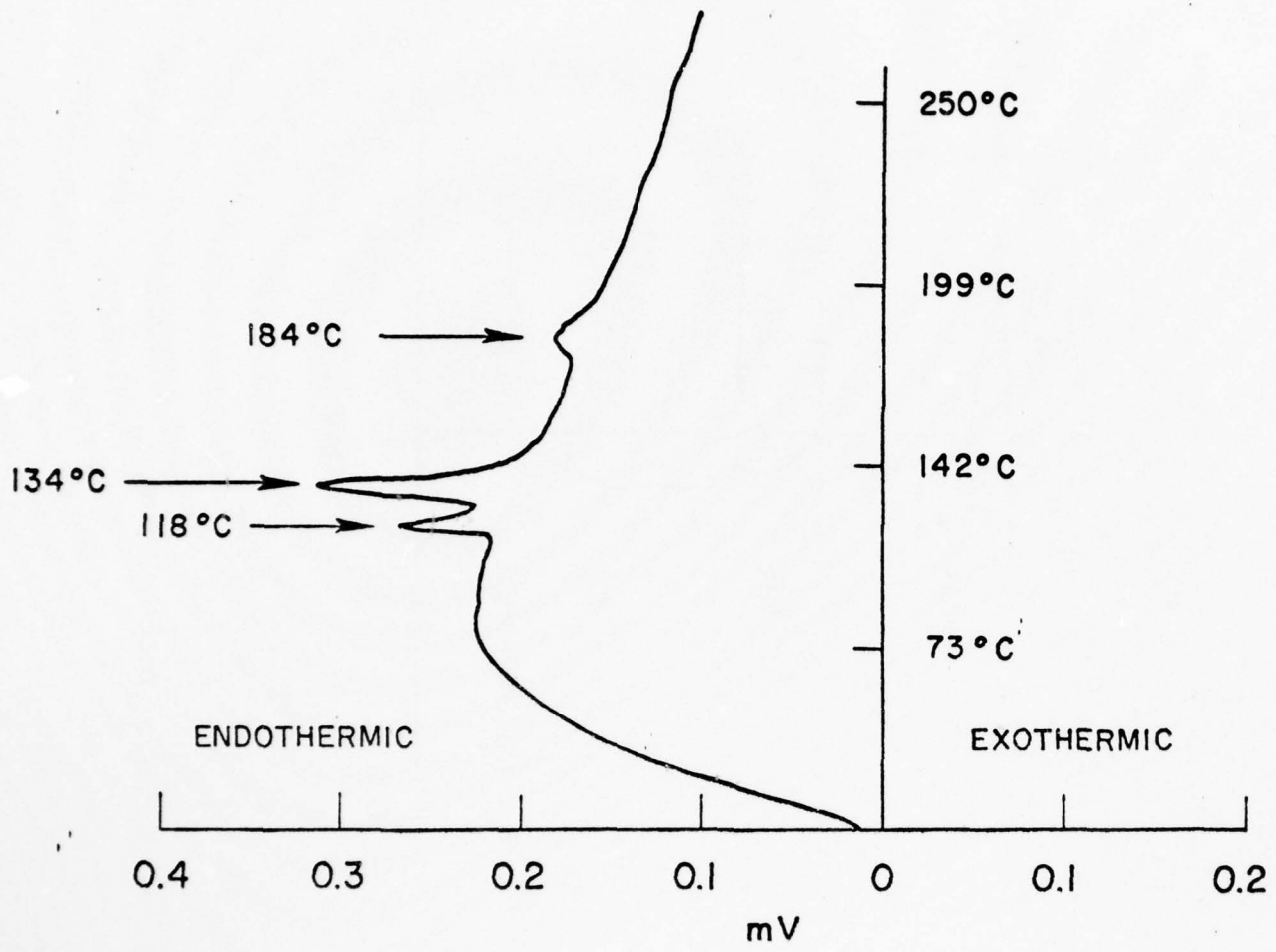

Fig. 71. Thermogram of S (0.060) + Cathode Mix (0.017), Sample #28

20. $S + Li_2S$

The thermogram has only two small endothermic transitions at 116° and 122° corresponding to the melting of two types of sulfur.

21. $S + Li_2SO_3$

The thermogram of $S + Li_2SO_3$, H_2O (monohydrate) contains two endothermic peaks at 105° and 120° corresponding to the melting of two types of S and two additional endothermic peaks at 163° and 207° corresponding to the dehydration of Li_2SO_3 (see Fig. 60). The thermogram of $S + Li_2SO_3$ (anhydrous) contains only two endothermic peaks corresponding to the melting of two types of S.

22. Carbon Cathode + Li_2SO_3

The thermogram of carbon cathode + Li_2SO_3, H_2O (monohydrate) showed a large endothermic peak at 209° corresponding to the dehydration. The glass tube was found to be broken at the end of the run most likely due to the excessive pressure of H_2O vapor. The thermogram of cathode + Li_2SO_3 (anhydrous) showed no transitions at all.

23. Li + 1(M) $LiAlCl_4$, $SOCl_2$ (Electrolyte)

The thermogram is very similar to the thermogram of Li + $SOCl_2$ (Fig. 62) consisting of a small endotherm at 169° followed by a large exothermic blast at 223°C with visible flames.

24. Li + S + Ni Tab

This DTA run was taken in order to ascertain whether the presence of Ni in the form of foil caused any change to the thermograms of Li + S. Ni is present in the thionyl D cell in the can, the tabs, and in the cathode grid. The thermogram is shown in Fig. 72. There is only a very minor difference; the two endothermic peaks corresponding to the melting of sulfur are separated, one occurring at 92°C and the other at 134°C. The large exothermic peak corresponding to Li + S combustion occurred at 182°C as before. There was no change in the intensity of the exothermal combustion of Li and S in the presence of the Ni foil.

25. Li + S + $SOCl_2$

We examined the Li + S, Li + $SOCl_2$ and the S + $SOCl_2$ combinations separately. It is of interest to see whether there is any peculiarity when all three are present together. The thermogram of the ternary combination, Li + S + $SOCl_2$ is shown in Fig. 73. Note that the endothermic transitions related to S are indistinguishable because the endothermal shifting of the baseline resulted from a difference in the thermal conductivity between the reference and the sample chemicals. The sharp endothermic peak at 194°C corresponding to the melting of

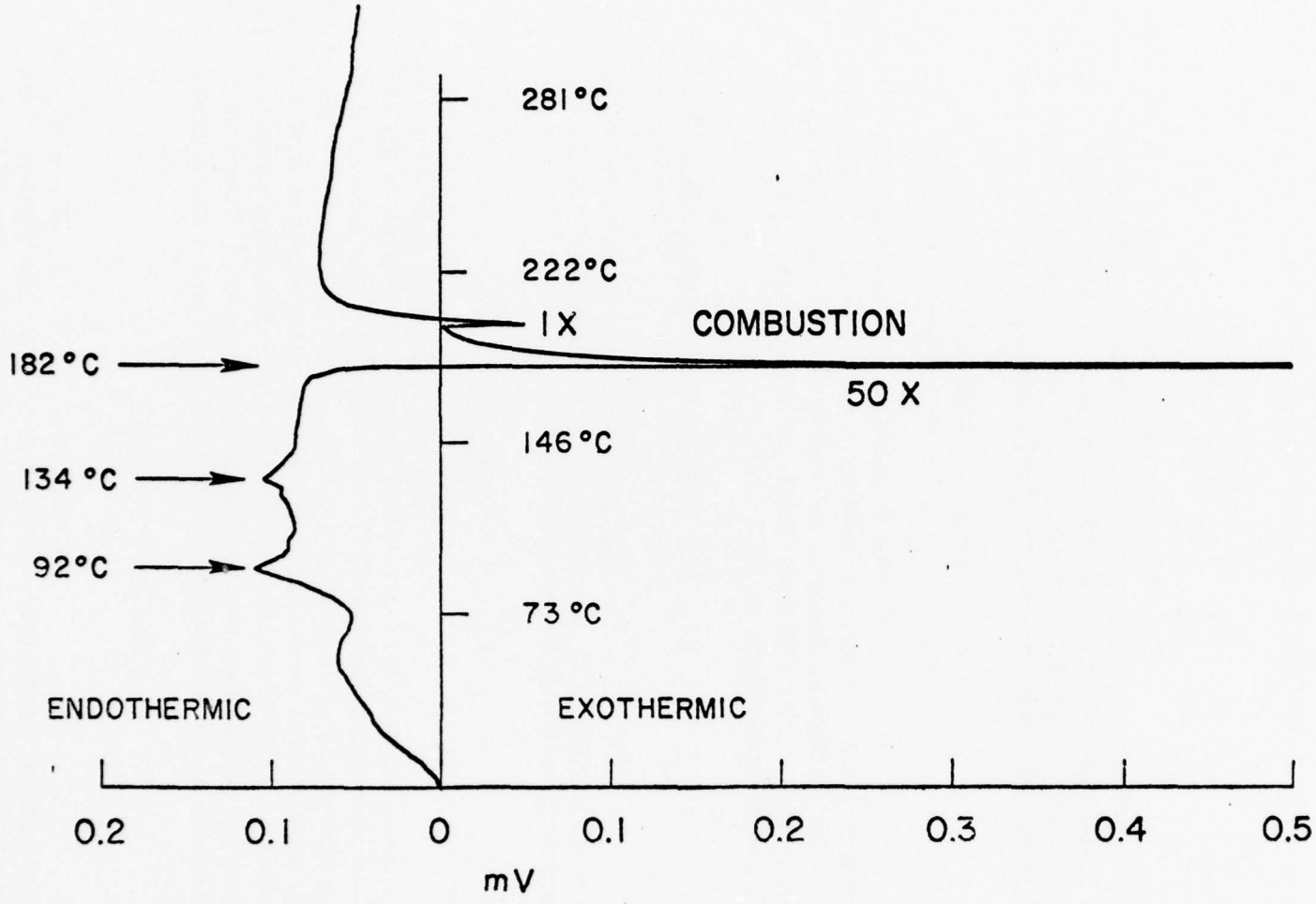

Fig. 72. Thermogram of Li (0.012) + Ni (0.012) + S (0.034) Sample #40

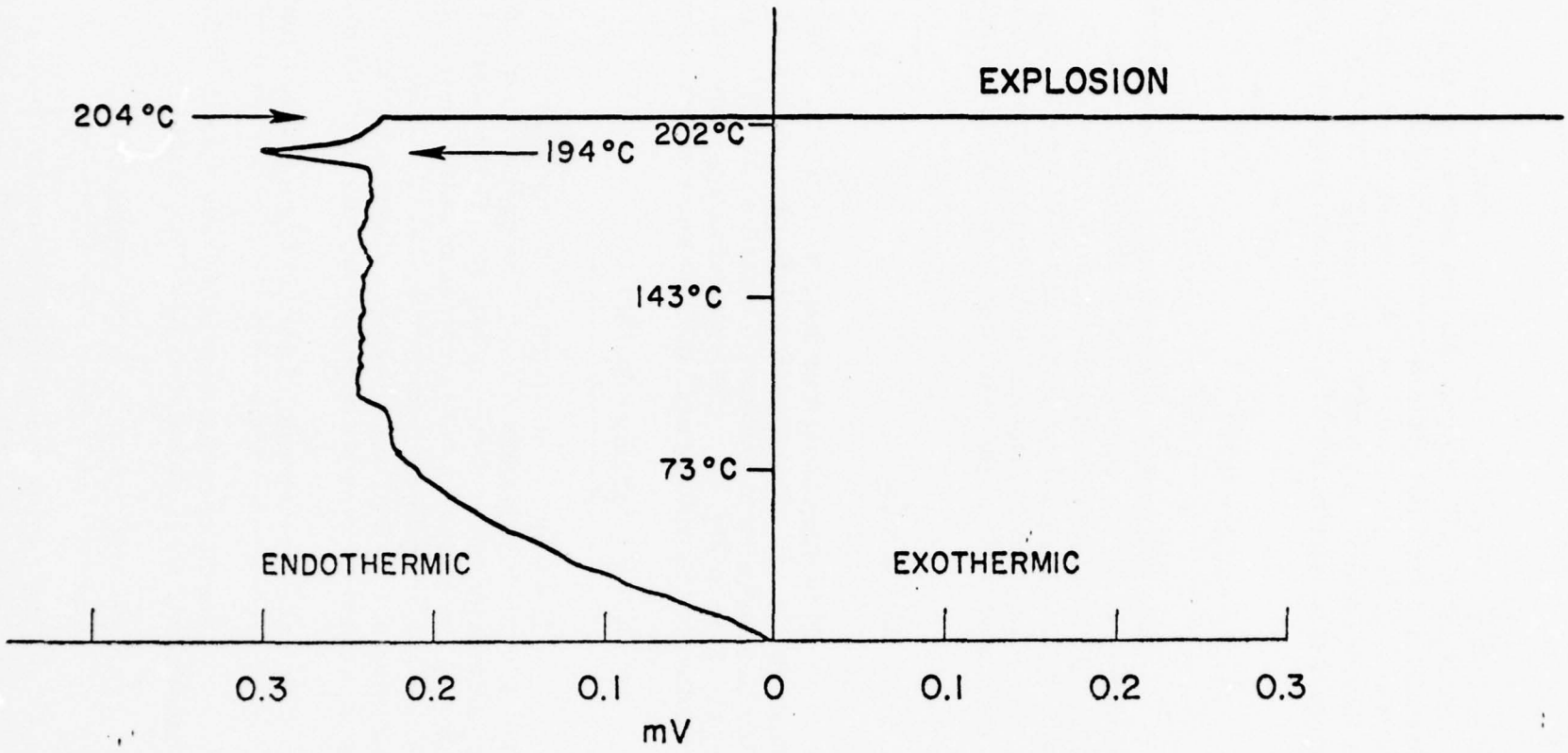

Fig. 73. Thermogram of Li (0.013) + S (0.045) + $SOCl_2$ (0.161), Sample #25

Li and the exothermic explosion at 204°C is similar to that observed in the thermogram of Li + $SOCl_2$ (Fig. 62). In general, the thermogram is similar to the Li + $SOCl_2$ thermograms and does not contain any features of the Li + S and the S + $SOCl_2$ thermograms. In the Li + S system, the combustion occurred at a temperature lower than the melting point of Li, whereas, in the Li + S + $SOCl_2$ system, the exothermic explosion occurred at a temperature higher than the melting point of Li.

26. Li + Li_2S + $SOCl_2$

The thermogram is shown in Fig. 74 and it consists of one relatively large exotherm at 134°C, very similar to that observed in the thermogram of Li_2S + $SOCl_2$ (Fig. 69), and a small endotherm at 169° corresponding to the melting of Li and finally the exothermic thermal runaway at 214°C, similar to Li + $SOCl_2$ thermogram (Fig. 62). Thus, the thermogram of the ternary system roughly represents a combination of the thermograms of the two binary systems, Li + $SOCl_2$ and L_2S + $SOCl_2$.

27. Li + S + Li_2S

This experiment was done in triplicate. The typical thermogram as shown in Fig. 75, shows small endotherms representing the transitions corresponding to S and a large exothermic transition at 177°C corresponding to the combustion of Li + S as in Fig. 65. Characteristically, there was no endothermic transition corresponding to the melting of Li prior to the exothermic combustion.

28. Carbon Cathode + S + $SOCl_2$

The effect of $SOCl_2$ on the thermogram of S + cathode mix was investigated in these DTA experiments. The experiments were done in triplicate. A typical thermogram is shown in Fig. 76. The typical two endothermic peaks corresponding to the transitions of two types of sulfur were replaced by one endothermic peak occurring at a lower temperature, 101°C. This may indicate the endothermic dissolution of S in $SOCl_2$. At higher temperature, 219°C, the sample container burst with a sharp endotherm corresponding to a pressure burst.

29. Carbon Cathode + 1(M) $LiAlCl_4$ - $SOCl_2$ (Electrolyte)

The thermograms consist of only a small endotherm at 88°C followed by the endothermic pressure burst at 238°C as usual.

30. S + 1(M) $LiAlCl_4$ - $SOCl_2$ (Electrolyte)

The thermogram consists of one endotherm at 93°, corresponding to the dissolution of S followed by the endothermic pressure burst at 193°C very similar to Fig. 76. This experiment was done in duplicate.

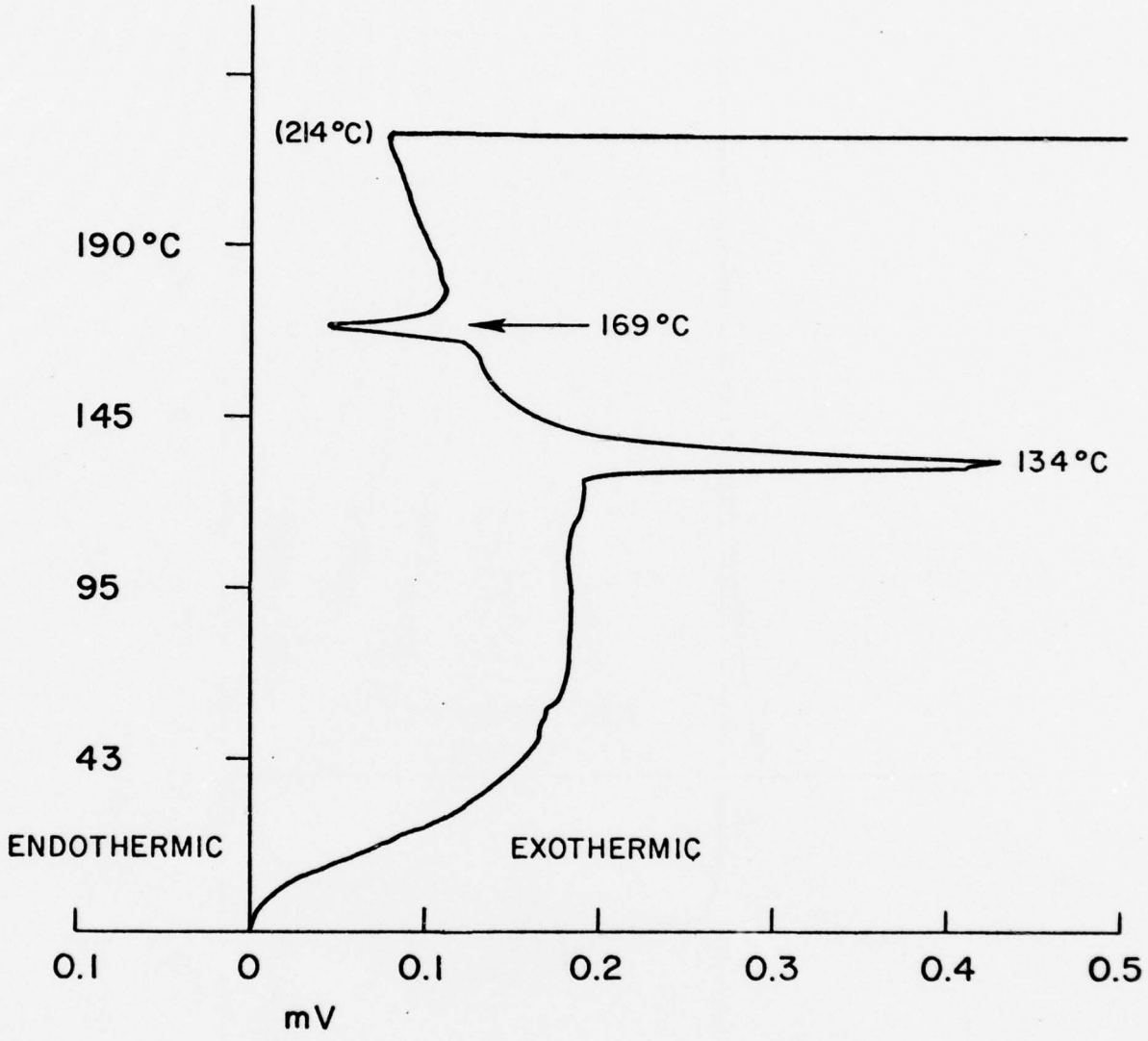

Fig. 74. Thermogram of Li + Li_2S + $SOCl_2$, Sample #66

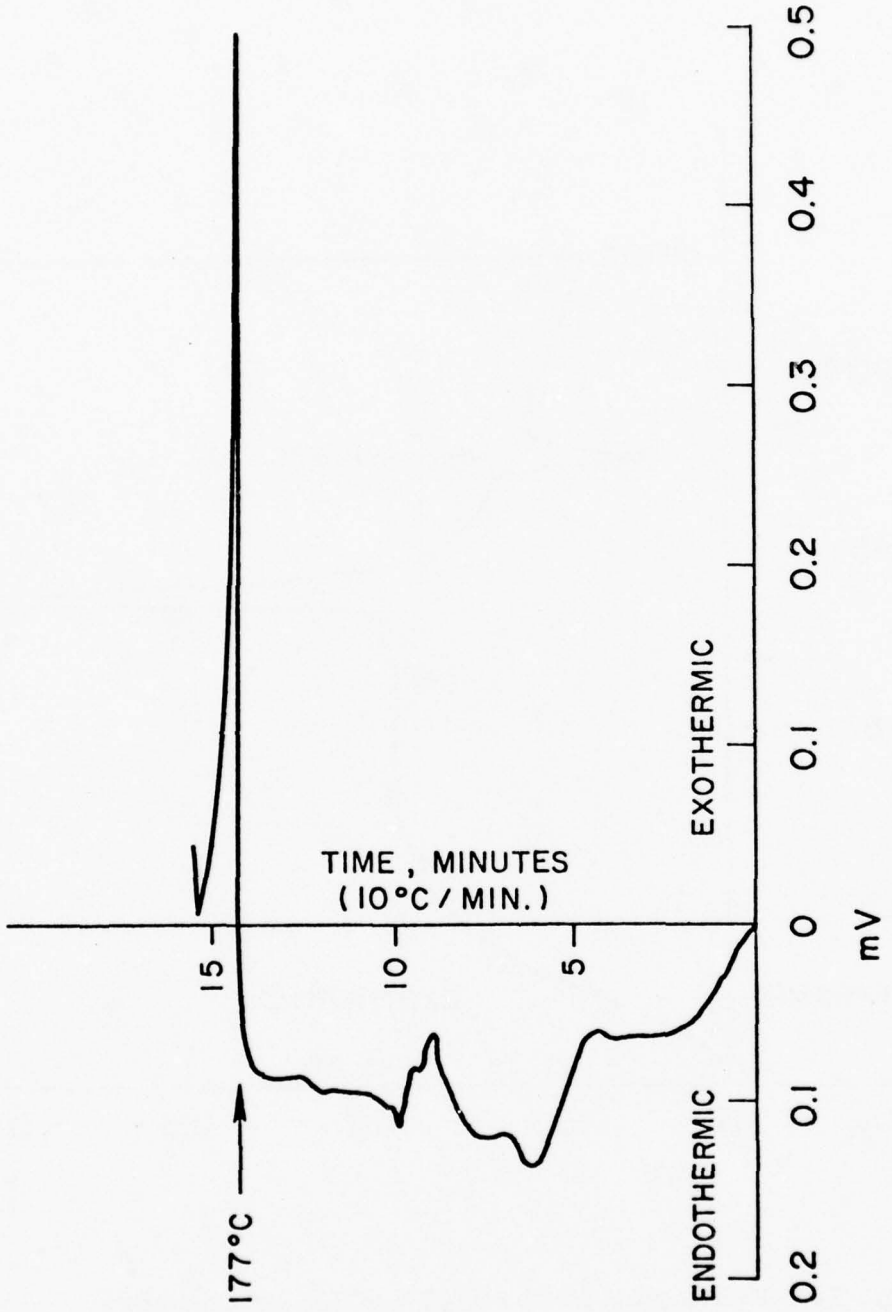

Fig. 75. Thermogram of Li + S + Li_2S, Sample #35

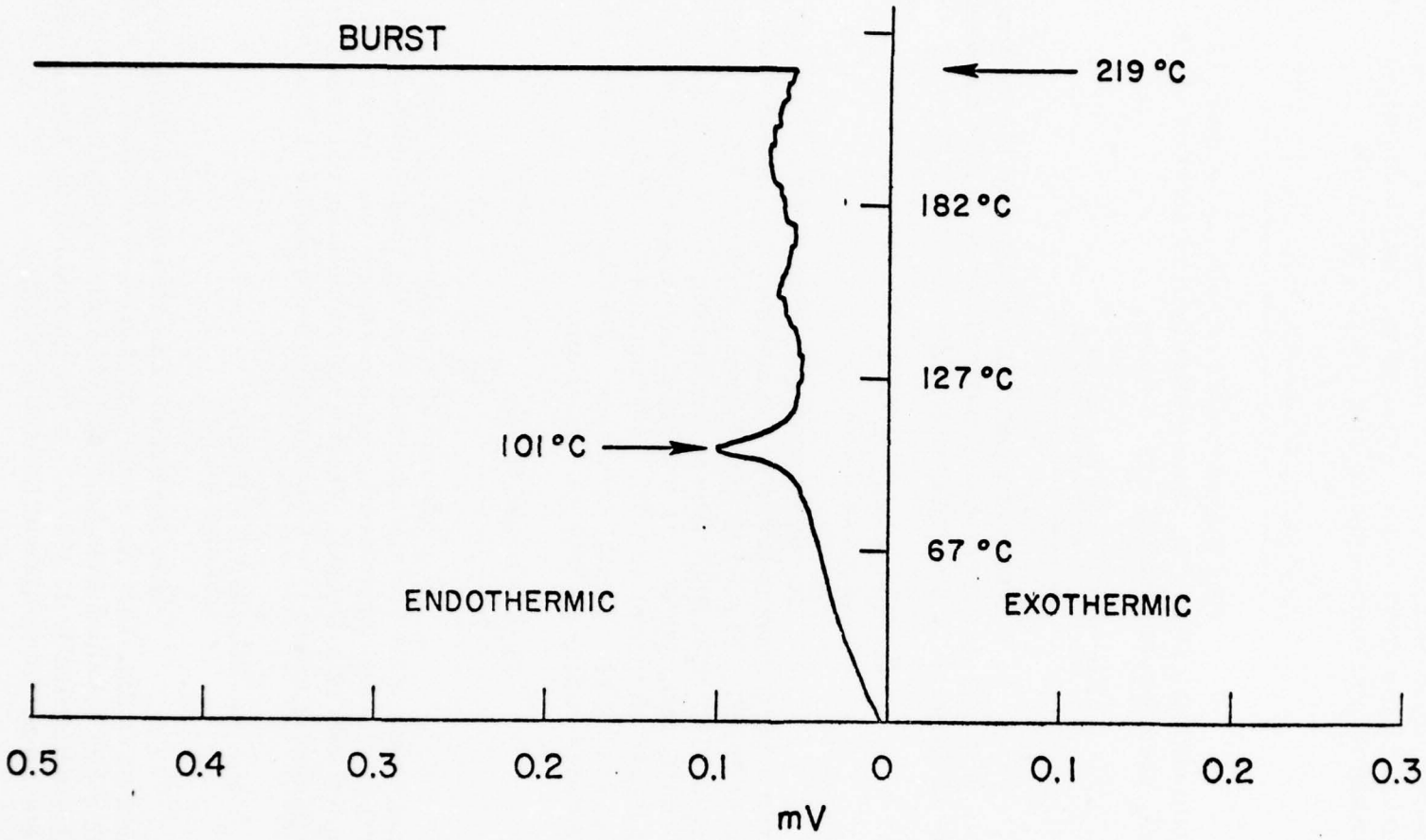

Fig. 76. Thermogram of S (0.050) + Cathode Mix (0.012) + $SOCl_2$ (0.145), Sample #23

31. Li_2S + 1(M) $LiAlCl_4$ - $SOCl_2$ (Electrolyte)

The thermogram consists of one small exotherm at 80°C, two somewhat larger exotherms at 109° and 118° and another small exotherm at 149° followed by the endothermic rupture of the sample container. The thermogram is very similar to the thermogram of Li_2S + $SOCl_2$ (Fig. 69).

32. Li_2SO_3 + 1(M) $LiAlCl_4$ - $SOCl_2$ (Electrolyte)

The thermogram is completely featureless except for the endothermic bursting at 184°C, characteristic of all samples containing $SOCl_2$. The Li_2SO_3 used was anhydrous.

33. Li + Li_2SO_3 + $SOCl_2$

The thermogram was identical to the thermogram of Li + $SOCl_2$ (Fig. 62) and consisted of one endotherm at 188° corresponding to the melting of Li followed by an exothermic explosion at 204°C.

34. Li + S + S_2Cl_2

The thermogram as shown in Fig. 77 consists of a small endotherm at 185°C corresponding to the melting of Li, followed by an exothermic explosion at 302°C. The second thermogram, shown in Fig. 78 consists of a small endotherm at 73°C most likely due to the dissolution of S, and then a second endotherm at 183°C corresponding to melting of Li, followed by a large endotherm at 191° and larger exotherms at 197°, 205° and 224°C. The tube was found to be broken and stuck to the sample container. The results of the second run were somewhat ambiguous because of the tube breakage.

35. Li + S + CS_2

This experiment was also done in duplicate. Both the thermograms were quite featureless other than the exothermic explosion at 169° and 178°C for the two experiments. In the second run, the explosion was accompanied with blue flames. These explosions occurred before the melting of Li at temperatures where Li - S combustions were observed (Fig. 65).

36. Li + S + $POCl_3$

This experiment was also done in duplicate. One thermogram is shown in Fig. 79. The small endotherms at 107° and 115° are most likely related to S and the third endotherm at 184° represent the melting of Li. The sample exploded exothermically at 309°C. In the second run the sample exploded after it was removed from the furnace at the end of the run.

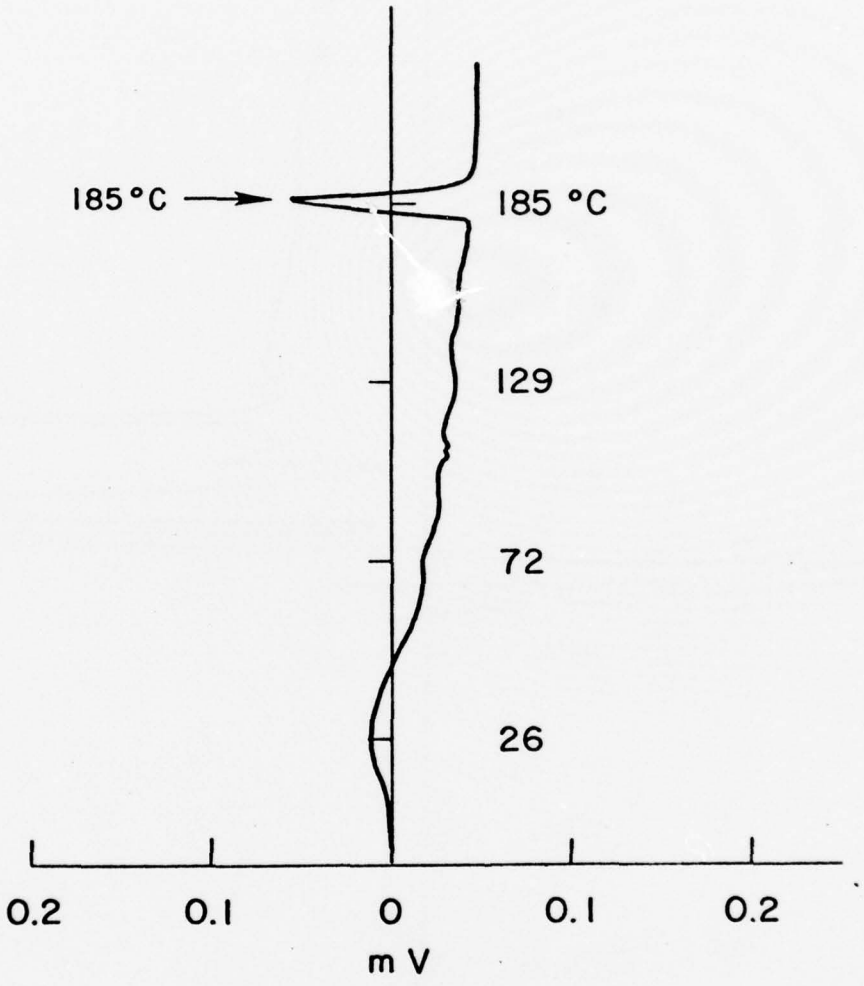

Fig. 77. Thermogram of Li + S + S_2Cl_2, Sample #95

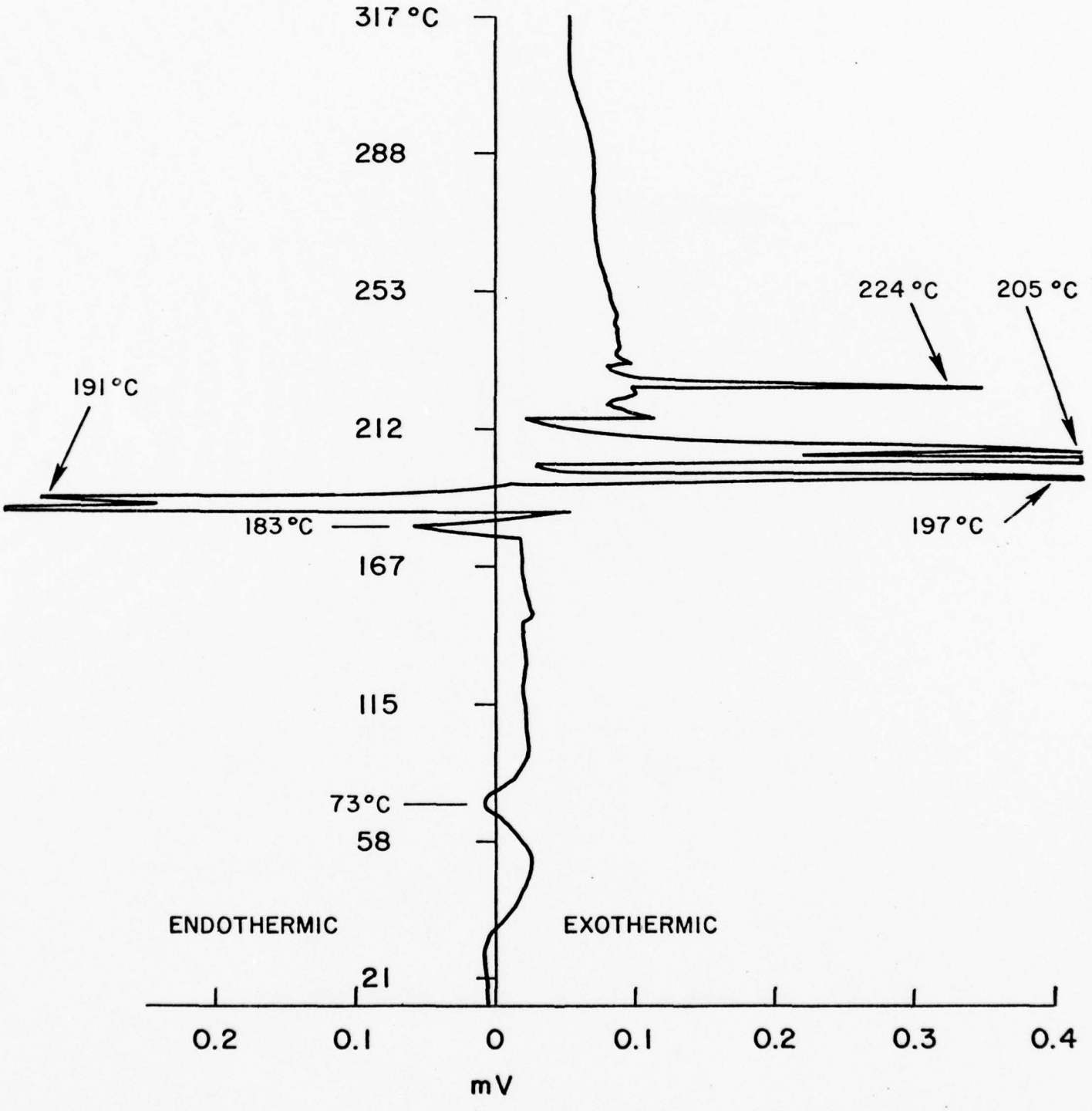

Fig. 78. Thermogram of Li + S + S_2Cl_2, Sample #96

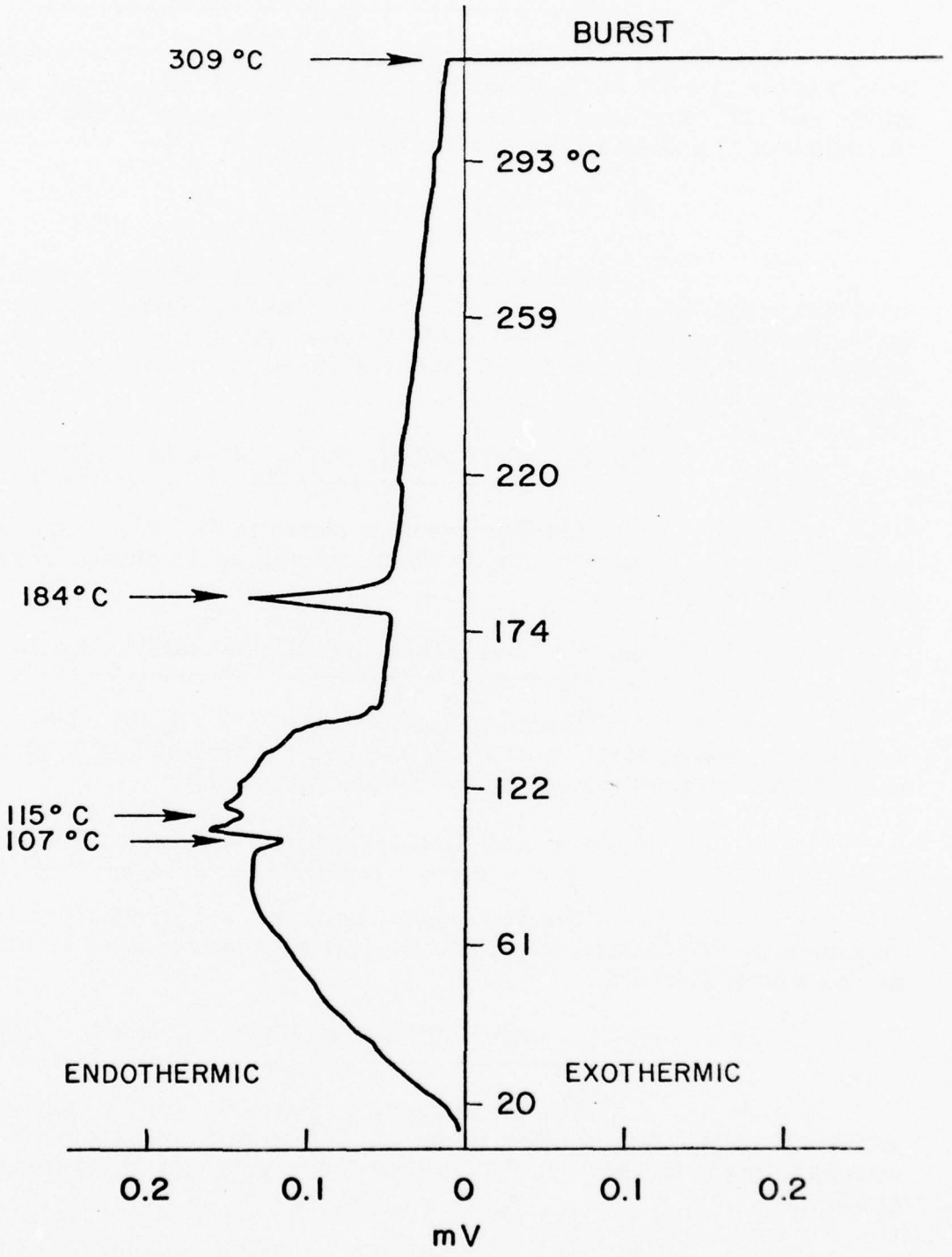

Fig. 79. Li + S + $POCl_3$, Sample #100

37. $Li + S + 1(M)\ LiAlCl_4 - SOCl_2$ (Electrolyte)

The thermogram as shown in Fig. 80 was very similar to that of the $Li + S + SOCl_2$ thermogram (Fig. 73) consisting of two small endotherms at 99° and 122, most likely related to S, a large endotherm at 188° corresponding to melting of Li and an exothermic blast at 273°C.

38. $Li + S + SOCl_2 + S_2Cl_2$

This experiment was done in triplicate. One thermogram is shown in Fig. 81. Very small endothermic peaks are related to the interactions with S and the endothermic peak at 185°C represents the melting of Li. The sample exploded exothermically at 234°C, very similar to that of the $Li + S + SOCl_2$ sample (Fig. 73).

39. $S + 1(M)\ LiAlCl_4, SOCl_2$ (90 vol%) + S_2Cl_2 (10 vol%)

The thermogram is shown in Fig. 82. It consists of an endotherm at 96°C corresponding to the dissolution of S followed by an endothermic pressure burst at 208°C.

40. $S + 1(M)\ LiAlCl_4, SOCl_2$ (90 vol%) + CS_2 (10 vol%)

The thermogram, as shown in Fig. 83, consists of two endotherms, one at 93°C, most likely due to the dissolution of S, and another at 224°C and surprisingly no endothermic pressure burst.

41. $S + 1(M)\ LiAlCl_4, SOCl_2$ (90 vol%) + $POCl_3$ (10 vol%)

The thermogram, as shown in Fig. 84 consists of one endotherm at 107°C corresponding to the S dissolution followed by the endothermic pressure burst at 215°C.

42. $Li + S + 1(M)\ LiAlCl_4, SOCl_2$ (90 vol%) + S_2Cl_2 (10 vol%)

The thermogram, as shown in Fig. 85, consists of one endotherm at 83° corresponding to the dissolution of S, one endotherm at 185° corresponding to the melting of Li followed by a very violent exothermic explosion at 261°C.

43. $Li + S + 1(M)\ LiAlCl_4, SOCl_2$ (90 vol%) + CS_2 (10 vol%)

The thermogram, as shown in Fig. 86 consists of one endotherm at 88°C corresponding to the dissolution of S, another small endotherm at 185°C corresponding to Li melting, followed by a violent exothermic explosion at 210°C.

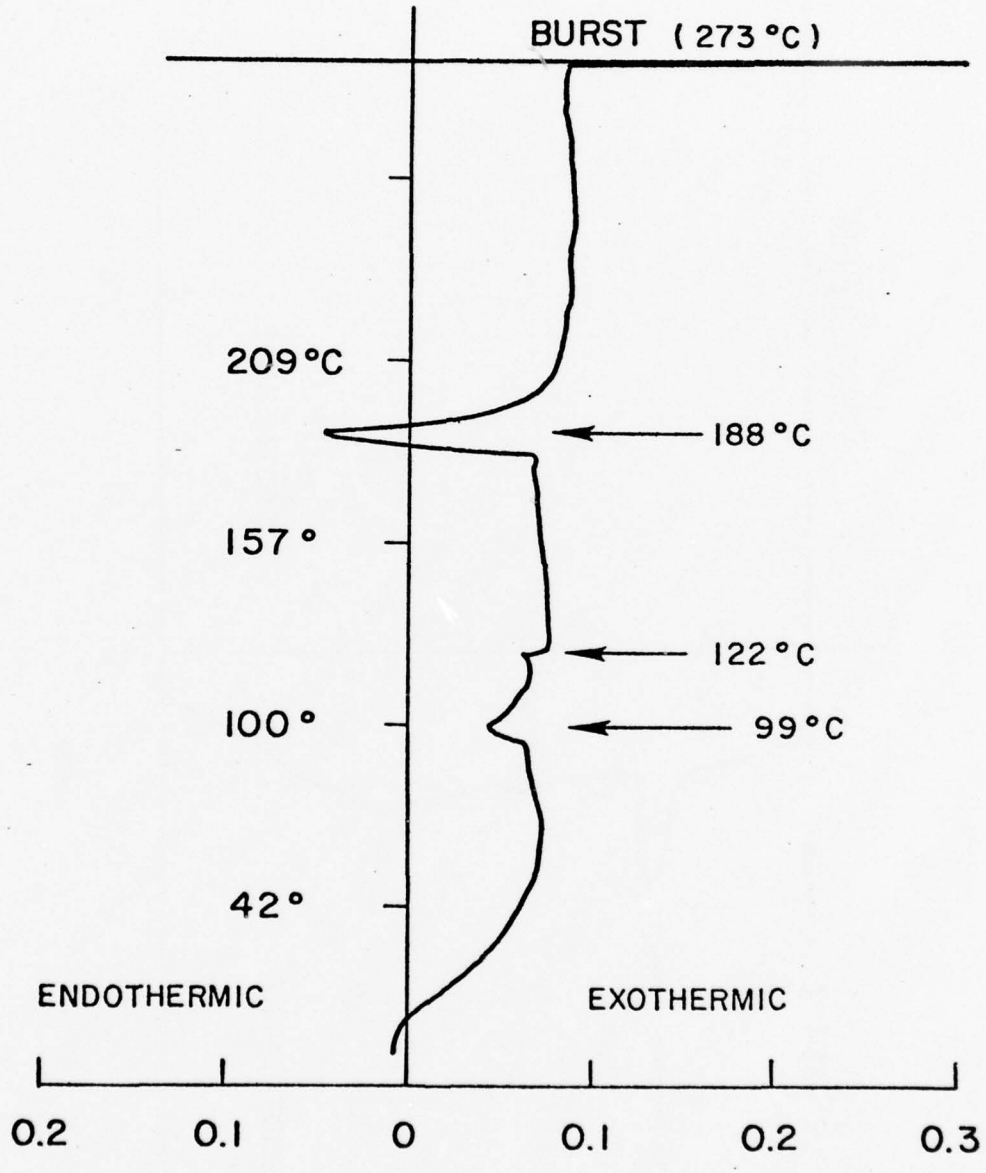

Fig. 80 Thermogram of Li + S + 1M $LiAlCl_4$-$SOCl_2$, Sample #84

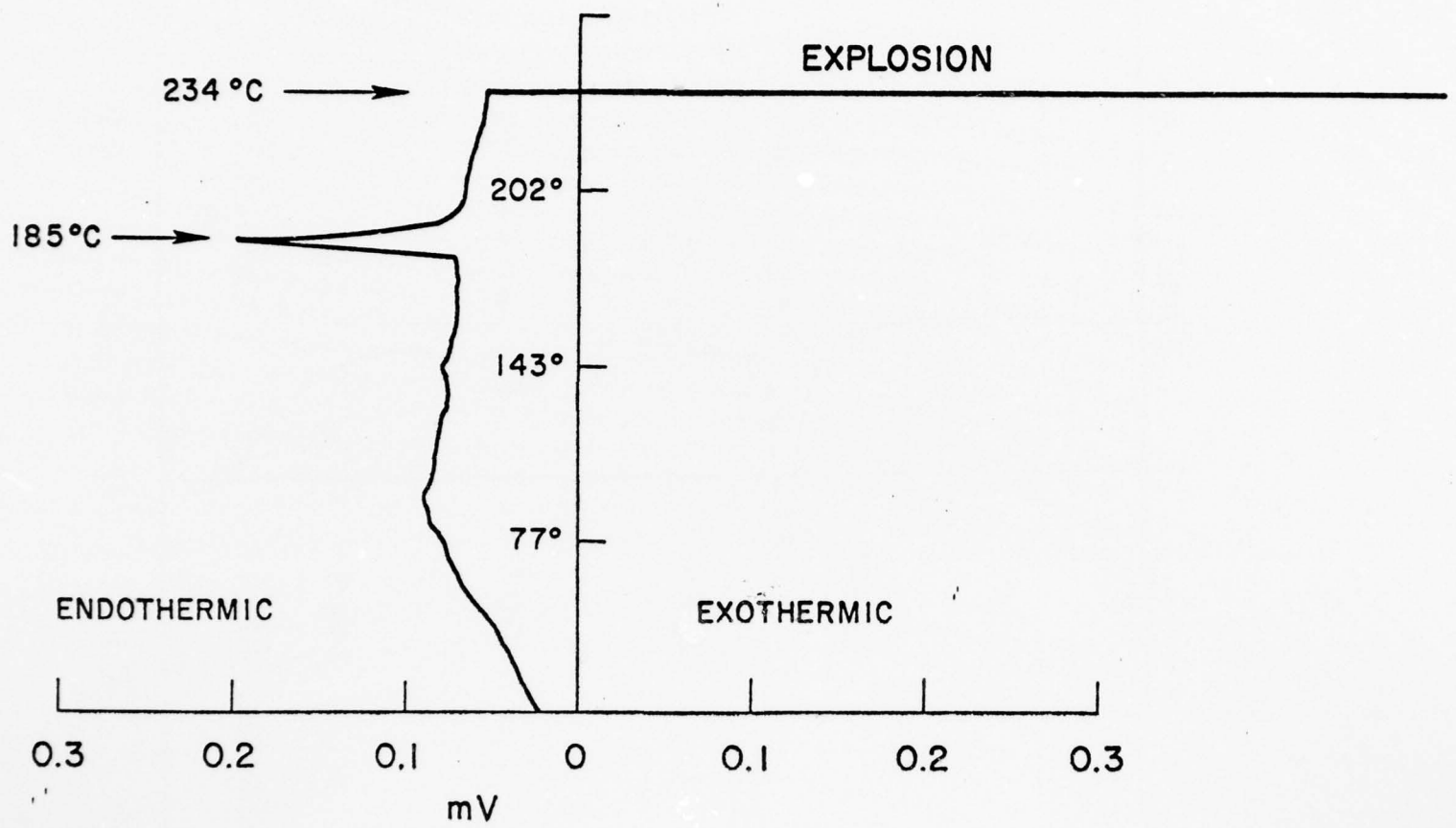

Fig. 81. Thermogram of Li (0.012) + S (0.031) + equal volumes of $SOCl_2$ + S_2Cl_2 mixture (0.092), Sample #33

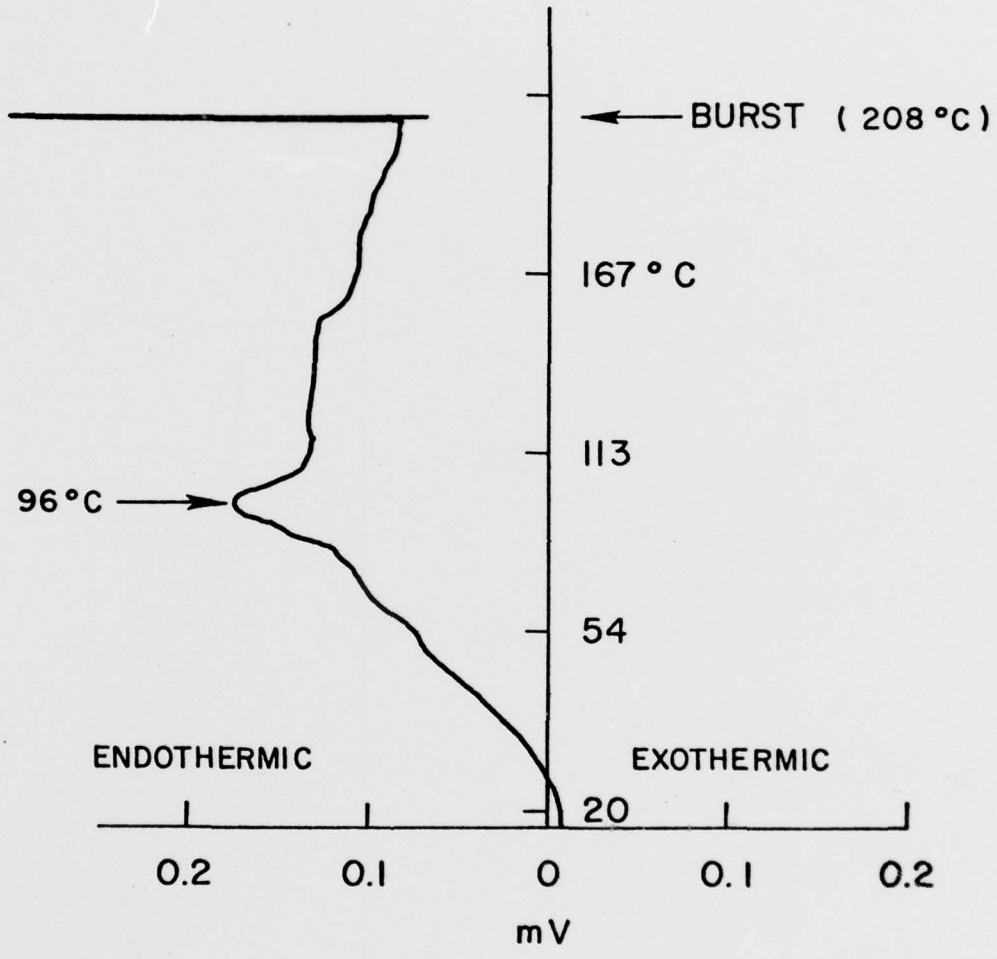

Fig. 82. Thermogram of S + 1M $LiAlCl_4$-$SOCl_2$ (90 vol%) + S_2Cl_2 (10 vol%), Sample #88

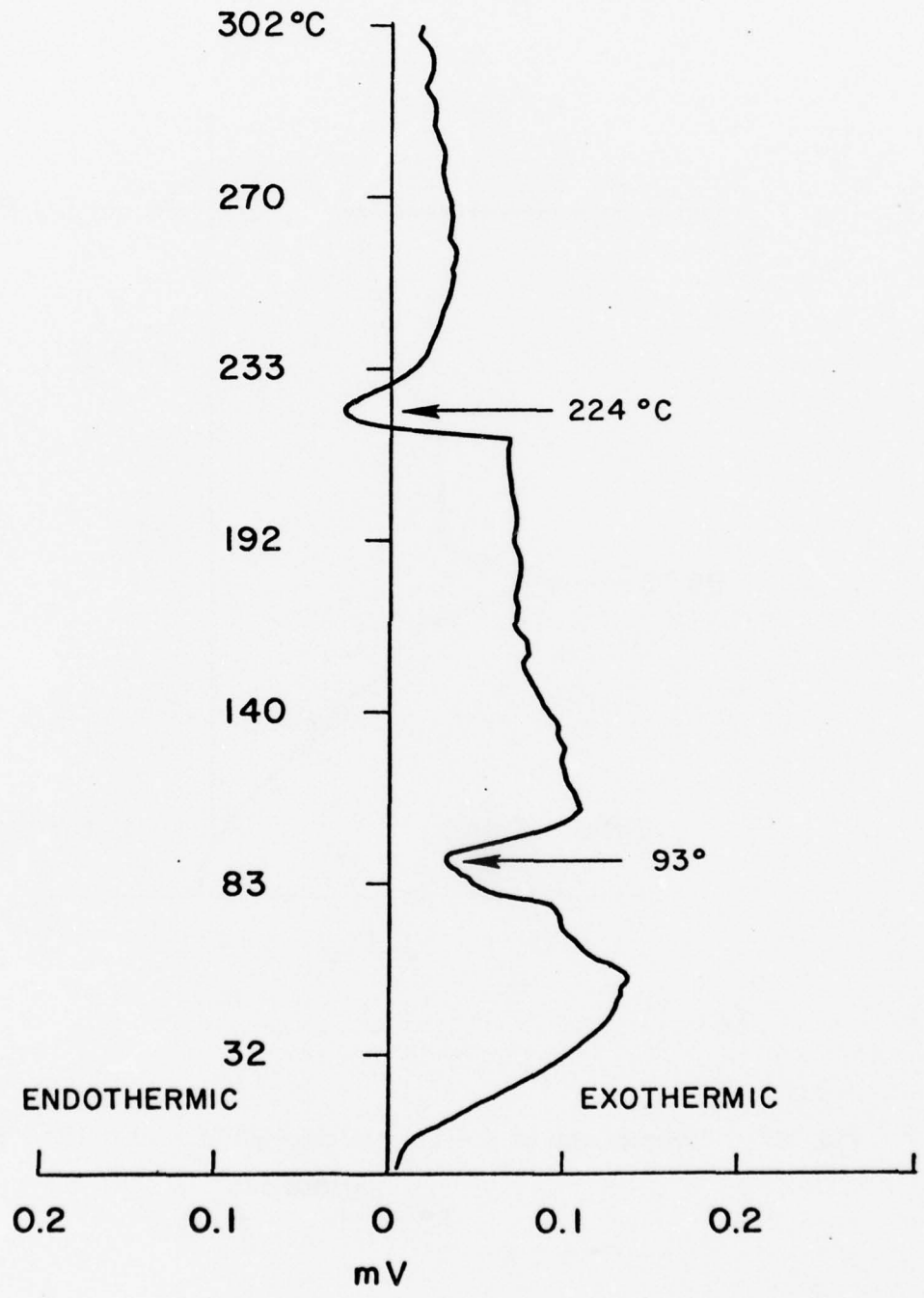

Fig. 83. Thermogram of S + 1M $LiAlCl_4$-$SOCl_2$ (90 vol% + CS_2 (10 vol%), Sample #89

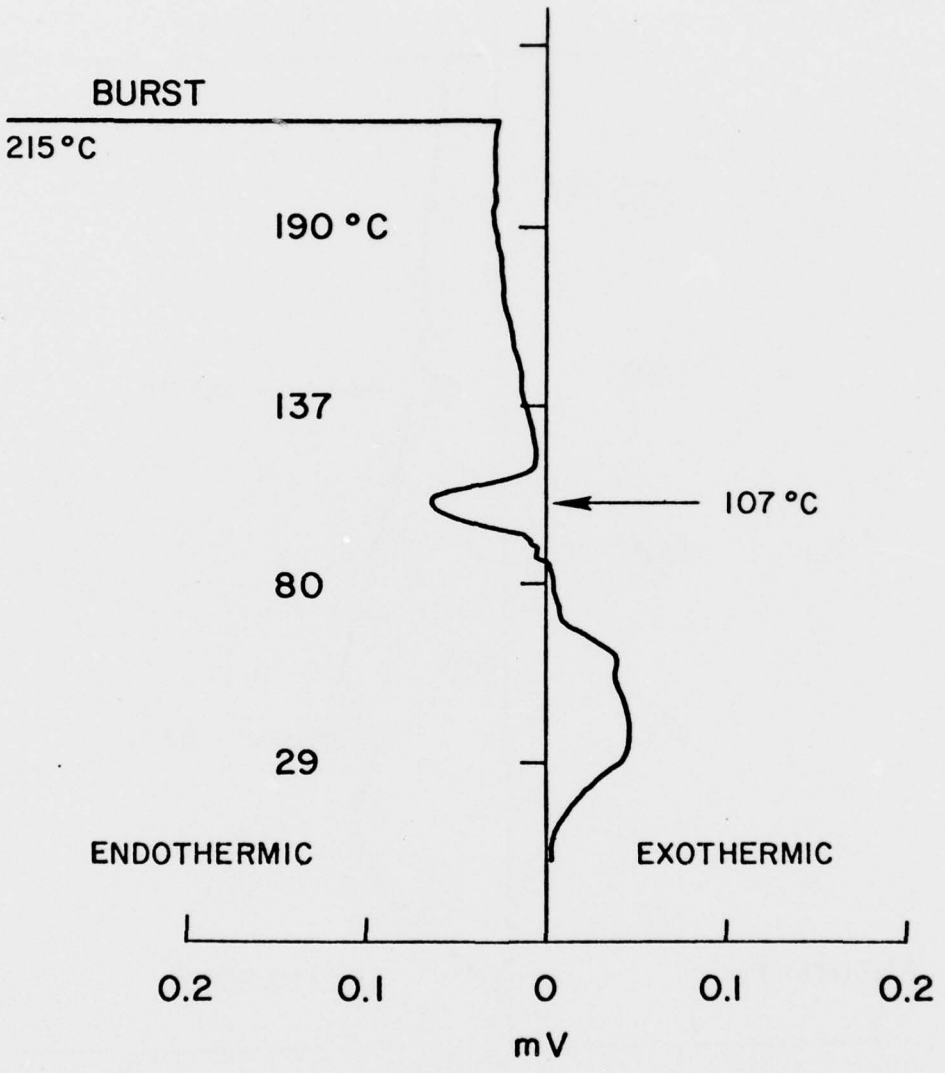

Fig. 84. Thermogram of S + 1M $LiAlCl_4$-$SOCl_2$ (90 vol%) + $POCl_3$ (10 vol%)
Sample #90

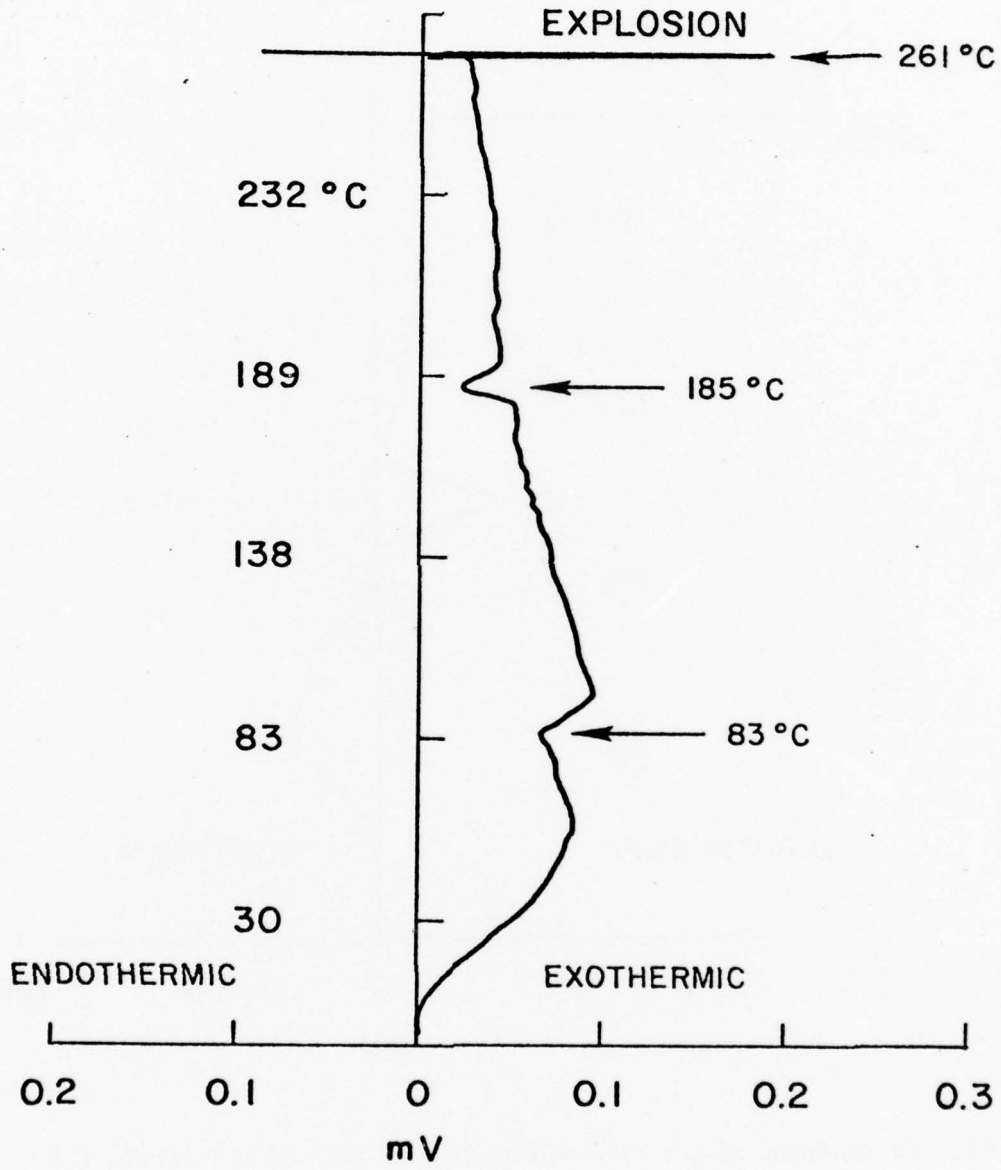

Fig. 85 Thermogram of Li + S + 1M $LiAlCl_4$-$SOCl_2$ (90 vol%) + S_2Cl_2 (10 vol%)
Sample #92

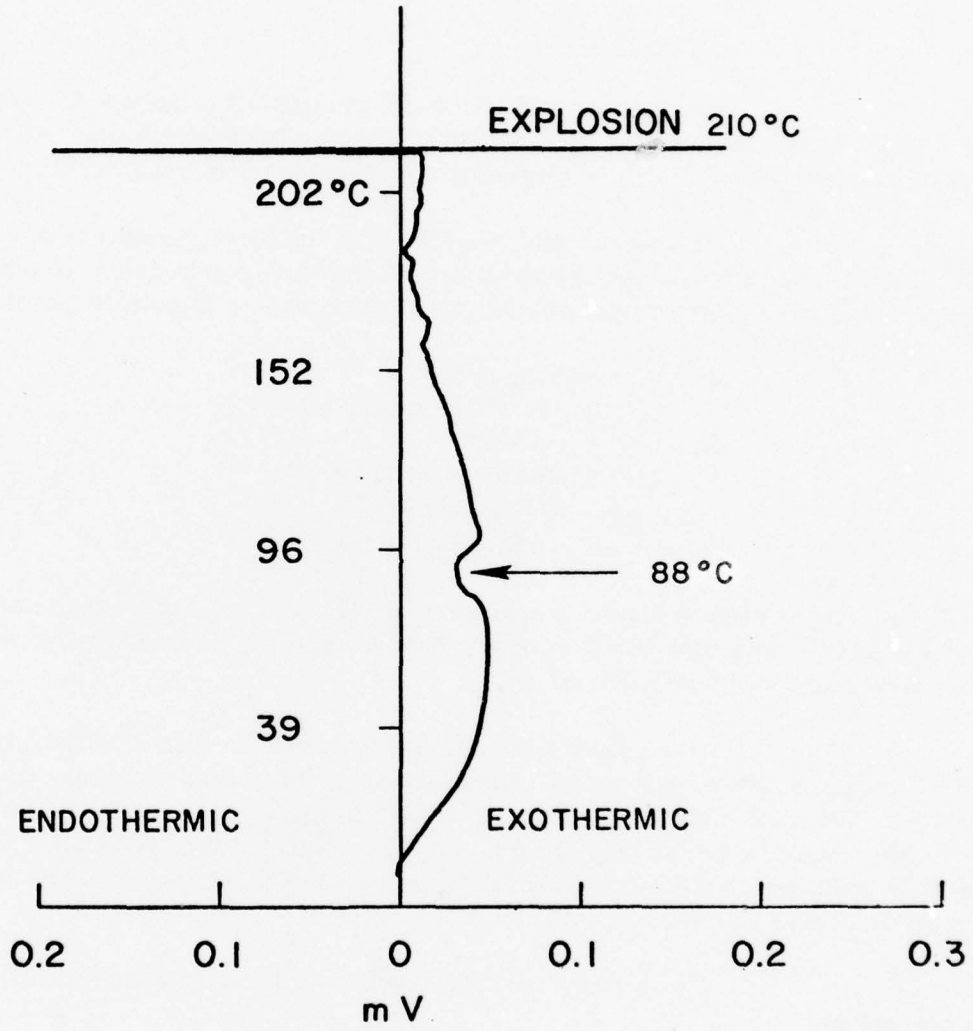

Fig. 86. Thermogram of Li + S + 1M $LiAlCl_4$-$SOCl_2$ (90 vol%) + CS_2 (10 vol%)
Sample #93

44. Li + S + 1(M) $LiAlCl_4$, $SOCl_2$ (90 vol%) + $POCl_3$ (10 vol%)

The thermogram, as shown in Fig. 87, consists of two endotherms at 105° and 185°C corresponding to the dissolution of S and the melting of Li respectively. The sample exploded violently with an exotherm at 225°C.

All the above DTA results are summarized in Table 18.

6.1.3 Conclusions

In general, all the cell constituents except Li and $SOCl_2$ were found to be quite inert when tested singly. Li showed exothermic reaction with glass sample container and $SOCl_2$ underwent endothermic pressure burst.

In binary combination, the following chemicals were found to be capable of initialing and propagating an exothermic combustion and/or thermal runaway. The lowest temperature at which it occurred is shown in parenthesis.

1. Li + $SOCl_2$ (192°C)
2. Li + glass filter paper (207°C)
3. Li + S (153°C)
4. Li + Li_2SO_3, H_2O (139°C)
5. Li_2S + $SOCl_2$ (145°C)
6. Li_2SO_3 + $SOCl_2$ (167°C)

In all the above binary combinations except (1) and (2), the exotherms occurred below the melting point of Li whereas in the case of (1) and (2) the exotherm occurred at or above the melting point of Li.

Also, note that the presence of Li is not essential for the initiation and/or propagation of a thermal runaway, as in the case of binary combinations (5) and (6). Although the presence of Li_2S and Li_2SO_3 in a partially discharged cell has not been completely established as yet, it is reasonable to assume that the chemical reaction between Li and S or SO_2 which are present in the cell may lead to the formation of Li_2S and Li_2SO_3.

The binary combinations which caused endothermic pressure bursts were:

7. Li_2S + $SOCl_2$ (207°C)
8. S + $SOCl_2$ (236°C)
9. Carbon cathode + $SOCl_2$ (241°C)
10. $Li_2SO_3 \cdot H_2O$ + $SOCl_2$ (76°C)
11. Li_2SO_3 + $SOCl_2$ (171°C)

All the combinations contained $SOCl_2$ which decomposed to SO_2 and Cl_2 leading to a pressure burst. In the case of the binary combination (10) water of hydration catalyzed this decomposition so that the pressure burst occurred at as low a temperature as 76°C. This demonstrated the importance of the catalytic effects of minor amounts of impurities on the safety of the Li/$SOCl_2$ system.

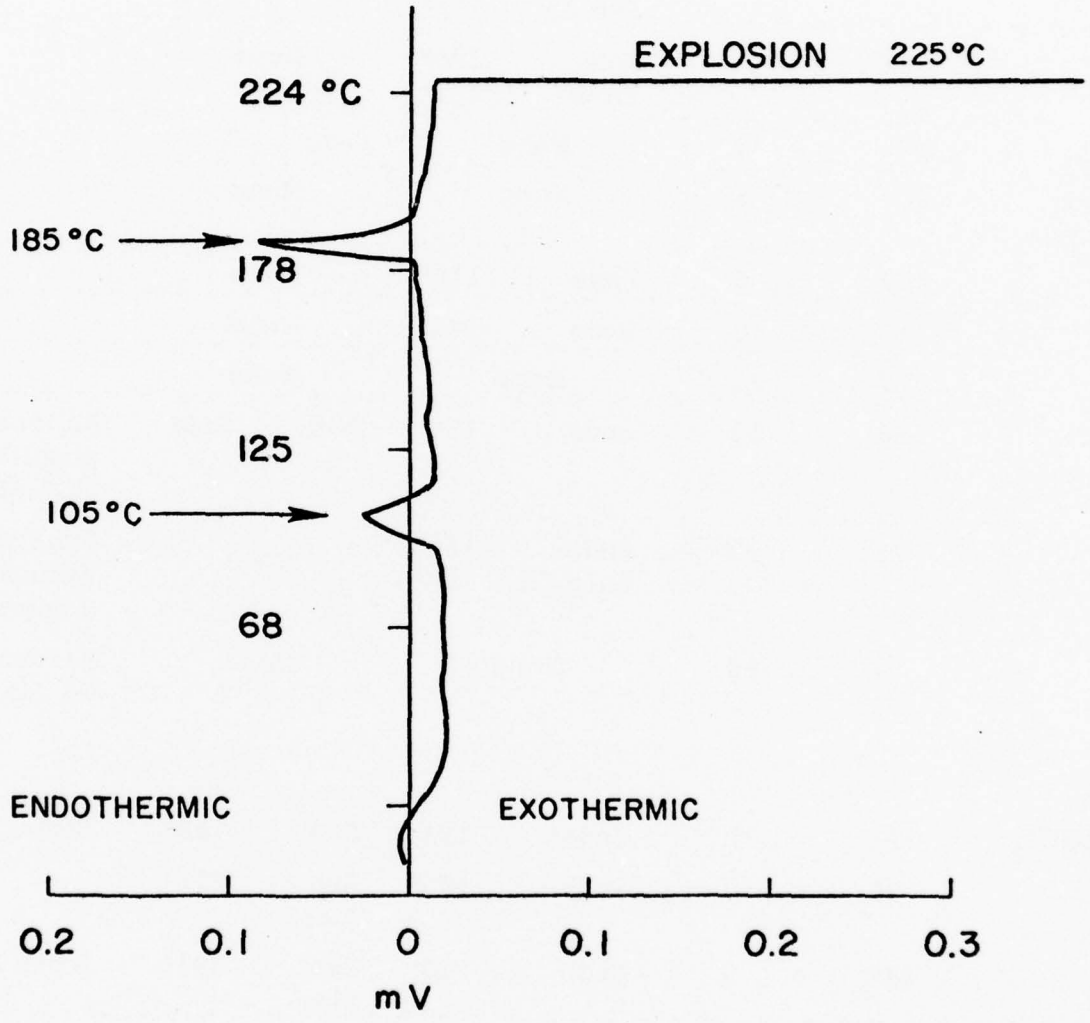

Fig. 87. Thermogram of Li + S + 1M $LiAlCl_4$-$SOCl_2$ (90 vol%) + $POCl_3$ (10 vol%) Sample #94

TABLE 18

Summary of the DTA Results

Materials	Tube Number	Heating Rate (°C/Min)	Peaks Type	Peaks Temp	Explosions Type	Explosions Temp	Remarks
Li	101	5	Endo Exo 2X Exo 2X	180° 195° 202°	None		Tube broken and stuck in block
S	102	5	Endo Endo	106° 121°	None		
$SOCl_2$	105	5	None		Endo	231°	
Carbon Cathode	103	5	None		None		
$LiAlCl_4$	112	5	Endo	118°	None		
LiCl	113	5	Endo	143°	None		
Li_2S	37	10	None		None		
Li_2SO_3	60	10	Endo	183°	Endo	214°	As received from supplier contains H_2O of hydration
	71	10	Endo Endo 5X	162° 199°	None		Tube Broken Vacuum dried 75°C 8 hours.
	74	10	None		None		Vacuum dried 135°C 20 hours.
$Li+SOCl_2$	21	10	Endo	183°	Exo	192°	Broke TC's
	26	10	Endo	189°	Exo Blast	227°	
	107	5	Endo	180°	Exo Blast	291°	Broke DTC
Li + Cathode	65	10	Endo Exo 5X	170° 187°	None		Tube broken and stuck in block
	85	10	Endo Exo 5X Exo 50X	184° 197° 199°	None		Tube broken and stuck in block.
	86	10	Endo Exo	183° 214°,224°	None		Tube broken and stuck in block

Materials	Tube Number	Heating Rate (°C/Min)	Peaks Type	Peaks Temp	Explosions Type	Explosions Temp	Remarks
Li + Glass Paper	38	10	Endo	187°	None		Tube broken and stuck in block
			Exo	207°			
			Exo 10X	214°			
	39	10	Endo	187°	None		Tube broken and stuck in block TC weld broken
			Exo 50X	208°			
Li_2S+$SOCl_2$	34	10	Exo	77°			
			Exo 5X	142°	Endo	219°	
	51	10	Exo	74°			
			Exo 10X	145°	Endo	207°	
			Exo	167°			
	52	10	Exo	76°			
			Exo 5X	147°	Endo	229°	
			Exo	163°			
S + $SOCl_2$	27	10	sm.Endo	71°			
			Endo	107°	Endo	236°	
Li + S	41	10	Exo	93°			
			Endo	113°	None		Small crack in tube
			Endo	128°			
			Exo 5X	174°			
	42	10	sm. Endo	113°			
			Endo	126°	None		
			Exo 50X	168°			
	43	10	Endo	112°			
			Endo	122°	None		Tube broken
			Exo 20X	184°			
	44	10	sm.Endo	126°			
			Exo 50X	172°	None		
	45	10	sm. Endo	126°			
			Endo	132°	None		
			Exo 20X	164°			
	46	10	Endo	117°			
			Endo	127°	None		
			Exo 50X	178°			
	47	10	sm.Endo	116°			
			Endo	126°	None		Tube cracked
			Exo 20X	172°			
	48	10	Endo	120°			
			Endo	126°	None		Tube broken and stuck in block
			Exo 10X	159°			
			sm.Endo	252°			
	49	10	Endo	118°			
			Endo	124°	None		Tube broken and stuck in block
			Exo 50X	153°			
			sm.Exo	290°			

Materials	Tube Number	Heating Rate (°C/Min)	Peaks Type	Peaks Temp	Explosions Type	Explosions Temp	Remarks
Li + S	50	10	Endo Endo Exo 50X	118° 129° 157°	None		Tube broken and stuck in block
Li_2O	73	10	None		None		
	80	10	sm Exo sm Endo	147° 153°	None		
S + Cathode	28	10	Endo Endo sm Endo	124° 134° 184°	None		
Li + Li_2S	58	10	Endo	194°	None		
Li_2S + S	59	10	Endo Endo	116° 122°	None		
Li + Li_2SO_3	61	10	Exo Endo Exo 5X	139° 169° 174°	None		Tube broke and stuck in block
	75	10	Endo Exo Exo 20X	162° 171° 179°	None		Vac dried 135° 20 hrs. Li_2SO_3. Tube broken and stuck
S + Li_2SO_3, H_2O	62	10	Endo Endo Endo Endo	105° 120° 163° 207°	None		Tube stuck in heating block
S + Li_2SO_3	76	10	sm Endo Endo Endo	71° 105° 115°	None		Vac dried 135° 20 hrs Li_2SO_3
Li_2SO_3, H_2O +$SOCl_2$	63	10	None		Endo	76°	
Li_2SO_3+$SOCl_2$	82	10	Exo Exo Exo	83° 112° 167°	Endo	171°	Vac dired 135° 20 Hr. Li_2SO_3
Cathode + Li_2SO_3, H_2O	64	10	Endo	209°	None		Bottom of tube broken
Cathode+Li_2SO_3	78	10	None		None		Vac dried 135° 20 hr Li_2SO_3
Li+$LiAlCl_4$+ $SOCl_2$	67	10	sm Endo	169°	Exo	223°	Blast and flames broke TC and insulators

Materials	Tube Number	Heating Rate (°C/Min)	Peaks Type	Peaks Temp	Explosions Type	Explosions Temp	Remarks
$Li+S+SOCl_2$	25	10	Endo	194°	Exo	204°	Broke TC's and insulator
Li+S+Ni tab	40	10	Endo	92°			
			Endo	134°	None		
			Exo 50X	182°			
	57	10	sm Endo	115°			
			Endo	126°	None		
			Exo 50X	174°			
Cathode+S+ $SOCl_2$	19	10	Endo	105°			
			Exo	121°	Endo	228°	
	23	10	Endo	100°			
			sm Endo	154°	Endo	219°	
			sm Endo	197°			
	29	10	Endo	105°	Endo	197°	
$Li+S+Li_2S$	35	10	Endo	81°,96°			
			Endo	117°,131°	None		Small crack in tube
			Exo 10X	179°			
			Endo	290°			
	53	10	sm Endo	127°			
			sm Endo	149°	None		
			Exo 50X	172°			
	54	10	sm Endo	116°			
			sm Endo	123°	None		
			Exo 50X	173°			
$Li+Li_2S+$ $SOCl_2$	66	10	Exo	134°			
			Endo	169°	Exo	214°	Broke TC and insulator
$S+1(M)LiAlCl_4$ $+SOCl_2$	68	10	Endo	93°	Endo	193°	
	87	10	Endo	103°	Endo	227°	
Cathode+1(M) $LiAlCl_4+SOCl_2$	69	10	Broad				
			Endo	88°	Endo	238°	
$Li_2S+1(M)$ $LiAlCl_4+SOCl_2$	70	10	sm Exo	80°			
			Exo 2X	109°	Endo	197°	
			Exo 2X	118°			
			sm Exo	149°			
$Li_2SO_3+LiAlCl_4$ $+SOCl_2$	81	10	None		Endo	184°	Vac dried 135° 20 hrs Li_2SO_3
$Li+Li_2SO_3+$ $SOCl_2$	83	10	Endo	188°	Exo	204°	

Materials	Tube Number	Heating Rate (°C/Min)	Peaks Type	Peaks Temp	Explosions Type	Explosions Temp	Remarks
$Li+S+S_2Cl_2$	95	10	Endo	185°	Exo	302°	
	96	10	Endo 73°, Endo 5X	183°, 191°			
			Exo 20X	197°	None		Tube broken, bottom half stuck in block
			Exo 5X	205°			
			Exo	224°			
$Li+S+CS_2$	97	10	None		Exo	169°	
	98	10	None		Exo	178°	Blue flames
$Li+S+POCl_3$	99	10	Endo	108°	Exploded when furnace was lifted off after the run		
			Endo	184°			
	100	10	Endo	107°			
			Endo	115°	Exo	309°	Broke TC and insulator
			Endo	184°			
$Li+S+LiAlCl_4+SOCl_2$	84	10	Endo	99°			
			Endo	122°	Exo	273°	Blast, broke TC and insulator
			Endo	188°			
	91	10	Endo	98°			
			Endo	184°	None		All liquid gone from tube
			Broad Endo	236°-288°			
$Li+S+SOCl_2+S_2Cl_2$	22	10	sm Endo	88°			
			sm Endo	139°	Exo	238°	Blast, broke TC and insulator
			sm Endo	191°			
	32	10	Endo	103°			
			Endo	187°	Exo	256°	
	33	10	sm Endo	90°			
			sm Endo	146°	Exo	234°	Broke TC and insulator
			Endo	184°			
$S+LiAlCl_4+SOCl_2+S_2Cl_2$	88	10	Endo	96°	Endo	208°	
$S+LiAlCl_4+SOCl_2+CS_2$	89	10	Endo	93°			
			Broad Endo	224°	None		
$S+LiAlCl_4+SOCl_2+POCl_3$	90	10	Endo	107°	Endo	215°	
$Li+S+LiAlCl_4+SOCl_2+S_2Cl_2$	92	10	Endo	83°			
			sm Endo	185°	Exo	261°	Blast, broke TC and all TC insulators
$Li+S+LiAlCl_4+SOCl_2+CS_2$	93	10	Endo	88°			
			Endo	160°	Exo	210°	Broke TC and in-
			sm Endo	185°			
$Li+S+LiAlCl_4+SOCl_2+POCl_3$	94	10	Endo	105°			Broke TC insulators
			Endo	185°	Exo	225°	

The DTA results of the ternary and the quarternary combinations indicate that the addition of $LiAlCl_4$ to all the binary combinations containing $SOCl_2$ did not alter their thermograms in any significant way. The electrolyte salt has little effect on the safety of the $Li/SOCl_2$ system.

On the other hand, the addition of $SOCl_2$ to the binary combinations such as (3) and (4), resulted in significant changes in the thermograms. The temperatures at which the exothermic explosion occurred was increased above the melting point of Li. This leads us to conclude that the presence of excess $SOCl_2$ at the end of the discharge may be beneficial from a safety standpoint.

The effect of additives such as S_2Cl_2, $POCl_3$ and CS_2 was found to be insignificant in all samples containing $SOCl_2$. However, in samples containing no $SOCl_2$, the presence of S_2Cl_2 and $POCl_3$ increased the temperature at which the exothermic explosion occurred from (200-252°C) to (302°-309°C). This leads us to conclude that the effect of S_2Cl_2 and $POCl_3$ on the safety of a fresh and/or partially discharged cell is negligible but it may be significant in the case of a completely discharged cell which contains no $SOCl_2$.

In summary, the following conclusions were arrived at from the DTA studies:

1. If the cells can be designed to maintain all of cell interior at temperatures below 100°C at all times, *including all local sites in the cell*, the cells will probably not experience thermal run-aways or explosions.

2. The electrolyte salts may not have any significant effects in the safety of the $Li/SOCl_2$ system.

3. The catalytic affects of trace quantities of impurities may lead to unpredictable hazardous conditions, not yet fully explored.

4. Usefulness of additives such as S_2Cl_2 and $POCl_3$ in enhancing the safety of the cells could not be demonstrated.

5. The development of chemical inhibitors remains an open question.

6. The effects of unstable reaction intermediates remain to be studied (SO and its intermediate reaction products).

6.2 Exothermicity Measurements

The primary objective of these experiments was to identify the chemical combinations present in a partially discharged cell that may generate heat locally by spontaneous chemical reaction at room temperature, leading to a spontaneous thermal runaway as experienced with some Li/$SOCl_2$ cells. We measured the differential temperatures of the various chemicals that may be present in the cell when they are combined at room temperature. We call it the "exothermicity" of the chemical mixture.

6.2.1 Experimental

The apparatus is shown schematically in Fig. 88. It consists of two identical glass sample holders with a special thermocouple trough at the bottom. One sample holder contains alumina at room temperature. The other sample holder contains the first chemical A to be examined. The second chemical B is added from the inlet tube in the form of liquid or vapor and mixes with the first chemical. The temperature changes occurring during the mixing and/or reaction between A and B is monitored on a strip chart recorder. The entire system is maintained in a thermostatic bath. A rise in the temperature indicates any exothermic reactions, including the heat of mixing. We carried out these measurements with: Li, $SOCl_2$, Li_2S, Li_2O, LiOH, H_2O, O_2 in order to identify the exothermic combinations.

6.2.3 Results and Discussion

The experiments were carried out in three parts. In the first part we added dry $SOCl_2$ vapor to the various materials to check the exothermicity. The results are summarized in Table 19. The experiments were done in sequence according to the columns under chemical B from left to right of Table 19. Note that passage of argon through the chemicals Li_2S, Li_2O, LiOH, $Li_2S + Li_2O$, Li, Li + S and $Li + S + Li_2S$ caused no reaction, exothermic or endothermic, as expected. Next, on passage of $SOCl_2$ vapor with argon (bubbling argon through $SOCl_2$) through the above chemicals caused exothermic reactions with all the above chemicals except Li and Li + S. It indicates that spontaneous heat generation is possible when $SOCl_2$ comes in contact with chemicals such as Li_2S that may be produced in the cells.

In the second part we added liquid $SOCl_2$ to the various chemicals and also moisture along with the liquid $SOCl_2$. The results are summarized in Table 20. Again going from left to right of column under chemical B note that argon produced no reaction as before. But addition of liquid $SOCl_2$ along with the continuing argon flow caused strong exothermic reactions in all cases except with Li and Li + S where endothermic reactions were observed because of

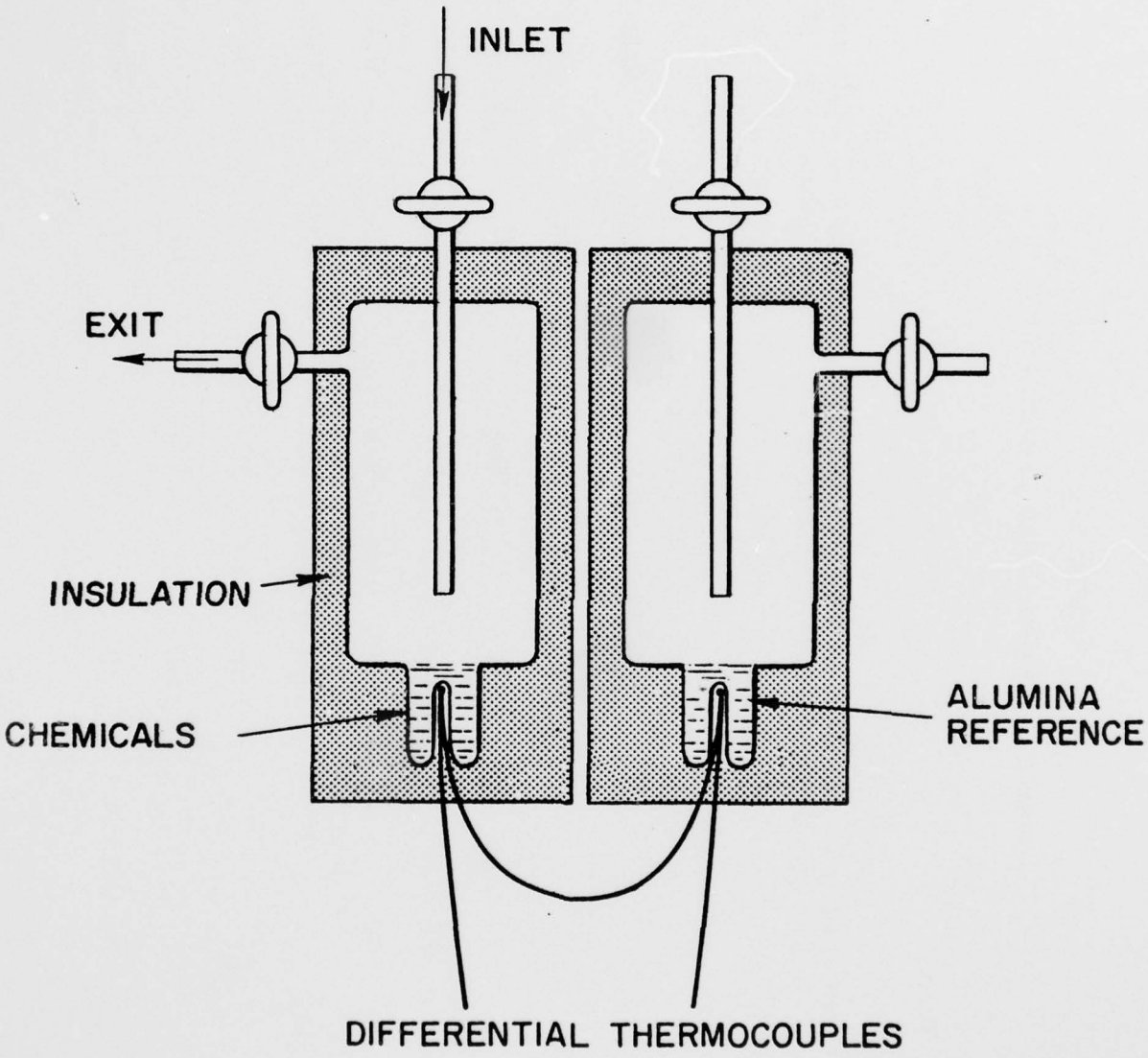

Fig. 88. Apparatus for Exothermicity Measurements

TABLE 19

Summary of Exothermicity Experiments

Part 1: Dry $SOCl_2$ Vapor

Procedure: Weigh sample in container in dry box, attach to apparatus and begin recording of differential temperature. Flow gas through sample container as follows: (1) argon only, (2) argon through $SOCl_2$, (3) argon only.

Chemical A	Chemical B			
Materials and Weight	Argon	Argon $SOCl_2$	Argon	Appearance After
Li_2S = .190	NR	Exo	NR	Unchanged
Li_2O = .274	NR	Exo	NR	Unchanged
H_2O = .714 (not weighed in dry box)	Endo	Exo 2X	Endo	Unchanged
LiOH = .288	NR	Exo	NR	Unchanged
Li_2S = .085 + Li_2O = .122	NR	Exo	NR	Small amt. turned yello
Li = .048	NR	NR	NR	Unchanged
Li = .042 + S = .257	NR	NR	NR	Unchanged
Li = .023 + S = .309 + Li_2S = .048	NR	Exo	NR	Unchanged

N.R. = No Reaction

2X = Magnification of the differential temperature measuring scale. Higher x values indicate stronger exothermic reactions.

TABLE 20

Summary of Exothermicity Experiments

Part 2: $SOCl_2$ Liquid and H_2O Vapor

Procedure: Sample prepared as in Part 1. Flow gas and add liquid as follows: (1) argon only, (2) add .1ml $SOCl_2$ while continuing dry argon, (3) argon through H_2O, (4) in some cases, add another .1ml $SOCl_2$ while continuing argon through H_2O, in several experiments this step of H_2O vapor continued overnight, (5) argon only.

Chemical A	Chemical B					
Materials & Weight	Argon	Argon $SOCl_2$ liq.	Argon H_2O	Argon/H_2O $SOCl_2$ liq.	Argon	Appearance After
Li_2S = .294	NR	Exo 20X	Exo	-	Endo	Black liquid soaked into yellow powder.
Li = .035	NR	Endo	Exo 2X	-	Endo	Li turned white - no liquid - grey top layer.
Li_2O = .239	NR	Exo 50X	Exo	Exo	Endo	Yellow streak along side, bottom white liquid on top.
Li = .024 + S = .341	NR	Endo	Exo	-	Endo	Li white, S not reacted, liquid on top.
LiOH = .213	NR	Exo 20X	Small Exo	Exo 5X	Endo	Color unchanged - liquid soaked in about halfway.
Li_2S = .109 + Li_2O = .079	NR	Exo 2X	Exo	Exo 50X White Smoke	Endo	Yellow & black liquid soaked in about halfway. Bottom unreacted.
Li = .021 + S = .270 + Li_2S = .044	NR	Exo	Exo 10X	Exo 2X	Endo	Yellow and a few dark lines, flaky particles floating in liquid. Li not visible.

N. R. = No Reaction

20X = High X values indicate stronger exothermic reaction.

the evaporation of $SOCl_2$ by flowing argon. Next, addition of H_2O vapor by means of argon caused exothermic reactions in all cases, as expected. The results indicate that ingress of moisture into $Li/SOCl_2$ cells may lead to a hazardous condition by setting off exothermic reactions which may lead to a thermal runaway. Such a condition might occur if an alleged hermetic seal lost its hermeticity due to corrosion, or if electrolyte were transferred from a cell under conditions of perceptible humidity.

In the third part, as summarized in Table 21, we determined the effect of O_2 and we repeated some of the experiments of part two. The results indicate that O_2 has no effect and confirm the previous results of part two concerning the strong exothermic reaction of liquid $SOCl_2$ and moisture with all the above chemicals.

6.2.3 Conclusions

Several exothermic chemical combinations have been identified. The $Li_2S + SOCl_2$ combination undergoes spontaneous exothermic reaction. Since a partially discharged cell contains both Li and S dissolved in $SOCl_2$, the formation of Li_2S according to the reaction

$$2\ Li + S \longrightarrow Li_2S \qquad (20)$$

is likely. This could explain the incidence of explosions of partially discharged cells on storage at ambient temperature. The spontaneous exothermic reaction between $Li_2S + SOCl_2$ may serve as a trigger for the thermal runaway. Moisture enhances the reactions and the system becomes more exothermic in the presence of moisture. Thus, total hermeticity of $Li/SOCl_2$ cells at all stages of discharge, storage and disposal appears to be a pre-requisite for safety.

6.3 Differential Thermal Analysis of Hermetic $Li/SOCl_2$ D Cells

We found the undischarged $Li/SOCl_2$ hermetic D cells to be more stable and predictable than the discharged cells. Also, the thermal runaways experienced by the undischarged D cells on accidental shorting (internal or external) was intrinsically preventable by means of low pressure venting. No such prevention was possible in the case of spontaneous thermal runaway of discharged cells. The latter is also unpredictable. The purpose of this study is to identify and characterize the nature of the instability that may have been generated as a result of the discharge of the $Li/SOCl_2$ D cells. We chose to use a thermal method to characterize the instability of the hermetic D cells since this is the most direct approach and the results may complement our DTA studies of the cell constituents.

TABLE 21

Summary of Exothermicity Experiments

Part 3: $SOCl_2$ Liquid and H_2O Vapor and O_2

Procedure: Sample prepared as in Part 1. Flow gas and add liquid as follows: (1) argon only, (2) O_2 only, (3) add .1ml $SOCl_2$ while continuing dry O_2, (4) O_2 through H_2O, (5) add another .1ml $SOCl_2$ while continuing O_2 through H_2O, (6) O_2 only and (7) argon only

Chemical A	Chemical B							
Materials and Weight	(1)	(2)	(3)	(4)	(5)	(6)	(7)	Appearance After
Li_2S = .138gm	NR	NR	Exo 2X	Exo 100X Smoke	Exo 2X	Endo	Endo	Yellow with a few dark lines, layer of liquid.
Li = .021gm	NR	NR	Endo	Exo 2X	Exo 2X	Endo	Endo	White, thicker, no liquid layer
Li_2O = .159	NR	NR	Exo	Exo	Exo 50X Smoke	Endo	Endo	Black liquid on top, bottom white.
LiOH = .159	NR	NR	Exo 10X	Exo	Exo 2X	Endo	Endo	No color change in powder, top half wet.
Li = .026 + S = .243	NR	NR	Endo	Exo	Endo, then Exo	Endo	Endo	Li partly reacted - S no change.
Li = .024 + S = .239 + Li_2S = .040	NR	NR	Exo	Exo	Exo 2X	Endo	Endo	Top 1/3 powder reacted can't see Li.
Li_2S = .079 + Li_2O = .079	NR	NR	Exo	Exo	Small Exo	Endo	Endo	Top 1/4 reacted - turned yellow, clear liquid on top, bottom unchanged.

N.R. = No Reaction

10X = High X values indicate stronger exothermic reactions.

6.3.1 Experimental

Hermetic D cells were made by winding carbon cathodes (20" x 1.75" x 0.025"), Li anodes (21.25" x 2.0" x 0.015") and two layers of glass filter paper separators into cylindrical spools and packaging them in D size (OD: 1.30", L: 2.38") nickel cans. The cell top was designed with three feedthroughs, two of which are tubes extending halfway down the cell. The tubes are closed at the bottom end and are used as thermocouple wells. The third (short) feedthrough is also a tube and it acts both as an electrolyte fill port and the anode terminal. This tube is closed at the top after the electrolyte filling. The cross-sectional view of the cell is shown in Fig. 89. The thermocouple well that was used for the differential temperature measurements was the one located halfway between the center and the wall of the cell.

The cross-sectional view of the heating fixture developed for carrying out the DTA of the D cells is shown in Fig. 90. It consists of a split aluminum block with two cylindrical cavities for the D cells and three thermocouple wells located at three positions shown in Fig. 90. The two halves of the aluminum block are put together after placing the two D cells in the proper cavities and securing them by means of screws. In this manner good thermal contact is ensured between the D cell and the aluminum block. The aluminum block is then wrapped with heating elements which are connected to a power supply that provides an approximately linear temperature rise. The aluminum fixture is thoroughly insulated on all sides to prevent heat dissipation.

The DTA of D cells was carried out by heating the aluminum fixture so that the temperature of the fixture rose approximately linearly and monitoring the differential temperature of the two D cells, one of which served as the reference.

6.3.2 Results

The sensitivity of the DTA system was checked by running a DTA of two undischarged D cells. The thermogram is shown in Fig. 91. The differential temperature response is shown in millivolts and the temperature of the aluminum fixture is shown in °C. The temperature limit of the experiment was kept relatively low, viz. between room temperature and 70°C. The heating rate was approximately 0.2°C/minute. The absence of any transitions indicate that the D cells were identical in terms of their thermal properties. The open circuit voltage (OCV) of both the cells was monitored during the experiment. It was 3.59V at 25°C and it decreased to 3.57V at 70°C.

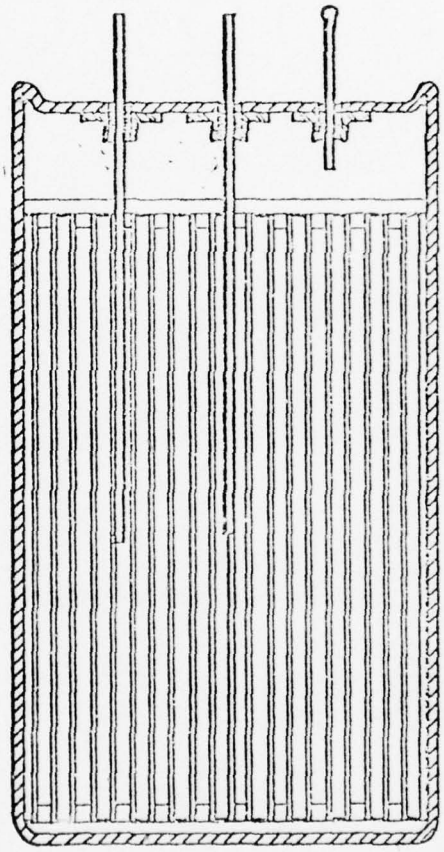

Fig. 89 Cross sectional view of the Li/$SOCl_2$ D cell with thermocouple wells

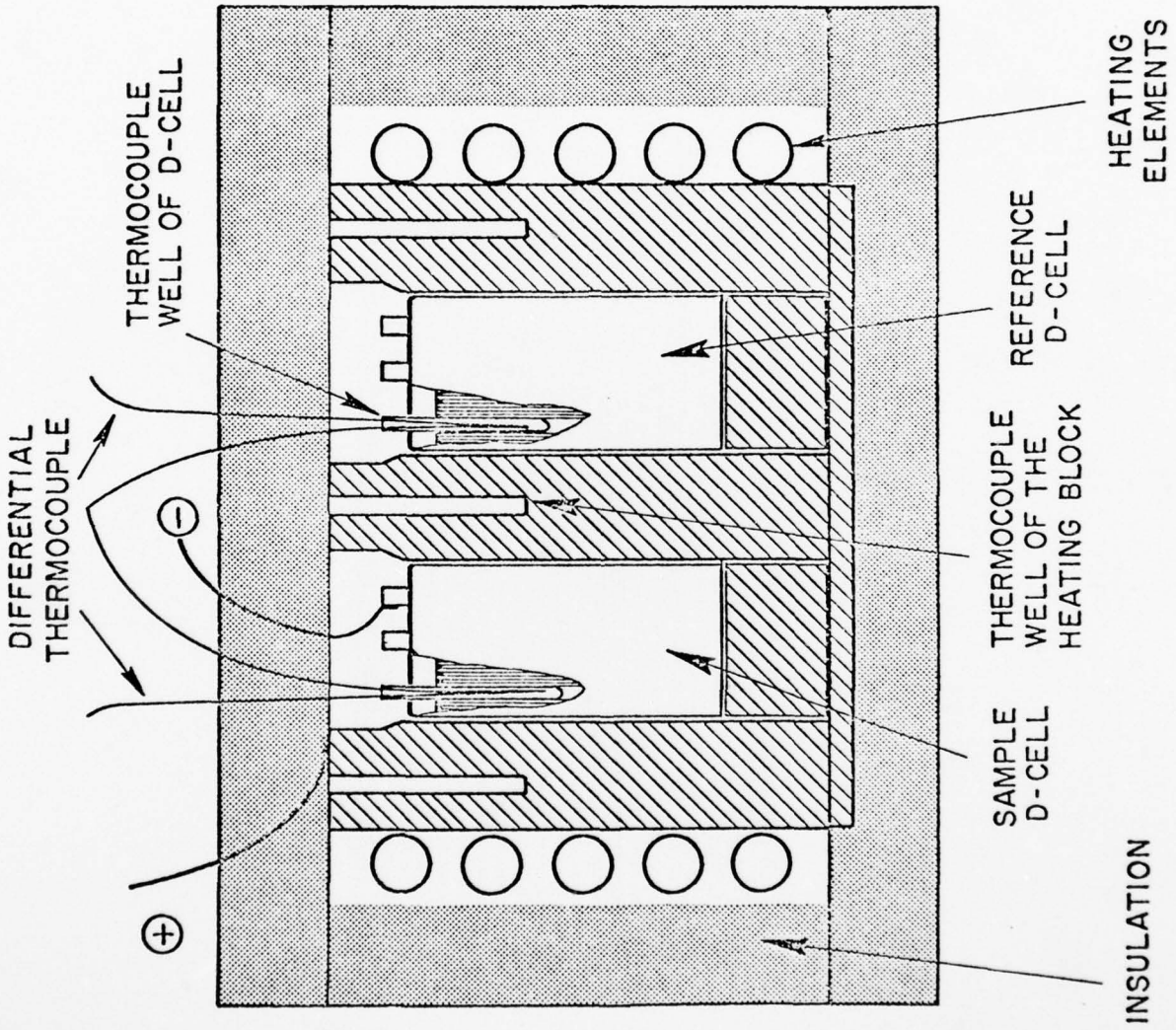

Fig. 90 Fixture for DTA of $Li/SOCl_2$ D cells

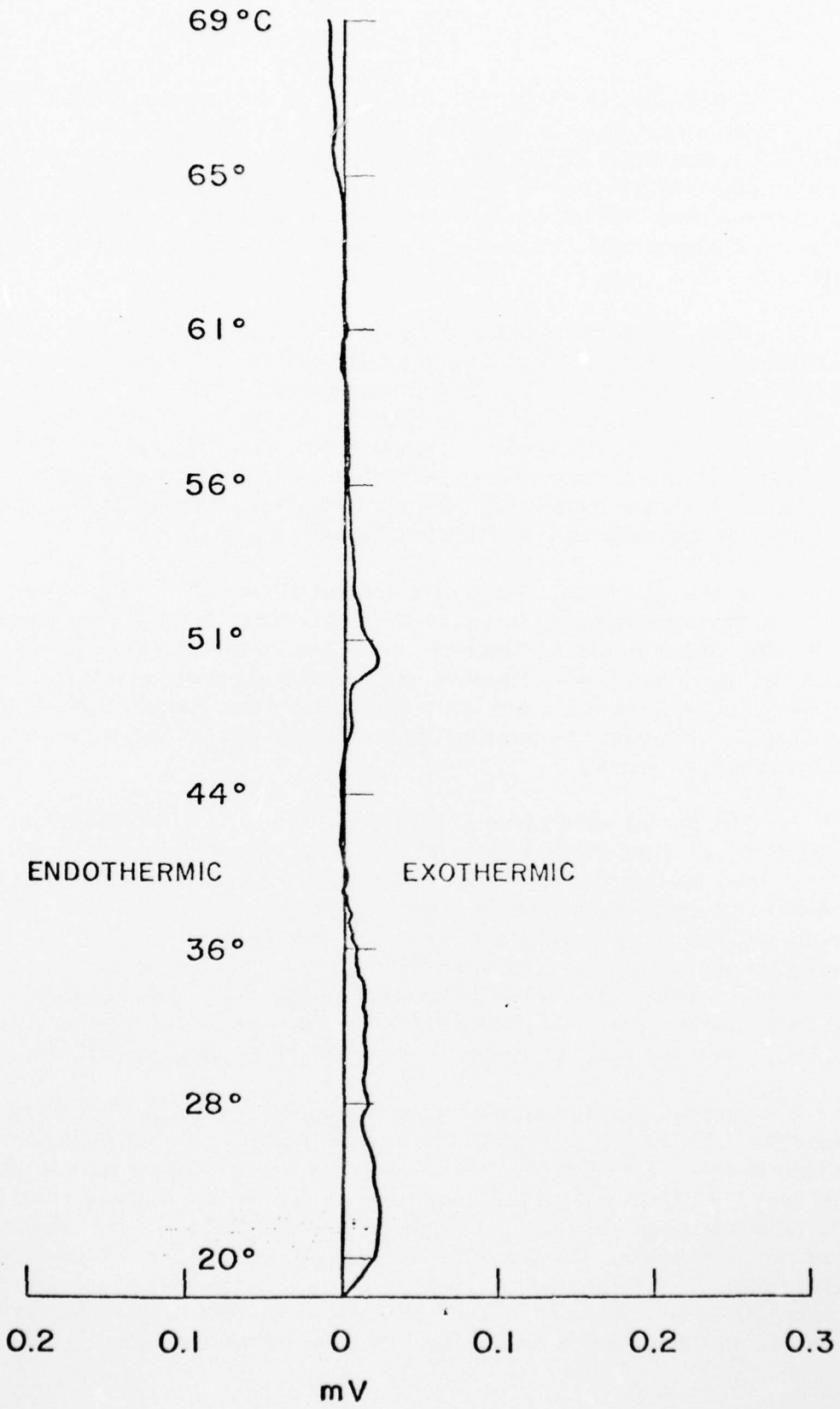

Fig. 91 Thermogram of two fresh $Li/SOCl_2$ D cells

A DTA run of an undischarged D cell using another D cell filled with Al_2O_3 as a reference is shown in Fig. 92. The gradual drift of the differential temperature at the start is attributed to the difference in the thermal characteristics of the $Li/SOCl_2$ cell and the reference cell. Again, the absence of any transitions indicate that Al_2O_3 filled D cells can be used as a reference cell. The temperature was increased to almost 100°C in this run.

Next, we discharged a D cell at 0.25A to remove 6A.Hr of its capacity and then ran a DTA of this partially discharged D cell against a D size can filled with Al_2O_3. The thermogram is shown in Fig. 93. The initial drift was due to Al_2O_3 as before. A very broad exothermic peak around 80°C was observed. A second run, Fig. 94, using the same discharged cell and a fresh cell as reference, showed no exothermic transitions. The use of fresh cell as a reference instead of Al_2O_3, prevents the drifting of the base line of the thermogram.

In the above runs we kept the upper limit of the temperature at 100°C. In the next run we increased the upper limit of the temperature to 163°C. The thermograms of two fresh cells are shown in Fig. 95. The absence of the drifting base lines as well as the absence of any transitions indicate that the fresh cells are quite similar in their thermal characteristics up to 163°C. An upper temperature limit of about 170°C was maintained for all the subsequent runs.

The D cell which was discharged at 6A.Hr and subjected to DTA runs earlier was discharged further at 0.25A for an additional capacity of 7.1A.Hr; thus making the total removed capacity 13.1A.Hr. This discharged cell was used again for a DTA run with a fresh cell as a reference. The thermogram showed no transitions from room temperature up to 70°C. The thermogram at temperatures between 70° and 163°C is shown in Fig. 96. The average heating rate was 0.35°/minute. The thermogram showed two exothermic peaks close together at 92° and 103°; and a third smaller one at 148°C. A repeat run, as shown in Fig. 97, showed no transitions.

Another D cell was discharged completely at 0.25A, realizing a capacity of 12.7A.Hr. The DTA thermogram of this cell with a fresh cell as a reference is shown in Fig. 98. There are two sharp exothermic peaks at 99° and 112° followed by the beginning of another exothermic peak at 164°. The sharpness of the peaks and the increase of the peak temperatures of this run compared to the previous run (Fig. 96) may be due to the increased heating rates, 0.8°C/minute which is more than twice that of the previous run. The exothermic behavior of the discharged cell appears to be reproducible. The repeat run of the same cells (Fig. 99) showed no transitions as before.

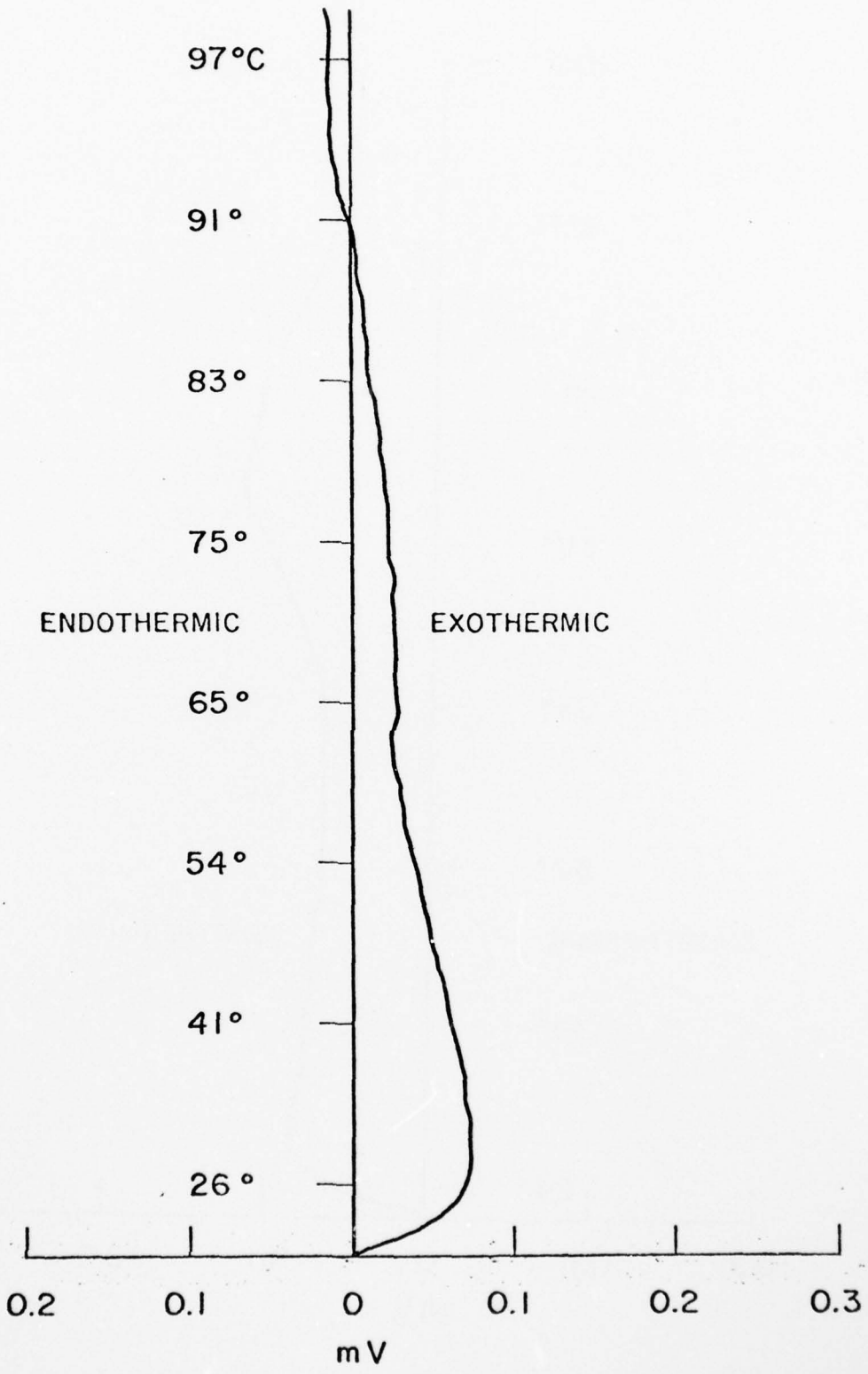

Fig. 92 Thermogram of a fresh $Li/SOCl_2$ D cell against a D size can filled with Al_2O_3

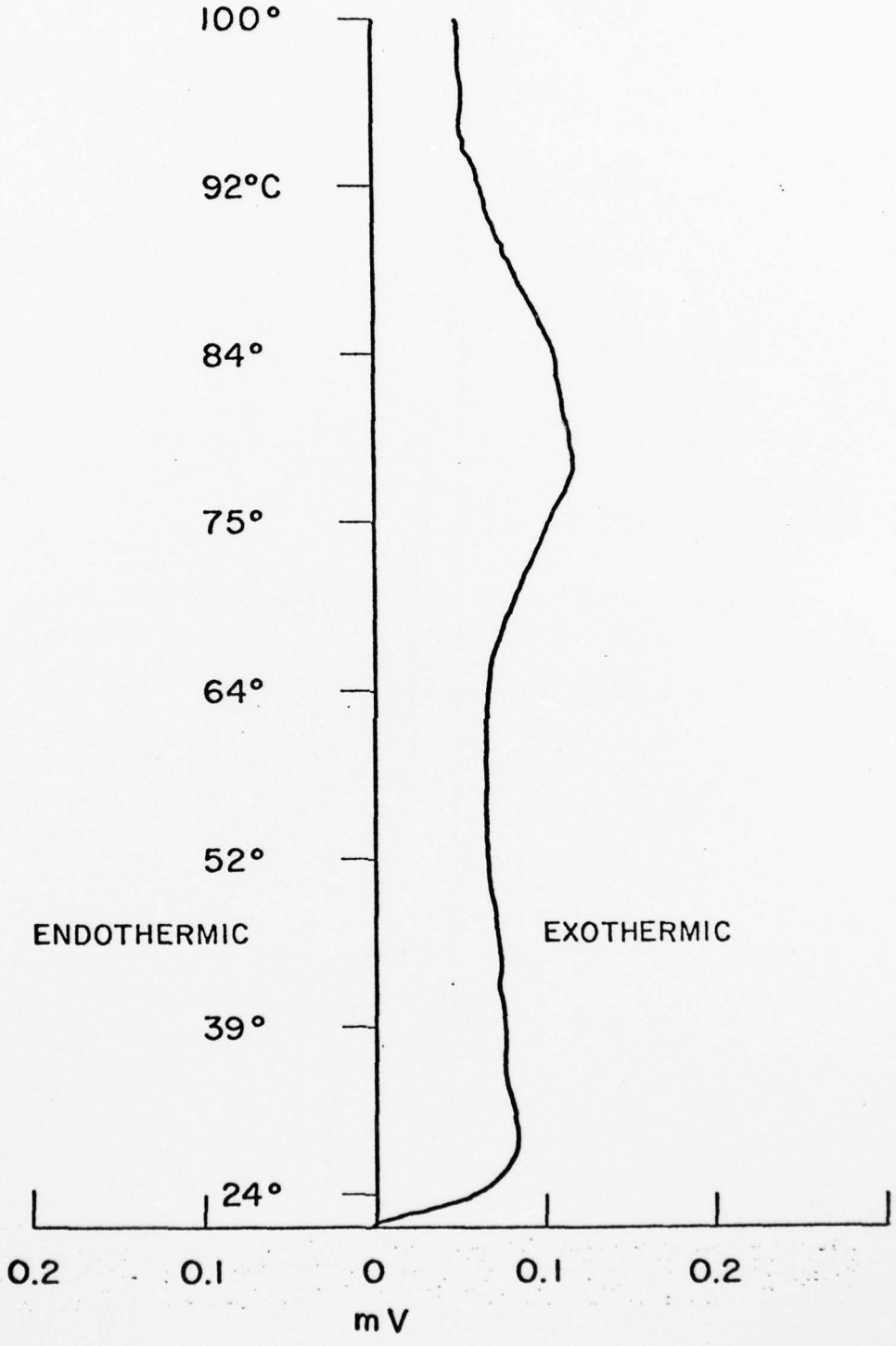

Fig. 93 Thermogram of a partially discharged (6 A.Hr) $Li/SOCl_2$ D cell against Al_2O_3

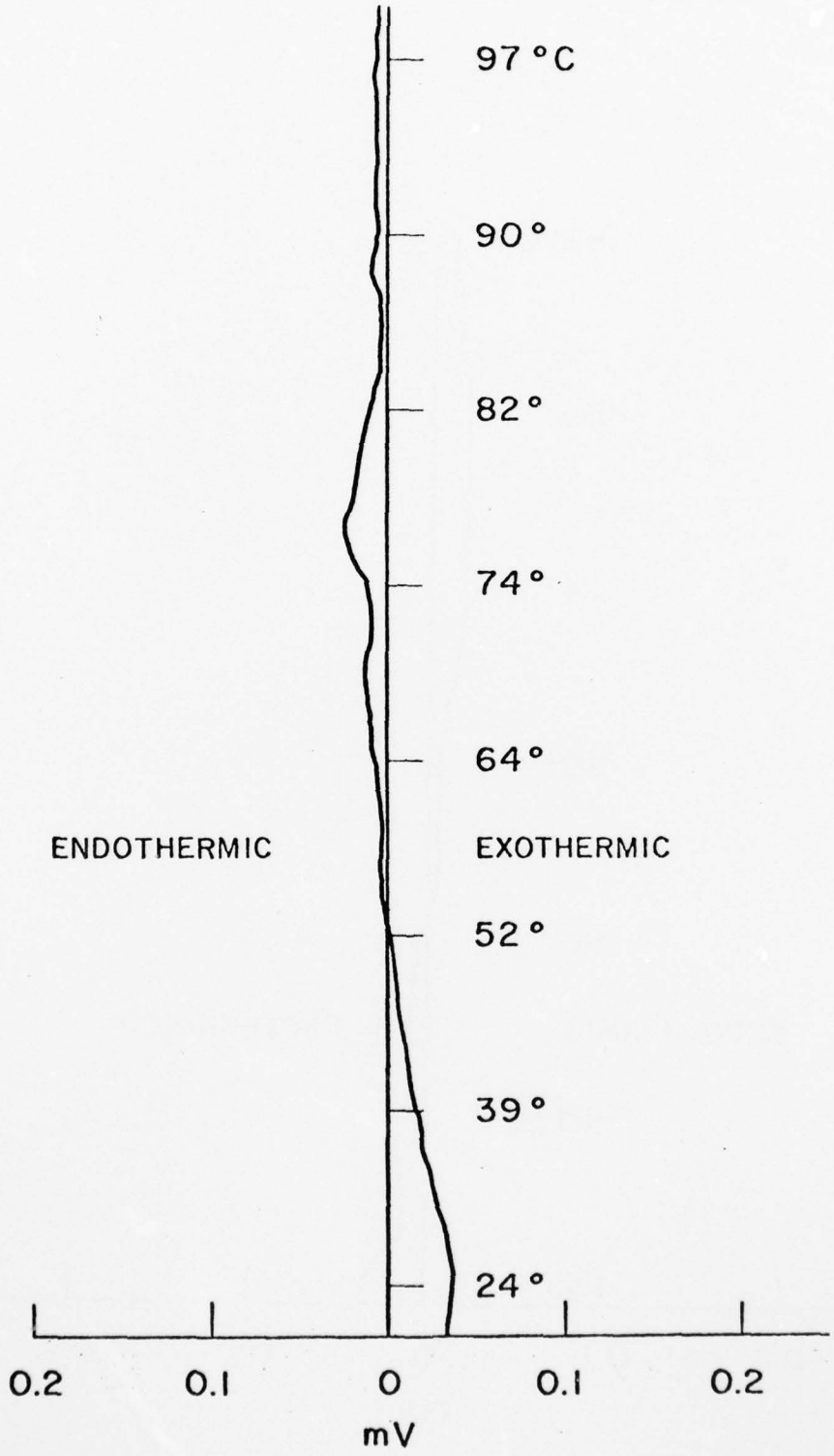

Fig. 94 Thermogram of the partially discharged (6 A.Hr) D cells (second run) against a fresh D cell

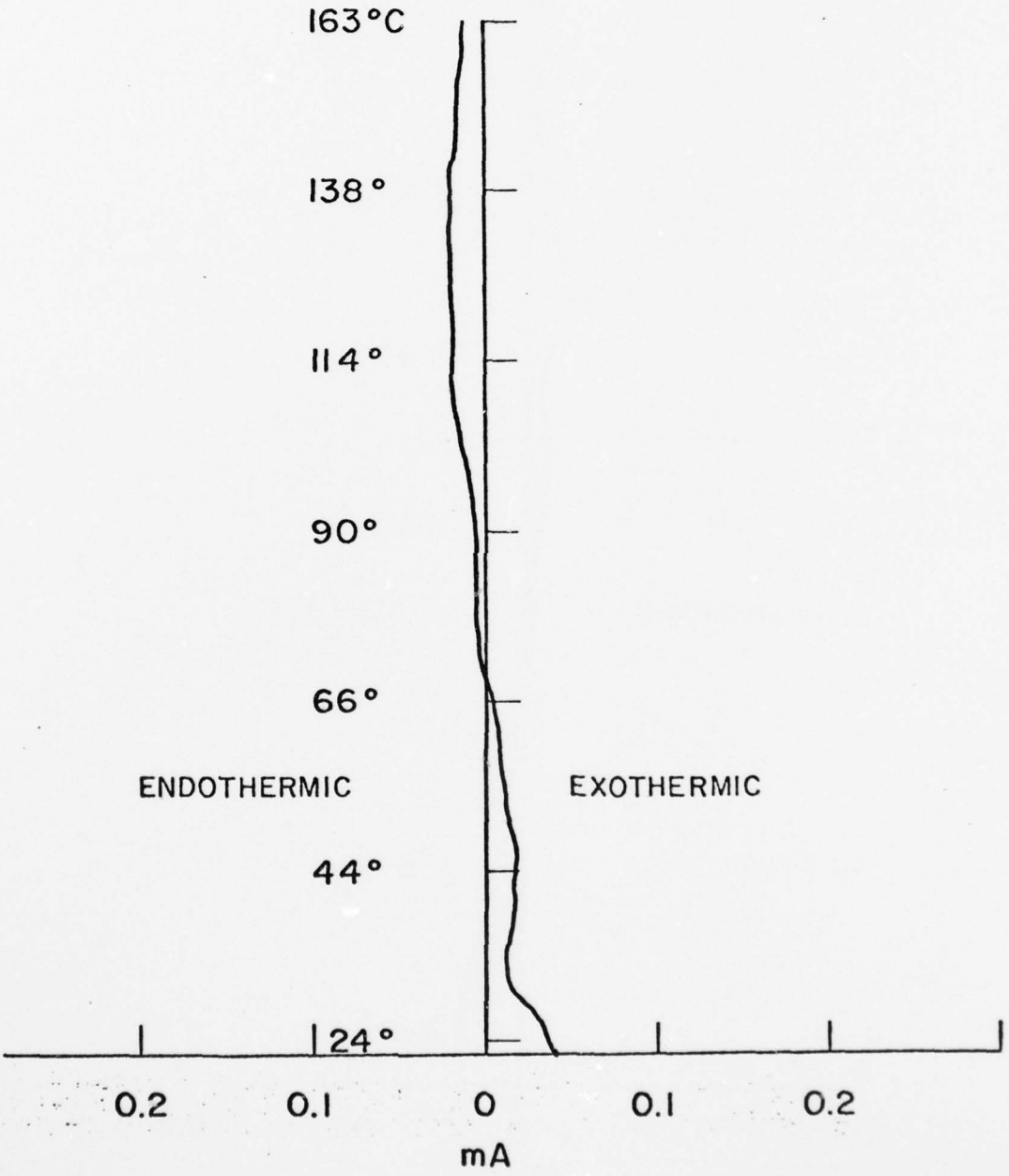

Fig. 95 Thermogram of two fresh $Li/SOCl_2$ D cells

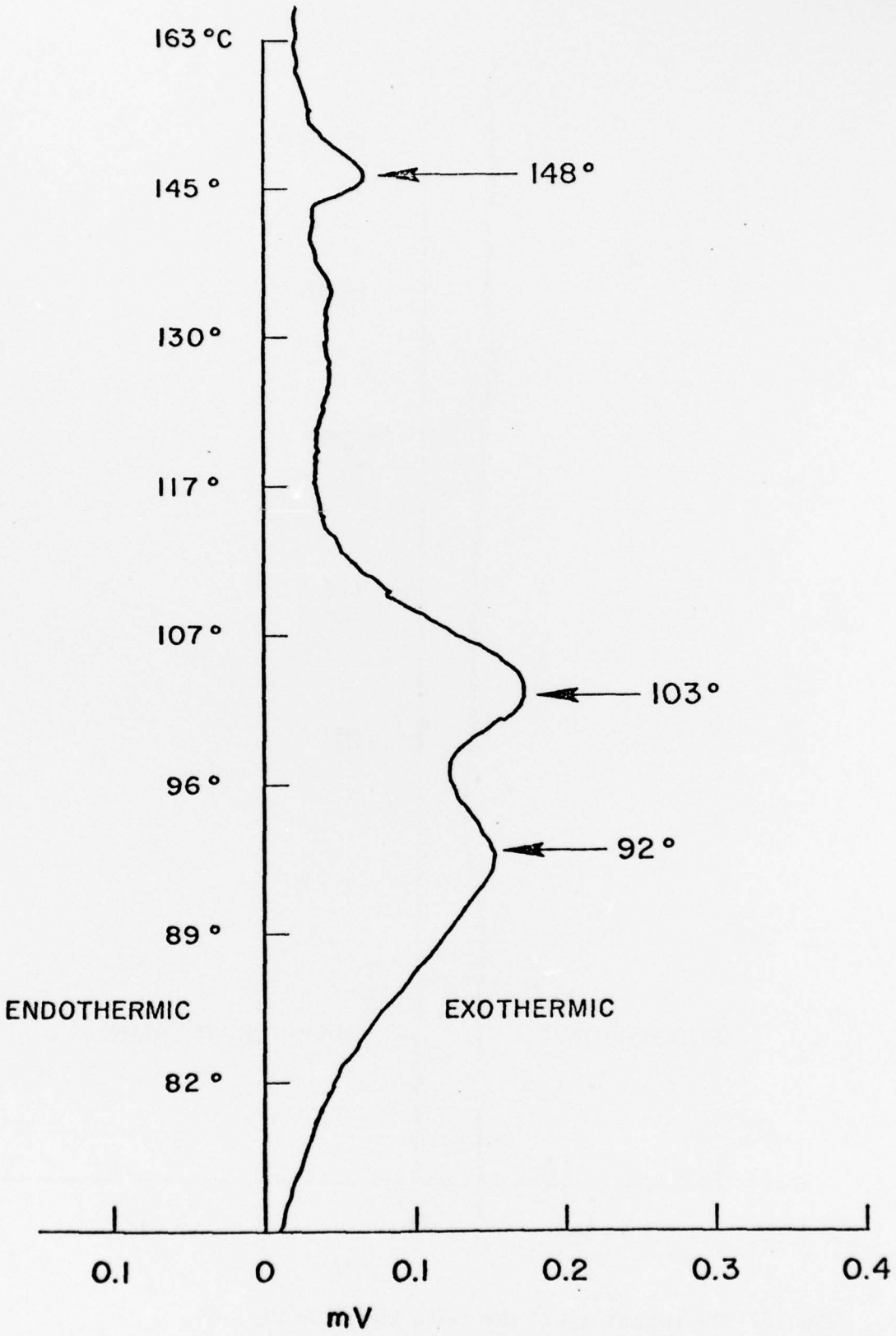

Fig. 96 Thermogram of a completely discharged (13.1 A.Hr) D cell against a fresh cell

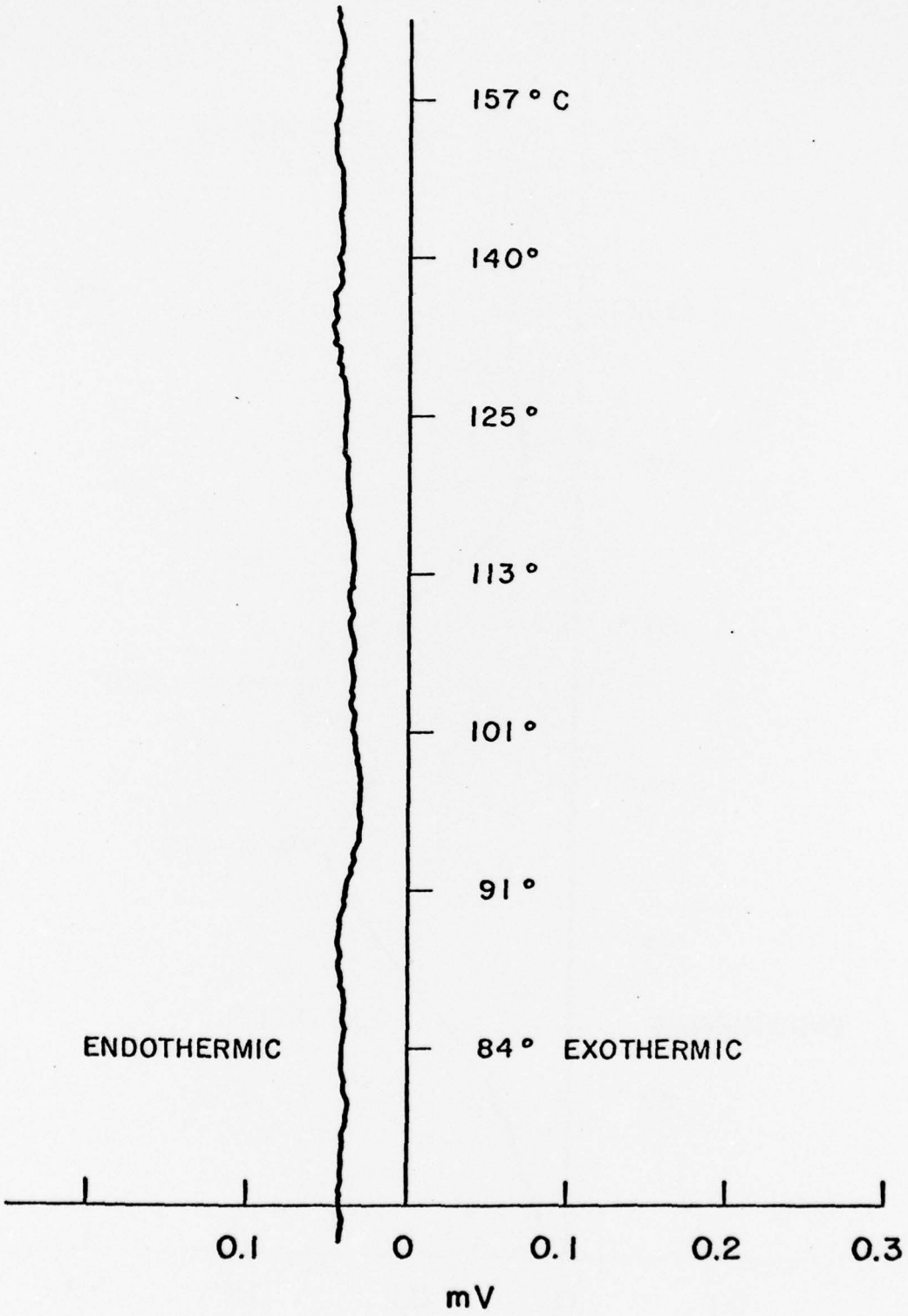

Fig. 97 The repeat run of the cells shown in Fig. 96

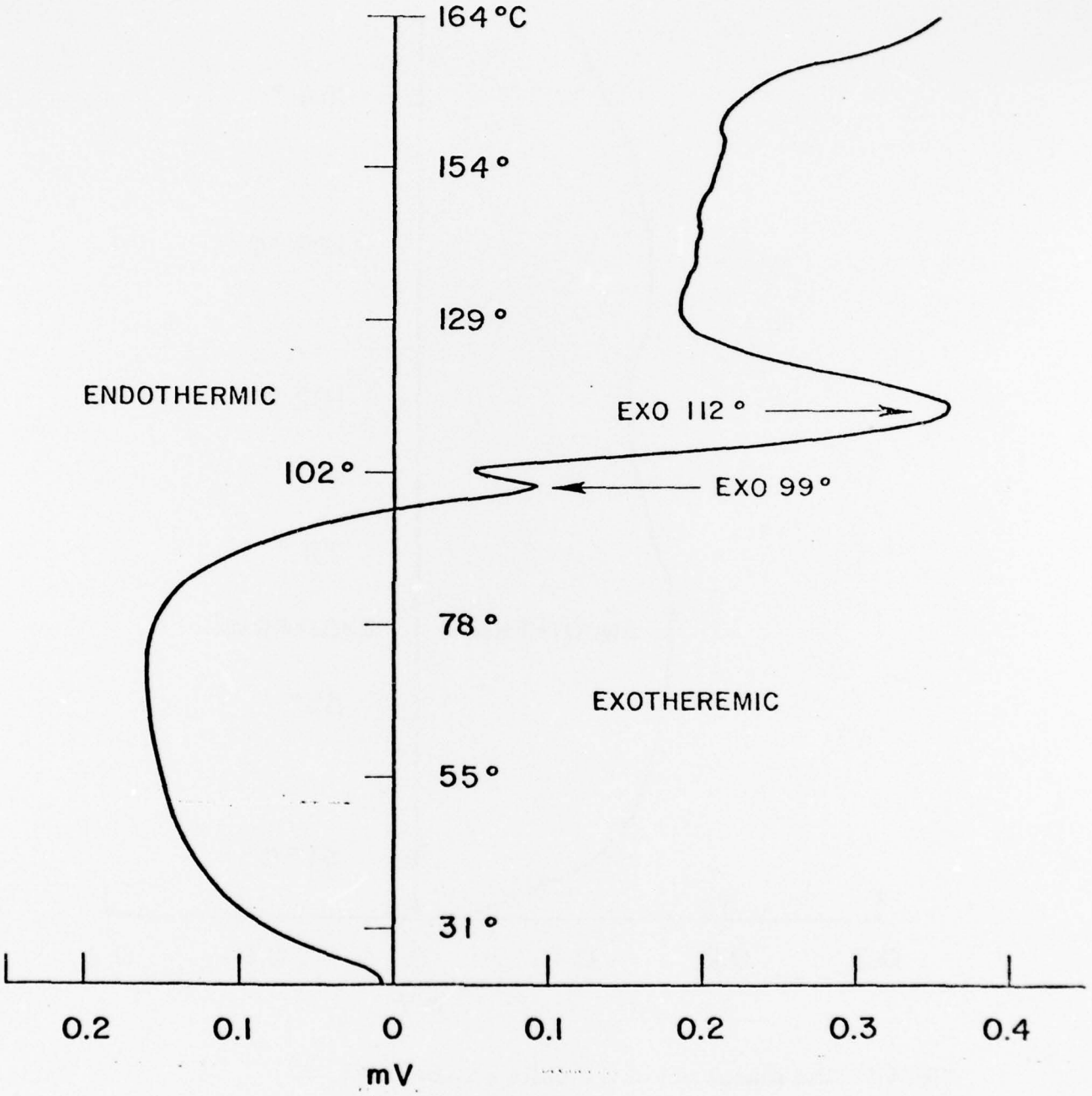

Fig. 98 Thermogram of a completely discharged (12.7 A.Hr) D cell against a fresh cell

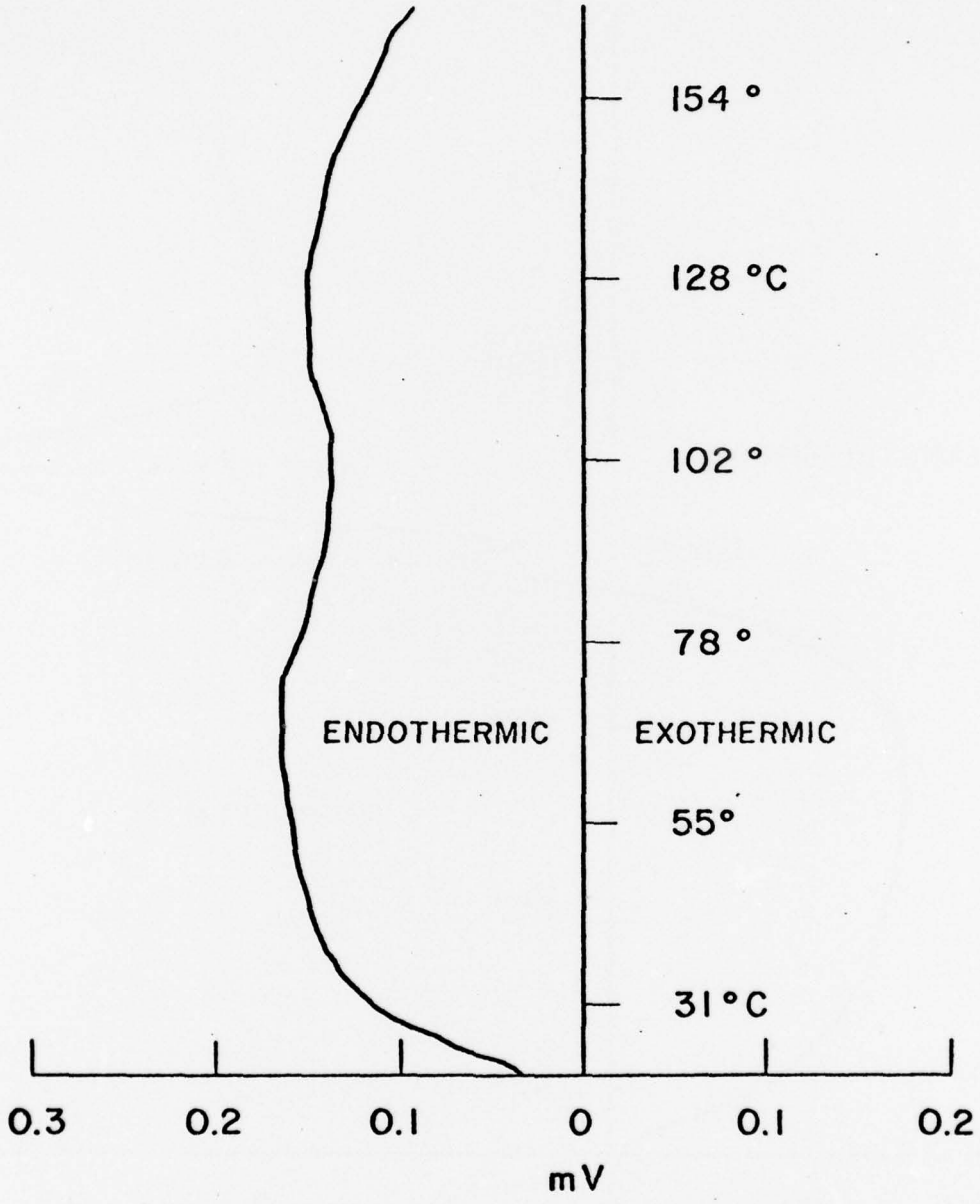

Fig. 99 The repeat run of the cells shown in Fig. 98

We discharged another D cell at 0.25A and realized a capacity of 12.0A.Hr to 2.0 volt. This cell was also subjected to a DTA run using Al_2O_3 (in D can) as reference. The thermogram is shown in Fig. 100. The two sharp exotherms at 90° and 113° followed by the beginning of a third one at 166° are similar to the ones seen in the previous run. The apparent endotherm at 133° is most likely due to the drifting of the base line. The reproducibility of the pehnomenon appears to be quite good. The repeat run of the same cell, (Fig. 101) shows no exothermic transitions except towards the end of the thermogram, where it shows the beginning of an exothermic transition.

We measured the differential temperatures of another D cell during the course of its discharge at 0.25A using Al_2O_3 as reference. We found that the differential temperature remained virtually constant during the discharge and began an exothermic rise towards the end of the discharge. The cell delivered 12.3A.Hr to 2.0 volts. The behavior is quite expected and is shown in the thermogram (Fig. 102) of the cell against Al_2O_3. The differential temperature of the cell was measured at room temperature after passing 0.25A through the previously discharged cell. The differential temperature showed a sharp exothermic rise corresponding to the sharp polarization of the cell voltage. On turning off the current, the differential temperature dropped back and a DTA run was started. The thermogram again showed the two typical exotherms at 101° and 110°. The beginning of the third one is barely noticeable at 168°C. Again, the repeat run (Fig.103) showed only the beginning of an exotherm at 164°C.

All the discharged D cells were examined after the first DTA run and were found to have developed severe bulging of the cell top. The elapsed time between the discharge and the first DTA run was varied from 2 to 6 days and it did not seem to have any effect on the DTA thermogram. Similarly, the elapsed time between the first and the second DTA run was varied from 1 to 7 days and it did not affect the second thermogram.

6.3.3 Discussion

The relative stability of the undischarged $Li/SOCl_2$ cells is demonstrated by the lack of exothermic transistions in the DTA thermogram of undischarged D cells against Al_2O_3 reference. This corroborates the earlier DTA results which showed the absence of any exothermic interactions between the materials present in a fresh cell in the temperature regime below the melting point of Li. The materials that are present in a fresh cell are Li, glass, carbon, Teflon, Ni, $SOCl_2$, $LiAlCl_4$ and trace impurities.

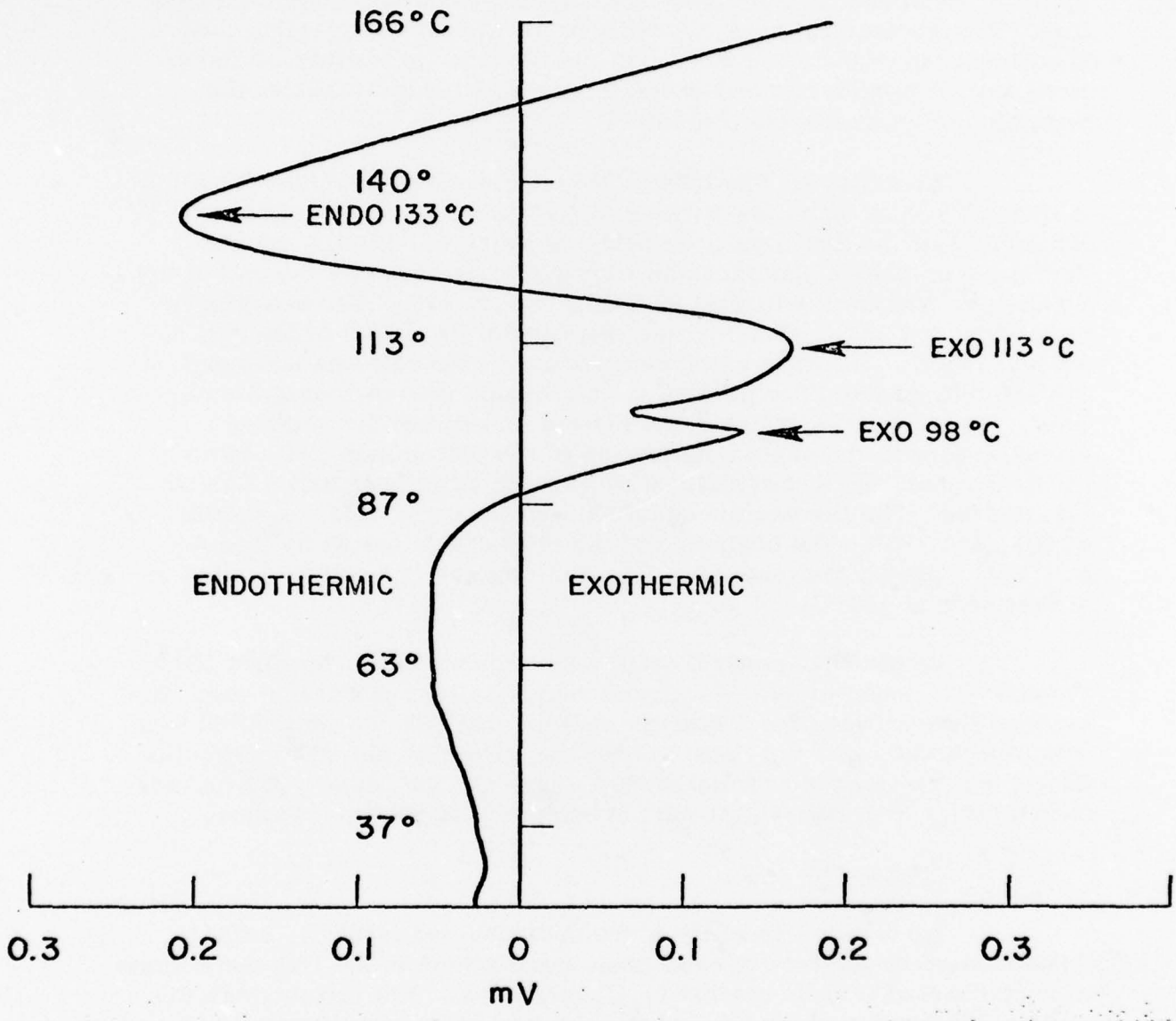

Fig. 100 Thermogram of a completely discharged (12 A.Hr) D cell against Al_2O_3

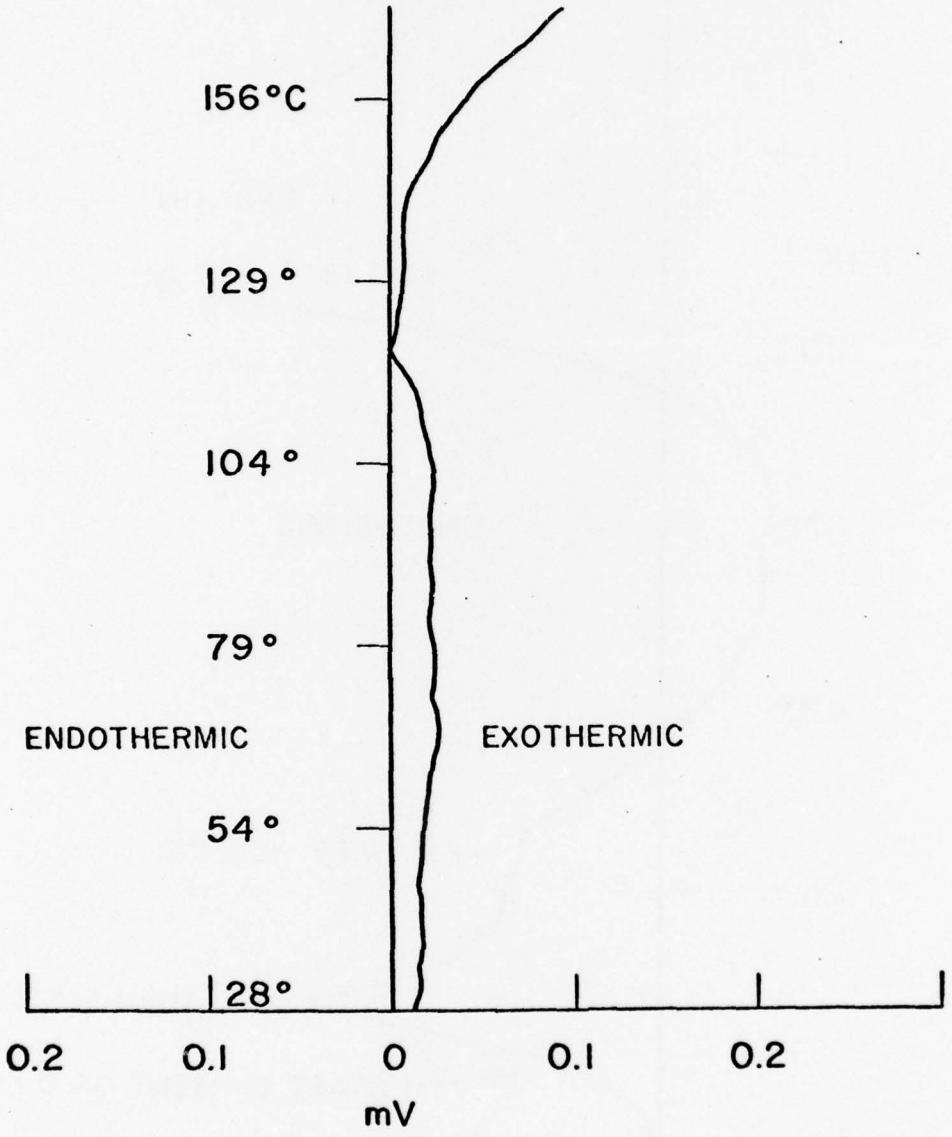

Fig. 101 The repeat run of the cell shown in Fig. 100

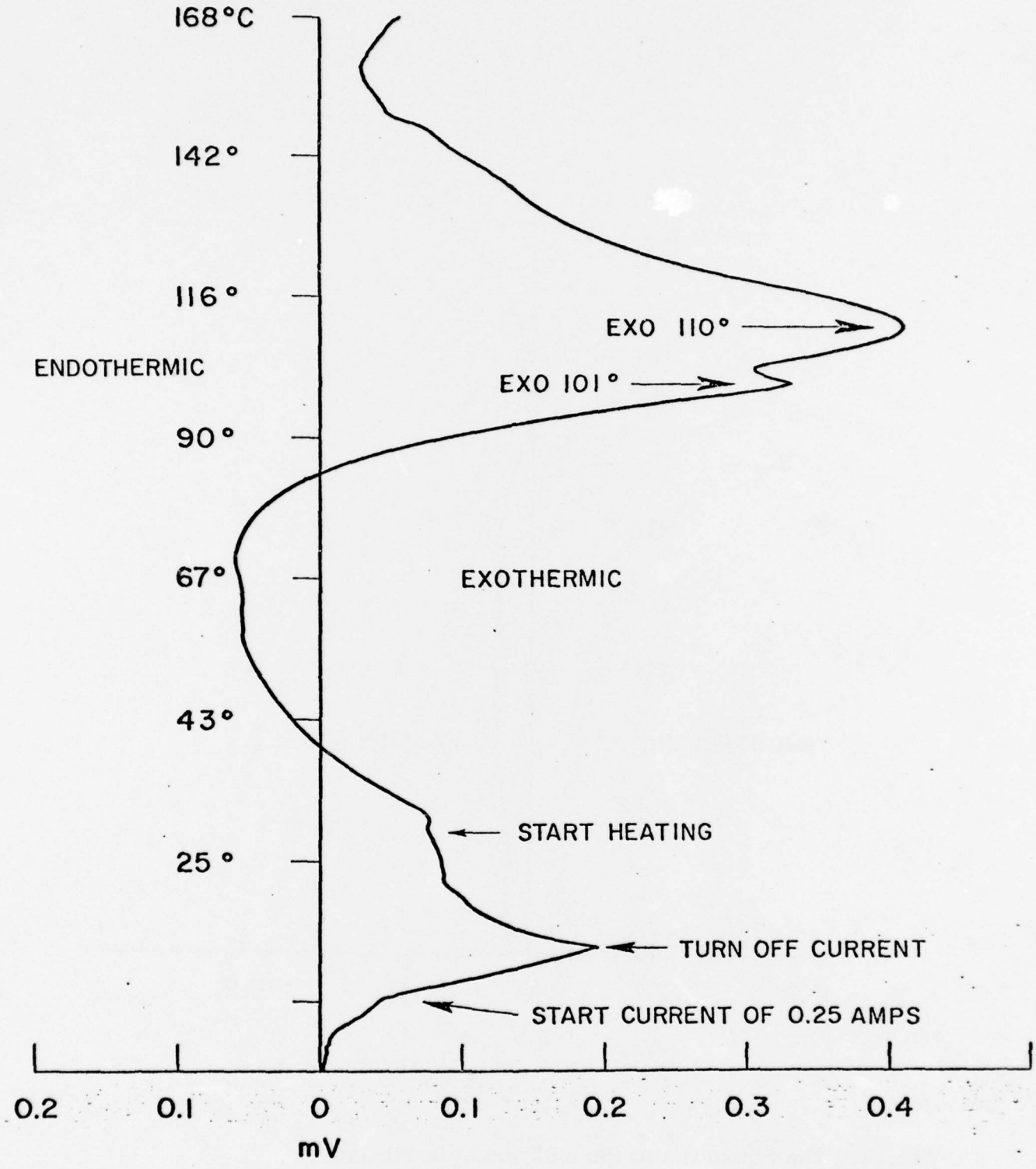

Figure 102 The thermogram of a completely discharged (12.3 A.Hr) D cell against Al_2O_3, showing the effect of overdischarge on the differential temperature

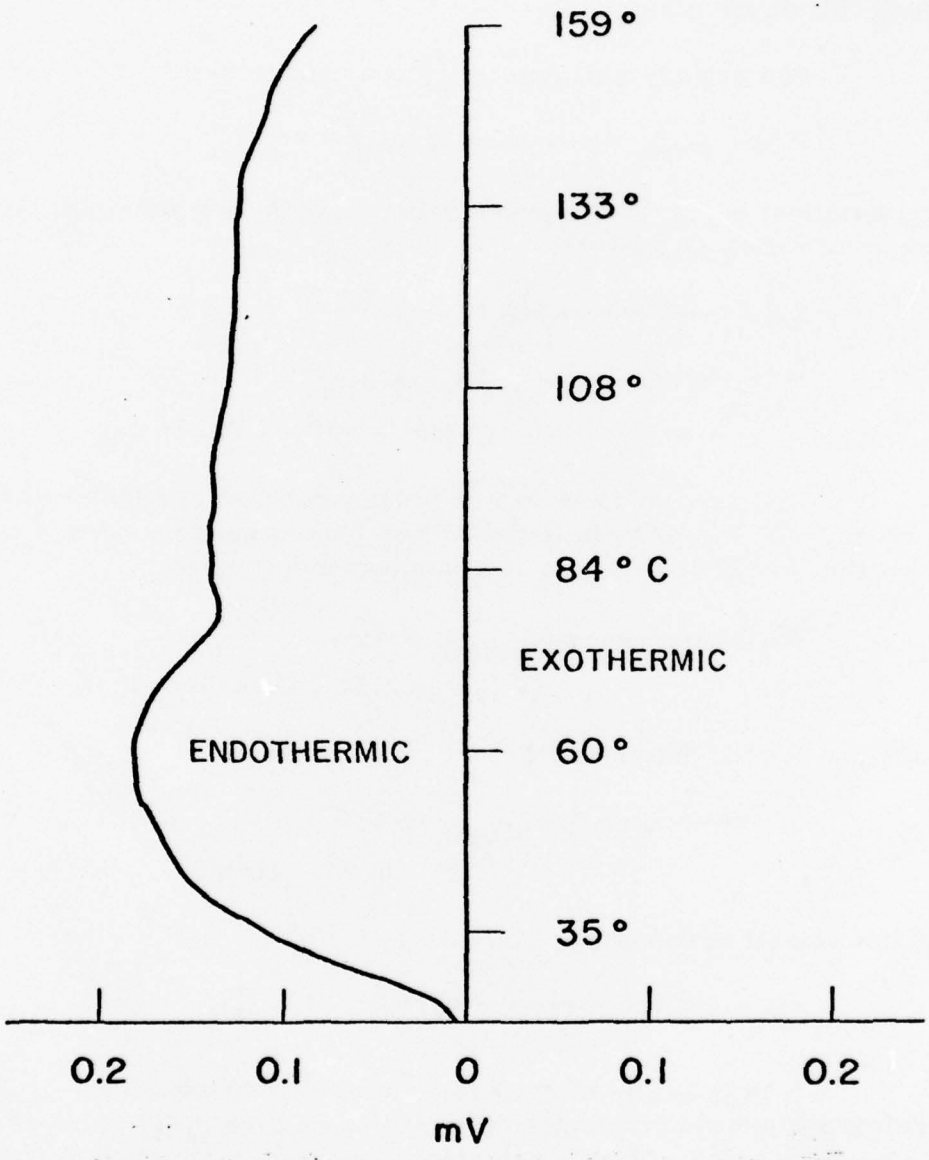

Fig. 103 The repeat run of the cell shown in Fig. 102

The instability of the discharged $Li/SOCl_2$ cell is demonstrated by the presence of two strong exothermic reactions occurring in the temperature range of 80-100°C. The reactions are irreversible and may involve transient species since no exothermic transitions are observed during the repeat DTA runs. It is reasonable to conclude that some of the chemical species involved in these exothermic reactions are generated in the cell as a result of the discharge.

The primary cell reaction is thought to be:

$$2\ Li + SOCl_2 \longrightarrow 2\ LiCl + SO \qquad (21)$$

The bi-radical SO is thermodynamically unstable and may undergo further reactions as follows:

$$2\ SO \longrightarrow (SO)_2 \qquad (22)$$

$$(SO)_2 + SO \longrightarrow S_2O + SO_2 \qquad (23)$$

$$\Delta H^\circ = -97.8K\ Cal/mole.$$

S_2O may polymerize to a yellow solid at low temperature. However, both the polymer and S_2O may undergo decomposition reaction on heating to 100°C or above in a quantitative manner.

$$2S_2O \longrightarrow 3S_{rhomb} + SO_2 \qquad (24)$$

$$\Delta H^\circ = -12.5K\ Cal/mole\ of\ S_2O$$

Thus, the overall decomposition reaction would be:

$$SO \longrightarrow 1/2S_{rhomb} + 1/2\ SO_2 \qquad (25)$$

$$H^\circ = -36.8K\ Cal/mole$$

and the overall cell reaction:

$$4Li + 2SOCl_2 \longrightarrow 4LiCl + S + SO_2 \qquad (26)$$

It is possible to calculate the thermodynamic EMF of the cell according to the reactions (21) and (26), using the ΔG° value of $SOCl_2$ in a gaseous state. The $E_\circ$ calculated based on reaction (21) is 3.05 volt whereas the $E_\circ$ calculated based on reaction (26) is 3.72 volt. The experimental value of 3.60 volt indicate further the instability of SO and that the cell voltage is probably a mixed potential corresponding to a mixture of reactions (21) through (25) depending upon the discharge temperature.

In view of the fact that the above E_o values were calculated using $\Delta G°$ of gaseous $SOCl_2$, the small difference between the experimental and the calculated value may indicate the reaction (26) to be the predominant overall cell reaction.

Based on this, the species that are thought to be formed as a result of discharge would be SO, $(SO)_2$, S_2O $(S_mO)_x$ polymer, S, LiCl. Of these, all except LiCl are reactive. The chemical reactions (23) through (25) are all exothermic and could cause the irreversible exothermic transitions observed in the DTA thermograms of the D cells. The reactions are also homogeneous (gas or liquid phase) and therefore, they could occur at relatively high rates at room temperature.

In addition, the reactions of the above species with $SOCl_2$ and Li should also be considered. For example

$$2\,Li + S \longrightarrow Li_2S \qquad (27)$$

$$\Delta G° = -120K\ Cal/mole\ of\ Li_2S$$

is an extremely exothermic reaction and is particularly prone to occur since S is in solution in $SOCl_2$. Furthermore, we showed earlier that Li_2S undergoes spontaneous exothermic reactions with $SOCl_2$. We are in the process of determining the ΔH values for this reaction which is speculated to be

$$SOCl_2 + Li_2S \longrightarrow S_2O + 2LiCl \qquad (28)$$

The nature of the "instability" generated in a thionyl cell by discharge is rather complex; although it manifests itself rather simply in the form of

(a) Two exothermic peaks in the DTA of the discharged cell, and

(b) Occasional spontaneous explosion of partially discharged cells on storage.

It is intriguing to speculate whether the two manifestations are related.

It is possible that the exothermic reactions, corresponding to the noted peaks in the thermogram, could occur at room temperature at a slower rate and build up heat locally inside the cell thereby accelerating the reactions even further thus providing a trigger for the remaining active materials such

as Li, S, SO_2, $SOCl_2$ causing a thermal runaway. According to this model, the exothermic peaks and the occasional cell explosions are related. This suggests an interesting approach towards alleviating the spontaneous cell explosion problem. Since, the second DTA runs do not show any exothermic peaks, it indicates that the chemicals responsible for the exothermic reactions are completely exhausted during the first run. Thus, a controlled thermal excursion may provide a means to deactivate the discharged cells.

6.4 General Conclusions

It was demonstrated from the DTA studies that there are several constituents in the $Li/SOCl_2$ cell which could create a thermal runaway when heated to a suitable temperature. Li is one of the most important exothermic components. It was shown from the exothermicity measurements that there are several chemical combinations which may be present in a partially discharged $Li/SOCl_2$ cell that are capable of undergoing spontaneous exothermic reaction to produce heat inside the cell. Moisture accelerated this heat generation. Thus, a cell should have a totally hermetic cell enclosure to prevent moisture ingress.

The instability of the discharged $Li/SOCl_2$ D cells was characterized using the DTA technique. The DTA thermograms of discharged D cells showed two sharp exothermic transitions in the 80-100°C temperature range corresponding to exothermic reactions of the discharged products. The absence of these peaks in repeat runs indicate the possible exhaustion of the unstable species during the first run. This suggests a possible approach of deactivating the discharged cells by subjecting them to a controlled thermal defusing.

7. Task VI - Local Internal Heating of D Cells to Test the "Hot Spot" Theory of Cell Explosion

According to the "hot spot" theory, the spontaneous explosion of discharged Li/$SOCl_2$ cells is caused by chemical reactions (discussed in the previous Section) which create a local "hot spot" in the cell by virtue of their exothermic nature and this "hot spot" then serves as a trigger for the other active cell compoments such as Li, S, SO_2, $SOCl_2$, Teflon and glass which feed the thermal runaway. The local hot spot may also be involved in the explosion of cells or low current (10 mA) reversals where the hot spot may be generated by the electrical current, although the involvement of chemical triggering cannot be ruled out. In order to test this theory, we attempted to create local "hot spots" inside the D cell by various means. The experimental details and the results are reported here.

7.1 Internal Heating by Means of Heating Wire Located Inside the D Cell

7.1.1 Experimental

Hermetic D cells were made with the electrode dimensions mentioned in the previous Section of this report. The cell tops were fitted with G/M seals having sealed Kovar tube feedthroughs. The location of the three feedthroughs are shown in Fig. 104. The center feedthrough was used for electrolyte filling and as the anode terminal. The other two feedthroughs extended halfway down the cell and the tips were sealed by welding. The tips were fitted with heating wires as well as spark gaps. We carried out some experiments with automobile ignition coils and a power supply to generate sparks between the tips of the two feedthroughs. Although, we were able to generate sparks in this manner, we were not successful in creating a thermal-runaway of a discharged cell by this means. We then continued our tests with heating wires connected between the tips of the insulated feedthroughs. Attempts to initiate an explosion by a current pulse generated by discharging a capacitor (330,000μF) through the heating wire were unsuccessful. We then carried out a series of exploratory experiments by applying DC through the heating wire to generate local hot spots inside the cell. The cell voltage, the wall temperature and the temperature at the tip of the feedthroughs where the heating wire was connected were monitored during these experiments. Next, we made cells having the heating wire located (i) on the Li anode, (ii) on the carbon cathode and (iii) on the separator insulated from botht the anode and the cathode. We discharged these cells partially and then carried out the local internal heating as above. Results are discussed below.

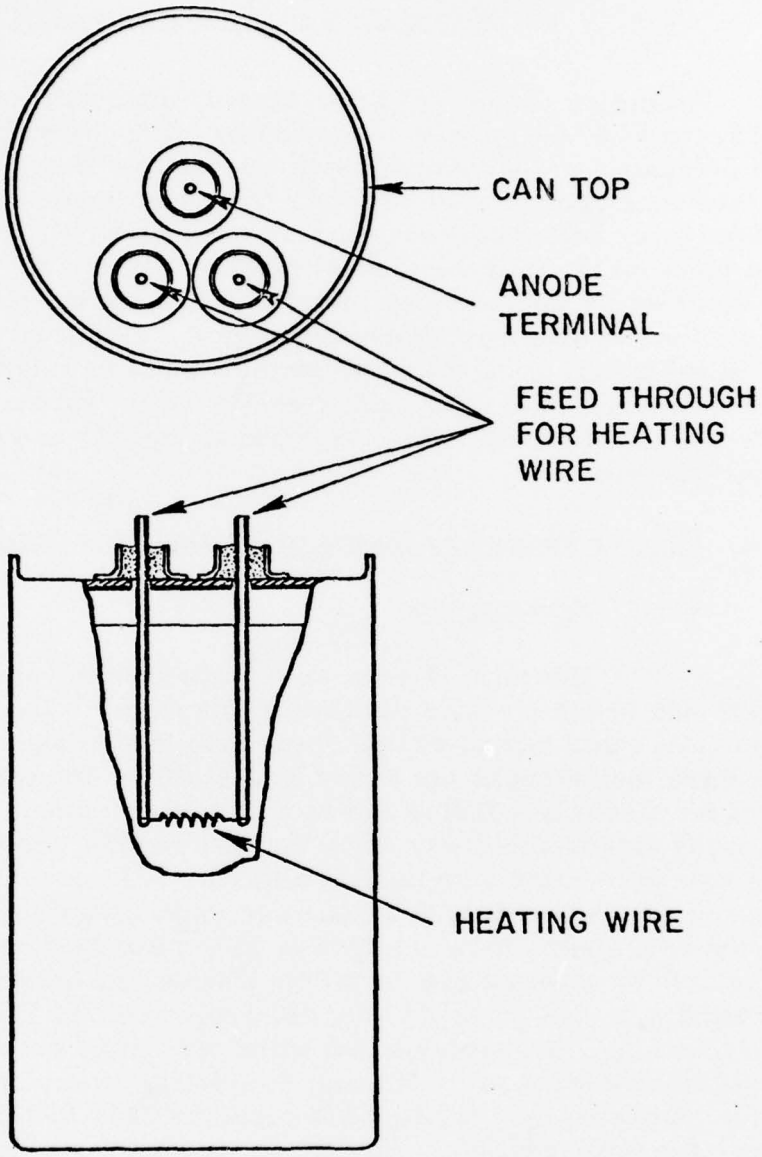

Fig. 104 The schematic representation of the D cell showing the feedthroughs for internal heating

7.1.2 Results and Discussion

We tested six cells having heating wires located near the cathode side within the electrode coil. The Li anode was electrically insulated from the heating wire by the separator.

The first cell had been completely discharged at 0.25A yielding a capacity of 12A.Hr. The local hot spot was created by passing 3A through the heating wire for 0.6 minute. During that time the cell wall temperature rose to 26° and the tip temperature rose to 53°, at which point an electrical discontinuity developed in the heating wire. There was no cell explosion.

The second cell was completely discharged at 0.1A yielding a capacity of approximately 15 A.Hr. The local hot spot was created by passing 3A for 1 minute, in which time the tip temperature rose to 55°C. The current was then increased to 4A; the tip temperature rose to 75°, the wall temperature to 28° in 0.3 minute and the heating wire fused and disconnected at that point. The cell voltage of 3.68 volt indicated that there was no cell shorting. There was no explosion.

The third cell was discharged completely at 0.25A to a capacity of 13.4A.Hr. The cell was internally heated using a 3A current through the heating wire for 95 minutes. During that time, the cell wall temperature rose to 63° and the tip temperature rose to 107°. Nothing happened. Next day, the cell was subjected to internal heating starting at 3A and then increasing to 7A in increments of 1A at 1 minute intervals. At 7.0A, the heating wire fused in 0.3 minute, causing the cell to develop internal short and thereafter both the cell voltage and the cell temperature gradually declined with time without any explosion.

The fourth cell was partially discharged at 0.5A to a capacity of 8A.Hr and then subjected to internal local heating at 3A for 1 minute followed by 4A for 1 minute, then 5A for 2 minutes and 6A for 3 minutes. During the 5A heating, the heating wire failed and caused an internal short. The OCV of the cell dropped to 3.50 volt indicating a high resistance short. The wall temperature rose to 40°. The current was shut off for a few minutes during which the wall temperature kept on rising slowly. After this, we heated the cell again starting at 3A and increasing to 8A in 1A increments in 1 minute stages. The cell wall temperature rose to 52° and the tip temperature was 72°C. The cell was then kept at room temperature for 22 hours during which time the cell voltage gradually declined from 3.60 volt to 2.2 volt due to the discharge through the internal short near the heating wires. The wall temperature dropped to 31°C and the tip temperature dropped to 33°C. At that point we turned on the internal heating using 4A and the cell exploded in less than 2 seconds.

The above exploratory experiment provides some support for the "hot spot" theory. The discharge of the cell through the internal short near the heating wire may have caused the accumulation of the active discharge products such as S, S_2O, $(SmO)_x$, etc. near the heating wire. The subsequent heating with 4A caused these products to ignite very quickly thus resulting in an explosion. The failure of the other three cells to explode was probably due to the fact that the discharge products were distributed uniformly throughout the cathode and were not concentrated enough near the heating wire to explode. Also, in those experiments, the cells were discharged 3 to 8 days prior to the heating experiment and the active discharge products may have been distributed evenly by diffusion and were not in sufficient concentration near the heating wire to ignite.

In the case of the fifth cell which was discharged at 0.1A yielding a capacity of approximately 15A.Hr., the heating wire broke off on 3A heating without shorting the cell. No explosion occurred.

The sixth cell was internally heated without discharging it previously. The heating started at 3A and increased to 5A in 1A increments with 1 minute stages. The heating wire broke off at 5A within 0.2 minute. At that point the wall temperature was 30° and the tip temperature was 77°C.

The above experiments, though exploratory in nature, demonstrate that a cell can be exploded by local "hot spots."

We next attempted to determine the effect of the position of the heating wire on the explodability of the cells by local heating. One D cell, made as described above (Fig. 104) with the heating wire touching the cathode was discharged first at 0.5A for 16 hours corresponding to a capacity of 8A.Hr. This cell was then heated internally by passing a DC of 3-12A increments of 1A/minute through the heating wire. The heating wires (NiChrome) used for these cells were able to withstand 12A without any fusing. Both the wall temperature and the temperature at the heating wire (via the hollow Kovar tube feedthrough) were measured during this experiment. The internal temperature (at the heating wire) was allowed to rise to 175°C in stages with the wall temperature rising to 56°C without any cell explosion. We then subjected this cell to several 1-minute pulses of 12A with a maximum internal temperature of 158°C without any explosion. The cell was then subjected to a 10A forced discharge for 45 minutes when the cell voltage remained negative (beyond scale) and the cell internal and the wall temperatures rose to 86° and 70°C respectively without any cell explosion. Up to this point, the cell appeared to be extremely abuse resistant. However, before abandoning the experiment,

we subjected the cell again to internal heating by 12A DC through the heating wire. The cell internal temperature was allowed to rise to 203°C, at which point, the 12A DC was shut off, and the internal temperature began to drop sharply. The wall temperature was 82°C when the 12A DC was shut off, and it continued to rise rather rapidly to 106° and began to level off. After 0.5 minute of shutting the DC, when the internal temperature was about to level off at 119°C and the wall temperature was at 106°C, the cell exploded.

Another D cell with the heating wire located on the separator and insulated from both the anode and the cathode was discharged at 0.5A for 16 hours and then subjected to several internal heating regimes consisting of 3A to 12A DC in 1-minute stages as well as direct 12A heating to as high as 222°C without any explosion. Finally, the cell was again subjected to a 12A DC internal heating and the cell internal temperature was allowed to rise indefinitely. The cell blew up when the internal temperature was 210°C, and the wall temperature was 63°C.

Another D cell with the heating wire located on the Li anode was first discharged at 1A corresponding to a capacity of 9A.Hr. and then it was subjected to an internal heating regime with DC of 3-12A in 1 minute stages as before the maximum internal temperature reached was only 47°C. This must be due to the high electrical and thermal conductivity of Li metal. After many attempts we were able to achieve a maximum internal temperature of 145°C using 12A DC through the heating wire. The cell did not explode.

7.1.2 Conclusion

The results indicate that a thermal runaway can be initiated by the local internal heating of a discharged thionyl D cell. Although the importance of the location of the hot spot is not very clear as yet, improved thermal conductions of the cell interior appears to be beneficial in preventing thermal runaways.

7.2 Internal Heating by High Current Pulses to Initiate an Instantaneous Thermal Runaway

The time required to induce a thermal runaway by means of heating wire as described earlier was of the order of several minutes or longer. Also, the incidence of thermal runaway was rather infrequent. An alternate method of inducing a thermal runaway more quickly and reliably was sought. One of the objects was to make these explosions amenable to study by high-speed photography. At a modest film speed of 1000 frames per second (fps), photography of explosions with induction periods of minutes or longer becomes impractical because of excessive wastage of films. Furthermore,

film speeds of 2000 to 10,000 fps are desirable for studying the details of a thermal runaway. Therefore, a method of inducing the thermal runaway within a fraction of a second of triggering the high-speed camera is highly desirable. Although, we have not carried out any high-speed photography of exploding $Li/SOCl_2$ D cells, we have developed a method by which a $Li/SOCl_2$ D cell can be induced to explode within less than a second. The experimental details and the results of the various exploratory experiments are described here.

7.2.1 Experimental

$Li/SOCl_2$ D cells were made as described in Section 7.1.1. The feedthroughs for the heating wires were used to measure the internal temperatures, instead of using them for heating purposes. The D cells were subjected to a high-current pulse by means of a 12V automobile battery and a shunt. The electrical arrangement is shown in Fig. 105. The direction of the current was the same as used for discharging the cell. The current and the internal temperature of the cell was monitored using a high-speed Brush recorder during the pulsing experiments. The cell explosion was noted from the loud noise and was correlated with the current and the temperature profiles on the high-speed recorder.

7.2.2 Results and Discussion

The results of all the individual experiments are discussed in detail in the Appendix of this report. Only the general characteristics are discussed here.

Fresh, partial as well as completely discharged cells were used for the pulsing experiments. The current pulses varied from 100-200A depending upon the condition of the D cells. In general, the cells did not explode during the pulse but they exploded a short time after the pulse. Also, in several cases multiple explosions were observed. The data on the discharge capacity, maximum pulse current, pulse length and the time to explosion of the various cells are shown in Table 22. Note that one cell exploded on a 0.096 second pulse of 198A through a heating wire located inside the cell instead of through the electrodes. Also, in almost all cases there was an induction period between the pulse and the actual cell explosion. The amount of energy used by a 1-second pulse of 200A (12V) is approximately 0.7WHr which is insignificant compared to the total energy of the D cell (72 WHr). Thus, it is clear that pulses initiated the explosion which was fueled by the energetic chemicals present in the cell. The partially discharged cells exploded much more readily and some times more violently than the undischarged cells.

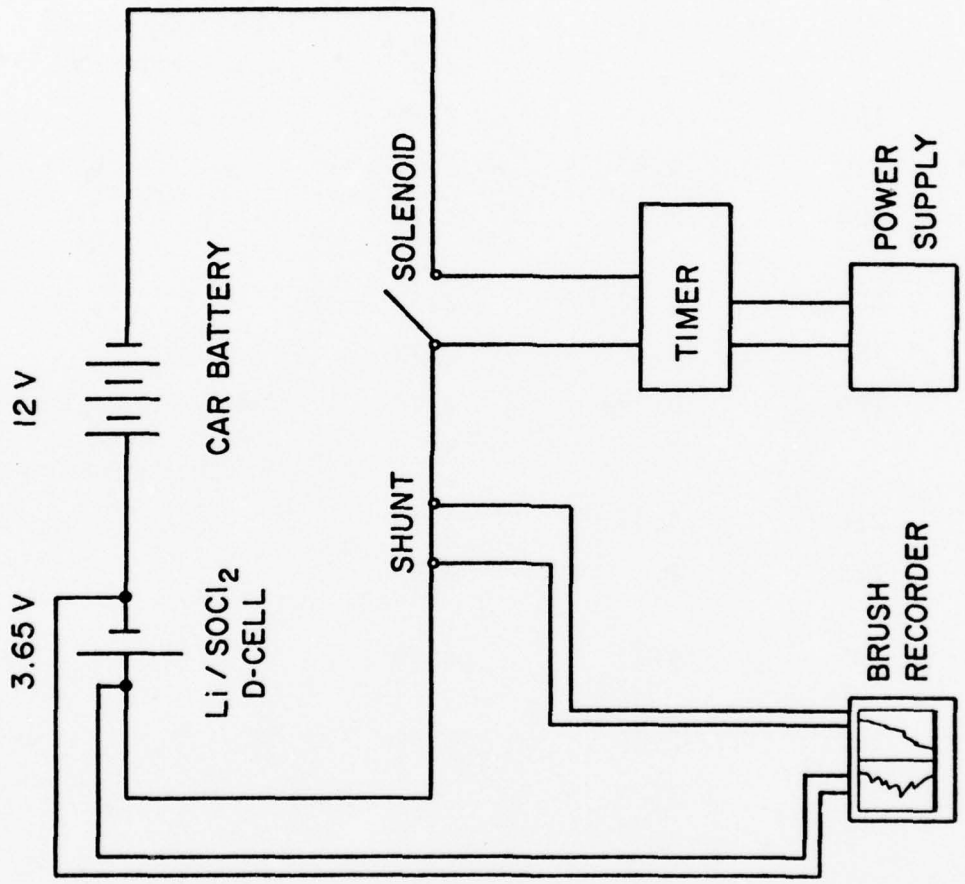

Fig. 105 Circuit for providing high current pulse to $Li/SOCl_2$ D cell from a 12V can battery

TABLE 22

The Results of High Current Pulsing of $Li/SOCl_2$ D Cells
By a 12V Automobile Battery

Discharged Capacity A.Hr	Maximum Pulse Current (A)	Pulse Width (sec)	Time to Explosion (sec)	Remarks
8	210	0.75	0.8 0.9 1.2	Multiple explosion
8	220	0.60	0.8 3.5	Mild explosion Loud explosion
Fresh	155	2.7	2.78	
4.5	210	1.0	1.50	
Undischarged (stored)	100	2.7	4.20	
2.0	200	0.32	2.50	
12	198	0.48	0.72	
10	198	0.096	0.70	Pulse through separate heating wire. Unusually loud explosion
8	210	0.90	1.1	
Undischarged (stored)	125	3.7	3.8	
Undischarged (stored)	105	4.44	4.60	
12	180	1.06	1.42	

7.2.3 Conclusions

1. High current pulse was effective in initiating a cell explosion.

2. The length of the pulse was found to be shortest for the completely discharged D cell, viz, 1 second or less. This is adequate for carrying out high-speed cinematography with speeds of 1000-2000 fps with minimum wastage of film.

3. The initiation of the explosion was most likely thermal in origin as opposed to electrochemical.

4. The results support the local "hot spot" theory of cell explosion.

8. Some Empirical Approaches to Alleviate the Explosion Hazard on Forced Overdischarge

The conditions which lead to a cell explosion, as discussed in Section 5 and 6 of this report, are:

a. Short circuiting
b. Casual storage of discharged cells
c. Forced discharge into voltage reversal

The explosions from accidental short circuiting is preventable by means of low pressure vent as discussed in Section 5.1.3.

The explosions of discharged cells on casual storage may be prevented by maintaining the hermeticity of the cells as well as by subjecting the discharged cells to a controlled thermal cycling as discussed in Section 6.3.

The explosions on voltage reversal, as discussed in Section 5.1.4, are not preventable by low pressure venting and remain a problem. We have, therefore, focussed our attention on this area in an attempt to find a solution. We chose to evaluate the efficacy of various empirical approaches that we developed from our up-to-date knowledge of the system.

Assuming that the initiation of an explosion is a thermal phenomenon, the mechanisms of internal heating on voltage reversal can be identified by examining the possible electrochemical reactions taking place on reversal. Since all the cells made and tested so far had excess Li, the anodic reaction during reversal should remain unchanged and consist of lithium dissolution.

$$Li \longrightarrow Li^+ + e \tag{29}$$

The cathodic reaction changes from the reduction of $SOCl_2$

$$2SOCl_2 + 4e \longrightarrow S + SO_2 + 4LiCl \tag{30}$$

to the reduction of Li^+ to form Li

$$Li^+ + e \longrightarrow Li \tag{31}$$

The cathode polarization from 2.0 volt to slightly negative voltage (versus Li) caused the rise in the internal temperature (Fig. 45). The temperature is expected to stabilize after this end point, since both the anodic reaction (29) and the cathodic reaction (31) are fairly reversible and should not cause any significant heat evolution. The triggering of the cell to explode must therefore be due to either the exhaustion of Li or the exhaustion of the electrolyte, (the source of Li^+) or both. Assuming that the exhaustion of Li is the cause, the empirical approaches consisting of (a) increasing the amount of Li in the anode, as well as (b) providing a current collector in the Li anode to ensure efficient utilization, are suggested for the alleviation of the explosion hazard on reversal.

Exploratory experiments in Section 7.1.2 indicated that localized accumulation of the discharge products such as sulfur may make the process of thermal initiation much easier and thus contribute to a thermal runaway. Thus, an approach consisting of improved electrode designs to make the cathodic reduction more uniform was considered. We showed (20) that at high currents, the cathodic reaction occurs preferentially near the tab because of the excessive electrical resistance of the expanded Ni grid. Thus, improvement of the current distribution of the cathode by means of multiple tabs should make the cathodic reaction more uniform and constitute another (c) approach for the alleviation of the explosion hazard.

The fourth (d) approach was strictly intuitive and it consisted of the use of duplex glass separators consisting of one layer of non-woven glass separator without a binder and another layer of a somewhat stronger non-woven glass separator having an organic binder. The idea is simply to reduce the degree of inhomogeneity of the separator which may contribute to the safety of the cells.

Accordingly, we made hermetic thionyl D cells having the above four concepts and subjected them to a constant current reversal. The experimental details and the results are discussed here.

8.1 Experimental

8.1.1 Standard Hermetic D Cells with Excess Li

The D cells made according to the specification described in Section 6.3.1 have an excess of Li (21 A.Hr). Hermetic D cells were made using the same electrode dimension and electrolyte volumes. We connected a piece of Li to one of the thermocouple feedthroughs and used this as a Li reference electrode. The potentials of both the cathode and the lithium anode were monitored against the Li reference electrode when the cell was discharged and overdischarged.

8.1.2 Hermetic D Cell With Current Collector In the Li Anode

Hermetic D cells were made in the same manner as described in Section 6.3.1, except that the Li anode was made of a sandwich of an expanded Ni exmet current collector between two layers of Li. The Li anode was in excess in terms of the stoichiometric capacity (24 A.Hr). These cells did not have a Li reference electrode. Cell voltage and the cell internal temperature were recorded while the cells were being discharged and overdischarged at a constant current.

8.1.3 Hermetic D Cells With Multiple Tabs on the Cathode

Hermetic D cells were made in the same manner as described in Section 6.3.1, except that the carbon cathode had four nickel tabs spaced equally apart instead of just one tab. These cells did not have any reference electrodes. The cell voltage and the internal temperatures were monitored during the constant current discharge and overdischarge.

8.1.4 Hermetic D Cell With Duplex Glass Filter Paper Separators

Hermetic D cells were made in the same manner as described in Section 6.3.1, except that the separator consisted of two layers of glass filter papers, one layer consisting of a soft non-woven material without any binder and the other consisting of a stronger non-woven material with an organic binder. The cathodes of these cells were thinner than those of Section 6.3.1. These cells had a Li reference electrode located inside the cell as in Section 8.1.1. The potentials of both the cathode and the Li anode were monitored during the cell discharge and the overdischarge.

8.2 Results and Discussion

8.2.1 Standard Hermetic D Cells With Excess Li

The cathode and the Li anode potentials of one D cell on a 3A constant current regular discharge of 8.6 A.Hr followed by a 10A forced discharge are shown in Fig. 106. During the discharge the Li anode potential remained constant all throughout, only the cathode polarized at the end of the discharge and became slightly negative. The cell was then forced discharged at 10A for another 11 hours before the cell exploded. Note that both the Li anode potential and the cathode potential remained constant for most of the time. Prior to explosion, the Li anode showed signs of polarization, but the cathode potential remained constant. The total capacity corresponding to the discharge and the forced discharge was approximately 119 A.Hr. This is approximately five times greater than the stoichiometric amount of Li present in the anode. Therefore, the constancy of the electrode potentials during the forced discharge must be due to an electrical short inside the cell generated during the forced discharge. The dendritic Li formed in the cathode might cause this short to occur. However, the fact that the Li anode finally polarized after 11 hours indicates that part of the current was used for electrochemical reactions and the electrical short was of a high resistance kind. The examination of the electrode potentials revealed no spike or any other non-uniformity to indicate the point at which the shorting occurred. It is most likely that the process of shorting is a gradual one. This provides an interesting example of increasing the apparent abuse resistance of a cell by creating of an internal short.

8.2.2 Hermetic D Cells With Current Collector in the Anode

The cell voltage and the internal temperature of one D cell on 1A discharge and forced discharge are shown in Fig. 107. The internal temperature rose at the end of the discharge and then declined and gradually leveled off to room temperature during the 1A reversal for 34 hours during which time the cell voltage remained constant at -0.2 volt. The total capacity including reversal (42 A.Hr) was significantly greater than the stoichiometric capacity of Li, and yet the absence of cell polarization indicates internal shorting. The current was then increased to 10A, and the cell internal temperature began to rise and the cell exploded.

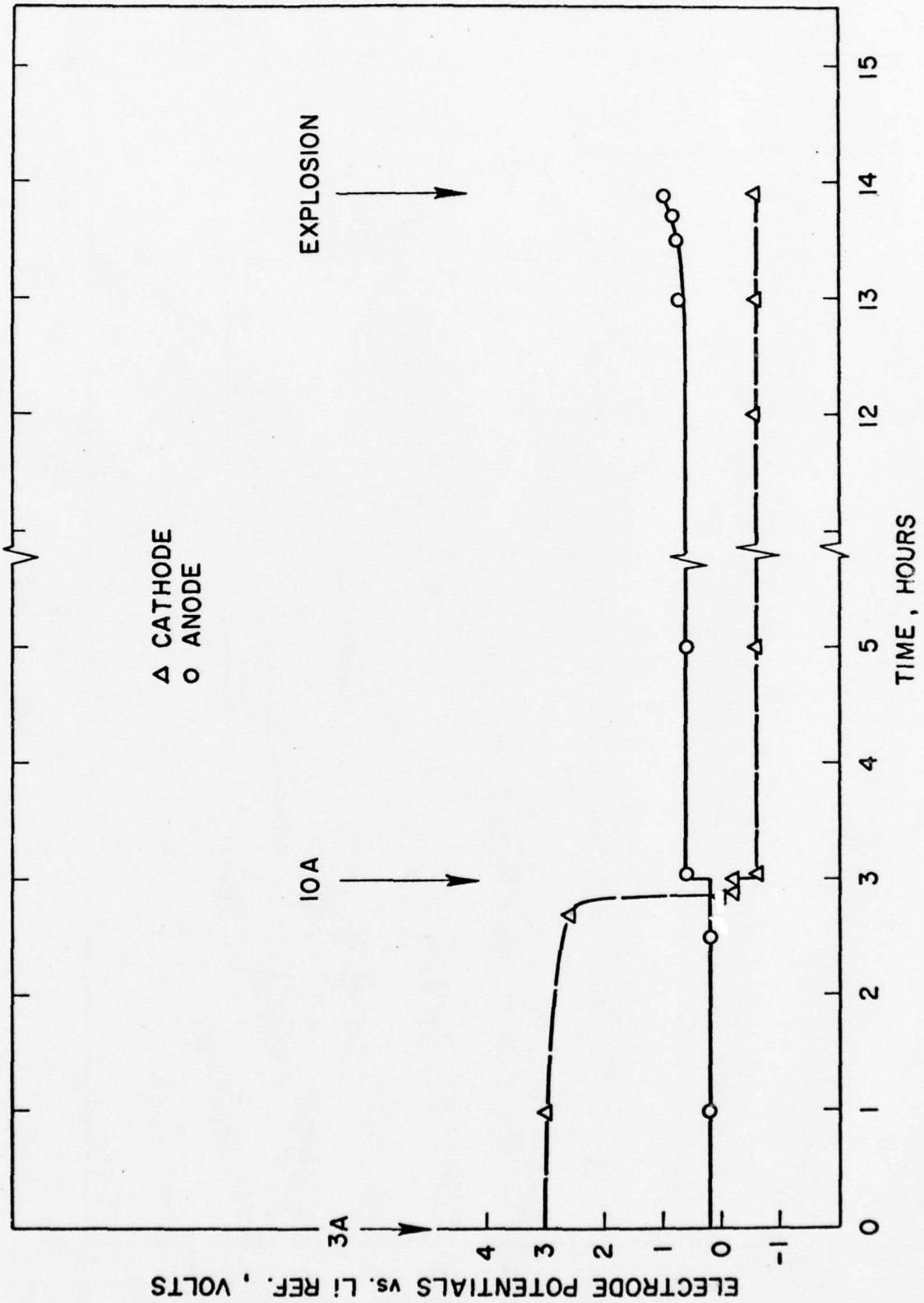

Fig. 106 Electrode potentials of hermetic Li/$SOCl_2$ D cell of standard construction with excess Li on 3A discharge followed by a 10A forced discharge

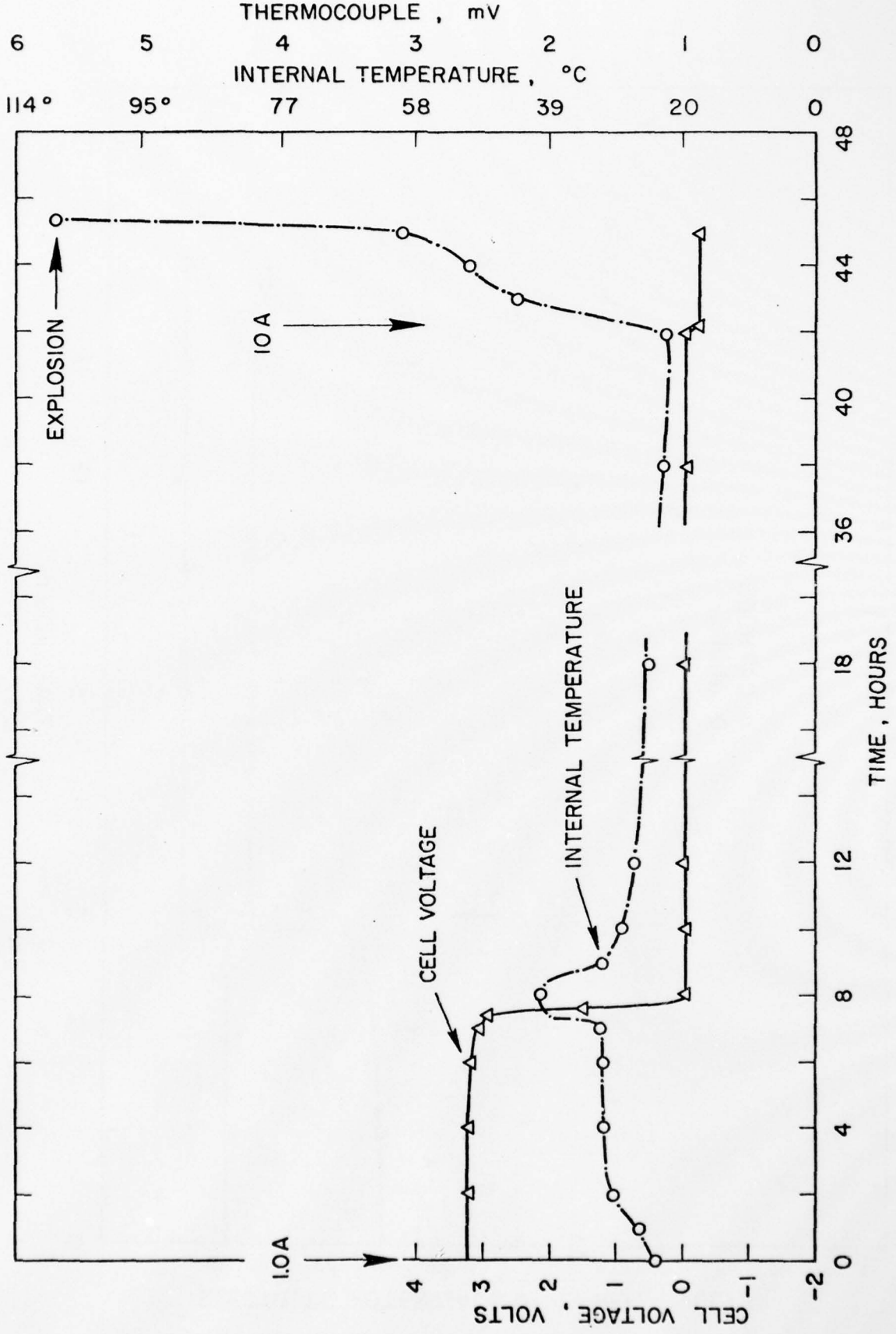

Fig. 107 Cell voltage and internal temperature of hermetic $Li/SOCl_2$ D cell with Ni exmet in Li anode on 1A discharge and forced discharge followed by 10A forced discharge

The voltage and the internal temperature of another D cell on 3A discharge and forced discharge are shown in Fig. 108. The discharge and the forced discharge was continued for 42 hours at 3A corresponding to a capacity of 126 A.Hr; the cell voltage remained constant at -0.3 volt all throughout. The current was then increased to 10A, the cell internal temperature increased and began to level off. The test was discontinued at that point. The cell did not explode at that point. However, the cell exploded from the shock of the explosion of the previous cell which was in the vicinity. We speculate that part of the current during the prolonged reversal is used for lithium deposition on the cathode whereas the remainder flows through the short without any electrochemical reaction. The presence of this finely divided dendritic Li on the cathode and S constitute a potent mixture which may be shock sensitive.

The voltage and the internal temperature profile of another D cell on 1A discharge and forced discharge for 90 hours are shown in Fig. 109. The cell potential remained at -0.15 volt throughout the reversal. There was no cell explosion.

We discharged another D cell 6.8 A.Hr to 2.0 volt at 3A and then continued to force discharge it for 70 hours without any explosion. The current was then increased to 10A and the cell exploded in 0.75 hour.

Another D cell was discharged 10.1 A.Hr to 2.0 volt at 0.3A, and then forced-discharged at 3A for 18 hours and 10A for 5 hours when the cell exploded.

Another five D cells were discharged at 0.3A to completion corresponding to a capacity of approximately 10 A.Hr., then the cells were force-discharged at 1A for 240 hours without any explosion. These cells were then subjected to an impact test consisting of a 12 lb weight dropped from a height of 2 ft. Three of the five cells exploded violently on impact.

The abuse resistance of all the cells on forced discharge was found to be exceptionally good.

8.2.3 Hermetic D Cells with Multiple Tabs on the Cathode

The voltage and the internal temperature profile of a D cell on 1A discharge and forced discharge is shown in Fig. 110. The cell voltage remained constant at -0.1 volt throughout the 1A reversal. The current was then increased to 10A, the cell voltage increased to -0.2 volt, the cell temperature increased rather steadily and the cell exploded.

The abuse resistance of this cell was found to be similar to that of the previous cells.

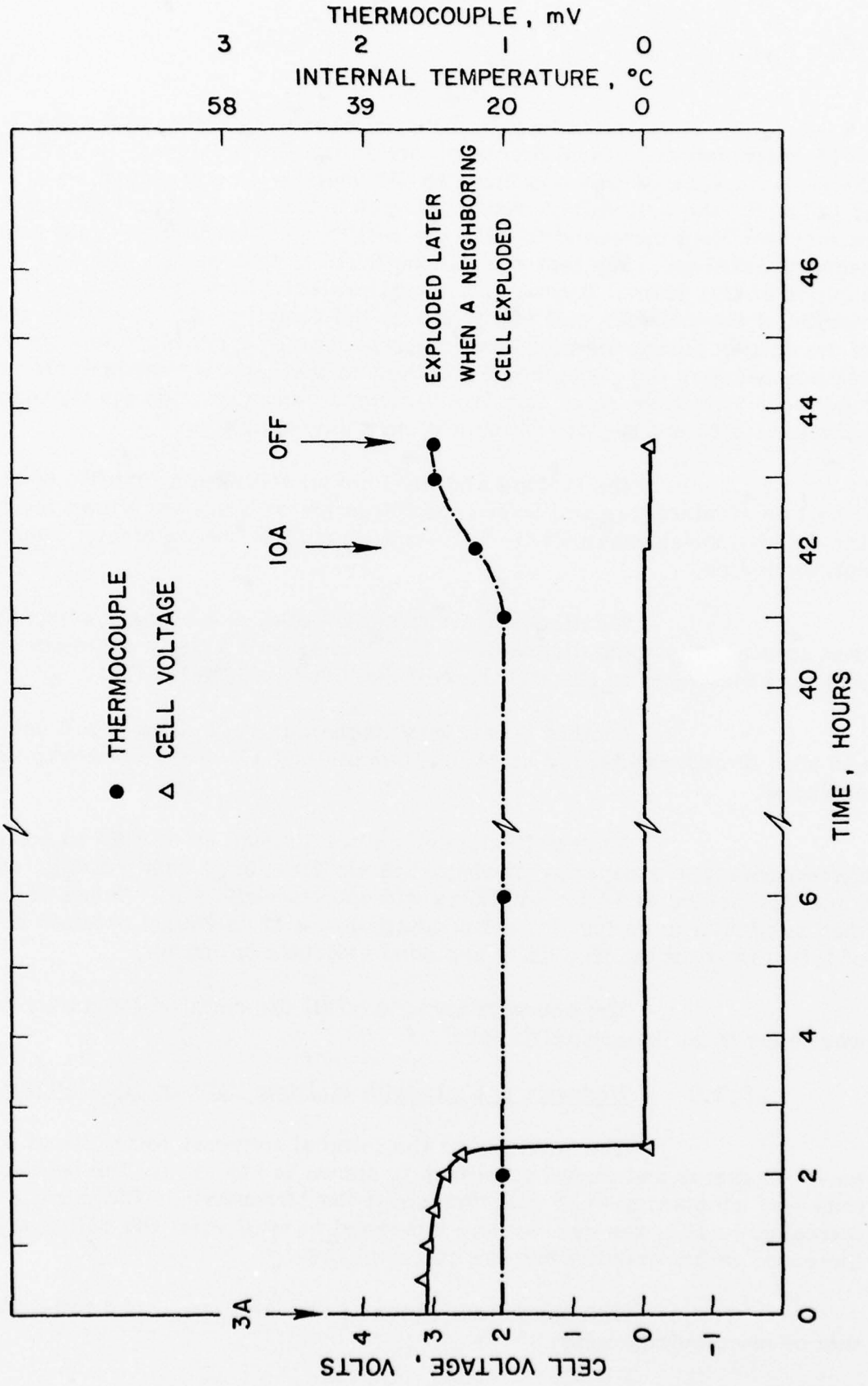

Fig. 108 Cell voltage and internal temperature of hermetic Li/$SOCl_2$ D cell with Ni exmet in Li anode on 3A discharge and forced discharge followed by 10A forced discharge

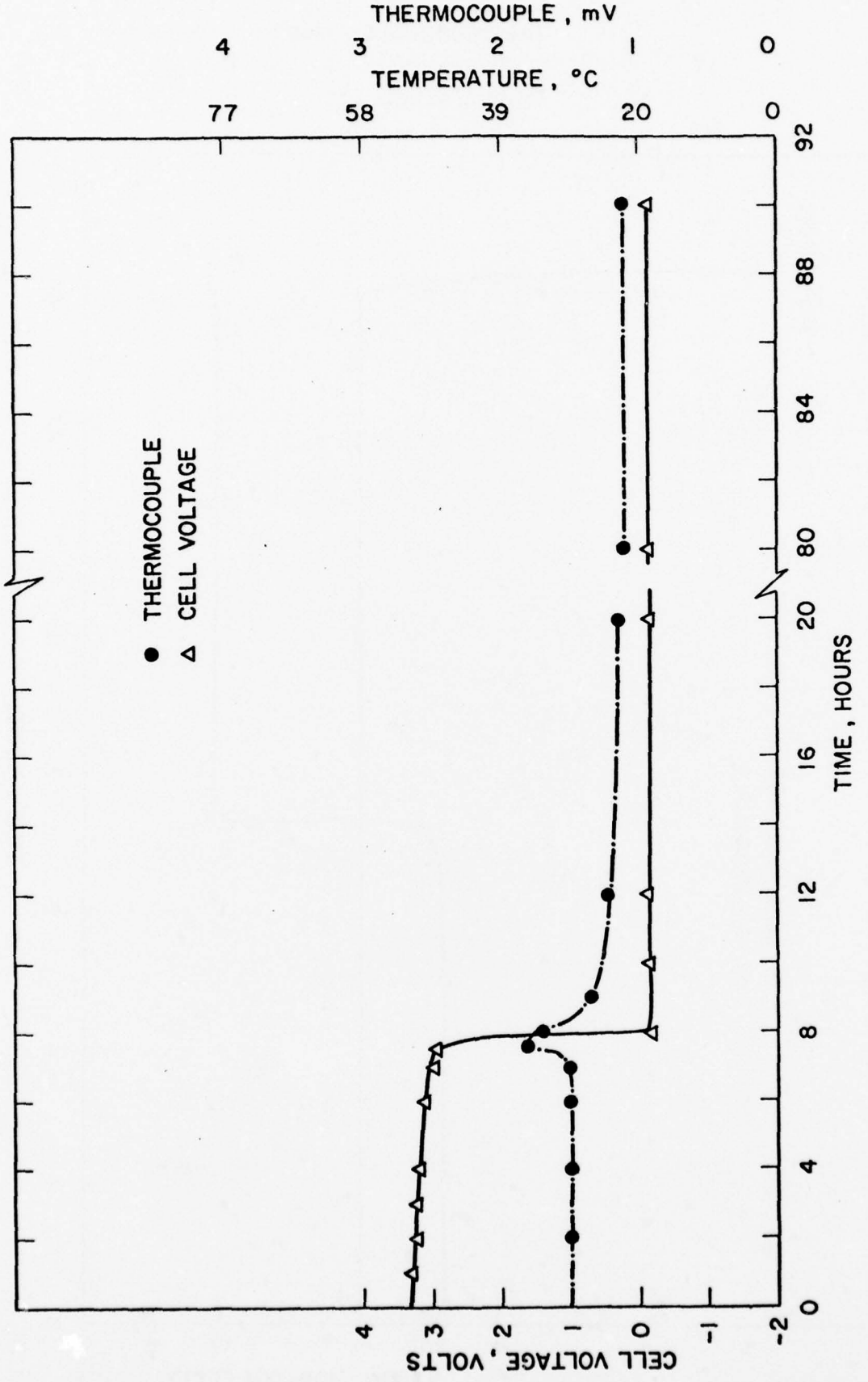

Fig. 109 Cell voltage and internal temperature of hermetic Li/$SOCl_2$ D cell with Ni exmet in Li anode on 1A discharge and forced discharge

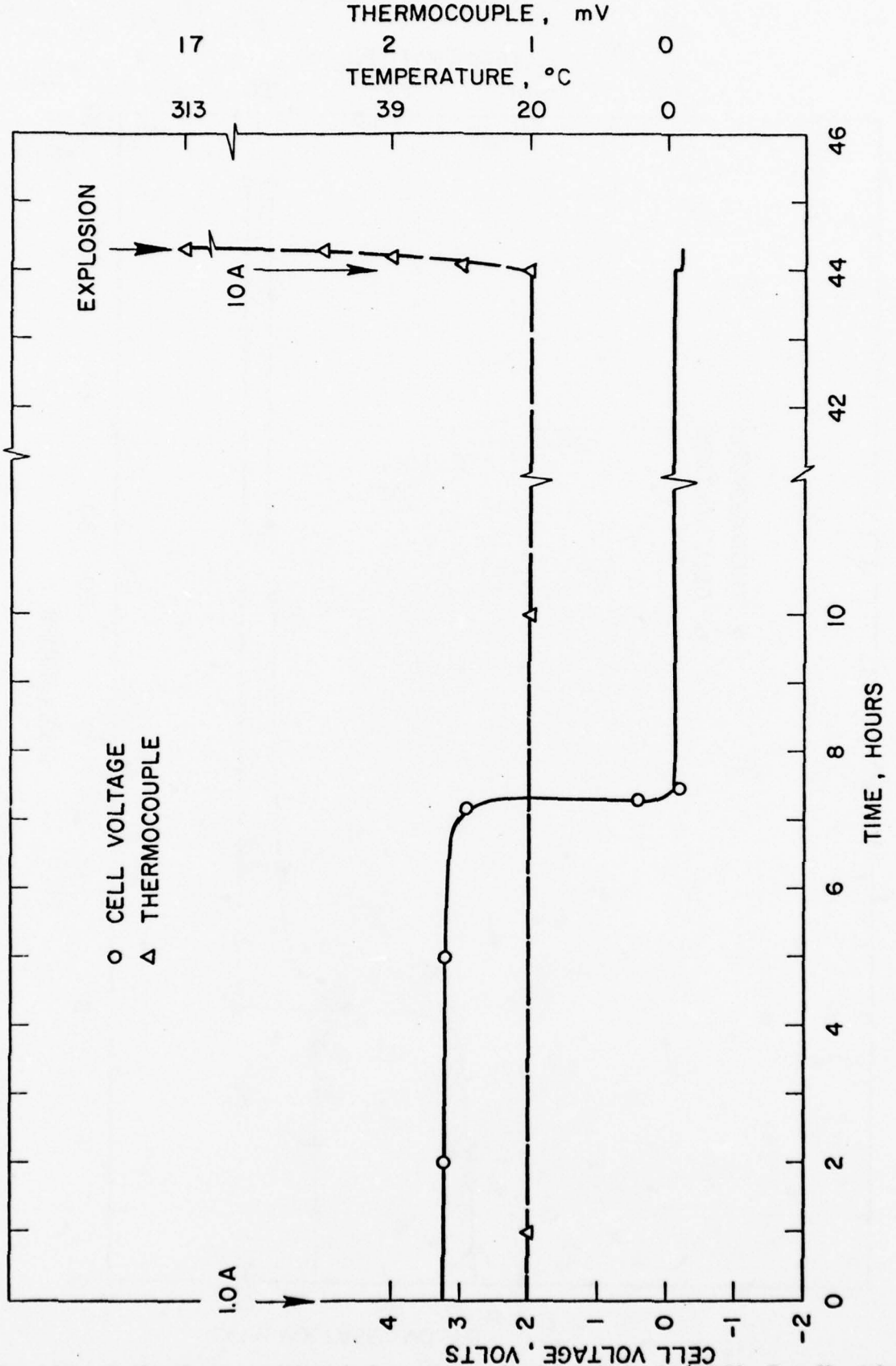

Fig. 110 Cell voltage and internal temperature of hermetic Li/$SOCl_2$ D cell with multiple tab in the cathode on 1A discharge and forced discharge followed by 10A forced discharge

8.2.4 Hermetic D Cell with Duplex Glass Filter Paper Separators

The cathode and the anode potential versus Li reference and the internal temperature of one D cell on 0.3A discharge and 1A forced discharge are shown in Fig. 111. The cathode polarized after 29 hours corresponding to a cell capacity of only 8.7 A.Hr. The 1A reversal continued for approximately 21 hours, when both the cathode and the anode potential remained constant, the temperature gradually declined during this process. There was no cell explosion. The cell was then subjected to an impact consisting of a 12 lb weight dropped from a height of 2 ft. The cell did not explode.

The cathode and the anode potentials of another D cell on 1A discharge and forced discharged are shown in Fig. 112. There was no explosion after 17 hours of reversal.

The electrode potentials and the internal temperature of another D cell on 1A discharge and force discharge is shown in Fig. 113. The behavior was similar to that observed before.

The electrode potentials of another D cell on 3A discharge and forced discharge for 75 hours are shown in Fig. 114. The cell did not explode as before. This cell also was impact tested with a 12 lb weight dropping from a 2 ft height. The cell did not explode on impact. We repeated this test with another D cell which was discharged and force-discharged fro 90 hours at 3A and then impact tested as above without any explosion.

The electrode potentials of a D cell on 3A discharge and forced discharge for 14.5 hours followed by a 10A forced discharge for another 15.5 hours are shown in Fig. 115. The cell finally exploded. Interestingly, the anode potential remained unchanged throughout the discharge, only the cathode potential showed a slight increase in polarization before the explosion.

The abuse resistance of the D cells were found to be exceptionally good, although the performance of the cells in terms of the capacity delivery at various currents was found to be poor compared to the cells described in Section 3.3.1.

8.3 Conclusions

The results indicate that all the four empirical approaches are effective to some extent in improving the abuse resistance of the hermetic D cells on reversal. The occurrence of internal cell shorting on reversal has been inferred from the experimental results. This was found to be beneficial in that it provided a path for the current to flow within the cell without coulombically consuming or producing any chemical products. It was conjectured that the shorting was caused by the formation of dendritic Li which deposited on the cathode. It is reasonable to suggest that a safer cell design is one in which conditions exist at the end of discharge where Li deposition may continue without any mass transfer problem.

This necessitates the presence of sufficient electrolyte and electrodes at the end of the discharge. Excess Li and a current collector in the Li anode ensures the integrity of the electrode, whereas the less active carbon cathodes ensure the low utilization of $SOCl_2$ and provide sufficient electrolytic conductivity for lithium deposition to progress to a shorting situation. The formation of the finely divided Li (dendritic deposits) on the cathode along with sulfur causes an over-discharged D cell to be shock sensitive.

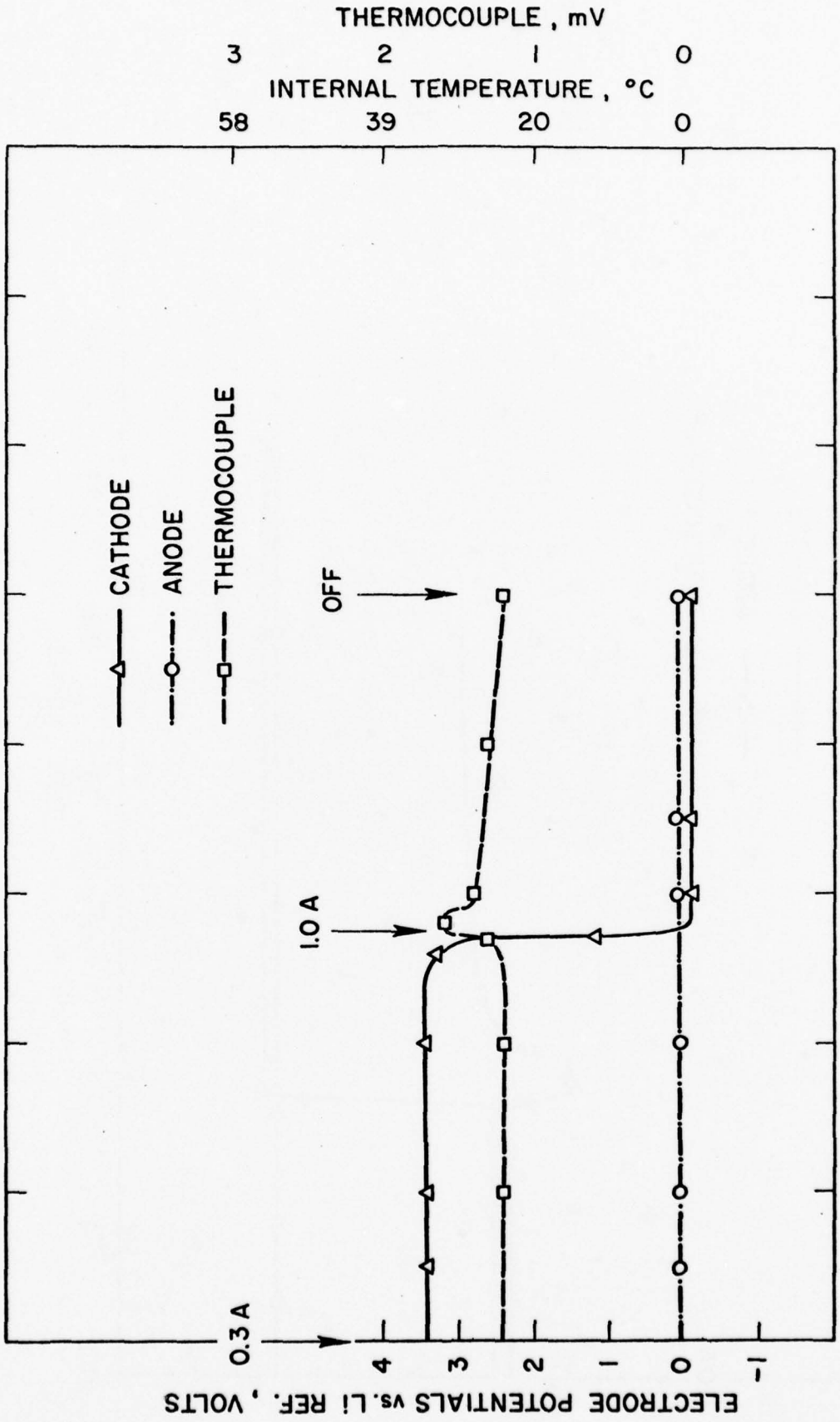

Fig. 111 Electrode potentials and internal temperature of hermetic Li/$SOCl_2$ D cells with duplex glass separator on 0.3A discharge and 1A forced discharge

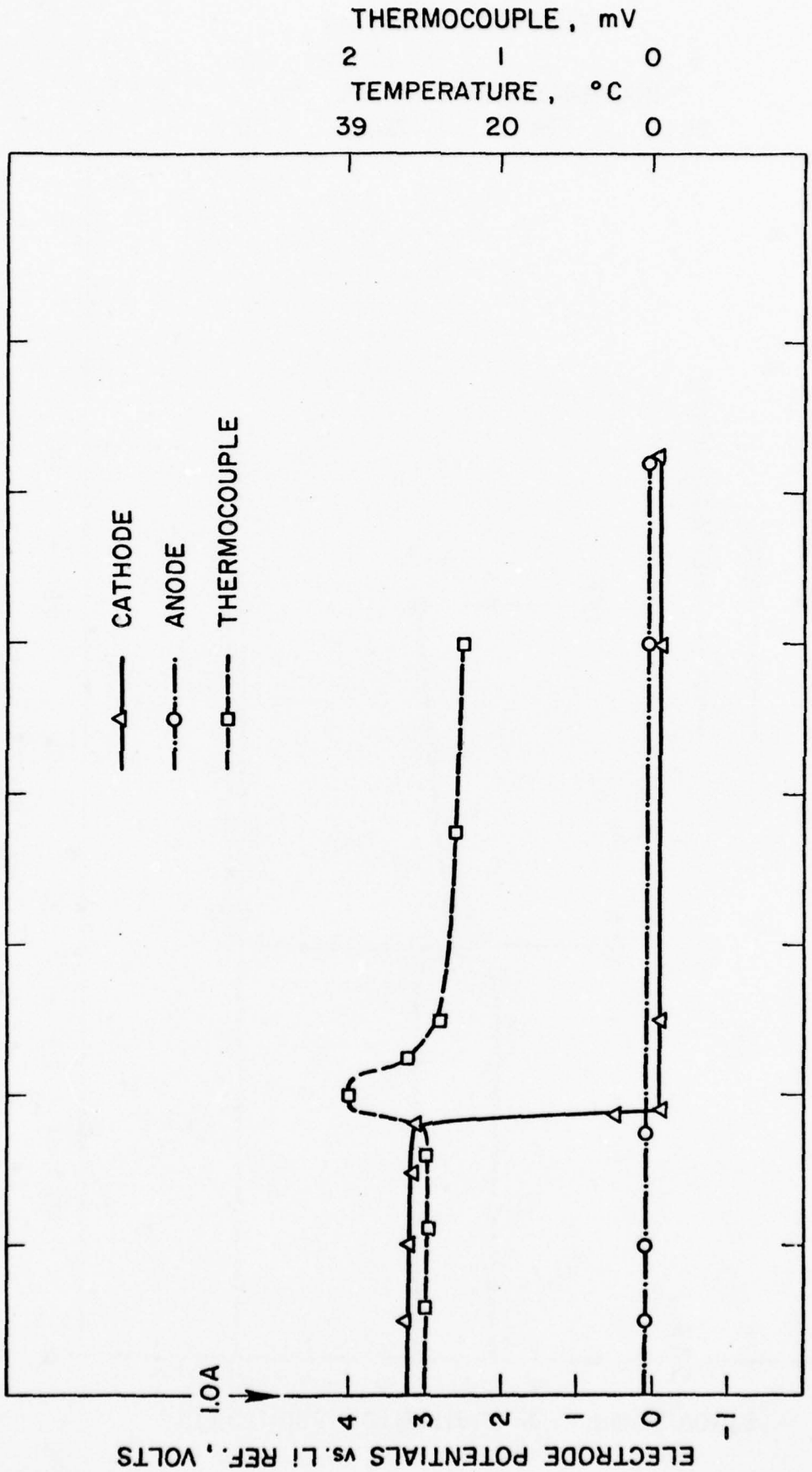

Fig. 112 Electrode potentials and internal temperature of hermetic Li/$SOCl_2$ D cell with duplex glass separator on 1A discharge and forced discharge

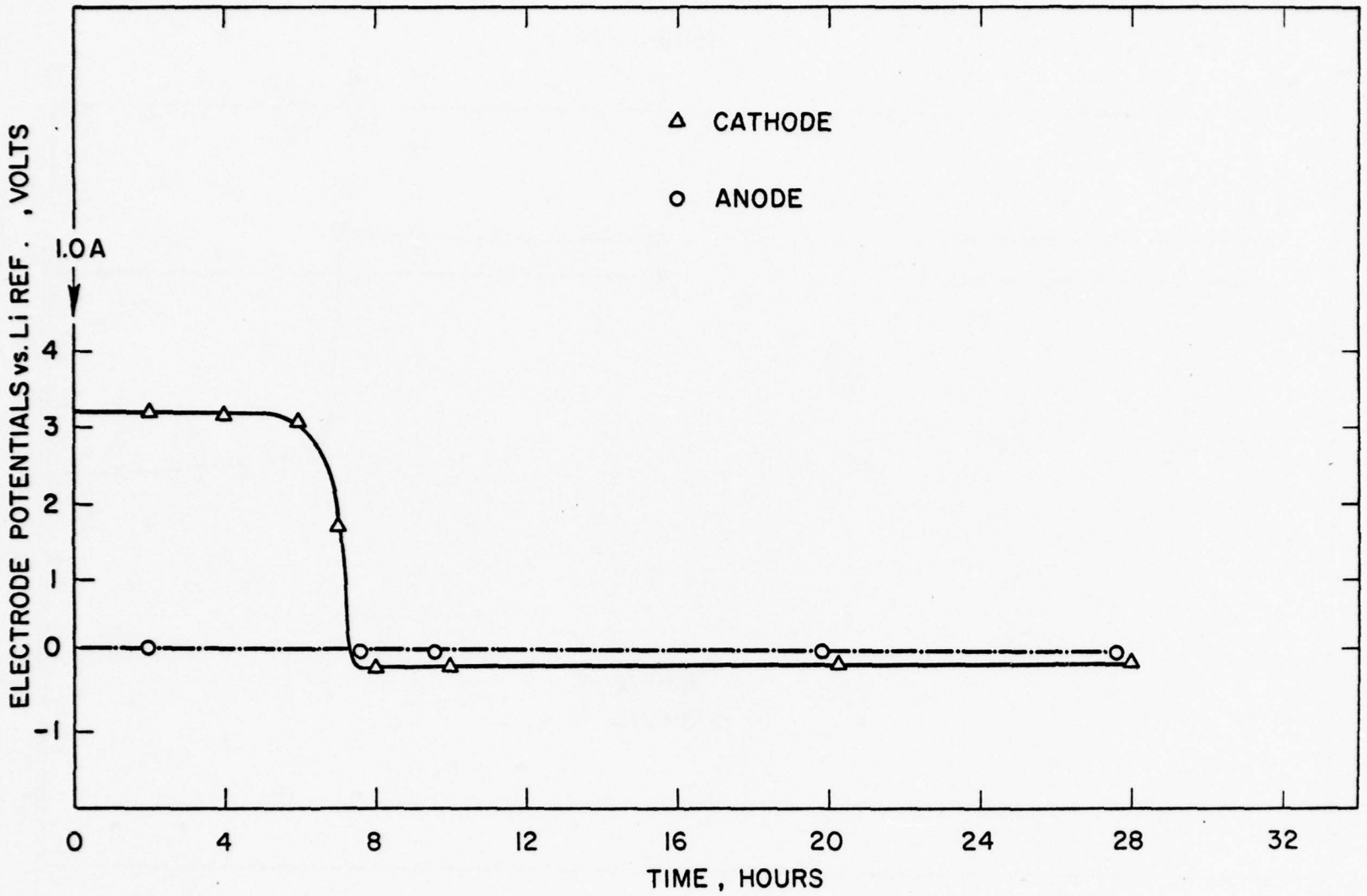

Fig. 113 Electrode potentials of hermetic Li/$SOCl_2$ D cell with duplex glass separators on 1A discharge and forced discharge

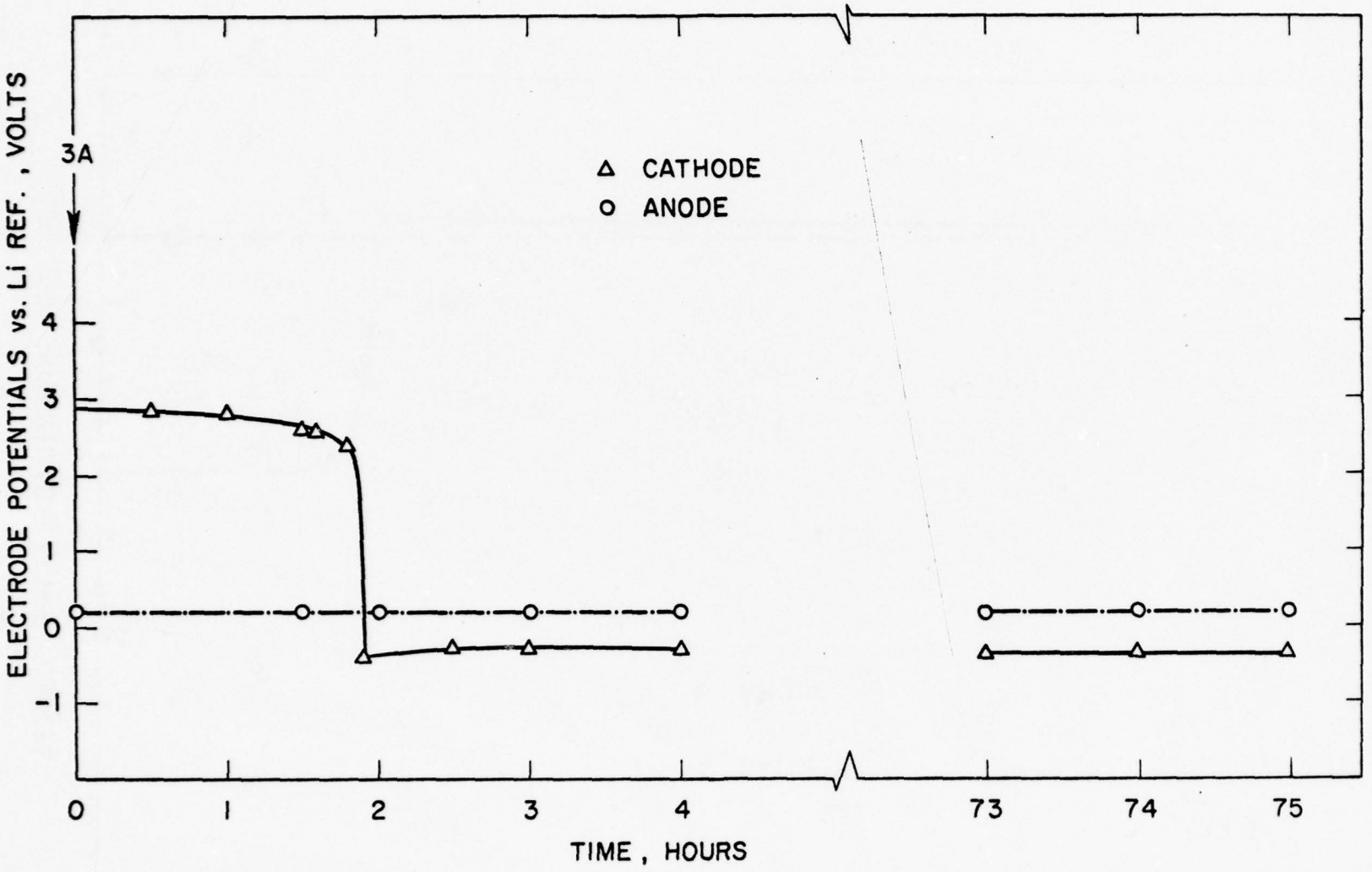

Fig. 114 Electrode potentials of hermetic Li/$SOCl_2$ D cells with duplex glass separators on 3A discharge and forced discharge

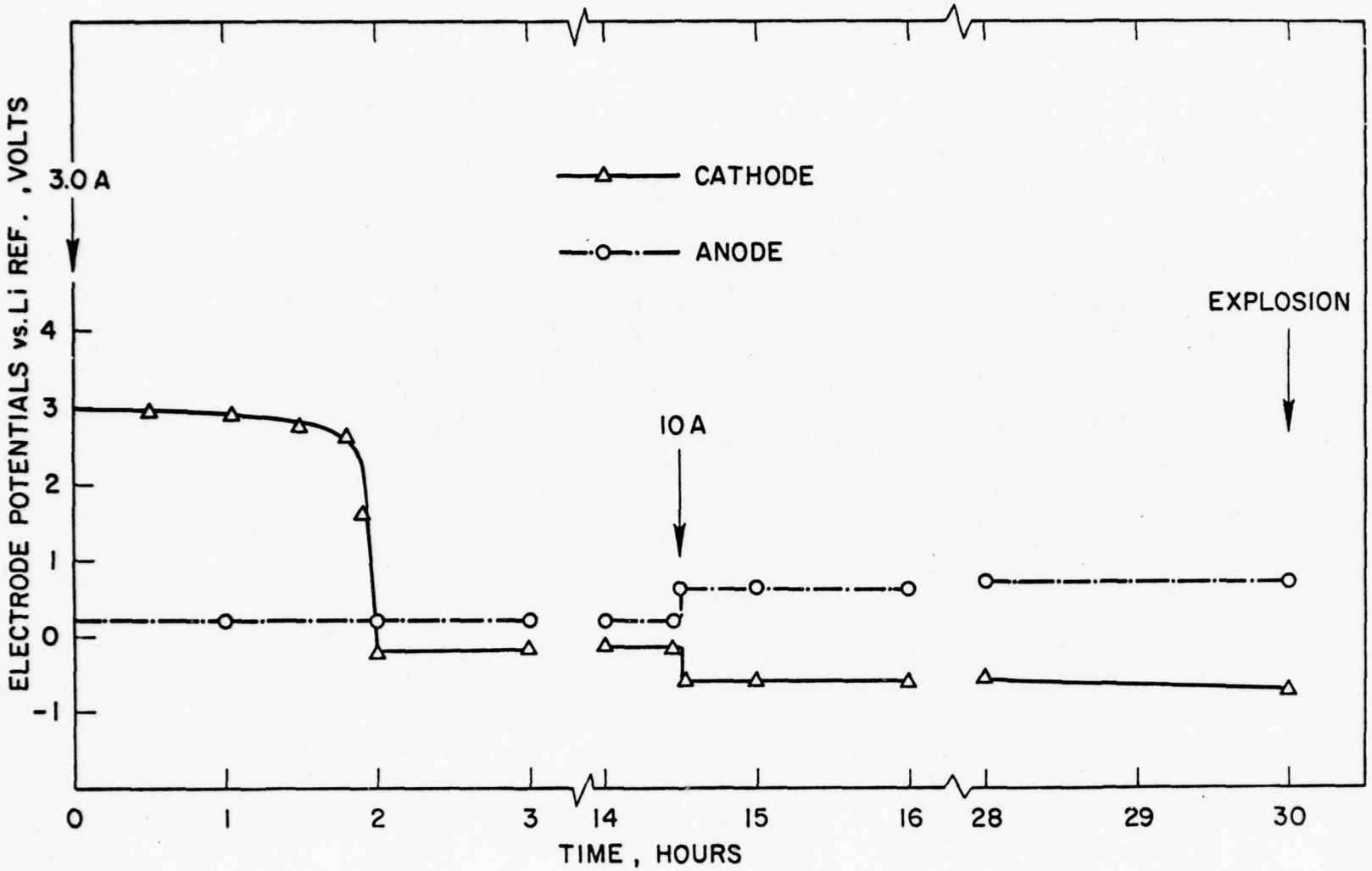

Fig. 115 Electrode potentials of hermetic Li/$SOCl_2$ D cells with duplex glass separators on 3A discharge and overdischarge and 10A reversal.

9. Conclusion

1. The $Li/SOCl_2$ hermetic D cells developed by us are capable of delivering energy densities of 290 WHr/lb and 20 WHr/in^3 at low rates (0.01-0.03A) and 156 WHr/lb and 11 WHr/in^3 at high rates (1.0A).

2. The capacity retention of the cells were found to be excellent on storage at 72°, 55°, 45° and 25°C for periods of 3 months, 6 months, 1 year and 2 years, respectively.

3. The voltage-delays experienced by cells initially on 72°C storage and -30°C test, were alleviated sufficiently as a result of a systematic study of the problem, that the cells now are suitable for a wide variety of military applications.

4. The thermal-runaways, forced or spontaneous, were found to be due to the exothermic reactions of the chemical constituents present in the cell on heating either by abuse (shorting, etc.) or spontaneously by chemical reactions.

A possible mechanism for the observed spontaneous thermal runaway of partially discharged cell on storage, has been developed.

5. An approach to prevent spontaneous explosion of discharged cell on casual storage has been developed. The efficacy of the approach needs to be demonstrated.

6. It was shown experimentally that a thermal runaway may be induced by a local "hot spot".

7. Several empirical approaches showed promise in improving the abuse resistance of the hermetic D cell on forced discharge, but the cells may exhibit percussion sensitivity after a prolonged reversal.

10. References

1. W. K. Behl, J. A. Cristopulos, M. Ramirez and S. Gilman, J. Electrochem. Soc., 120, 1619 (1973).
2. J. J. Auborn, K. W. French, S. I. Lieberman, V. K. Shah and A. Heller, ibid, 120, 1613 (1973).
3. D. L. Maricle et al, U.S. Pat. 3,567,515 (1971); G. E. Blomgren and M. L. Kronenberg, German Pat. 2,262,256 (1973).
4. A. N. Dey and C. R. Schlaikjer, Proc. 26th Power Sources Symposium, Atlantic City, April 1974.
5. J. R. Driscoll and G L. Holleck, Abstract 34, p. 91 The Electrochemical Society Extended Abstracts, Fall Meeting, Dallas, Texas, Oct. 5-9, 1975.
6. M. L. B. Rao, J. Electrochem. Soc., 114, 13 (1967).
7. A. N. Dey, ibid., 118, 1547 (1971).
8. R. Selim and P. Bro, ibid., 118, 830 (1971).
9. P. Bro, Brighton Power Sources Conference (1974).
10. A. N. Dey, Electrochim. Acta, 21, 377 (1976).
11. A. N. Dey and C. R. Schlaikjer, unpublished results.
12. A. N. Dey, "Sealed Primary Lithium Inorganic Electrolyte Cell", Second Quarterly Report, ECOM-74-0109-2, November 1974.
13. N. Marincic and A. Lombardi, "Sealed Lithium Inorganic Battery", Seventh Quarterly Report, ECOM-74-0108-7, March 1976.
14. K. French, P. Cuker, C. Persiahi and J. Auborn, J. Electrochem. Soc., 121, 1045 (1974).
15. D. L. Chua, Proc. 27th Power Source Symp., Atlantic City, N.J., 1976.
16. M. M. Markowitz and D. Z. Boryta, J. Electrochem. Eng. Data, 7, 586 (1962).
17. N. B. Pilling and R. E. Bedeworth, J. Inst. Met., 29, 577 (1923).
18. A. N. Dey, J. Electrochem. Soc., 123, 1262 (1976).
19. A. N. Dey, "Sealed Primary Lithium Inorganic Electrolyte Cell", First Quarterly Report, ECOM 74-0109-1, July 1974.
20. P. Bro and A. N. Dey, Abstract 23, p. 63. The Electrochemical Society Extended Abstracts, Fall Meeting, Las Vegas, Nevada, October 17-22, 1976.

11. Acknowledgement

Helpful suggestions from Dr. Sol Gilman and Dr. Per Bro and experimental assistance of John Miller, Sarah Spencer and Robin Granelli are gratefully acknowledged.

12. Appendix

Detailed Results on High Current Pulsing Experiments

The experimental results on the initiation of a thermal runaway by high current pulsing are listed in the order the experiments were performed.

1. One D cell was partially discharged 8 A.Hr and then subjected to a high current from a 12V battery. The current and the internal temperature profiles were recorded with a dual channel recorder and are shown in Fig. 116. The initial current was 210A which gradually declined to 125A in 0.75 sec. and then suddenly became zero most likely because of the melting of the tab connecting the cell electrodes to the terminal. The cell exhibited three separate explosions as judged from the sound. The cluster of spikes in the current profile corresponded with the three explosions as indicated in the figure. This multiple explosion appears to be peculiar to this mode of initiation of a thermal runaway since we have not observed this phenomenon in the earlier experiments involving thermal runaways. The sensitivity of the temperature measurement was too low to measure any temperature rise during the high current pulse, and showed fluctuations and a substantial rise after each explosion.

2. Another D cell was partially discharged 8 A.Hr and then subjected to two 16 milisecond pulses of 220A followed by a 40 milisecond pulse of 220A. The cell did not explode. The pulse width was then increased to 0.1 second using the 12V battery. The cell still did not explode. The pulse width was then increased further to approximately 0.6 second. The cell exhibited two separate explosions. The first explosion was muffled and was considerably less noisy than a typical cell explosion, whereas the second one was much louder and sounded like a typical cell explosion. The current and the internal temperature profiles are shown in Fig. 117. The first explosion corresponded with the first set of current and temperature spikes at around 0.8 seconds. The internal temperature gradually rose thereafter and the second explosion took place after approximately 3.5 seconds of the initiation of the pulse; there was only one current spike corresponding to this explosion.

3. One fresh D cell was subjected to high current pulses of increasing durations starting from 0.18 second. The cell was allowed to cool to room temperature after each pulse. The purpose of the experiment was to determine the pulse width needed to explode the cell. The pulse widths, the maximum current and the maximum internal temperature after each pulse is given below.

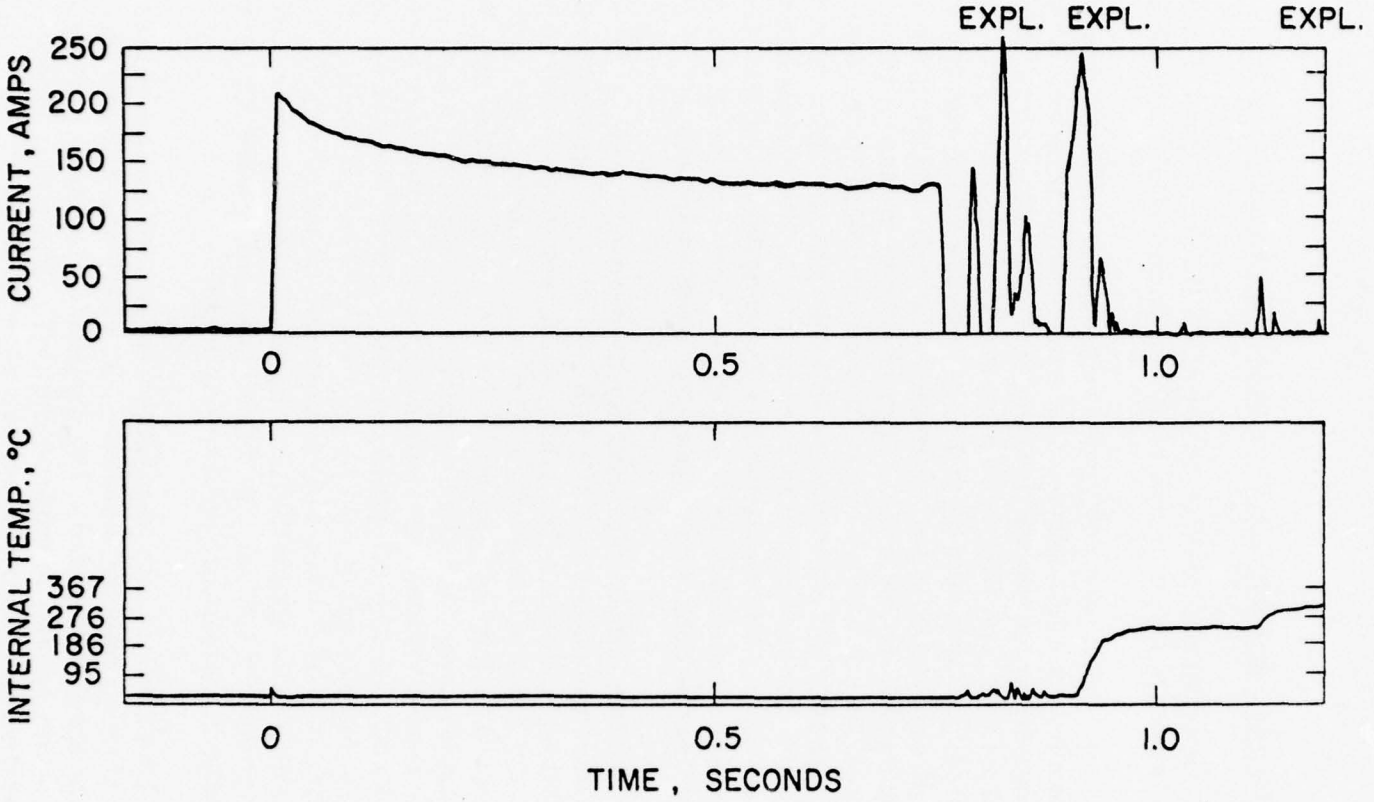

Fig. 116 Current and internal temperature profiles on pulsing a $Li/SOCl_2$ D cell

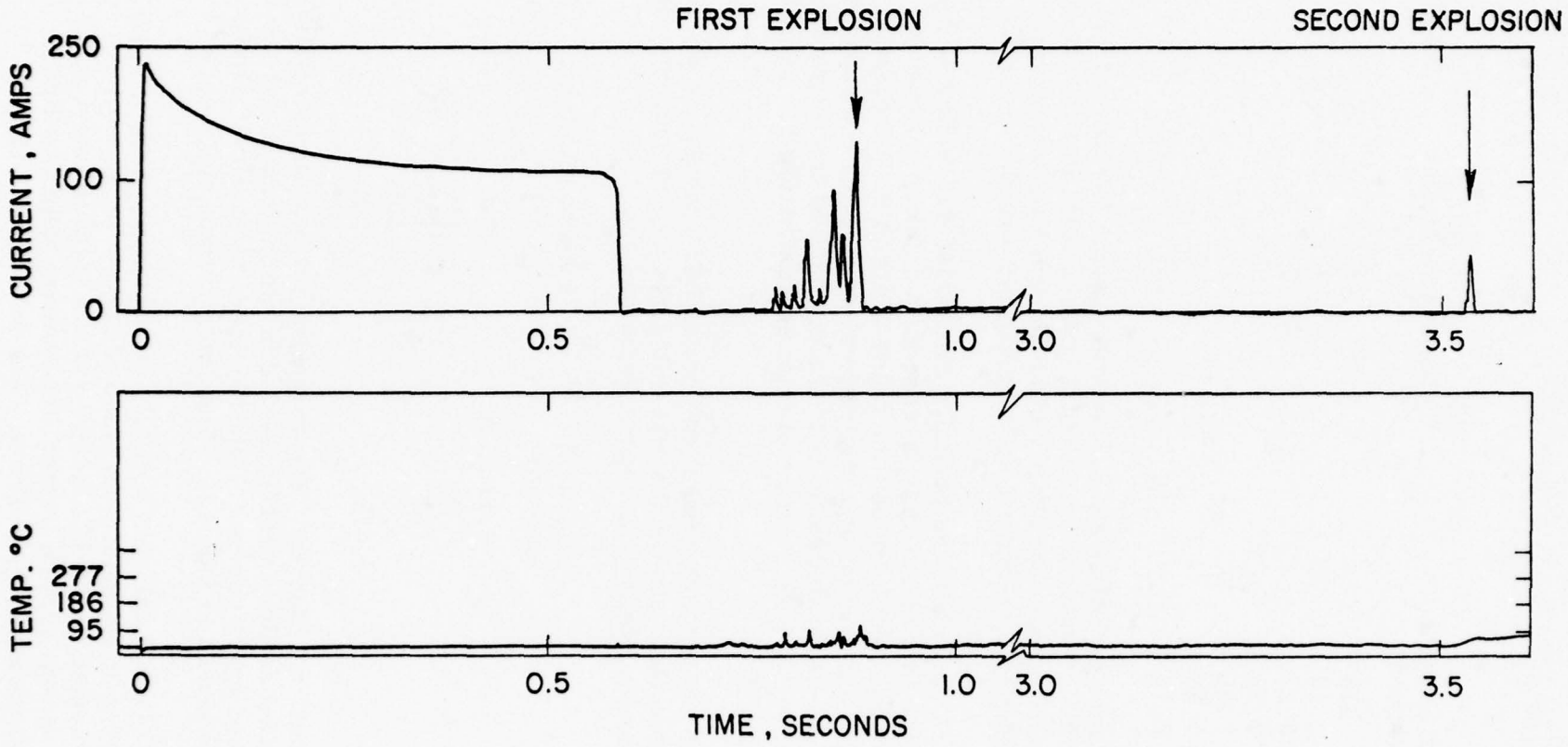

Fig. 117 Current and internal temperature profiles on pulsing a Li/$SOCl_2$ D cell

Pulse Width (second)	Maximum Current (A)	Internal Temperature (°C)
0.18	195	30
0.18	140	30
0.21	180	30
0.35	195	35
0.45	175	35
1.36	175	35
2.70	155	Exploded

The cell exploded after the 2.7 second pulse. The current and the internal temperature profiles of this particular pulsing experiment is shown in Fig. 118. The explosion occurred very shortly after the pulse corresponding to the temperature spike, there was no current spike at the point of the explosion.

4. One D cell was partially discharged 4.5 A.Hr and then subjected to a pulse which was set to be 0.06 second in duration. However, the malfunction of the switching circuit caused the pulse width to be increased to approximately 1 second. The current and the temperature profiles are shown in Fig. 119. There were considerable fluctuations of the current and the temperature towards the end of the pulse. The cell exploded after approximately 1.5 seconds of initiation of the pulse.

5. One undischarged D cell which had been stored at ambient temperature for approximately six months was subjected to high current pulses of increasing durations starting at 0.11 second as below.

Pulse Width (second)	Maximum Current (A)
0.11	110
0.35	110
1.4	135
3.6	100
4.6	75

The cell did not explode. The pulse current was substantially lower than the cells tested earlier, most likely due to the increased cell impedance. The cell was pulsed again with a 2.7 second pulse and the cell exploded. The current profile is shown in Fig. 120. The sharp current spike coincided with the explosion.

6. One D cell was partially discharged to a capacity of 2.0 A.Hr and then subjected to a 20 milisecond pulse of 200A without any explosion. The cell was then connected to the 12V battery via the solenoid without the switching circuitry and the current and the internal temperature were monitored. The cell exploded after approximately 2.5 second. The current and the internal temperature profiles are shown in Fig. 121. The maximum pulse current of 200A dropped sharply after 0.32 second to 20A most likely due to tab melting. Both the current and the

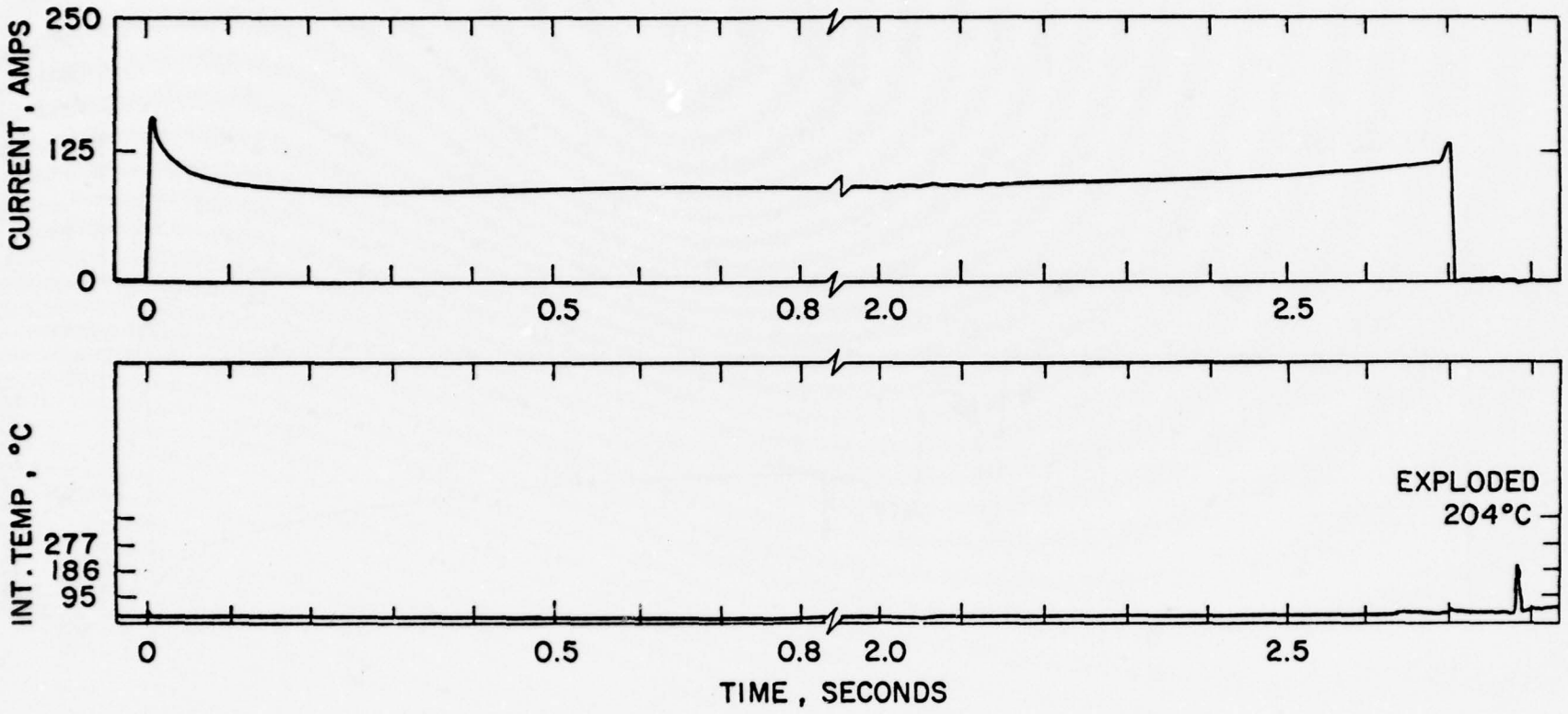

Fig. 118 Current and internal temperature profiles on pulsing a Li/$SOCl_2$ D cell

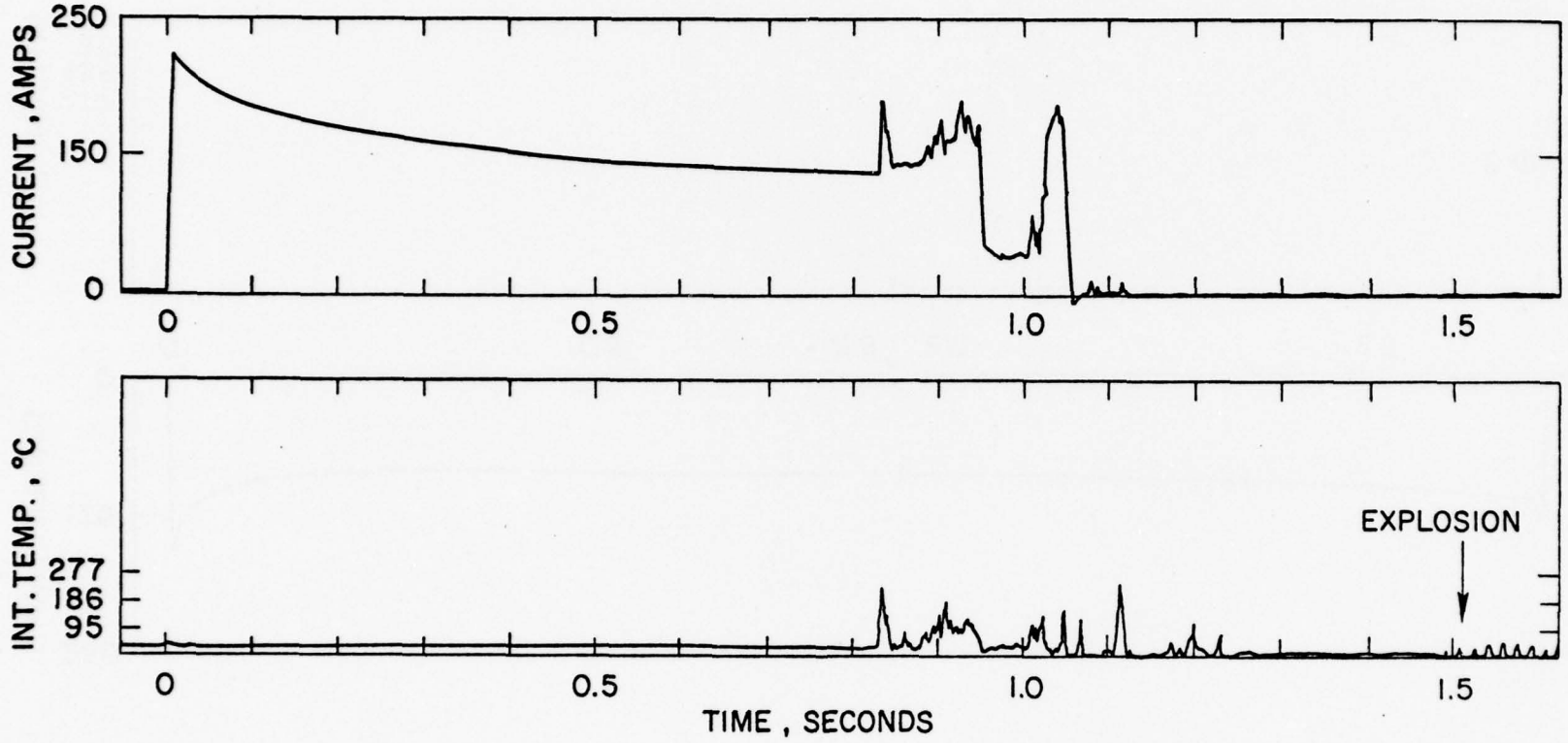

Fig. 119 Current and internal temperature profiles on pulsing a $Li/SOCl_2$ D cell

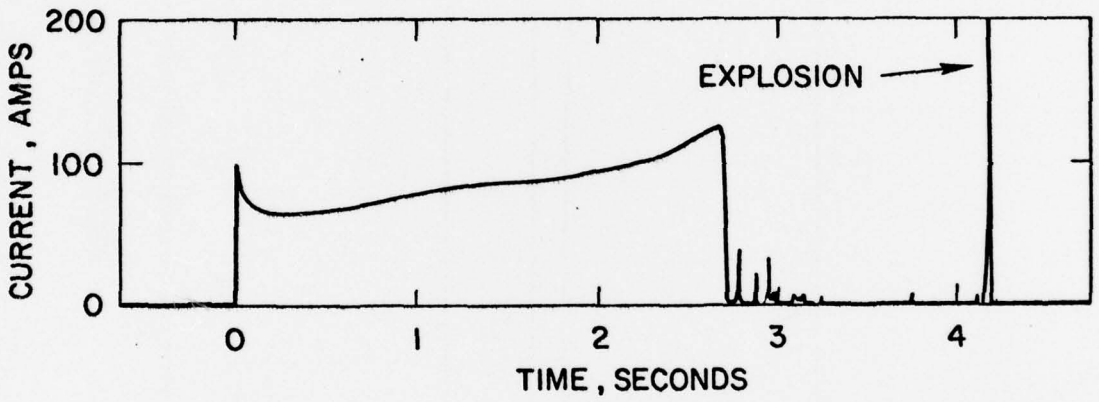

Fig. 120 Current profile on pulsing a $Li/SOCl_2$ D cell

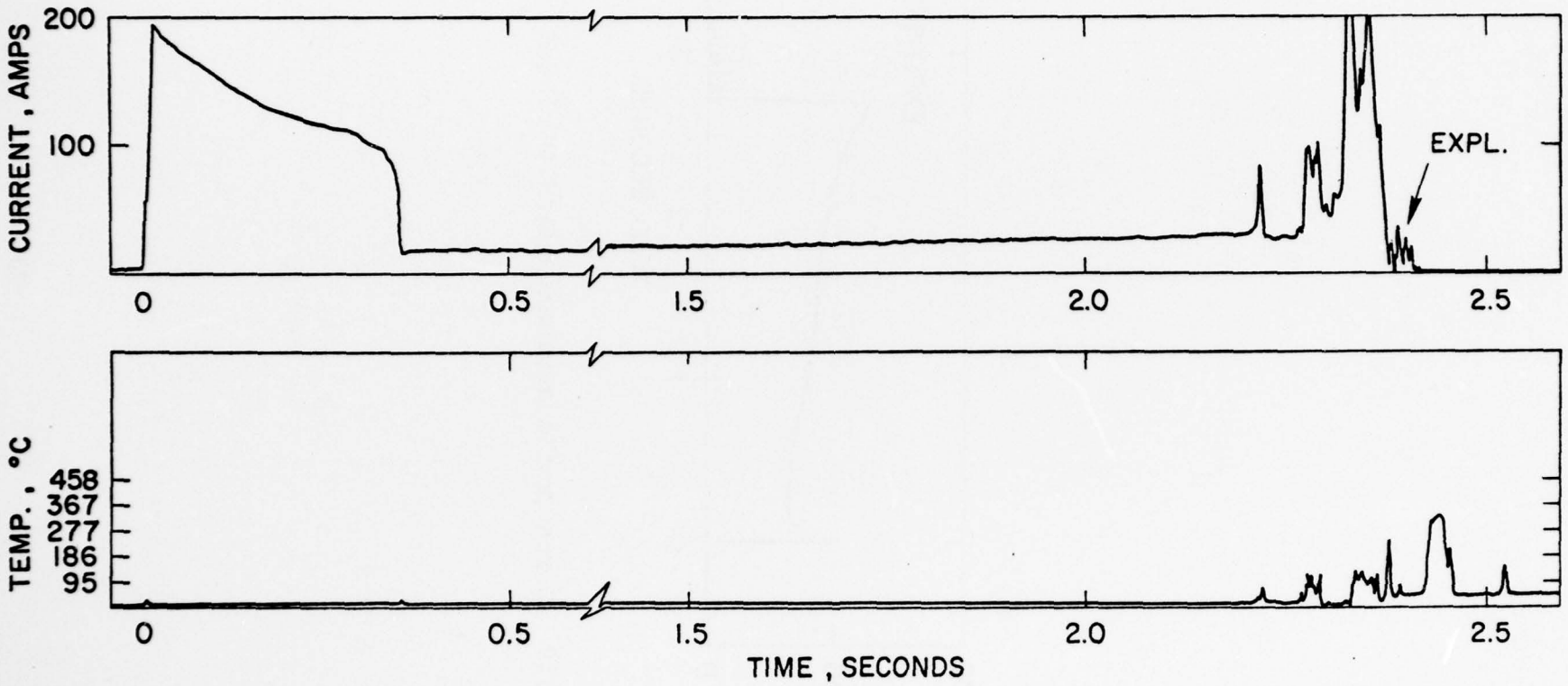

Fig. 121 Current and internal temperature profiles on pulsing a $Li/SOCl_2$ D cell

temperature fluctuated considerably prior to the explosion.

7. One D cell was completely discharged to yield a capacity of 12A.Hr and then subjected to several pulses of increasing durations starting from 0.024 second as below:

Pulse Width (second)	Maximum Current (A)
0.024	172
0.040	190
0.216	188
0.360	198

Finally the cell was pulsed with a 1.2 second duration pulse. The pulse terminated spontaneously (most likely due to the melting of the tab) at 0.48 second and the cell exploded after 0.72 second as shown in the voltage profile in Fig. 122.

The results so far indicate a general trend of shorter pulses for the explosion of a discharged D cell to occur compared to the explosion of a partially discharged or a fresh cell.

8. In this experiment we applied the high current pulse through the heating wire located inside the cell (touching the cathode) instead of through the electrodes in order to isolate any electrochemical effect (if any) on the initiation of an explosion. The D cell was partially discharged 10 A.Hr. The first pulse through the heating wire was 0.04 second long and the maximum current was 200A. The cell interior heated to 48°C as a result of this pulse, but the cell did not explode. Next, the pulse duration was increased to 0.096 second. This time the cell exploded. The current and the internal temperature profiles are shown in Fig. 123. The explosion occurred right after the current and the temperature spikes. The explosion was found to be unusually loud.

This experiment demonstrated that the initiation of the cell explosion is mostly a thermal phenomenon and not an electrochemical one, since no current was passed through the cell electrodes.

9. We attempted to carry out another experiment similar to above by applying high current pulses through the heating wire of another D cell which was partially discharged 8 A.Hr. The pulse width and the maximum currents are as follows.

Pulse Width (second)	Maximum Current (A)
0.04	200
0.06	200
0.08	200
0.10	200

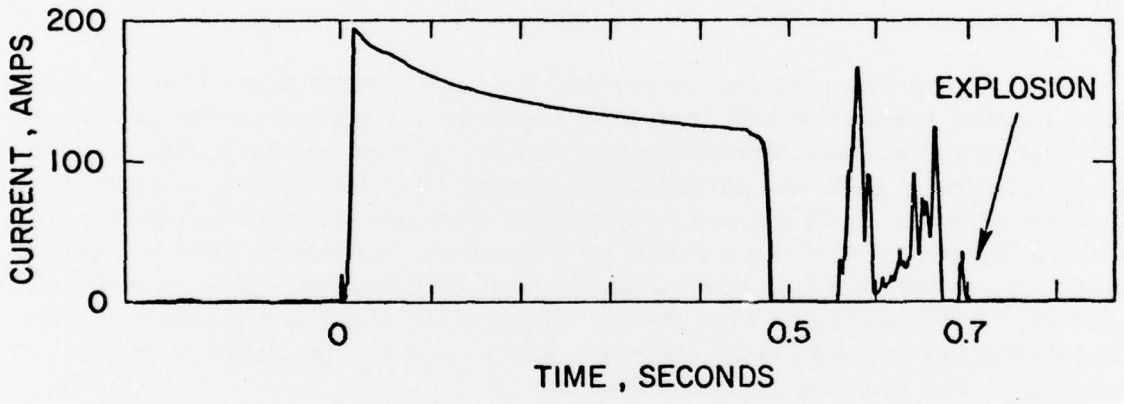

Fig. 122 Current profile on pulsing a $Li/SOCl_2$ D cell

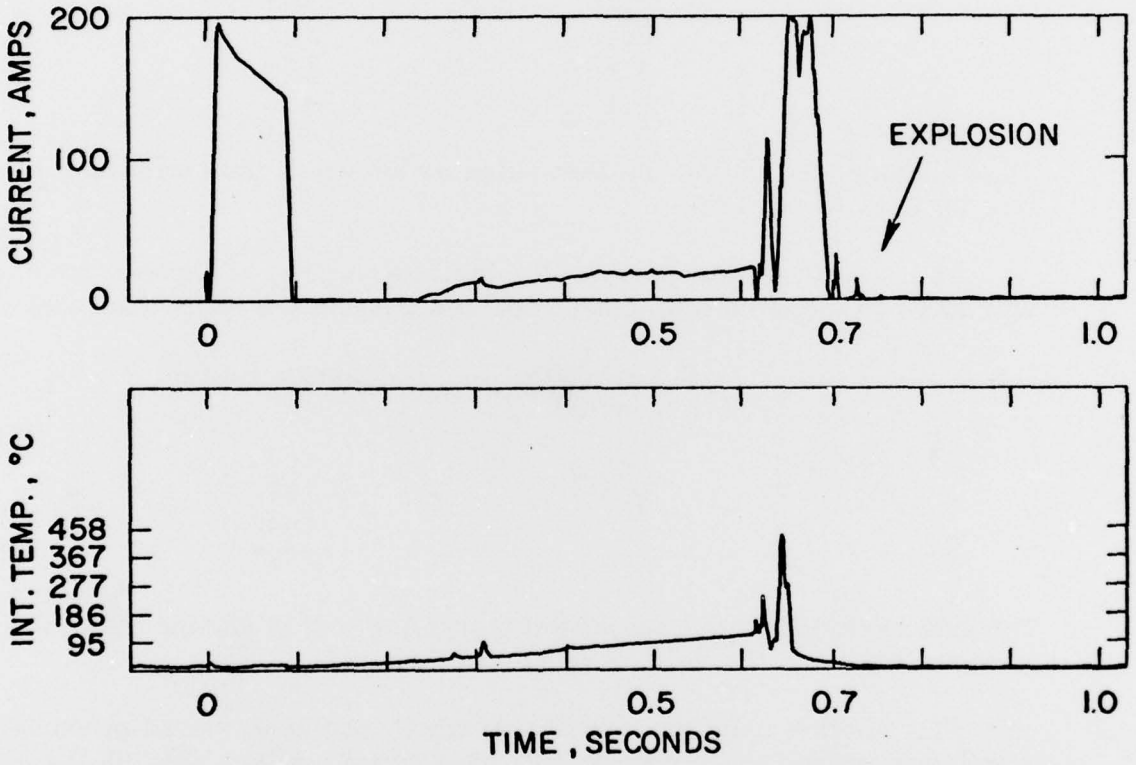

Fig. 123 Current and internal temperature profiles on pulsing a $Li/SOCl_2$ D cell

The heating wire burnt out during the last pulse.

Next we pulsed the cell through the electrodes as below.

Pulse Width (second)	Maximum Current (A)
0.03	190
0.06	188
0.08	190
0.10	188
0.20	188
0.25	190
0.70	190
1.1	190

The cell exploded during the last pulse as shown in the current and the temperature profiles in Fig. 124.

10. One undischarged D cell which was stored at ambient for one month was subjected to repeated high current pulses through the electrodes as below.

Pulse Width (second)	Maximum Current (A)
1.1	108
1.4	108
2.2	104
3.8	136

The cell exploded at the end of the last pulse of 3.8 second duration as shown in the current and the voltage profile in Fig. 125.

11. Another undischarged D cell which had been stored at ambient for one month was subjected to consecutive high current pulses through the electrodes as below.

Pulse Width (second)	Maximum Current (A)
1.1	90
2.2	112
2.9	124
4.6	112

The cell exploded at the end of the last pulse as shown in the current and the voltage profile in Fig. 126.

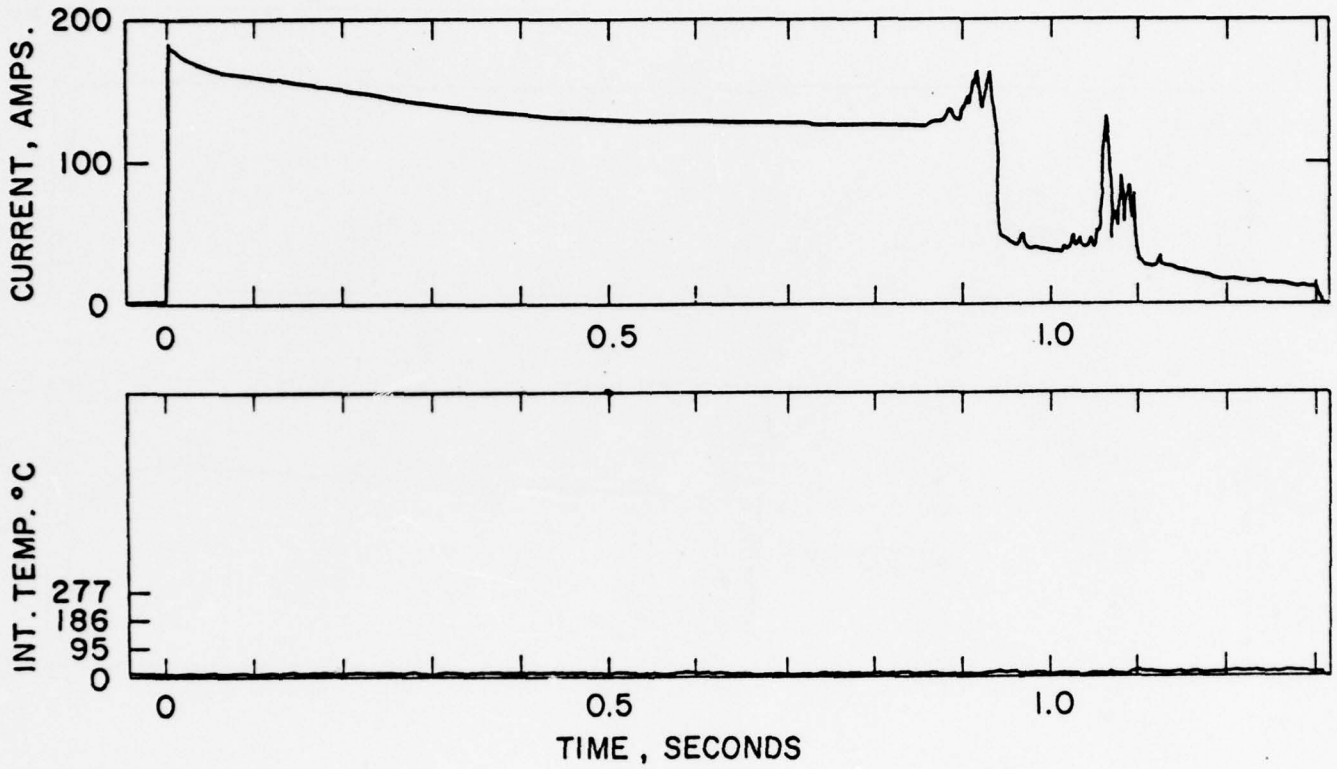

Fig. 124 Current and internal temperature profiles on pulsing a $Li/SOCl_2$ D cell

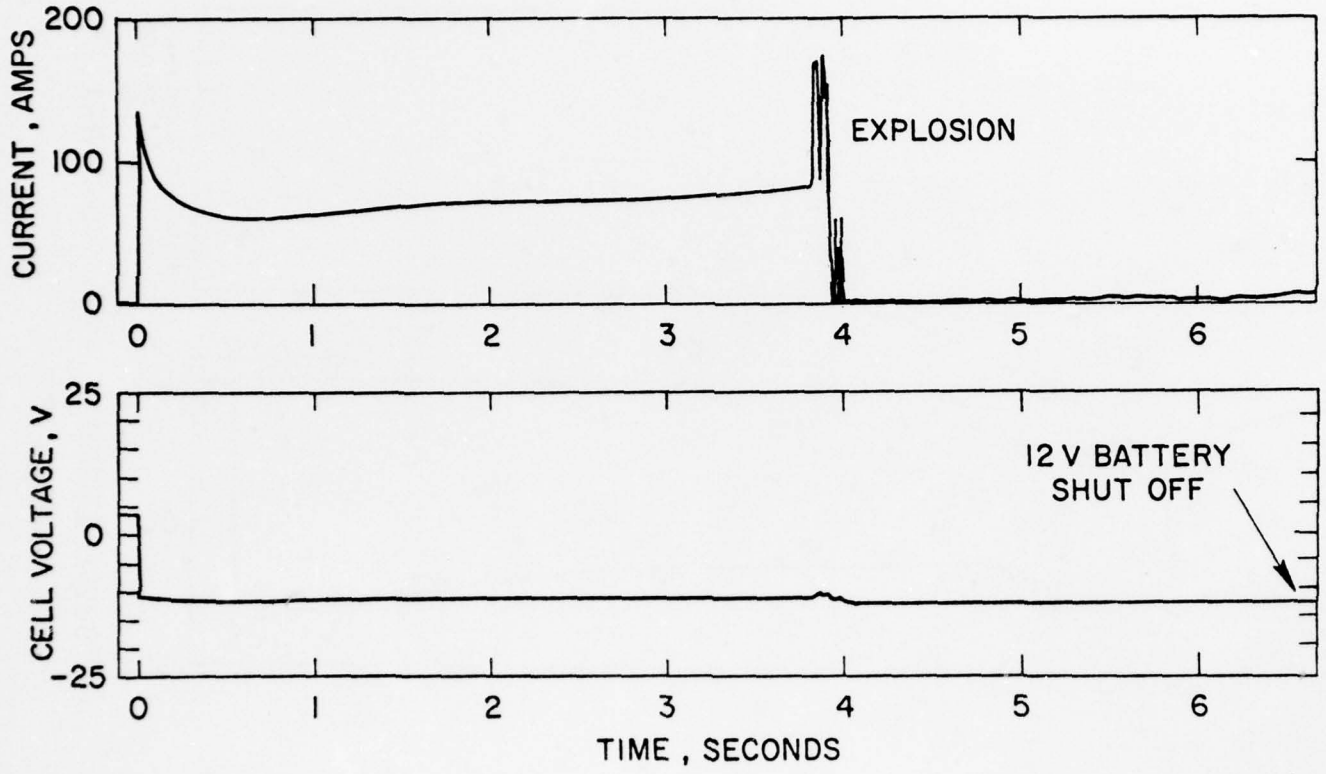

Fig. 125 Current and internal temperature profiles on pulsing a $Li/SOCl_2$ D cell

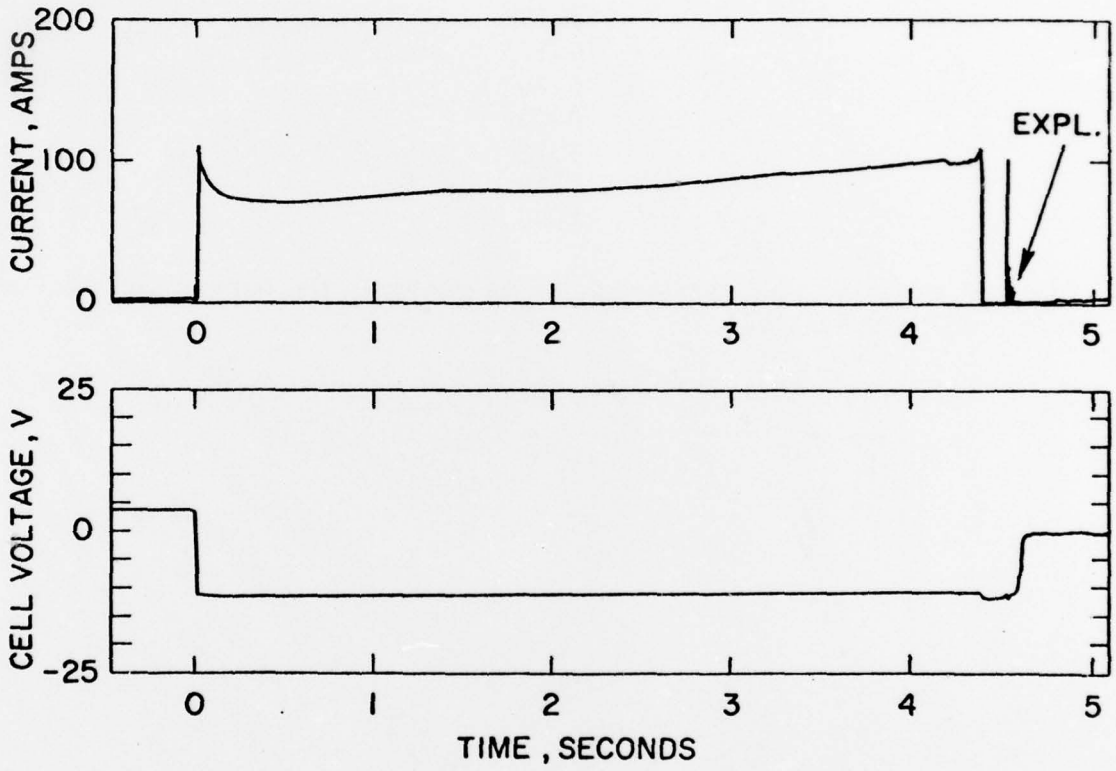

Fig. 126 Current and internal temperature profiles on pulsing a $Li/SOCl_2$ D cell

12. One completely discharged D cell ($\sim$12 A.Hr) was first subjected to pulses through the heating wire which burnt out during the pulse without any cell explosion. The cell was then subjected to consecutive high current pulses through the electrodes in the following sequence. The maximum current was approximately 180A.

Pulse Width (second)
0.024
0.068
0.080
0.104
0.136
0.20
0.23
0.18
0.30
1.06

The cell exploded after the last pulse as shown in the current and the temperature profiles in Fig. 127.

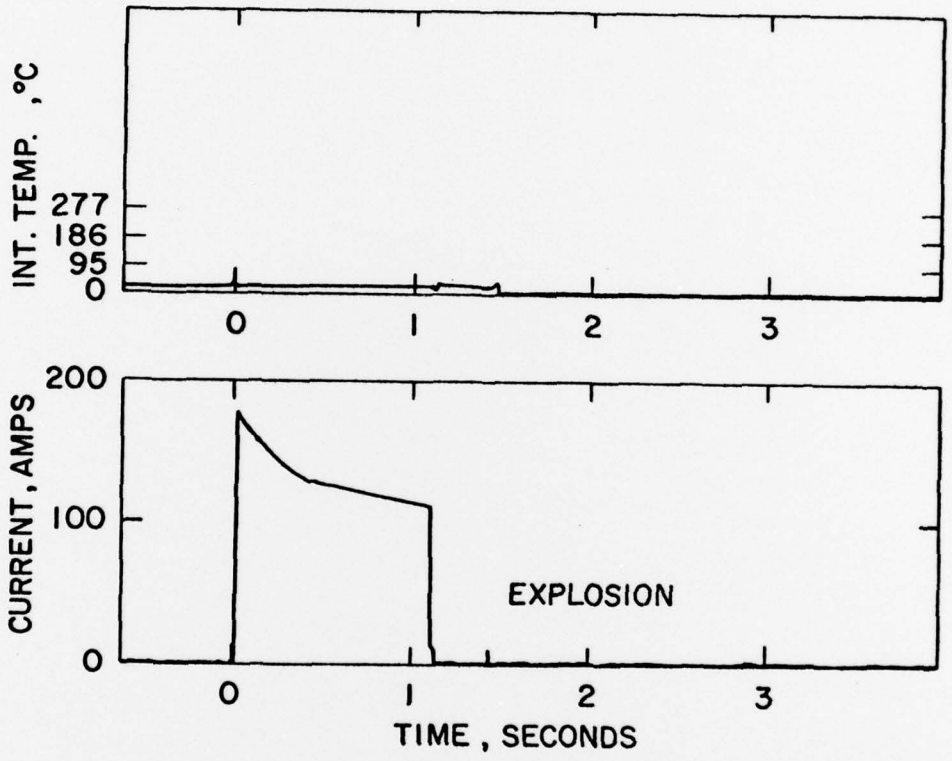

Fig. 127 Temperature and current profiles on pulsing a $Li/SOCl_2$ D cell

DISTRIBUTION LIST

Defense Documentation Center (12)
ATTN: CCD-TCA
Cameron Station (Bldg. 5)
Alexandria, VA 22314

Commander (1)
Naval Electronics Laboratory Center
ATTN: Library
San Diego, CA 92152

Commander (1)
Naval Surface Weapons Center
White Oak Laboratory
ATTN: Library, Code WX-21
Silver Spring, MD 20910

Commandant, Marine Corps (2)
HQ, U.S. Marine Corps
ATTN: Code LMC
Washington, DC 20380

Rome Air Development Center (1)
ATTN: Documents Library (TILD)
Griffiss AFB, N.Y. 13441

HQ ESD (DRI) (1)
L.G. Hanscom AFB
Bedford, MA 01731

HDQA (DAMA-ARZ-D)/ (1)
Dr. F. D. Verderame)
Washington, D.C. 20310

Commander (1)
Harry Diamond Laboratories
ATTN: Library
2800 Powder Mill Road
Adelphi, MD 20783

Commander (1)
U.S. Army Research Office
ATTN: DRXRO-IP
PO Box 12211
Research Triangle Park, NC 27709

Commander (1)
U.S. Army Signals Warfare Lab
ATTN: DELSW-OS
Arlington Hall Station
Arlington, VA 22212

Commander (1)
U.S. Army Mobility EQP Res & Dev Cmd
ATTN: DRXFB-R
Fort Belvoir, VA 22060

NASA Scientific & Tech Info Facility (1)
Baltimore/Washington Intl Airport
PO Box 8757, MD 21240

Commander
U.S. Army Electronics R&D Command
Fort Monmouth, N. J. 07703

DELSD-L-S	(2)
DELET-DD	(1)
DELET-DT	(2)
DELET-P	(1)
DELSD-L (Tech Lib)	(1)
DELSD-MR	(7)

Commander
U.S. Army Communications R&D Command
Fort Monmouth, N. J. 07703

USMC-LNO (1)

Distribution List Continued

Yardney Electric Company (1)
82 Mechanic Street
Pawcatuck, CT 02891
ATTN: Mr. William E. Ryder

Exxon Research and Engineering Co. (1)
Corporate Research Laboratory
Linden, N.J. 07036
ATTN: Dr. R. Hamlen

Argonne National Laboratories (1)
9700 South Cass
Argonne, IL 60439
ATTN: Dr. E. C. Gay

GTE Sylvania, Inc. (1)
77 A Street
Needham Heights, MA 02194
ATTN: Mr. Richard Pabst

General Motors Corp. (1)
Research Laboratories
General Motors Technical Center
12 Mile and Mounds Roads
Warren, MI 48090
ATTN: Dr. J. L. Hartman

Union Carbide Corporation (1)
Parma Research Center
P. O. Box 6116
Cleveland, OH 44101

P. R. Mallory & Co. Inc. (1)
S. Broadway
Tarrytown, N.Y. 10591
ATTN: J. Dalfonso

North American Rockwell Corp. (1)
Atomics International Division
Box 309
Canoga, Park, CA 91304
ATTN: Dr. L. Heredy

General Electric Research & (1)
Development Center
P. O. Box 8
Schenectady, N.Y. 12301
ATTN: Dr. Stefan Mitoff

University of California (1)
Department of Science & Research
Santa Barbara, CA 93100
ATTN: Dr. J. Kennedy

The Electric Storage Battery Co. (1)
Carl F. Norburg Research Center
19 W. College Avenue
Yardley, PA 19067
ATTN: Dr. A. Salkind

Gulton Industries, Inc. (1)
Metuchen, N.J. 08840
ATTN: Mr. S. Charlip

Electrochimica (1)
2485 Charleston Road
Mountain View, CA 94040
ATTN: Dr. Eisenberg

Dr. Hugh Barger (1)
P.O. Box 2232
Davidson, N.C. 28036

Energy Storage & Conversion Dept. (1)
T.R.W. Systems
One Space Park
Redondo Beach, CA 90278
ATTN: Dr. H. P. Silverman

Sanders Associates, Inc. (1)
24 Simon Street
Mail Stop NSI-2208
Nashua, N.H. 03060
ATTN: J. Marshall

Power Conversion Inc. (1)
70 MacQuesten Pkwy
Mount Vernon, N.Y. 10550
ATTN: Stuart Chodosh

Distribution List Continued

Dr. D. Pouli (1)
Portfolio Manager
Hooker Chemicals & Plastics Corp.
M.P.O. Box 8
Niagara Falls, N.Y. 14302

Dr. Leonard Nanis (1)
G207
S.R.I.
Menlo Park, CA 94025

Frank Murphy/SB331 (1)
Naval Underwater Systems Center
Newport Laboratory
Newport, R.I. 02840

NASA Lewis Research Center (1)
Mail Stop 302-1
2100 Brookpark Road
Cleveland, OH 44101
ATTN: Dr. Stuart Fordyce

Mr. Joe McCartney (1)
Naval Undersea Center
Code 608
San Diego, CA 92132

EIC, Inc. (1)
ATTN: S.B. Brummer
Newton, MA 02158

Altus Corp. (1)
ATTN: Douglas Glader
440 Page Mill Road
Palo Alto, CA 94306

J. Bene MS488 (1)
NASA Langley Research Center
Hampton, VA 23665

Mr. Eddie T. Seo (1)
Research and Development Division
The Gates Rubber Company
999 S. Broadway
Denver, Colorado 80217

Transportation Systems Center (1)
Kendall Square
Cambridge, MA 02142
ATTN: Dr. Norman Rosenberg

GTE Laboratories, Inc. (1)
40 Sylvan Road
Waltham, MA 02154

Foote Mineral Company (1)
Route 100
Exton, PA 19341
ATTN: Dr. H. Grady

Honeywell, Inc. (1)
104 Rock Road
Horsham, PA 19044
ATTN: C. Richard Walk

Sanders Associates, Inc. (1)
Sonobuoy Division
95 Canal Street
Nashua, N.H. 03060
ATTN: Dr. David Dwyer

Eagle-Picher Industries, Inc. (1)
Electronics Division
ATTN: Mr. Robert L. Higgins
P. O. Box 47
Joplin, Missouri 64801

SUPPLEMENT TO DISTRIBUTION LIST

13 January 1978

Other Recipients

Mr. Donald Mortel (1)
AF Aero Propulsion Lab
ATTN: AFAPL-POE-1
Wright-Patterson AFB, Ohio 45433

Mr. Richard E. Oderwald (1)
Department of the Navy
Hqs., US Marine Corps
Code LMC 4
Washington, DC 20380

Commander (1)
Harry Diamond Laboratories
ATTN: DELHD-RDD (Mr. A. Benderly)
2800 Powder Mill Road
Adelphi, MD 20783

Power Information Center (1)
University City Science Center
3624 Science Center
Philadelphia, PA 19104